PB99-163198

Summary Report of Research on Permanent Ground Anchor Walls, Volume II: Full-Scale Wall Tests and a Soil-Structure Interaction Model

PUBLICATION NO. FHWA-RD-98-066

SEPTEMBER 1998

U.S. Department of Transportation
Federal Highway Administration

Research and Development
Turner-Fairbank Highway Research Center
6300 Georgetown Pike
McLean, VA 22101-2296

FOREWORD

This report is part of a four-volume series which summarizes a comprehensive study on permanent ground anchor walls. Volume I (FHWA-RD-98-065) discusses current practice and limiting equilibrium analyses. Volume II (FHWA-RD-98-066) presents results of full-scale wall tests and a soil-structure interaction model. Volume III (FHWA-RD-98-067) covers model-scale wall tests and ground anchor tests. Volume IV (FHWA-RD-98-068) summarizes the first three volumes and presents conclusions and recommendations.

Charles J. Nemmers, P.E.
Office of Engineering
Research and Development

NOTICE

This document is disseminated under the sponsorship of the Department of Transportation in the interest of information exchange. The United States Government assumes no liability for its contents or use thereof. This report does not constitute a standard specification or regulation.

The United States Government does not endorse products or manufacturers. Trademarks or manufacturers names appear herein only because they are considered essential to the object of this document.

Technical Report Documentation Page

1. Report No.	2. Government Accession No.	3. Recipient's Catalog No.
FHWA-RD-98-066		PB99-163198

4. Title and Subtitle	5. Report Date / 6. Performing Organization Code
SUMMARY REPORT OF RESEARCH ON PERMANENT GROUND ANCHOR WALLS, VOLUME II: FULL-SCALE WALL TESTS AND A SOIL-STRUCTURE INTERACTION MODEL	5. Report Date: September 1998 6. Performing Organization Code:

7. Author(s)	8. Performing Organization Report No.
Weatherby, D.E., Chung, M., Kim, N.-K., and Briaud, J.-L.	

9. Performing Organization Name and Address	10. Work Unit No. (TRAIS) / 11. Contract or Grant No.
Schnabel Foundation Company 45240 Business Court, Suite 250 Sterling, Virginia 20166	10. Work Unit No. (TRAIS): 3E3B0139 11. Contract or Grant No.: DTFH61-89-C-00038

12. Sponsoring Agency Name and Address	13. Type of Report and Period Covered / 14. Sponsoring Agency Code
U.S. Department of Transportation Federal Highway Administration, Research and Development 6300 Georgetown Pike McLean, Virginia 22101-2296	13. Type of Report and Period Covered: Final Report, September 1989–November 1997 14. Sponsoring Agency Code:

15. Supplemental Notes

FHWA Contracting Officer's Technical Representative (COTR): Albert F. DiMillio, HNR-10
FHWA Technical Consultant: Richard S. Cheney, HNG-31

16. Abstract

Research directed toward improving the design and construction of permanent ground anchor walls is presented. The research focused on tiedback soldier beam walls for highway applications. These walls are generally less than 25 ft high, and they are supported by one or two rows of permanent ground anchors.

This volume is part of a four-volume report summarizing the research. It presents the results of research on a 25-ft-high wall constructed in a medium dense sand, and the development of a numerical model to be implemented in a computer program for the design of soldier beams. Apparent earth pressure diagrams for one-tier and multi-tier walls are developed. Measured bending moments are compared with moments predicted by different design methods. Axial load behavior of the soldier beams is described. The behavior of drilled-in and driven soldier beams is compared. Axial loads, bending moments, wall and ground movements, and anchor loads for each stage of construction are included. A numerical model that combines apparent earth pressure diagrams to describe the pressure on the wall, and soil spring to model the lateral resistance below the bottom of the excavation, is presented.

This volume is the second in a series. The other three volumes are entitled:
- FHWA-RD-98-065 Volume I Current Practice and Limiting Equilibrium Analyses
- FHWA-RD-98-067 Volume III Model-scale Wall Tests and Ground Anchor Tests
- FHWA-RD-98-068 Volume IV Conclusions and Recommendations

In addition, a manual and computer program were developed that incorporate research results. They are entitled:
- FHWA-RD-97-130 Design Manual for Permanent Ground Anchor Walls
- FHWA-RD-98-093 TB Wall — Anchored Wall Design and Analysis Program for Personal Computers

17. Key Words	18. Distribution Statement
Ground anchor walls, tiebacks, retaining walls, apparent earth pressures, soldier beams, soil-structure interaction.	No restrictions. This document is available to the public through the National Technical Information Service, Springfield, Virginia 22161.

19. Security Classif. (of this report)	20. Security Classif. (of this page)	21. No. of Pages	22. Price
Unclassified	Unclassified	274	

Form DOT F 1700.7 (8-72) Reproduction of completed page authorized

SI* (MODERN METRIC) CONVERSION FACTORS

APPROXIMATE CONVERSIONS TO SI UNITS

Symbol	When You Know	Multiply By	To Find	Symbol
		LENGTH		
in	inches	25.4	millimeters	mm
ft	feet	0.305	meters	m
yd	yards	0.914	meters	m
mi	miles	1.61	kilometers	km
		AREA		
in^2	square inches	645.2	square millimeters	mm^2
ft^2	square feet	0.093	square meters	m^2
yd^2	square yards	0.836	square meters	m^2
ac	acres	0.405	hectares	ha
mi^2	square miles	2.59	square kilometers	km^2
		VOLUME		
fl oz	fluid ounces	29.57	milliliters	ml
gal	gallons	3.785	liters	l
ft^3	cubic feet	0.028	cubic meters	m^3
yd^3	cubic yards	0.765	cubic meters	m^3

NOTE: Volumes greater than 1000 l shall be shown in m^3.

Symbol	When You Know	Multiply By	To Find	Symbol
		MASS		
oz	ounces	28.35	grams	g
lb	pounds	0.454	kilograms	kg
T	short tons (2000 lb)	0.907	megagrams	Mg
		TEMPERATURE (exact)		
°F	Fahrenheit temperature	5(F-32)/9 or (F-32)/1.8	Celcius temperature	°C
		ILLUMINATION		
fc	foot-candles	10.76	lux	l
fl	foot-Lamberts	3.426	candela/m^2	cd/m^2
		FORCE and PRESSURE or STRESS		
lbf	poundforce	4.45	newtons	N
psi	poundforce per square inch	6.89	kilopascals	kPa

APPROXIMATE CONVERSIONS FROM SI UNITS

Symbol	When You Know	Multiply By	To Find	Symbol
		LENGTH		
mm	millimeters	0.039	inches	in
m	meters	3.28	feet	ft
m	meters	1.09	yards	yd
km	kilometers	0.621	miles	mi
		AREA		
mm^2	square millimeters	0.0016	square inches	in^2
m^2	square meters	10.764	square feet	ft^2
m^2	square meters	1.195	square yards	ac
ha	hectares	2.47	acres	mi^2
km^2	square kilometers	0.386	square miles	
		VOLUME		
ml	milliliters	0.034	fluid ounces	fl oz
l	liters	0.264	gallons	gal
m^3	cubic meters	35.71	cubic feet	ft^3
m^3	cubic meters	1.307	cubic yards	yd^3
		MASS		
g	grams	0.035	ounces	oz
kg	kilograms	2.202	pounds	lb
Mg	megagrams	1.103	short tons (2000 lb)	T
		TEMPERATURE (exact)		
°C	Celcius temperature	1.8C + 32	Fahrenheit temperature	°F
		ILLUMINATION		
lx	lux	0.0929	foot-candles	fc
cd/m^2	candela/m^2	0.2919	foot-Lamberts	fl
		FORCE and PRESSURE or STRESS		
N	newtons	0.225	poundforce	lbf
kPa	kilopascals	0.145	poundforce per square inch	psi

* SI is the symbol for the International System of Units. Appropriate rounding should be made to comply with Section 4 of ASTM E380.

(Revised August 1992)

TABLE OF CONTENTS

TABLE OF CONTENTS
(continued)

TABLE OF CONTENTS
(continued)

LIST OF FIGURES

LIST OF FIGURES
(continued)

LIST OF FIGURES
(continued)

LIST OF FIGURES
(continued)

LIST OF FIGURES
(continued)

LIST OF FIGURES
(continued)

LIST OF FIGURES
(continued)

LIST OF FIGURES
(continued)

LIST OF FIGURES
(continued)

LIST OF FIGURES
(continued)

LIST OF FIGURES
(continued)

LIST OF FIGURES
(continued)

LIST OF TABLES

LIST OF TABLES
(continued)

LIST OF TABLES
(continued)

LIST OF ABBREVIATIONS AND SYMBOLS

A	=	Cross-sectional area of a beam
A	=	Factor in API equation for determining R-y curve for a soldier beam toe
API	=	American Petroleum Institute
A_c	=	Area of concrete section
A_s	=	Area of steel beam section
A_s	=	Area of ground anchor tendon
A_s	=	Block perimeter surface area of the soldier beam toe
A_t	=	Block area of the tip
a	=	Factor in a beam torsion equation
BMCOL76	=	Computer program to solve beam-columns
BHST	=	Borehole shear test
b	=	Soldier beam width or drilled shaft diameter
C	=	Distance between the strain gauges on opposite flanges
CBEAMC	=	Computer program to solve beam-columns
COM624P	=	Laterally loaded pile computer program
CPT	=	Cone penetrometer
C_1	=	Distance between the neutral axis and the front flange strain gauge
C_1	=	Coefficient in the API laterally loaded pile equation
C_2	=	Distance between the neutral axis and the back flange strain gauge
C_2	=	Coefficient in the API laterally loaded pile equation
C_3	=	Coefficient in the API laterally loaded pile equation

LIST OF ABBREVIATIONS AND SYMBOLS
(continued)

c = Cohesion intercept

D = Toe depth

DMT = Dilatometer

d = Depth of toe embedment

d = Distance from the bottom of the excavation

E = Young's modulus for steel

FHWA = Federal Highway Administration

E_c = Young's modulus of concrete

E_s = Young's modulus for a steel soldier beam or an anchor tendon

E_s = Young's modulus for soil in compression

E_s' = Young's modulus for soil in extension

FHWA = Federal Highway Administration

f'_c = 28-day compressive strength of concrete

f_s = Average unit skin friction resistance

f_{yield} = Yield strength of an anchor tendon

G = Shear modulus of elasticity

H = Height of a cut, height of a wall, depth

H_1 = Depth to the upper ground anchor

h = Beam depth less flange thickness

h = Depth of cut

l = Distance from ground anchor to point of fixity

I = Moment of inertia of a soldier beam

LIST OF ABBREVIATIONS AND SYMBOLS
(continued)

$I_{x\text{-}x}$	=	Moment of inertia about the x-x axis
$I_{y\text{-}y}$	=	Moment of inertia around y-y axis
J	=	Polar moment of inertia
K	=	Lateral earth pressure coefficient for determining skin friction resistance for a driven soldier beam
K_a	=	Active earth pressure coefficient
K_h	=	Horizontal subgrade modulus
K_o	=	At-rest earth pressure coefficient
K_p	=	Passive earth pressure coefficient
k	=	Anchor tendon stiffness
k	=	Initial modulus of subgrade reaction
ksi	=	Kips per square inch
L_u	=	Effective unbonded length of an anchor tendon
M	=	Bending moment
MKT	=	McKiernan-Terry
M_{max}	=	Maximum bending moment resulting from a torsional load
NAVFAC	=	Naval Facilities Engineering Command
NSF	=	National Science Foundation
N_q	=	Bearing capacity factor
n	=	Modulus ratio = E_c/E_s
P	=	Axial force in a soldier beam section
P	=	Horizontal earth pressure acting on the wall
P_{active}	=	Active earth pressure

LIST OF ABBREVIATIONS AND SYMBOLS
(continued)

$P_{at\text{-}rest}$	=	At-rest earth pressure
PBPMT	=	Preboring pressuremeter
$P_{passive}$	=	Passive earth pressure
P_u	=	Ultimate lateral resistance
P_{ud}	=	API ultimate lateral resistance deep, flow resistance
P_{us}	=	API ultimate lateral resistance shallow, wedge resistance
pcf	=	Pounds per cubic foot
psf	=	Pounds per square foot
Q_s	=	Ultimate axial load-carrying capacity or resistance due to skin friction
Q_t	=	Ultimate axial load-carrying capacity or resistance due to tip resistance or end-bearing
Q_{ult}	=	Ultimate axial load-carrying capacity or resistance
q	=	Unit end bearing resistance of a soldier beam
R_a	=	Force in an R-y curve associated with active earth pressures
R_o	=	Force in an R-y curve associated with at-rest earth pressures
R_p	=	Force in an R-y curve associated with passive earth pressures
SPT	=	Standard penetration
s	=	Soldier beam spacing
s_c	=	Clear spacing between soldier beams
s_u	=	Undrained shear strength of a clay
T	=	Torque
T_1	=	Upper ground anchor design load
T_2	=	Second-tier ground anchor design load

LIST OF ABBREVIATIONS AND SYMBOLS
(continued)

t	=	Thickness
tsf	=	Tons per square foot
t/m^3	=	Tons per cubic meter
u	=	Porewater pressure
V	=	Shear
w_a	=	Offset deflection for R-y curve
w_o	=	Offset deflection for R-y curve
w_p	=	Offset deflection for R-y curve
y	=	Deflection of the wall
y_a	=	Active reference deflections
y_o	=	Deflection when the ground anchor load is zero
y_p	=	Passive reference deflections
y_s	=	Deflection when ground anchor is locked-off
y_u	=	Deflection when the anchor tendon ruptures
y_y	=	Deflection when the anchor tendon yields
z	=	Depth
α	=	Anchor inclination
α	=	Factor for determining adhesion with respect to the undrained shear strength of a clay
α	=	Friction angle between a drilled shaft and the ground, ϕ for dense sands, $\phi/3$-$\phi/2$ for loose sands
β	=	A factor in laterally loaded pile equations for determining the shape of the failure wedge, $45° + \phi/2$
γ	=	Total unit weight

LIST OF ABBREVIATIONS AND SYMBOLS
(continued)

δ	=	Angle of friction between soil and pile
δ	=	Wall friction angle
ϵ	=	Strain
ϵ_{axial}	=	Axial strain
ϵ_b	=	Strain at the back flange strain gauge
ϵ_{bb}	=	Bending strain at the back flange strain gauge
ϵ_f	=	Strain at the front flange strain gauge
ϵ_{ff}	=	Bending strain at the front flange strain gauge
ϵ_{rupt}	=	Rupture strain for an anchor tendon
σ	=	Stress in a soldier beam
σ_v	=	Total vertical stress
σ'_v	=	Effective vertical stress
σ'_{vave}	=	Average effective vertical stress along the toe of the soldier beam
σ_{bb}	=	Bending stress in a soldier beam
ϕ	=	Angle of internal friction of the soil, angle of shear resistance
Θ	=	Rotation angle in radians

CHAPTER 1
INTRODUCTION

This volume is part of a four-volume report summarizing research performed to improve the design of permanent ground anchor walls for highway applications. It presents the results of research on a 25-ft-high wall constructed in a medium dense sand, and the development of a numerical model that could be implemented in a computer program for the design of soldier beams. The chapters in Volume II include the following:

- Chapter 2 describes the construction of the wall, and presents axial loads, bending moments, wall and ground movements, and anchor loads for each stage of construction. The behavior of the wall is described in detail. Analyses of the measurements and recommendations for improving the design of permanent ground anchor walls constructed with soldier beams are made. Recommended apparent earth pressure (AEP) diagrams for walls supported by one row or multiple rows of ground anchors are presented. Guidelines for determining bending moments in the soldier beams, and the axial load behavior of the soldier beams are made.
- Chapter 3 presents the development and evaluation of a soil-structure interaction numerical model for the design of soldier beam walls. The use of springs to model the earth pressure behind the wall is evaluated, and recommendations for modeling the earth pressures behind the wall are presented. Relationships for determining the lateral resistance of the embedded portion of the soldier beams are adapted from laterally loaded pile models.

The other three volumes of the research report are entitled:

Volume I	Current Practice and Limiting Equilibrium Analysis (Long, et al., 1998)
Volume III	Model-scale Wall Tests and Ground Anchor Tests (Mueller, et al., 1998)
Volume IV	Conclusions and Recommendations (Weatherby, 1998)

The four volumes address the major elements of permanent ground anchor wall design and provide guidance and recommendations to be used in the development of a design procedure presented in a separate manual. Some research findings were incorporated in a computer code developed for the design or analysis of permanent ground anchor walls. The manual is entitled *Design Manual for Permanent Ground Anchor Walls* (Weatherby, 1997), and the computer program is named *TB Wall — Anchored Wall Design and Analysis Program for Personal Computers* (Urzua and Weatherby, 1998).

Recommendations presented in this report are intended to apply to permanent ground anchor walls for typical highway applications. They were not developed for temporary earth support systems, but many principles presented apply to both permanent and temporary construction.

CHAPTER 2
FULL-SCALE WALL STUDY

A 25-ft-high, instrumented, full-scale, tiedback, H-beam and wood lagging wall was constructed in an alluvial sand deposit to study various aspects of the behavior of anchored walls. The wall was constructed at Texas A&M's National Science Foundation (NSF) designated site for Geotechnical Experimentation.

2.1 OBJECTIVES OF THE STUDY

Objective 1: Determine the moments and stresses in the soldier beams and the deflected shape of the soldier beams under typical loading conditions. Investigate the changes that occur in the lateral earth pressure against the soldier beams as the ground anchors are stressed.

Objective 2: Determine whether the embedded length of a drilled-in soldier beam should be designed as a composite section when Class A concrete is used below grade.

Objective 3: Compare the measured moments and stresses in the soldier beam and the behavior of the embedded length of the soldier beam with predictions from current design procedures.

Objective 4: Determine how the vertical component of the ground anchor force is carried by the soldier beam.

Objective 5: Measure the lateral load in the soldier piles and establish the moment diagram for that portion of the soldier beam installed below subgrade.

Objective 6: Determine how much, if any, of the lateral load is carried by the soil between soldier piles.

Objective 7: Determine the concerns or problems associated with ground anchors installed eccentrically on a soldier beam.

Objective 8: Determine the appropriate load and safety factors that should be assigned to the structural and soil components (pressure magnitude and distributions) to prevent excessive inward wall deflection due to exceeding available passive resistance.

Objective 9: Monitor the performance of the various components of the permanent ground anchor wall system as the load is reduced in a ground anchor.

2.2 THE FULL-SCALE WALL

Eight soldier beams in the wall were instrumented and studied.

2.2.1 Subsurface Condition

The wall was constructed in an alluvial sand deposit. To characterize the soil at the site, a series of in situ and laboratory tests were done. The in situ tests include three Standard Penetration (SPT) borings, three Cone Penetrometer (CPT) soundings, three Preboring Pressuremeter (PBPMT) borings, one Dilatometer (DMT) boring, and one Borehole Shear Test (BHST) hole. Locations for the in situ tests are shown on the site plan for the wall in Figure 1. Laboratory tests were used to determine the natural moisture contents, the particle size distributions, the Atterberg limits, and the Unified Soil Classification for disturbed samples obtained from the SPT borings. Table 1 presents the results of the laboratory tests.

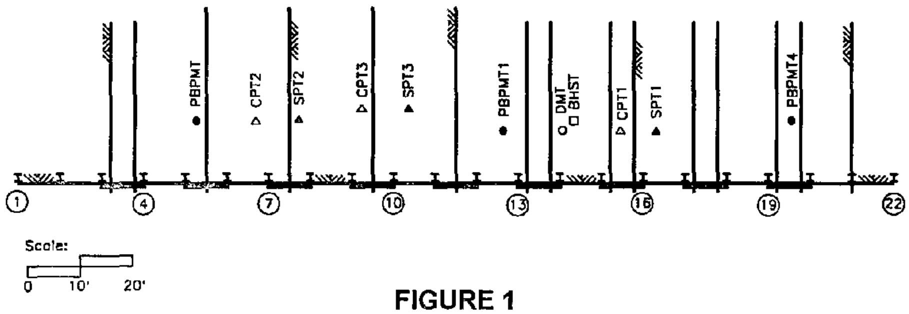

FIGURE 1
Site Plan and In Situ Test Locations

TABLE 1
Summary of the Laboratory Tests

DEPTH	SPT 1					DEPTH	SPT 2					SPT 3				
	W	Atterberg Limits					W	Atterberg Limits				W	Atterberg Limits			
(ft)	(%)	LL (%)	PL (%)	PI (%)	Soil Class.	(ft)	(%)	LL (%)	PL (%)	PI (%)	Soil Class.	(%)	LL (%)	PL (%)	PI (%)	Soil Class.
4	12.30					5	15.80	31.50	27.60	2.90	ML	13.21	30.40	15.70	14.70	SC
8						10	18.03					19.57	22.80	21.00	1.80	SM
12					SP	15	19.71					10.50				
16					SP	20	21.88					19.16				SP
20					SP	25	25.55					21.92				
24	28.60	47.90	18.18	29.72	SC	30	32.83	38.40	26.70	11.70	SM	20.22				SP
28						35	37.77					30.88				
32	34.90	48.16	23.48	24.68	SC	40	29.63					30.04	33.20	23.90	9.30	SC
36	28.50															
40	26.70	36.50	20.48	16.02	SC	Note: Depth based on preconstruction ground level.										
45	22.30	60.85	20.45	40.40	CH											

The SPT borings are denoted as SPT 1, SPT 2, and SPT 3. The average SPT values are shown in Figure 2, a cross-sectional view showing the soil profile at the center of the wall. The soils at the wall were classified as a loose clayey sand or a silty sand from 0 to 10 ft; a medium dense, clean, poorly graded sand from 10 to 25 ft; a medium dense, clayey sand from 25 ft to 40 ft; and a hard clay below 40 ft. Using the SPT tests, the angle of shear resistance, ϕ, was estimated to be between 29° and 33° and the total unit weight, γ, was estimated to be between 113 and 118 pcf.

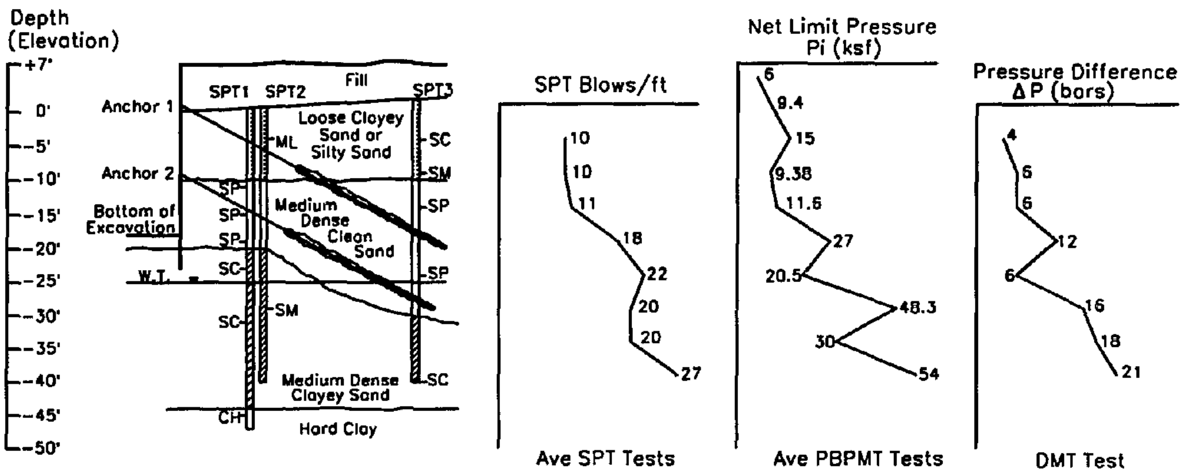

FIGURE 2
Wall Cross-sectional and In Situ Test Results

When wall construction commenced, readings from a groundwater observation well installed in SPT 1 indicated that the water table was approximately 25 ft below the original ground surface. This groundwater table level was higher than expected. To ensure that the water table would remain below the embedded portion of the soldier beams, a 7-ft-high fill was placed on top of the original ground surface. The fill was made using silty and clayey sand obtained on site. The fill was placed in 6- to 9-in lifts and compacted by making two passes of a fully loaded rubber tire pan scrapper.

The results of the CPT tests are presented in Figure 3. The CPT soundings were made from the original ground surface before the construction of the fill. The soil classifications shown on the CPT logs were determined using relationships developed by Schmertmann (1970). The angle of shear resistance, ϕ, was estimated to be between 30 and 32° using the correlation developed by Trofimenkov (1974). The relative density was estimated to be between 40 and 60 percent using the correlation developed by Schmertmann (1977). The soil classifications, ϕ angle, and relative densities are similar to those determined from the SPT tests.

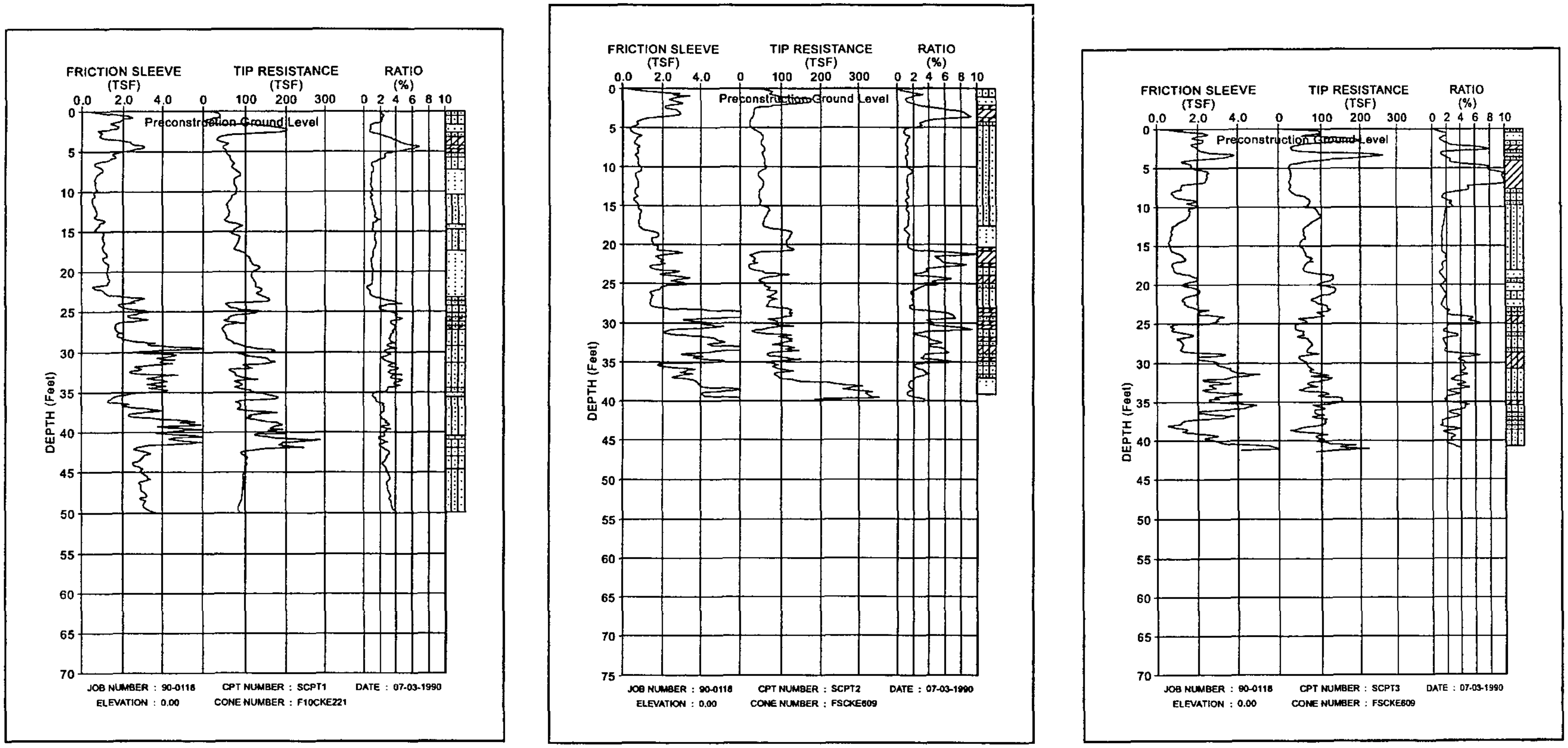

FIGURE 3
Cone Penetrometer Results for CPT 1, CPT 2, and CPT 3

The BHST results are plotted in Figure 4. The tests indicate that the angle of internal friction lies between 30° and 33°, and the soil had an average cohesion of 0.34 psi.

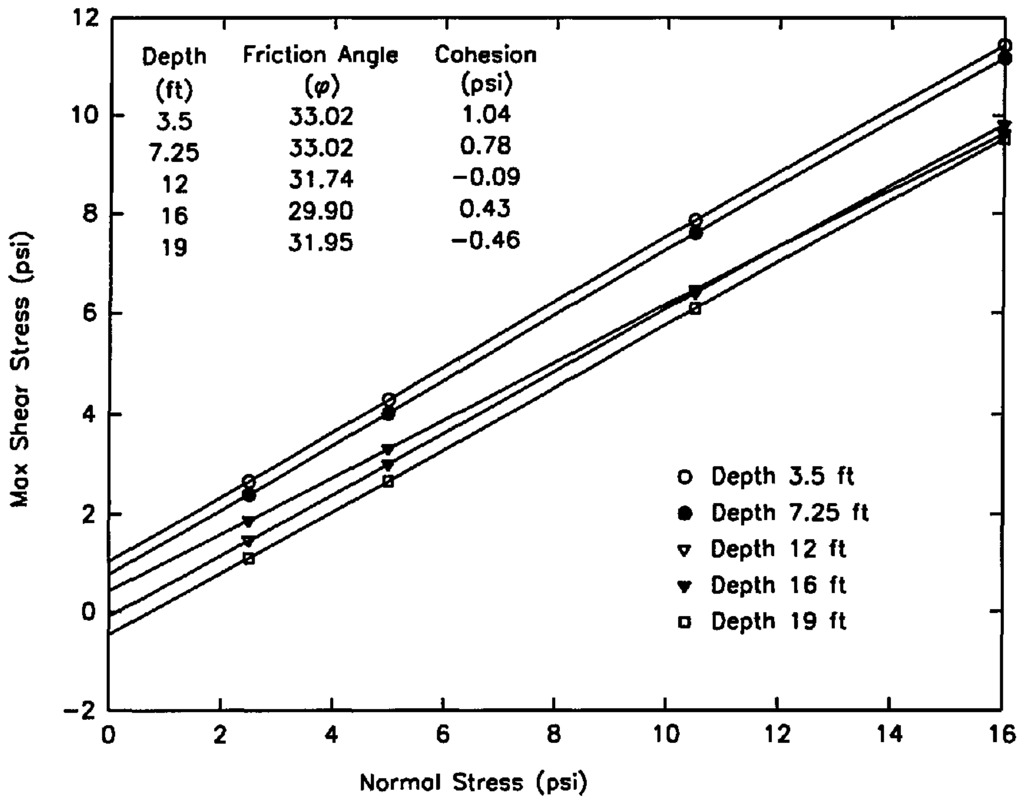

FIGURE 4
Borehole Shear Test Results

Summaries of the PBPMT tests are plotted in Figure 5 and the average net limit pressures are shown in Figure 2. PBPMT 1 and 2 tests were taken from the original ground surface. After the fill was placed, PBPMT 4 tests were conducted at 3-, 7- and 13-ft depths.

The pressure differences for the dilatometer test (DMT) are shown in Figure 2.

Based on the results of the tests, the soil was assigned a total unit weight, γ, of 115 pcf and an angle of internal friction, ϕ, of 32°. The SPT resistances, the net limit pressures from the pressuremeter tests, and the pressure differences from the dilatometer tests increase linearly with depth.

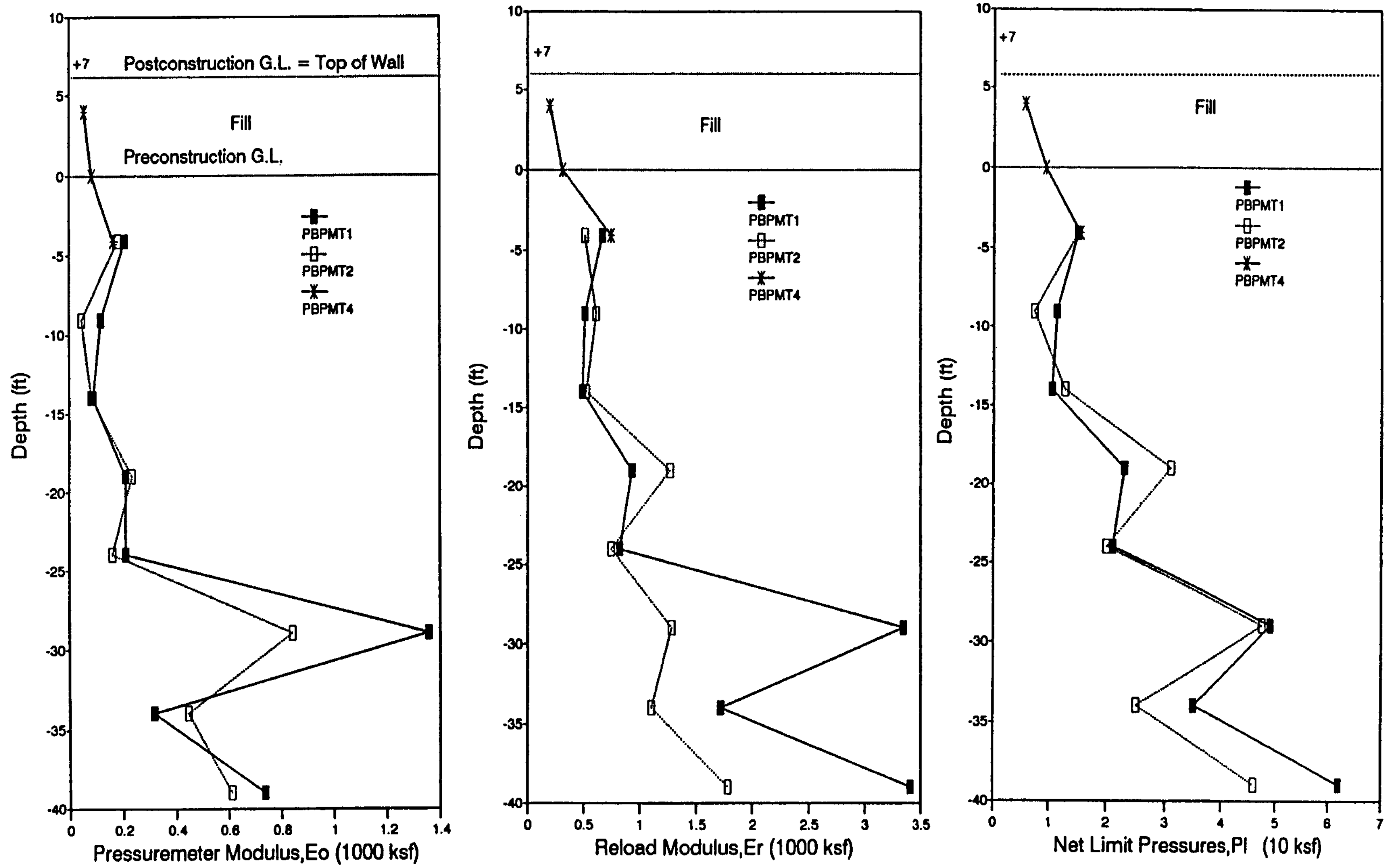

FIGURE 5
Pressuremeter Test Results

2.2.2 Wall Design and Construction

A tiedback retaining wall consisting of soldier beams and wood lagging, and supported by pressure-injected ground anchors, was selected for the study. A 25-ft-high wall was chosen since most highway walls are of similar height. The wall contained a section supported by one row of ground anchors and a section supported by two rows of anchors. Each section was divided into a driven beam and a drilled-beam portion.

Soldier beams and the ground anchors were designed to support the $25H$ trapezoidal apparent earth pressure diagram shown in Figures 6 and 7. Soldier beam bending moment and ground anchor load calculations are shown in the figures. Calculations for soldier beam moments and ground anchor loads were the same for the driven and the drilled-in soldier beams.

Internal stability of the wall was checked by ensuring that the ground anchors would develop their load-carrying capacity behind the critical failure surface. A Rankine failure surface extending from the bottom of the excavation up at an angle of $45+\phi/2 = 61°$ defined the critical failure surface. A distance of 9.5 ft was required to reach the critical failure surface for the upper anchor (highest anchor elevation) of the two-tier wall. Federal Highway Administration (FHWA) guidelines (Cheney, 1988) recommend that the unbonded length be extended behind the critical failure surface a minimum distance of 5 ft or 20 percent of the wall height. Using FHWA guidelines, the minimum unbonded lengths for the two-tiered wall were 14.5 ft for the upper anchor and 10 ft for the lower anchor. A minimum unbonded length of 13 ft was necessary for the one-tier wall. The unbonded lengths for the test wall were extended beyond the minimums. An unbonded length of 18 ft was selected for the upper anchor of the two-tier wall, and 15 ft unbonded lengths were used for the lower anchor and the anchor for the one-tier wall.

Anchor bond lengths were selected so the ultimate ground anchor capacity was at least twice the ground anchor design load. The maximum design load was 106.5 kips. Pressure-injected ground anchors in medium dense sand develop ultimate load-carrying capacities of about 10 kips/linear ft. Anchor bond lengths of 24 ft (estimated ultimate capacity of 240 kips) were selected.

The ground anchors had to be long enough to satisfy external stability. External stability is satisfied when all failure surfaces passing behind the backs of the anchors have a $FS \geq 1.3$. A 29-ft-long upper anchor and a 21-ft-long lower anchor satisfied external stability for the two-tier wall. Total anchor lengths for the two-tier wall were 42 ft for the upper anchor and 39 ft for the lower anchor. A 27-ft-long anchor satisfied external stability for the one-tier wall. A total anchor length of 39 ft was used.

A 5-ft-long toe embedment was selected for the wall. Experience with similar walls indicated that a 5-ft toe was adequate to support the lateral and vertical loads applied to the soldier beam.

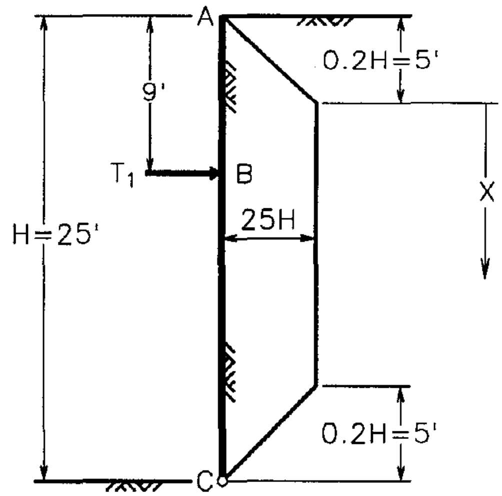

Calculate T_1 by $\Sigma\ M$ @ C

$$16\,T_1 = (25H)\,(8'\text{ soldier beam spacing})\,(8.0H)\,(0.5H)$$

$$T_1 = 78.1 \text{ kips}$$

Calculate M @ B

$$M_B = \left[\frac{(25H)\,(8)\,(5)}{2}\right]\,[9-5+5/3] + [(25H)\,(8)\,(9-5)]\left[\frac{(9-5)}{2}\right]$$

$$M_B = 70{,}833 + 40{,}000$$

$$M_B = 110{,}833 \text{ \#-ft.}$$

Calculate point where V = 0 below B

$$V = 0 = T_1\left[\frac{(25H)\,(8)\,(5)}{2}\right] - (25H)\,(8)\,X$$

$$0 = 78{,}100 - 12{,}500 - 5{,}000X$$

$$X = 13.1 \text{ ft.}$$

Calculate $M_X = 13.1'$

$$M_X = T_1\,(18.1-9) - \left[\frac{(25H)\,(8)\,(5)}{2}\right][13.1+5/3] - [(25H)\,(8)\,\frac{(13.1)^2}{2}]$$

$$M_X = 710{,}710 - 184{,}583 - 429{,}025$$

$$M_X = 97{,}102 \text{ \#-ft.}$$

FIGURE 6
Apparent Earth Pressure Diagram and Calculations for One-tier Wall

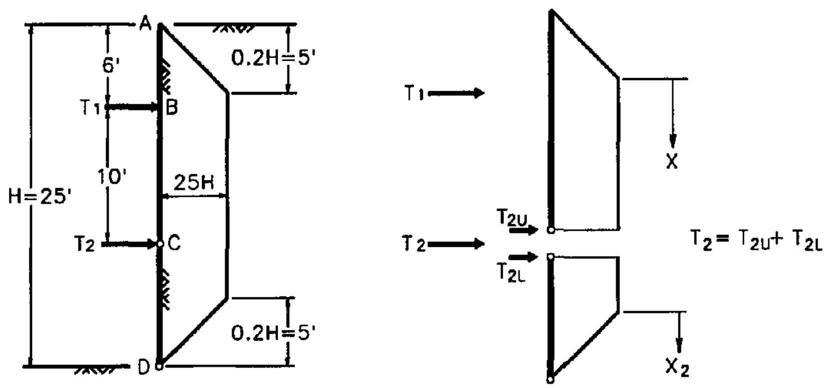

Calculate T_1 by $\Sigma\, M$ @ C

$$10T_1 = \left[\frac{(25H)(8' \text{ beam spacing})(5)}{2}\right][16-5+5/3] + [(25H)(8)(16-5)]\left[\frac{(16-5)}{2}\right] \quad T_1 = 46.08 \text{ kips}$$

Calculate T_{2u} by $\Sigma\, F$

$$T_{2u} = \frac{(25H)(8)(5)}{2} + (25H)(8)(11) - T_1 = 21.42 \text{ kips}$$

Calculate T_{2L} by ΣM@ D

$$9T_{2L} = \left[\frac{(25H)(8)(5)}{2}\right]\left[\left(\frac{2}{3}\right)(5)\right] + [(25H)(8)(9-5)]\,[5+2] \qquad T_{2L} = 20.19 \text{ kips}$$

Calculate T_2

$$T_2 = T_{2u} + T_{2L} = 21.42 + 20.19 = 41.61 \text{ kips}$$

Calculate M_B @ C

$$M_B = \left[\frac{(25H)(8)(5)}{2}\right][6-5+5/3] + [(25H)(8)(6-5)]\left[\frac{(6-5)}{2}\right] = 35{,}833 \text{ \#-ft.}$$

Calculate point where V = 0 between T_1 and T_2

$$V = 0 = T_1 - \left[\frac{(25H)(8)(5)}{2}\right] - (25H)(8)(X) = 46{,}080 - 12{,}500 - 5{,}000x$$

$$X = 6.7 \text{ ft.}$$

Calculate $M_x = 6.7'$

$$M = T_1\,(11.7-6) = \left[\frac{(25H)(8)(5)}{2}\right][6.7+5/3] - \left[\frac{(25H)(8)(6.7)^2}{2}\right] = 45{,}848 \text{ \#-ft.}$$

Calculate point where $V=0$ between T_2 & D

$$V = 0 = T_{2L} - (25H)(8)(4) - \left[\frac{25H + (25H - 5Hx_2)}{2}\right] 8x^2 = 20{,}190 - 20{,}000 - 5{,}000x_2^2$$

$$x_2 = 0.038 \text{ ft.}$$

Calculate $Mx_2 = 0.038$ since x_2 so small

$$M = T_{2L}\,(4+0.038)\,[(25H)(8)(4.038)]\,4.038/2 = 40{,}763 \text{ \#-ft.}$$

FIGURE 7
Apparent Earth Pressure Diagram and Calculation for Two-tier Wall

The toe of one drilled-in soldier beam in each section of the wall was backfilled with Class A structural concrete and the toe of the other drilled-in beam was backfilled with lean-mix backfill. The soldier beams were assumed to be continuous over the upper row of anchors and hinged at the second row of anchors and at the bottom of the excavation. Soldier beams were designed to resist bending moments but they were not designed for combined axial and bending stresses. The ground anchor angle was selected to be 30° from the horizontal so the ground anchors would apply a significant downward load on the soldier beams.

Figure 8 shows an elevation view of the wall and Figure 9 shows a plan view. Figures 10 and 11 are section views through the one-tier and the two-tier sections, respectively. Table 2 contains the soldier beam schedule and Table 3 contains the ground anchor schedule for the wall.

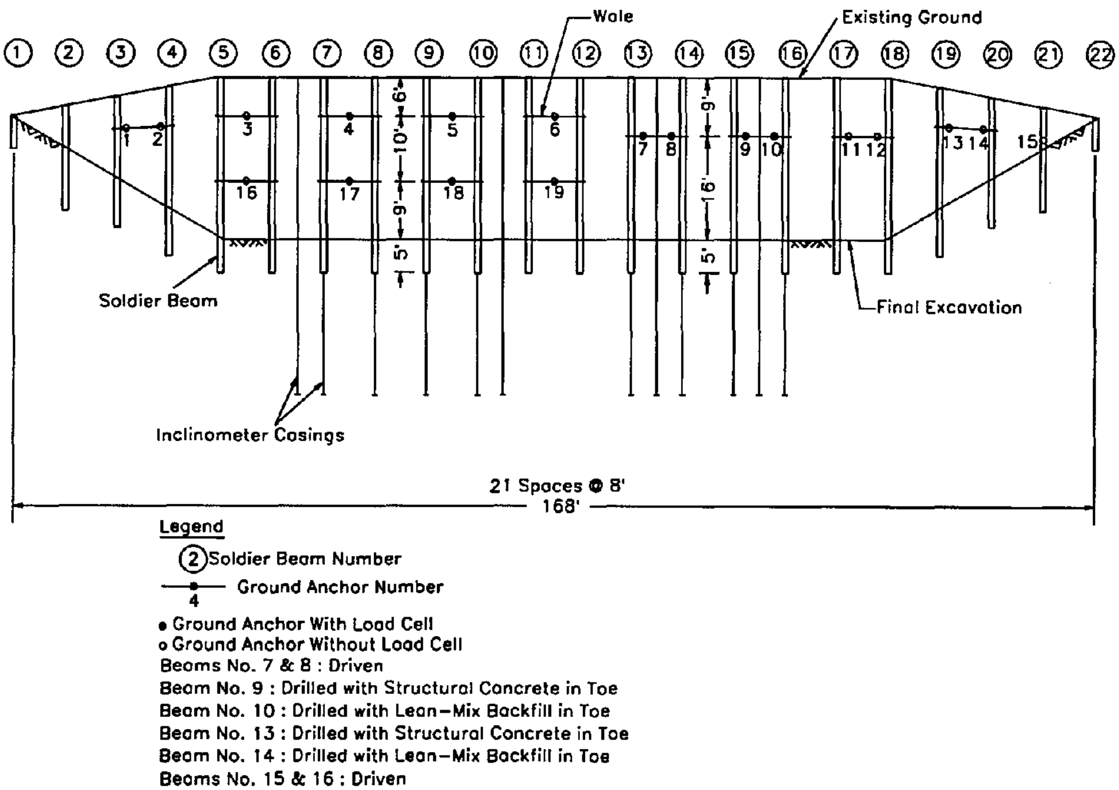

FIGURE 8
Elevation View of the Wall

TABLE 2
Soldier Beam Schedule

PILE NO.	PILE SIZE	INSTALLATION METHOD	COMMENT
1-2	HP 8×36	Driven	
3	HP 8×36	Drilled	Lean-mix in toe.
4	HP 12×53	Drilled	Lean-mix in toe.
5-6	HP 8×36	Driven	
7-8	HP 6×25	Driven	
9	HP 6×25	Drilled	Class A concrete in toe.
10	HP 6×25	Drilled	Lean-mix in toe.
11-12	HP 8×36	Driven	
13	HP 10×57	Drilled	Class A concrete in toe.
14	HP 10×57	Drilled	Lean-mix in toe.
15-16	HP 10×57	Driven	
17-19	HP 12×53	Driven	
20	HP 8×36	Driven	
21	HP 10×42	Driven	
22	HP 8×36	Driven	

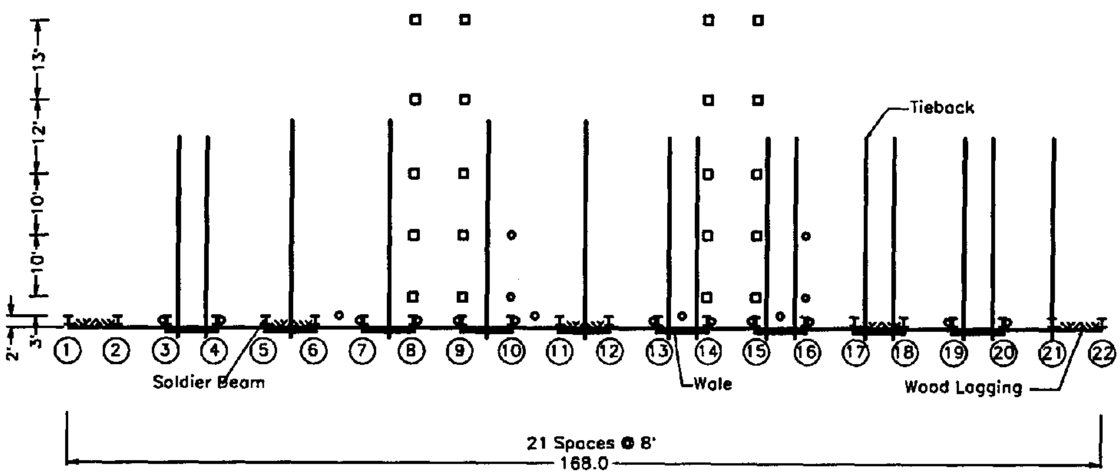

Legend
Soldier Beam
Inclinometer
Settlement Point
Beams No. 7 & 8 : Driven, Two Rows of Anchors
Beam No. 9 : Drilled, Structural Concrete in Toe, Two Rows of Anchors
Beam No. 10 : Drilled, Lean–Mix Backfill in Toe, Two Rows of Anchors
Beam No. 13 : Drilled, Structural Concrete in Toe, One Row of Anchors
Beam No. 14 : Drilled, Lean–Mix Backfill in Toe, One Row of Anchors
Beams No. 15 & 16 : Driven, One Row of Anchors

FIGURE 9
Plan View of the Wall

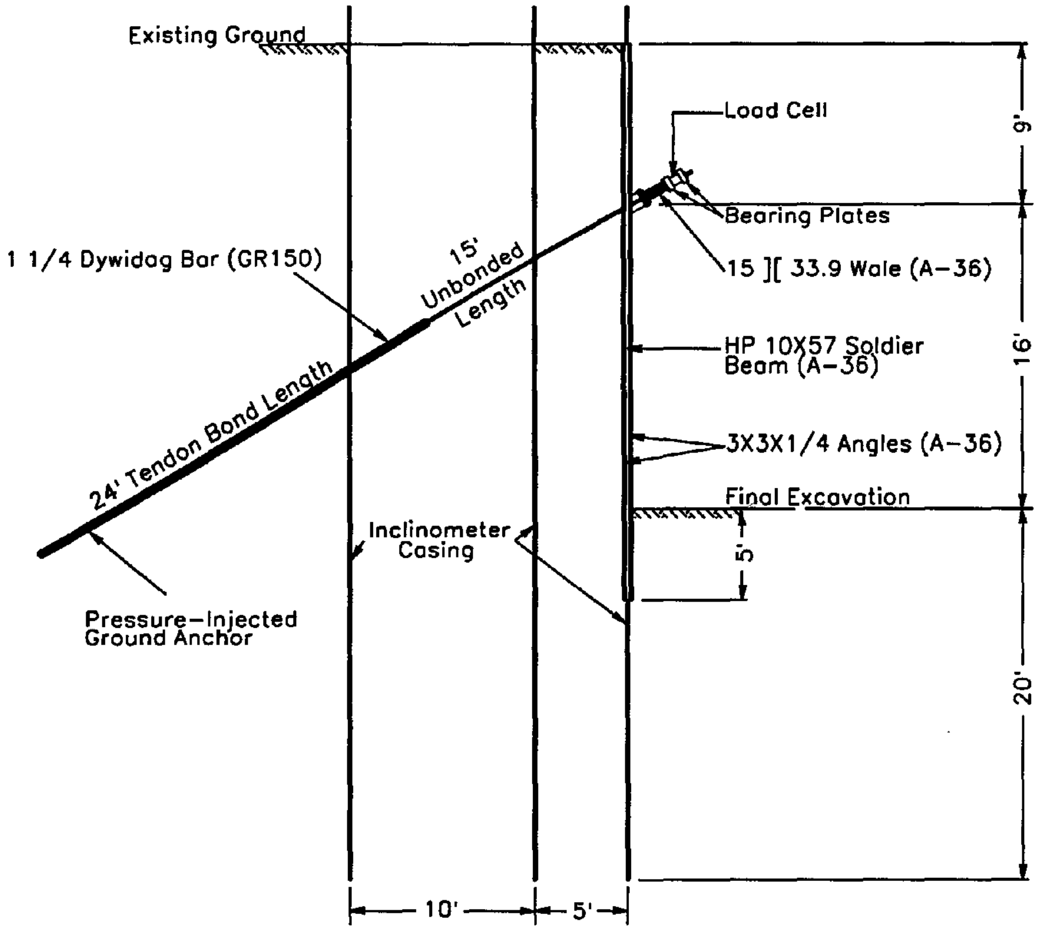

FIGURE 10
Section Through the One-tier Wall

TABLE 3
Ground Anchor Schedule

ANCHOR NO.	TENDON SIZE ϕ (in.)	DESIGN LOAD (kips)	LOCK-OFF LOAD (kips)
1	1-3/8	25.5	19.1
2	1-3/8	49.0	36.8
3-6	1-1/4	106.5	82.0
7-12	1-1/4	90.0	67.5
13	1-3/8	49.0	36.8
14	1-3/8	25.4	19.1
15	1-1/4	20.0	15.0
16-19	1-1/4	96.0	72.0

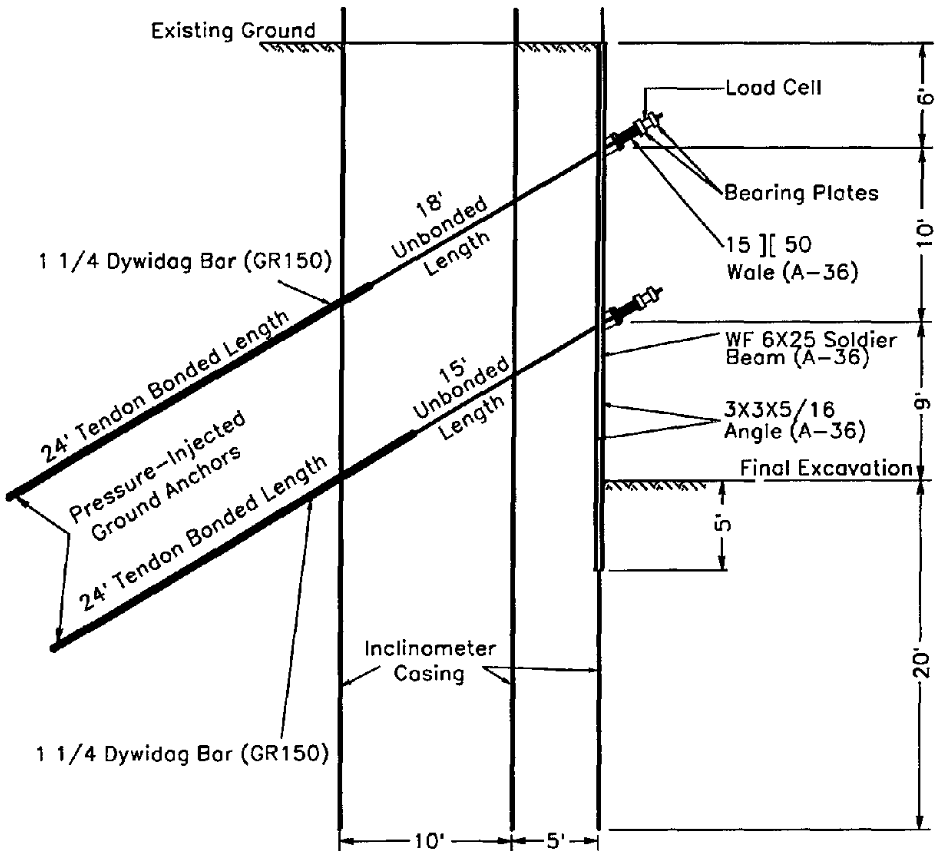

FIGURE 11
Section Through the Two-tier Wall

Soldier Beams 7 to 10 in the two-tier wall section and Soldier Beams 13 to 16 in the one-tier wall section were instrumented. To protect the vibrating wire strain gauges from damage during installation of the soldier beams, structural angles were welded over the gauges. Soldier Beams 13 to 16 had 3×3×1/4 angles welded to the HP 10×57 beams and Soldier Beams 7 to 10 had 3×3×5/16 angles welded to the WF 6×25 beams. The composite HP 10×57 and WF 6×25 beams had moments of inertia of 417.8 in^4 and 132.9 in^4 respectively. Figure 12 shows a cross-section of a typical instrumented soldier beam.

Soldier Beams 7, 8, 15, and 16 were driven to the desired depth using a MKT 9B3 air hammer. Beams 9, 10, 13, and 14 were installed in cased drilled shafts. Eighteen-in-diameter casing was used for Beams 9 and 10 and 24-in casing was used for Beams 13 and 14. A vibratory pile hammer was used to install the casing for the full length of the pile. Then, a truck-mounted drill was used to remove the soil from the casing. The soldier beams were placed in the cased holes and backfilled with concrete or lean-mix backfill. The casing was pulled as the concrete or backfill was placed.

Drill holes for Beams 9 and 14 were backfilled with lean-mix fill. Holes for Beams 10 and 13 were backfilled with Class A structural concrete below the bottom of the final excavation and with lean-mix backfill above the bottom of the excavation. The Class A concrete had an average 28-day compressive strength of 4770 psi. The lean-mix fill had an average 28-day compressive strength of 87 psi.

Pressure-injected ground anchors were used to support the wall. The anchors were installed by driving a closed-end, 3.5-in casing into the ground. After the casing reached the desired depth, then the ground anchor tendon was inserted in the casing and the closure point driven off. Neat-cement grout was pumped down the casing as the casing was extracted. The grout surrounding the bond length was placed at pressures exceeding 200 psi. The top row of anchors had an 18-ft unbonded length and the bottom row of anchors had a 15-ft unbonded length. A plastic tube was used as a bondbreaker over the unbonded length. Three days after the anchors were installed, each anchor was tested and stressed. Test loads were 133 percent of the design loads and the lock-off loads were 75 percent of the design loads.

Three-in-thick wood lagging was used to support the soil between the soldier beams as the excavation proceeded. In general, the excavation was made in 4-ft lifts.

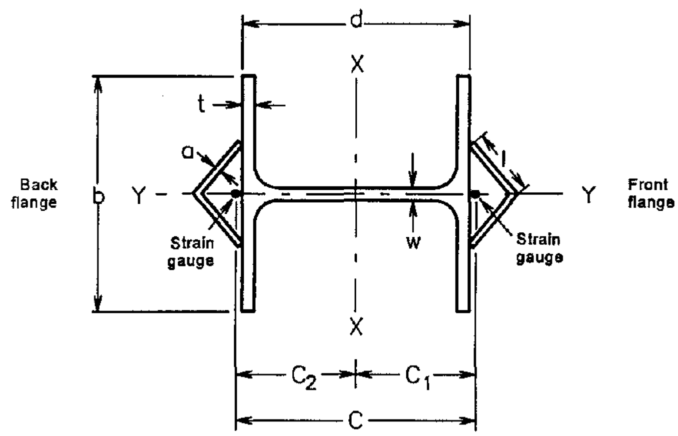

FIGURE 12
Cross-section of an Instrumented Soldier Beam

2.2.3 Instrumentation and Data Acquisition

The instrumentation for the wall consists of strain gauges, embedment strain gauges, load cells, inclinometers, and settlement points. Data acquisition for the strain gauges and embedment gauges was automated using a datalogger (Geokon, Micro-10 Datalogger) and a personal computer. The load cells were read using a strain indicator (Geokon, GK-401). Inclinometer readings were taken with an inclinometer reader (Geokon, Model GK-601) and the data files were saved in a personal computer. The optical settlement surveys were performed with an engineer's level (approximate accuracy ±0.14 in).

Surface-mounted vibrating wire strain gauges (Geokon Model VSM-4000) were used on the soldier beams. Twenty-eight strain gauges were installed on the extreme fibers of each flange. The upper and lower strain gauges were located 1.0 ft from the ends of the soldier beams and the second and third strain gauges, from the top of the beams, were placed 1.5 ft apart. The remaining gauges were installed every foot along the beams. Angles were welded to the soldier beam flanges to protect the strain gauges. The space between the angle and the flange was filled with polyurethane foam. A typical vibrating wire strain gauge installation is shown in Figure 13.

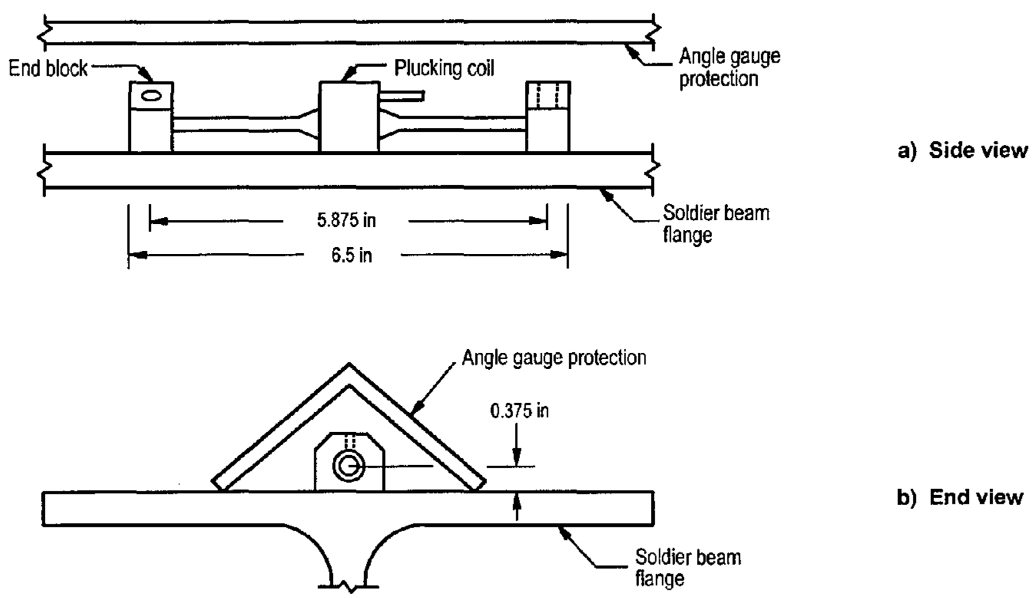

FIGURE 13
Vibrating Wire Strain Gauge Installation

Inclinometer casings were installed at each instrumented soldier beam, between the instrumented beams, and behind the wall face at the locations shown in Figure 9. The 1.9-in inclinometer casings were installed by driving a 3.5-in closed-end casing into the ground to ensure that no ground was lost during installation. The hole surrounding the casing was backfilled with a weak grout consisting of one bag of cement to three bags of lime. Inclinometer casings for the drilled-in soldier beams were installed through 4-in-diameter PVC pipes securely attached to the beams. Inclinometer casings were installed to a depth of 15 ft below the bottoms of the soldier beams. It was assumed that no movement would occur at that depth. A Sinco Digitilt Inclinometer Model 50325-E sensor was used with the inclinometer reader to measure and record the deflections of the casings.

Geokon Model 4900 vibrating wire load cells were installed on each ground anchor supporting an instrumented soldier beam. The locations of the load cells are shown in Figure 8. Two-in-thick bearing plates were used on each side of the load cells to minimize errors resulting from eccentric loading.

Embedment strain gauges were installed to measure strains in the concrete or fill surrounding the toes of the drilled beams (Figure 14). These gauges were modified Geokon Model VCE-4200 vibrating wire strain gauges. Five gauges were fixed inside a 1.0-in diameter times 0.025-in-thick steel tube. The tubes were sized to have the same axial stiffness as concrete with a Young's modulus of 3.0×10^6 psi. The tube positioned and protected the gauges during installation. The gauge tubes were located so their strain gauges were at the same level as the strain gauges on the soldier beam. Operating principles and the data acquisition procedures for the embedment gauges were the same as for the surface-mounted strain gauges.

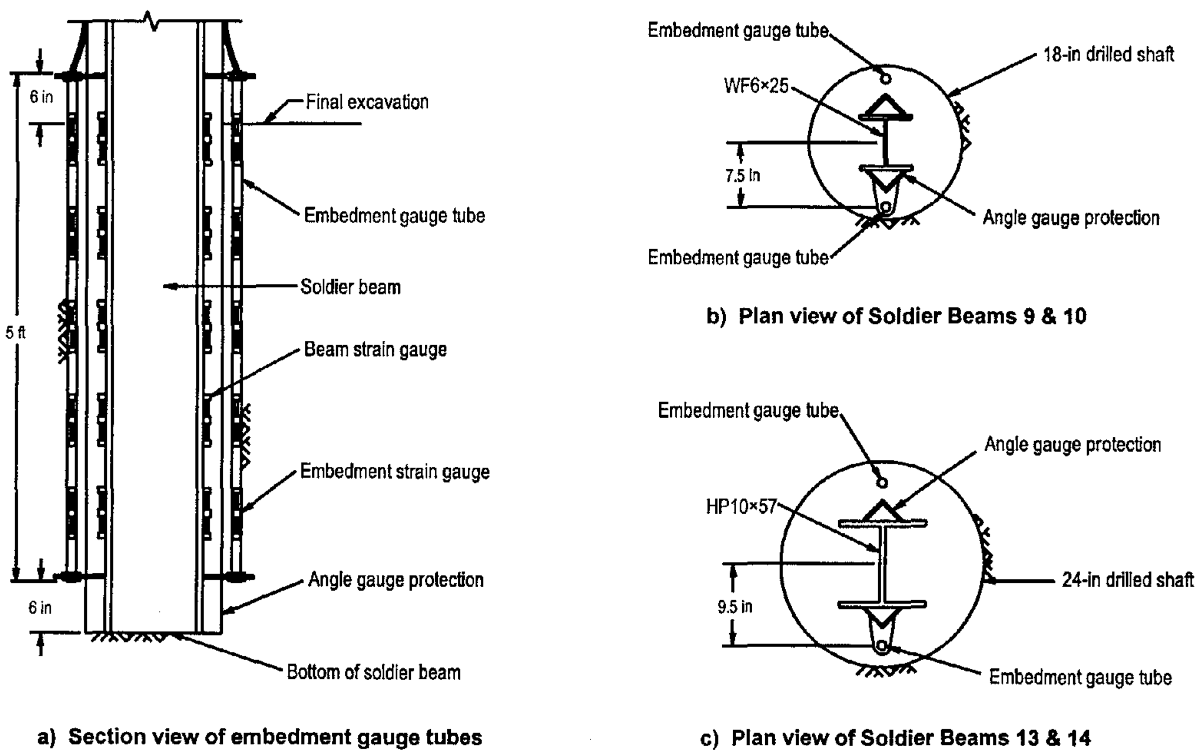

FIGURE 14
Embedment Gauge Details

Optical settlement points were installed at the locations shown in Figure 9. The settlement points consist of a 5-ft length of #5 rebar driven 4.5 ft into the ground. Soldier beam settlements were also measured.

2.3 DATA REDUCTION

2.3.1 Strain Gauge Data

The bending moments and the axial forces in the soldier beams were computed from the measured strains. Strains developed during construction in response to the earth pressures, the horizontal and vertical movements of the wall, and the applied ground anchor loads. The measured strains were separated into bending strains and axial strains using elastic theory.

Figure 15 shows the strain distribution in a cross-section of a soldier beam. The bending strains are proportional to the distance from the neutral axis. Therefore, the bending strains and the axial strains in the soldier beams are given by Equations 2.1 and 2.2:

$$\varepsilon_{bb} = \frac{\varepsilon_b - \varepsilon_f}{C} C_2 \qquad \text{. . . [2.1]}$$

$$\varepsilon_{axial} = \frac{\varepsilon_b C - \varepsilon_b C_2 + \varepsilon_f C_2}{C}$$

or

$$\varepsilon_b - \varepsilon_{bb} \qquad \text{. . . [2.2]}$$

where:

ε_{bb} = bending strain at the back flange gauge

ε_b = total strain at the back flange gauge

ε_f = total strain at the front flange gauge

C = distance between the two gauges

C_2 = distance between the neutral axis and the back gauge

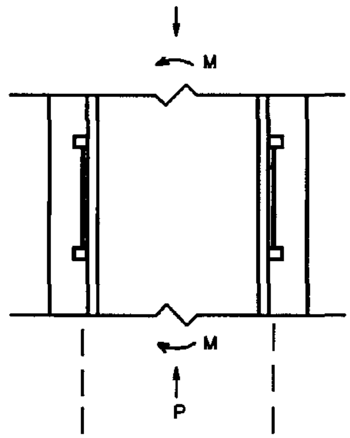

a) Soldier beam

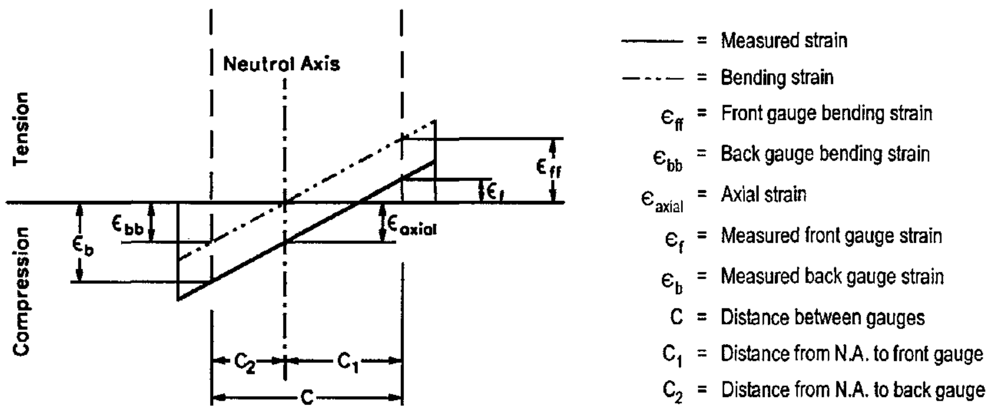

b) Strain diagram

FIGURE 15
Strain Distribution in Soldier Beams

For the soldier beams, where the neutral axis lies in the middle of the soldier beam, $c_1 = c_2 = c/2$. Then Equations 2.1 and 2.2 can be simplified to:

$$\varepsilon_{bb} = \frac{\varepsilon_b - \varepsilon_f}{2} \qquad \text{. . . [2.3]}$$

$$\varepsilon_{axial} = \frac{\varepsilon_b + \varepsilon_f}{2} \qquad \text{. . . [2.4]}$$

2.3.1.1 Calculation of Bending Moments

The stress, σ, at any location in a beam is related to the strain, ε, at that location by Equation 2.5:

$$\sigma = E\,\varepsilon \qquad \text{. . . [2.5]}$$

where E is Young's modulus for the steel. The bending stress, σ_{bb}, in a soldier beam with the neutral axis at the center of the beam is

$$\sigma_{bb} = \frac{M}{I}\,C_2 \qquad \text{. . . [2.6]}$$

where M is the bending moment in the beam and I is the moment of inertia of the beam. Combining Equations 2.5 and 2.6 leads to the following equation for the bending moment in a beam with the neutral axis at its center

$$M = \frac{EI}{C_2}\,\varepsilon_{bb} \qquad \text{. . . [2.7]}$$

Young's modulus for the steel (3×10^7 psi)and the moment of inertia of the beam sections were substituted in Equation 2.7 to calculate the bending moment. A cross-section of a soldier beam is shown in Figure 12. Soldier beam properties are presented in Table 4.

TABLE 4
Section Properties of Drilled and Driven Soldier Beams

CATEGORY	DRILLED BEAMS						DRIVEN BEAMS	
	Above Subgrade		Below Subgrade					
Beam No.	9 & 10	13 & 14	10	14	9	13	7 & 8	15 & 16
Concrete Used	Lean-mix Backfill		Lean-mix Backfill		Structural Concrete		n/a	n/a
Designation	W 6×25 L 3×3×5/16	HP 10×57 L 3×3×1/4	W 6×25 L 3×3×5/16	HP 10×57 L 3×3×1/4	W 6×25 L 3×3×5/16	HP 10×57 L 3×3×1/4	W 6×25 L 3×3×5/16	HP 10×57 L 3×3×1/4
b (in)	6.0	10.0	6.0	10.0	6.0	10.0	6.0	10.0
d (in)	6.38	9.9	6.38	9.9	6.38	9.9	6.38	9.9
t (in)	0.45	0.6	0.45	0.6	0.45	0.6	0.45	0.6
A_s (in^2)	10.9	19.68	10.9	19.68	10.9	19.68	10.9	19.68
h (in)	18.0	24.0	18.0	24.0	18.0	24.0	n/a	n/a
c_1 (in)	3.94	5.85	3.565	5.325	3.565	5.325	3.565	5.325
c_2 (in)	3.19	4.8	3.565	5.325	3.565	5.325	3.565	5.325
c (in)	7.13	10.65	7.13	10.65	7.13	10.65	7.13	10.65
$n = E_c/E_s$	0.0177	0.0177	0.1312	0.1312	0.1312	0.1312	n/a	n/a
$I(x\text{-}x)$ (in^4)	164.47	470.6	200.05	606.29	733.35	2198.55	132.94	417.8
A_c (in^2)	171.59	321.33	238.13	426.59	238.13	426.59	n/a	n/a

n = the modulus ratio = Ec/Es
E_s = Young's modulus of steel
E_c = Young's modulus of concrete
A_s = the sum of the soldier beam and angle areas
$I(x\text{-}x)$ = moment of inertia of the composite section about x-x line
A_c = the area of concrete

Drilled-in beams were placed in drilled shafts filled with lean-mix fill. Below the bottom of the excavation, Soldier Beams 9 and 13 were backfilled with Class A structural concrete. The lean-mix fill on the front of the drilled beams was removed during excavation. If the concrete or fill did not crack and the bond between the steel beam and the concrete was strong enough, then the beam would act as a composite section. The bending moments and the axial loads in the drilled-in soldier beams also were computed assuming that the beams behaved as a composite beam. Cross-sections of a composite, drilled in, beam above and below the excavation level are shown in Figure 16.

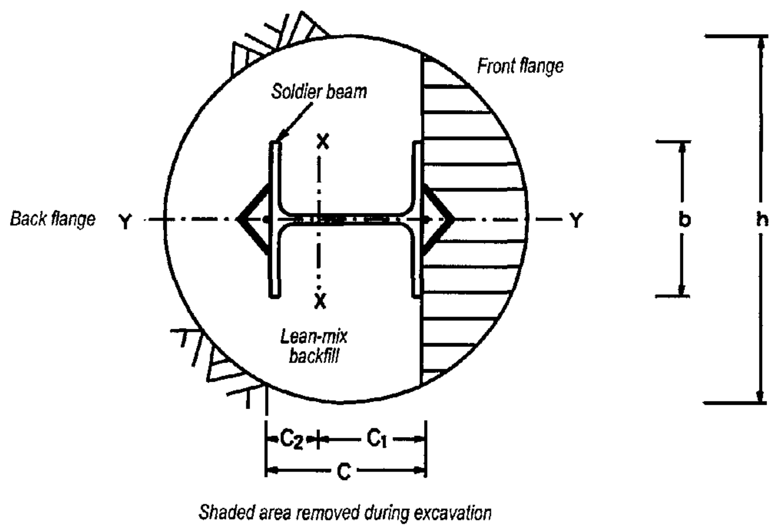

a) Above final excavation

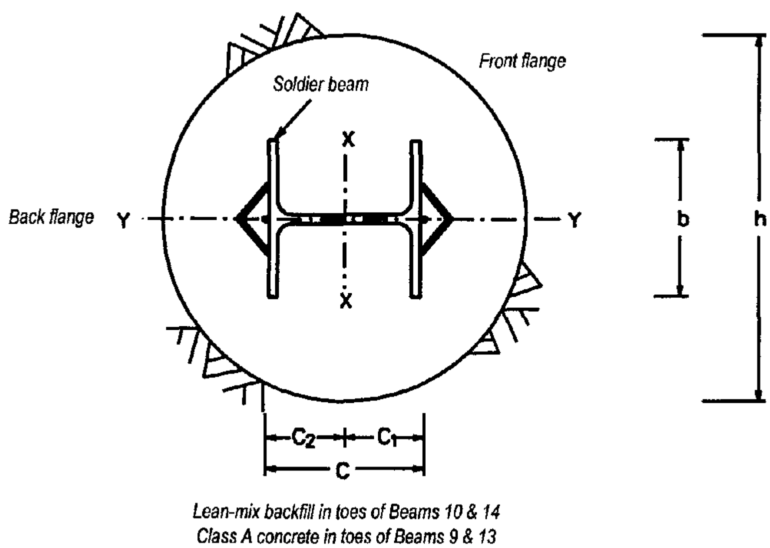

b) Below final excavation

FIGURE 16
Cross-section of Drilled-in Soldier Beam

Each composite beam was transformed into an equivalent steel beam. In the transformed section, the steel beam remained unchanged and the width of the concrete portion was reduced by the ratio of Young's moduli, concrete to steel. Young's modulus for concrete was estimated using the following equation:

$$E_c = 57000 \sqrt{f'_c}\ (psi) \qquad \ldots [2.8]$$

where f'_c is the 28-day compressive strength. The average 28-day compressive strength was 87 psi for the lean-mix fill and 4770 psi for the structural concrete. Using Equation 2.8, Young's moduli was computed to be 5.31×10^5 psi for the lean-mix fill and 3.94×10^6 psi for the structural concrete. Table 4 includes the section properties for the composite soldier beams.

Bending moments assuming composite behavior for the drilled-in beams were calculated using Young's modulus for steel and the section properties for the composite beams. At 25 ft, the bottom of the excavation, section properties for the beam above subgrade were used in the bending moment calculation.

2.3.1.2 Calculation of Axial Load

The axial stress in the beams was obtained from the stress-strain relationship

$$\sigma = \frac{P}{A} = E\ \varepsilon_{axial} \qquad \ldots [2.9]$$

where

P = axial force in the beam section
A = cross-section area of the beam
ε_{axial} = axial strain obtained in Equation 2.4

The equation for the axial forces in the beam can be written as

$$P = A\ E\ \varepsilon_{axial} \qquad \ldots [2.10]$$

For the drilled-in soldier beams, the axial forces also were computed assuming that they behaved as a composite beam. At 25 ft, section properties for the beam above subgrade were used in the axial force calculation. If the beams behaved as a composite section, then Equation 2.10 is rewritten as

$$P = (A_s E_s + A_c E_c)\ \varepsilon_{axial} \qquad \ldots [2.11]$$

where

A_s = area of steel beam section
E_s = Young's modulus of steel
A_c = area of concrete section
E_c = Young's modulus of concrete

Section 2.5.2 presents the results of the study to decide if the drilled-in soldier beams behaved as a composite section.

2.3.1.3 Data Reduction for Damaged Gauges

Some strain gauges installed on the soldier beams ceased to function because of damage during installation, fabrication of the wale connection, or other causes. The bending strains at a damaged gauge were approximated by estimating the axial strain at that location and computing the bending strain using either Equation 2.12 or 2.13. Equation 2.12 was used if the front flange gauge was damaged and Equation 2.13 was used if the back flange gauge did not function.

$$\varepsilon_{bb} = \varepsilon_b - \bar{\varepsilon}_{axial} \qquad \ldots [2.12]$$

$$\varepsilon_{ff} = \varepsilon_f - \bar{\varepsilon}_{axial} \qquad \ldots [2.13]$$

where ε_{bb} or ε_{ff} is the unknown bending strain on the back or front of the beam and ε_b or ε_f is the measured strain of the respective sides of the beam. The bending moment was calculated using either Equation 2.7 or 2.14

$$M = \frac{EI}{C_2} \varepsilon_{ff} \qquad \ldots [2.14]$$

2.3.2 Inclinometer Data

The horizontal deflections perpendicular to the wall face were obtained from the measurements made in the inclinometer casings. G-Tilt Inclinometer Data Reduction Computer Program (Mitre Software Corporation, 1989) was used to reduce the data. The deflection of the inclinometer casing at a given level was obtained by accumulating the calculated deviation of that level from the bottom of the casing. Deflection calculations assumed that the bottom of the inclinometer casing was fixed.

2.3.3 Load Cell Data

Ground anchor loads were determined from the vibrating wire load cell measurements. The sum of the six strain gauge readings in each load cell was subtracted from the initial value. Then the difference was converted into the ground anchor force by multiplying the difference by a gauge factor provided by the manufacturer.

2.3.4 Embedment Strain Gauge Data

Strains in the concrete or backfill surrounding the toes of the drilled-in beams were measured with embedment strain gauges. The strains were analyzed and compared with the strains in the beams at the same level to investigate whether or not the beams behaved as a composite. Embedment strain gauges were positioned as shown in Figure 14. The concrete or fill surrounding the toe of the piles was not excavated. Therefore, the neutral axis of the composite section was at the center of the beam. Section 3.5.2 discusses the analysis of the embedment strain gauges and the composite behavior of the soldier beams.

2.3.5 Optical Surveying Data

An optical level survey of the ground surface behind the wall and the tops of the soldier beams was conducted. Upon reducing the survey data, it became apparent that the original bench mark had been disturbed. The ground and pile settlements presented in the report were computed assuming the settlement points 50 ft from the wall were no a ffected by construction activities.

2.4 OBSERVED PERFORMANCE

The overall behavior of the wall is described in this section. Specific aspects of behavior are discussed in Section 2.5. Table 5 summarizes the construction activities affecting the wall. The zero readings for the instrumentation were taken on Day One, December 3, 1990. The last readings were taken on June 28, 1992, Day 573.

TABLE 5
Wall Construction Activities

STAGE NO.	ACTIVITY	DATE	DAY
00	Zero readings	12/03/90	1
01	4-ft Excavation	02/22/91	82
02	8-ft Excavation	02/26/91	86
03	Install anchors on SB 7-10	03/04/91	92
04	1. Test and stress anchors on SB 7-10 2. Excavate to 10-ft at SB 13-16	03/07/91 & 03/08/91	95 96
05	Install anchors on SB 13-16	03/08/91	96
06	Test and stress anchors on SB 13-16	03/12/91 & 03/13/91	100 & 101
07	14-ft Excavation	03/18/91	106
08	17-ft Excavation	03/20/91	108
09	Install 2nd row of anchors on SB 7-10	03/22/91	110
10	Test and stress anchors on SB 7-10	03/26/91	114
11	21-ft Excavation	03/28/91	116
12	25-ft Excavation	04/03/91 & 04/04/91	121 & 122
13	1st long-term reading	04/18/91	130
14	2nd long-term reading	05/15/91	163
15	3rd long-term reading	06/27/91	206
16	Reduce load in Anchors 4 & 9	07/17/91	226
17	2nd Reading after reducing load	11/27/91	360
18	3rd reading after reducing load	06/28/92	573

2.4.1 One-tier Wall

The one-tier portion of the wall had a drilled-in beam section and a driven beam section. Soldier Beams 13 and 14 were the instrumented beams in the drilled-in section. Beam 13 had structural concrete surrounding the toe, and Beam 14 had lean-mix fill surrounding its toe. Soldier Beams 15 and 16 were the instrumented beams in the driven section. The locations of these beams are shown in Figure 8.

Appendix A contains figures showing the bending moments, axial loads, inclinometer profiles and settlement profile for Soldier Beams 13 through 16 at different stages of construction. The axial loads and bending moments for the drilled-in beams were computed assuming the load was carried by the steel section. The drilled-in beams did not behave as a composite section. (Composite behavior of the drilled-in beams is discussed in Section 2.5.2.)

Figure 17 shows the ground anchor loads as a function of time. The average ground anchor lock-off load was 67.7 kips, approximately 75 percent of the 90-kip design load. The planned lock-off load was 67.5 kips. The average load in the ground anchors supporting Beams 13 to 16 was 72.5 kips upon completion of construction, an increase of 7.2 percent from the lock-off load. During the 84-day observation period, the average anchor load increased to 74.1 kips, with a maximum load of 80.9 kips. The average anchor load at the end of the observation period was 82 percent of the design load.

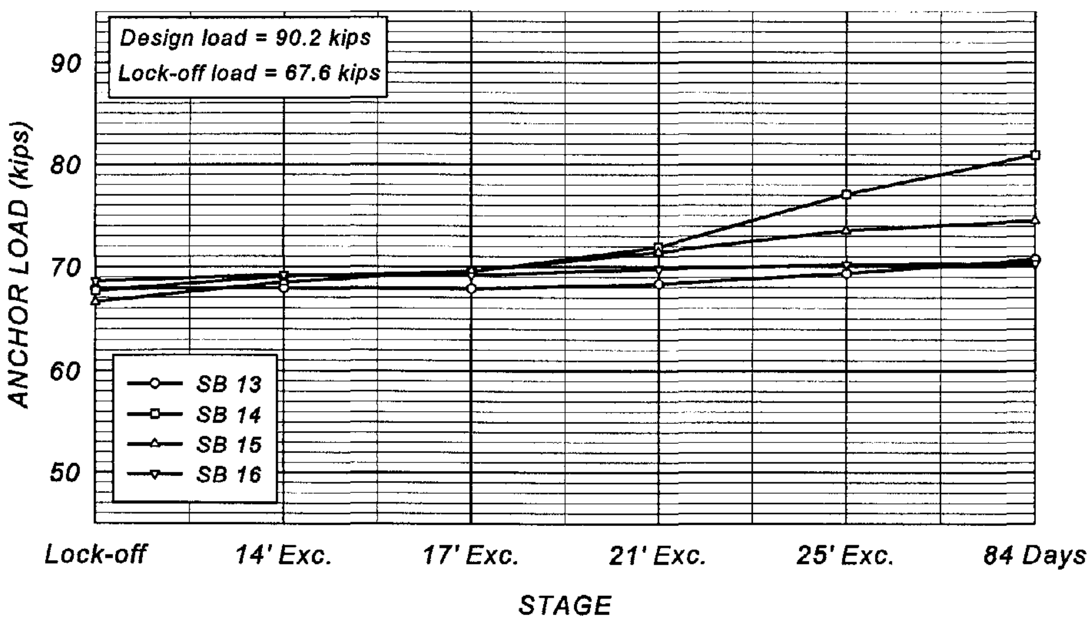

FIGURE 17
Ground Anchor Loads with Respect to Excavation Depth or Time for Soldier Beams 13 to 16

Table 6 presents some significant observations regarding the behavior of the one-tier wall. Maximum bending moments were the cantilevered moments at the anchors. The design moment at this location was 110.8 kip-ft. Upon completion of construction the average moment was 113.1 kip-ft, and at the end of the observation period the average bending moment was 120.1 kip-ft. Soldier beam bending moments at the anchors depended upon the magnitude of the ground anchor test load or lock-off load rather than the earth pressures.

The maximum design bending moment in the span below the ground anchor was 97.1 kip-ft. Average measured moments at this location were 41.7 kip-ft upon completion of the wall and 48.2 kip-ft at the end of the observation period. Bending moment between the anchor and the bottom of the excavation depended upon the earth pressure.

The design procedure assumed a hinge at subgrade. Small moments were observed at subgrade and in the toe, confirming the use of a subgrade hinge when computing bending moments. Bending moments in the toe of the drilled-in soldier beams were less than the moments in the driven beams. This difference may be the result of partial composite action between the steel beams and the concrete or lean-mix backfill. Unreasonably high bending moments were calculated when composite section properties were used.

The maximum axial loads in the soldier beams were almost twice the vertical components of the ground anchor forces and much larger than expected. The average maximum axial load was 65.4 kips upon completion of the wall while the average vertical component of the ground anchor load was 36.3 kips. Eighty-four days after completion of the wall the average, maximum axial load was 71.0 kips, an increase of 8.6 percent. After considerable investigation, it was determined that the large axial loads were the result of compression strains caused by the welding of 0.5-in studs to the exposed flange of each soldier beam. The studs were used to attach the wood lagging to the soldier beams. Section 2.5.1 discusses the compression strains in detail and Section 2.5.3 discusses the axial load applied to the soldier beams.

Lateral movements of the beams and settlement profiles are shown in the figures in Appendix A and selected readings are presented in Table 6. Average settlement was 0.63 in for the drilled-in beams, and 0.44 in for the driven beams. All four beams settled sufficiently to fully mobilize skin friction. Beam 13 continued to settle during the monitoring period. End bearing resistance of Beam 13 was fully mobilized. Beams 14 to 16 settled enough to mobilize a significant portion their end bearing resistance. The toe of Soldier Beam 13 was backfilled with structural concrete. Backfilling the toe with structural concrete did not improve the axial load-carrying capacity of Beam 13. The horizontal movement of the cantilever and the ground surface settlements are similar to those reported by Peck (1969), Goldberg, et al. (1976), and Clough and O'Rourke (1990).

TABLE 6
Summary of One-tier Wall Behavior

MOMENTS (kip-ft)	SOLDIER BEAM 13 (DRILLED-IN)		INCLINOMETER E5		SOLDIER BEAM 14 (DRILLED-IN)		SOLDIER BEAM 15 (DRIVEN)		INCLINOMETER E6		SOLDIER BEAM 16 (DRIVEN)	
	Stage 12	Stage 15	Stage 12	Stage 15	Stage 12	Stage 15	Stage 12	Stage 15	Stage 12	Stage 15	Stage 12	Stage 15
Cantilever	112.36	117.48			110.46	121.58	112.36	117.27			117.06	124.19
Max. Mid Span	-34.11	-38.04			-40.80	-47.98	-46.99	-55.00			-44.97	-51.44
Subgrade	-0.60	0.14			4.52	2.88	-19.41	-20.85			-19.76	-20.79
Max. Toe	0.60	0.97			5.72	6.06	-14.57	-15.61			-13.72	-13.67
ANCHOR LOAD (kips)	69.33	70.70			77.08	80.94	73.52	74.50			70.19	70.29
AXIAL LOAD (kips)	-64.15	-70.34			-67.28	-77.43	-70.61	-73.21			-59.66	-63.05
LATERAL MOVEMENT (in)												
Top	1.13 (0.0038H)	1.39 (0.0046H)	1.22 (0.0041H)	1.39 (0.0046H)	0.81 (0.0027H)	0.96 (0.0032H)	0.71 (0.0024H)	0.76 (0.0025H)	0.74 (0.0025H)	0.98 (0.0033H)	0.72 (0.0024H)	0.83 (0.0028H)
Anchor	0.48 (0.0016H)	0.70 (0.0023H)	0.73 (0.0024H)	0.83 (0.0028H)	0.33 (0.0011H)	0.48 (0.0016H)	0.29 (0.0010H)	0.38 (0.0013H)	0.50 (0.0017H)	0.67 (0.0022H)	0.26 (0.0009H)	0.36 (0.0012H)
Max. Mid Span	*	*	*	*	0.34 (0.0011H)	0.52 (0.0017H)	0.40 (0.0013H)	0.53 (0.0018H)	0.52 (0.0017H)	*	0.33 (0.0011H)	0.45 (0.0015H)
Subgrade	0.19 (0.0006H)	0.29 (0.0010H)	0.23 (0.0008H)	0.28 (0.0009H)	0.17 (0.0006H)	0.28 (0.0009H)	0.29 (0.0010H)	0.39 (0.0013H)	0.21 (0.0007H)	0.26 (0.0009H)	0.24 (0.0008H)	0.36 (0.0012H)
Tip	0.05 (0.0002H)	0.10 (0.0003H)	0.04 (0.0001H)	0.06 (0.0002H)	0.04 (0.0001H)	0.11 (0.0004H)	0.10 (0.0003H)	0.11 (0.0004H)	0.06 (0.0002H)	0.08 (0.0003H)	0.06 (0.0002H)	0.09 (0.0003H)
PILE SETTLEMENT (in)	0.76 (0.0025H)	0.85 (0.0028H)			0.50 (0.0017H)	0.43 (0.0014H)	0.41 (0.0014H)	0.41 (0.0014H)			0.46 (0.0015H)	0.43 (0.0014H)

* Lateral movements below the anchor level were less than the movements at the anchor location.

Figure 18 shows the inclinometer profiles for Beams 13 and 14 and Inclinometer E5, which was located between the beams and 2 ft behind the lagging. Figure 19 shows similar profiles for Beams 15 and 16 and Inclinometer E6. Above the bottom of the excavation, the inclinometers between the beams moved out about 0.2 in more than the adjacent soldier beams. This difference in movements reflects the bowing of the lagging boards between the soldier beams. Below subgrade, the lateral movements were small, and the beams and the ground moved together. Since the embedded portions of the beams did not move relative to the soil, the soldier beams could not develop significant lateral loads.

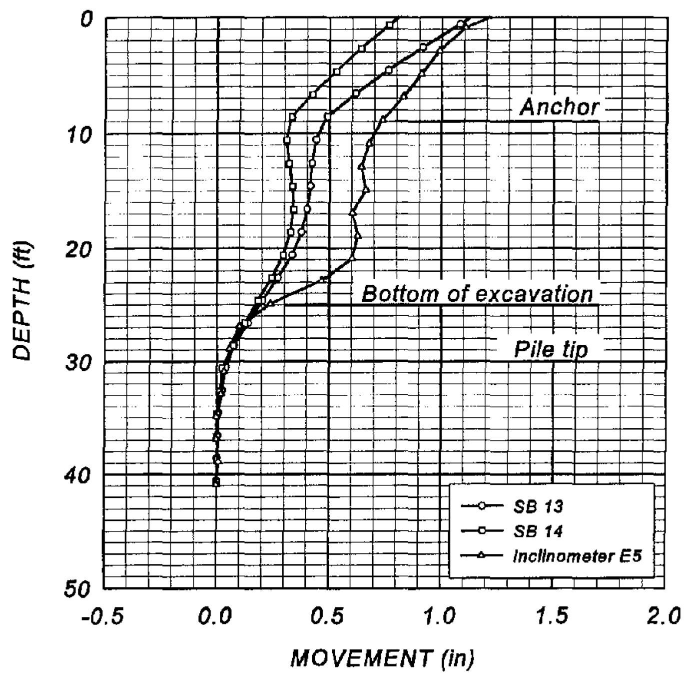

FIGURE 18
Lateral Movement of Soldier Beams 13 and 14 and Inclinometer E5; Day 206

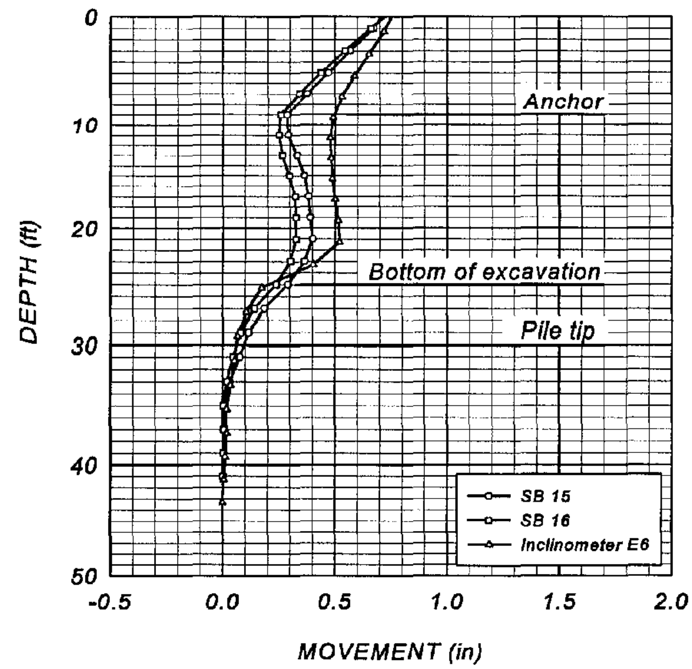

FIGURE 19
Lateral Movement of Soldier Beams 14 and 15 and Inclinometer E6; Day 206

2.4.2 Two-tier Wall

The two-tier portion of the wall had a driven beam section and a drilled-in beam section. Soldier Beams 7 and 8 were the instrumented beams in the driven section, and Beams 9 and 10 were the instrumented beams in the drilled-in beam section. Beam 9 had structural concrete surrounding the toe and Beam 10 had lean-mix fill surrounding its toe. The locations of these beams are shown in Figure 8.

Appendix A contains figures showing the bending moments, axial loads, inclinometer profiles, and settlement profile for Soldier Beams 7 to 10 at different stages of construction. Similar to the one-tier wall section, the axial loads and bending moments for the drilled-in beams were computed assuming all the load was carried by the steel section. (Composite behavior is discussed in Section 2.5.2.)

Figure 20 shows the ground anchor loads as a function of time. The average, upper-tier ground anchor lock-off load was 82.4 kips, approximately 75 percent of the 106.5-kip design load. The average, lower-tier anchor, lock-off load was 71.5 kips, approximately 75 percent of the 96-kip design load. Planned lock-off loads were 82 kips for the upper anchors, and 72 kips for the lower anchors. The average load in the upper anchors supporting Beams 7 to 10 was 90.9 kips upon completion of construction, an increase of 10.3 percent from the lock-off load. Upon completion of the wall, the average load in the lower anchors was 71.8 kips, an increase of 0.4 percent from the lock-off load. At the conclusion of the 84-day observation period, the average upper-row anchor load was 90.6 kips, 85.1 percent of the design load. The average anchor load in the lower row of ground anchors was 69.0 kips, 72 percent of the design load, at the end of the observation period. The maximum upper row anchor load was 99.4 kips, and the maximum lower row anchor load was 79.1 kips. These maximum loads were less than the design loads. Figure 20 shows that the lower ground anchor supporting Soldier Beams 7 and 8 lost load and the anchors supporting Soldier Beams 9 and 10 gained load. These changes resulted from the differences in the settlement of the beams. Beams 7 and 8 continued to settle during the observation period, while Beam 9 settled very little during the observation period. As the beams settled, the ground anchor load decreased as the anchor tendon shortened elastically.

Table 7 presents some significant observations regarding the behavior of the two-tier wall. The maximum bending moments were the cantilevered moments at the upper anchors. The design moment at this location was 35.8 kip-ft. Upon completion of construction, the average cantilever bending moment was 44.9 kip-ft, and at the end of the observation period the average moment was 45.2 kip-ft. Measured bending moments at the upper anchor location were about 26 percent larger than the design bending moment. This difference does not mean that the earth pressure diagram was too small. In fact the bending moment at the ground anchor locations is a response to the applied anchor test load or lock-off load. For the two-tier wall, the difference between the design and the measured bending moment at the upper anchor resulted from the use of a flexible soldier beam, the shape of the design apparent earth pressure diagram, and the moment "locked" into the beam during testing (Sections 2.5.7 and 2.5.9).

The maximum design bending moment in the span below the upper ground anchor was 45.8 kip-ft. Average measured moments at this location were 10.6 kip-ft upon completion of the wall and 8.5 kip-ft at the end of the observation period. The design procedure assumes hinges at the lower row of ground anchors and at subgrade. At these locations the design bending moment must be zero. When construction was completed, the average measured bending moment at the second row of ground anchors was 28.1 kip-ft. At the end of the 84-day observation period, the average moment at the second row of anchors had dropped slightly to 26.3 kip-ft. The design bending moment in the span below the second row of anchors was 40.8 kip-ft. When the excavation reached 25 ft, the maximum depth, the average measured bending moment was 19.4 kip-ft. At the end of the observation period the average bending moment had increased to 24.1 kip-ft. Small bending moments were observed at subgrade and in the toe, confirming the assumption of a hinge at subgrade. Similar to the behavior of the one-tier wall, bending moments in the toe of the drilled-in soldier beams were less than the moments in the driven beams. This difference may be the result of partial composite action between the steel beams and the concrete or lean-mix backfill. Full composite section properties would have given too high a bending moment for the measured strains (see Section 2.5.2).

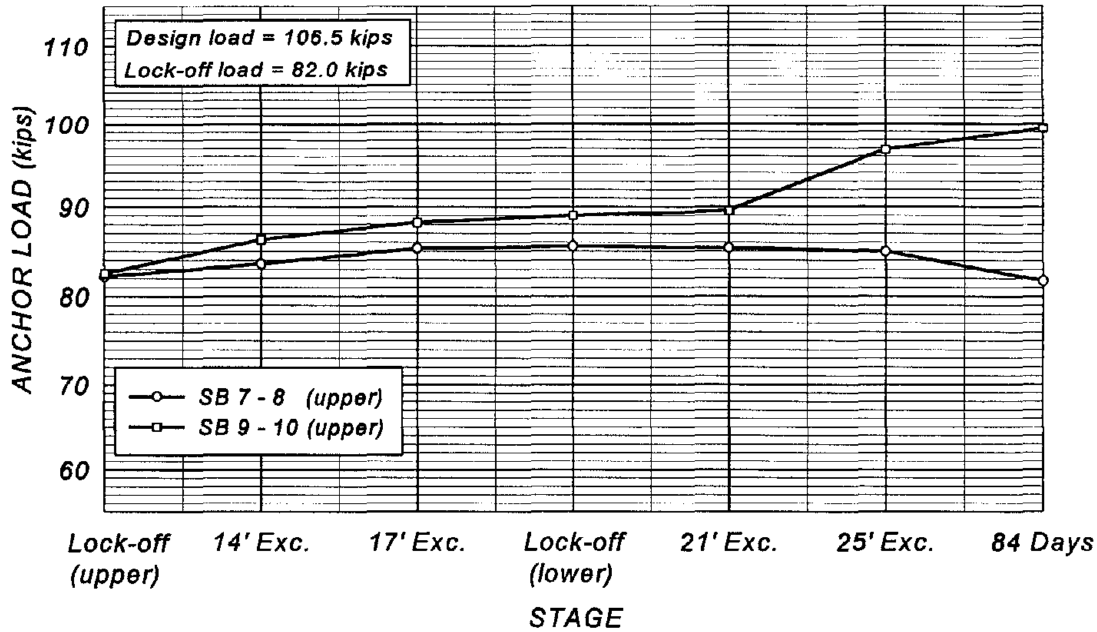

a) Upper ground anchor load

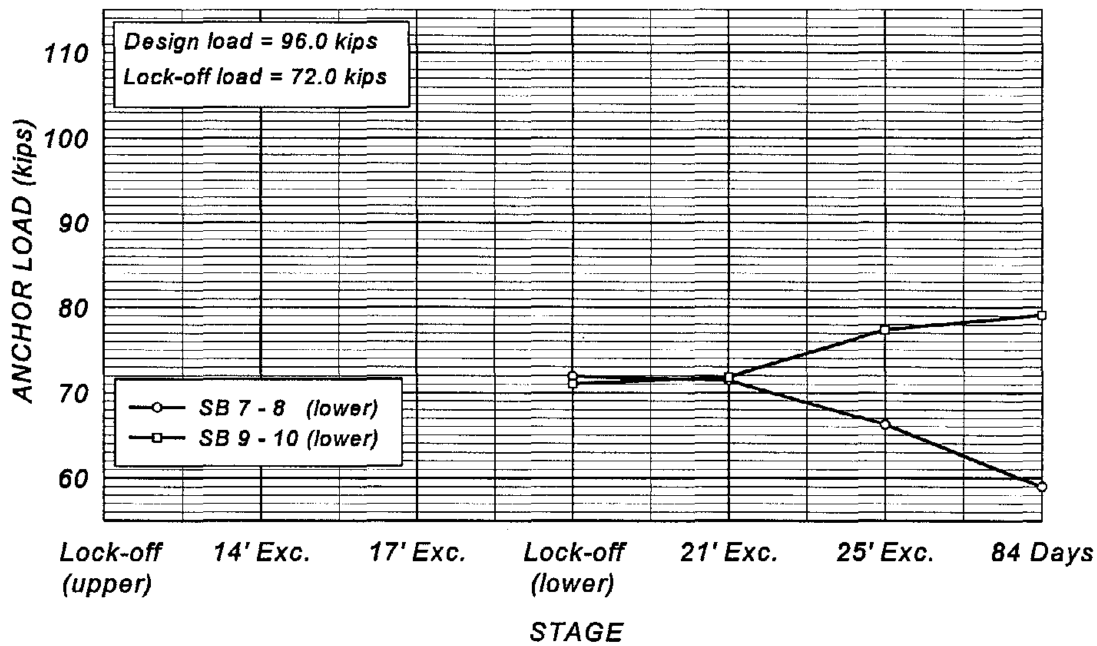

b) Lower ground anchor load

FIGURE 20
Ground Anchor Loads with Respect to Excavation Depth or Time for Soldier Beams 7 to 10

TABLE 7
Summary of Two-tier Wall Behavior

MOMENTS (kip-ft)	INCLINOMETER E1		SOLDIER BEAM 7 (DRIVEN)		SOLDIER BEAM 8 (DRIVEN)		SOLDIER BEAM 9 (DRILLED-IN)		SOLDIER BEAM 10 (DRILLED-IN)		INCLINOMETER E2	
	Stage 12	Stage 15	Stage 12	Stage 15	Stage 12	Stage 15	Stage 12	Stage 15	Stage 12	Stage 15	Stage 12	Stage 15
Cantilever			54.33	55.13	45.87	49.06	39.82	34.05	39.66	42.76		
Span			-9.29	-6.91	-6.02	-2.83	-16.01	-15.34	-10.94	-8.81		
2nd Anchor			24.24	17.53	29.74	25.13	31.65	34.10	26.59	28.49		
Span			-24.24	-26.18	-22.71	-24.85	-13.92	(1)	-16.82	-21.33		
Subgrade			-11.50	-12.04	-10.20	-12.24	3.57	2.38	-4.13	-7.72		
Max. Toe			-6.13	-5.96	-5.88	-6.81	1.58	1.93	-2.04	-4.55		
UPPER ANCHOR LOAD (kips)			84.99/2	81.74/2	84.99/2	81.74/2	96.80/2	99.45/2	96.80/2	99.45/2		
LOWER ANCHOR LOAD (kips)			66.25/2	58.97/2	66.25/2	58.97/2	77.35/2	79.10/2	77.35/2	79.10/2		
AXIAL LOAD (kips)			-39.52	-43.98	-37.93	-37.45	-78.33	-95.94	-46.38	-52.92		
LATERAL MOVEMENT (in)												
Top	1.15 (0.0038H)	1.85 (0.0062H)	(2)	(2)	1.35 (0.0045H)	1.80 (0.0060H)	0.95 (0.0032H)	1.22 (0.0041H)	1.18 (0.0039H)	1.57 (0.0052H)	1.51 (0.0050H)	2.13 (0.0071H)
Anchor	0.87 (0.0029H)	1.36 (0.0045H)	(2)	(2)	0.75 (0.0025H)	1.10 (0.0037H)	0.55 (0.0018H)	0.80 (0.0027H)	0.72 (0.0024H)	1.05 (0.0035H)	1.01 (0.0034H)	1.45 (0.0048H)
2nd Anchor	0.82 (0.0027H)	1.34 (0.0045H)	(2)	(2)	0.46 (0.0015H)	0.75 (0.0025H)	0.29 (0.0010H)	0.51 (0.0017H)	0.44 (0.0015H)	0.72 (0.0024H)	0.81 (0.0027H)	1.26 (0.0042H)
Subgrade	0.27 (0.0009H)	0.37 (0.0012H)	(2)	(2)	0.33 (0.0011H)	0.53 (0.0017H)	0.18 (0.0006H)	0.33 (0.0011H)	0.29 (0.0010H)	0.50 (0.0017H)	0.25 (0.0008H)	0.41 (0.0014H)
Tip	0.14 (0.0005H)	0.19 (0.0005H)	(2)	(2)	0.14 (0.0005H)	0.21 (0.0007H)	0.07 (0.0002H)	0.14 (0.0005H)	0.10 (0.0003H)	0.21 (0.0007H)	0.08 (0.0003H)	0.15 (0.0005H)
PILE SETTLEMENT (in)			1.18 (0.0039H)	1.51 (0.0050H)	0.88 (0.0029H)	1.27 (0.0042H)	0.41 (0.0014H)	0.45 (0.0015H)	0.91 (0.0030H)	1.09 (0.0036H)		

(1) Strain gauges did not function.

(2) Inclinometer casing for Beam 7 became blocked near the excavation level and could not be read after Stage 10.

The average maximum measured bending moment below the upper row of anchors was 28.1 kip-ft with a maximum value of 34.1 kip-ft at the lower anchor on Beam 9. This moment was 61 percent of the maximum design moment below the upper ground anchor. These measurements confirm the use of moment reduction factors recommended by Peck, et al. (1974). The design procedures did not predict the location of the maximum bending moments below the upper support.

The average of the maximum axial loads shown in Table 7 for Soldier Beams 7 and 8 was 38.7 kips at the conclusion of construction. Soldier Beams 7 and 8 were supported by two anchors and these anchors applied a vertical force of 37.8 kips to each beam. At the end of the 84-day observation period, the average maximum axial load in Beams 7 and 8 was 40.7 kips, and the calculated vertical component of the ground anchor force was 35.2 kips per beam. The axial loads carried by Beams 9 and 10 are discussed separately since they were significantly different from each other. The maximum axial load in Soldier Beam 9, upon completion of the wall, was 78.3 kips, and it increased to 95.9 kips at the end of the 84-day observation period. This load was much larger than the axial load in Beams 7, 8, and 10. When the excavation was completed, the maximum axial load in Beam 10 was 46.4 kips, and it increased to 52.9 kips at the conclusion of the observation period. The average of the maximum axial loads in Soldier Beams 9 and 10 at the conclusion of construction was 62.4 kips and the average vertical component of the ground anchor force in each beam was 43.5 kips. At the end of the observation period, the average vertical component of the ground anchor force in Beams 9 and 10 was 44.6 kips per beam. At the same time, the average maximum axial load in Beams 9 and 10 was 74.4 kips, almost 30 kips more than the vertical anchor force. This large difference was the result of the stain gauge errors (see Section 2.5.1) and the stiff axial behavior of Beams 9 and 10. Beam 9, in particular, settled less than the adjacent piles and as a result carried more downdrag load (see Section 2.5.3.1) than the other beams.

Lateral movements of the two-tier beams and settlement profiles are shown in Appendix A and selected readings are presented in Table 7. When construction was completed, driven Beam 7 had settled 1.18 in, driven Beam 8 had settled 0.88 in, drilled-in Beam 9 had settled 0.41 in, and drilled-in Beam 10 had settled 0.91 in. During the 84-day observation period, the vertical movement of Beams 7, 8, 9, and 10 increased to 1.51 in, 1.27 in, 0.45 in, and 1.09 in, respectively. Soldier Beams 7, 8 and 10 started to settle significantly when the excavation reached the 21-ft depth, 4 ft above the final excavation level. Soldier Beams 7, 8, and 10 continued to settle during the observation period, indicating that skin friction and end bearing were fully mobilized. Beam 9 did not settle during the observation period, indicating that it had additional end bearing resistance. Beam 9 settled sufficiently to fully mobilize skin friction. Beams 7, 8, and 10 settled more than twice as much as Beam 9. Drilled-in Beam 9 had structural concrete in the toe and the smallest settlements in the two-tier wall section. This is opposite from the behavior of the one-tier wall where Beam 13, structural concrete in the toe, settled the most and had the largest lateral movements. Horizontal movements and the ground surface settlements are at the upper range of the movements reported by Goldberg, et al. (1976), and Clough and O'Rourke (1990).

Figure 21 shows the inclinometer profiles for Soldier Beam 8 and Inclinometer E1, which was between Soldier Beams 6 and 7 and 2 ft behind the lagging. Figure 22 shows similar profiles for Beams 9 and 10 and Inclinometer E2. Inclinometer E2 was between Soldier Beams 10 and 11. Above the bottom of the excavation, Inclinometers E1 and E2 moved more than the adjacent beams. The large lateral movements measured in Inclinometers E1 and E2 below 12 ft resulted from local loss of ground during a heavy rain storm. Below subgrade, the lateral movements were small. Beams 8 and 10 moved about 0.1 in out with respect to Inclinometers E1 and E2. Beam 9 moved about the same amount as Inclinometer E2. Since Beams 8 and 10 settled more than twice the settlement of Beam 9, it is possible that the relative lateral movement between the inclinometers and Soldier Beams 8 and 10 is the result of settlement. The relative movement between the beams and the ground was small, suggesting that the mobilized lateral toe resistance was small.

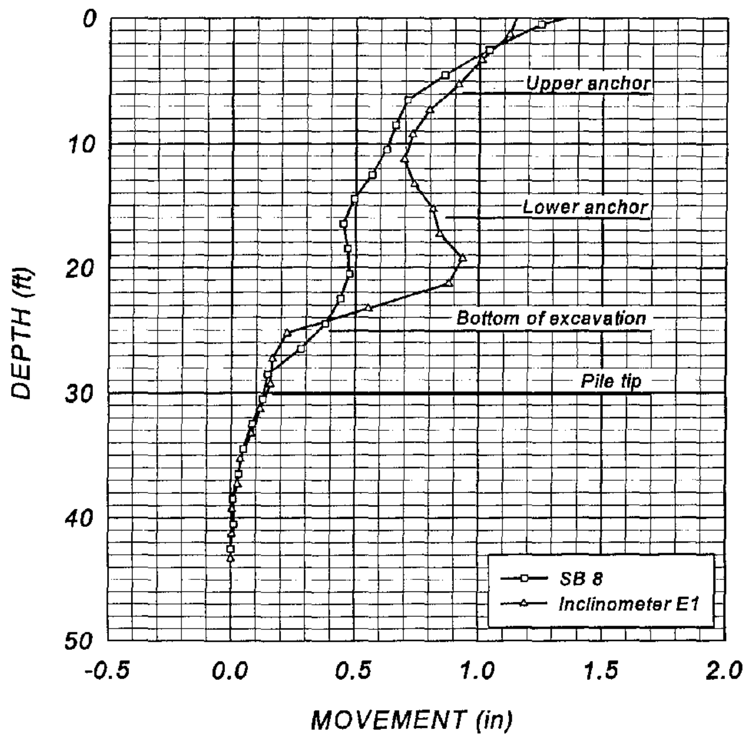

FIGURE 21
Lateral Movement of Soldier Beam 8
and Inclinometer E1; Day 206

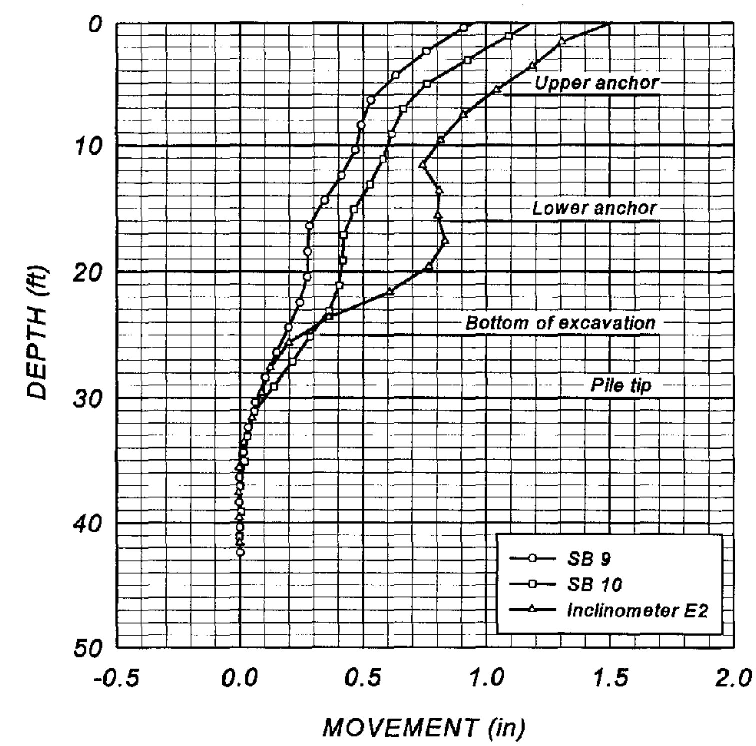

FIGURE 22
Lateral Movement of Soldier Beams 9 and 10 and Inclinometer E2; Day 206

2.5 SPECIFIC ASPECTS OF WALL PERFORMANCE

2.5.1 Large Axial Loads

Axial compression loads computed for the exposed portions of the soldier beams at each stage of construction were unreasonably large. Large axial loads were present in the exposed portions of the soldier beams even before the ground anchors were installed. Reasonable axial loads were computed at locations 1 ft below the bottom of the excavation. Axial load plots for each soldier beam at selected construction stages are shown in Appendix A.

When the excavation advanced to the 4-ft level, the compression loads in the exposed portions of Soldier Beams 7 to 10 varied between 5.7 and 25.6 kips with an average load of 13.3 kips. At the 4-ft depth, the average compression load in the upper portions of the Beams 13 to 16 was 25.0 kips with the compression loads ranging between 12.3 and 33.0 kips. Compression loads in the exposed portions of the Beams 7 to –10 varied between 2.9 and 25.2 kips with an average load of 13.1 kips when the excavation was deepened to 8 ft. At the 8-ft depth, the average compression load above the bottom of the excavation was 25.4 kips in Soldier Beams 13 to 16. The load in Beams 13 to 16 ranged from 2.5 kips of tension to 40.1 kips compression. The axial loads were similar for both the driven and drilled beams.

Ground movements, such as downdrag, could not have caused axial loads of these magnitudes or distributions. For example, after excavating only 4 ft, the average compression loads at the 2.5-ft level were 17.4 and 28.4 kips in Beams 7 to 10 and Beams 13 to 16, respectively. If downdrag or ground movements had been responsible for these loads, then the loads should have been smaller and approximately equal for all the piles. However, the compression loads were high and approximately proportional to the cross-sectional area of the beams.

Axial loads 1 ft below the bottom of each excavation stage were reasonable. For example, Figure 23 shows the average axial loads in the driven soldier beams immediately after locking off the ground anchors. The average load in Beams 7 and 8 at the 9-ft level was 19.1 kips. At this construction stage the average vertical component of the ground anchor force equaled 20.7 kips. When the excavation was 10 ft deep, the average compression load in Beams 15 and 16 was 28.9 kips at the 11-ft level. The average vertical component of the ground anchor force on Soldier Beams 15 and 16 equaled 33.7 kips at that stage of construction. Similar behavior was observed at each stage of construction. Section 2.5.3 presents a complete analysis of the axial loads below the excavation level for each stage of construction.

Schnabel Foundation Company and Barrie Sellers (president of Geokon, the gauge supplier), carefully studied the raw strain gauge data and concluded that an external factor caused the large compressive strains. Assuming that the back flange gauges were correct, and the beam was only subjected to bending at shallow depths, the false compression strains in the front flange gauges could be calculated. Given these assumptions, the front flange bending strains must be equal in magnitude to the back flange strains and opposite in sign. In addition, the false, front flange, axial strains have to be equal to the difference between the measured strains and the calculated bending strains. Table 8 contains the results of these calculations for the driven beams when the excavation was 8 ft deep. Average, false, front flange, compression strains in Beams 7, 8, 15, and 16 were 90.3, 86.3, 76.0, and 83.1 $\mu\epsilon$, respectively. Compression loads corresponding to these strains were 14.8, 14.1, 22.4, and 24.5 kips. These loads are very close to the axial loads computed from the measured strains when the excavation was 4 and 8 ft deep. This analysis further supports the conclusion that the measured front flange compression strains were shifted.

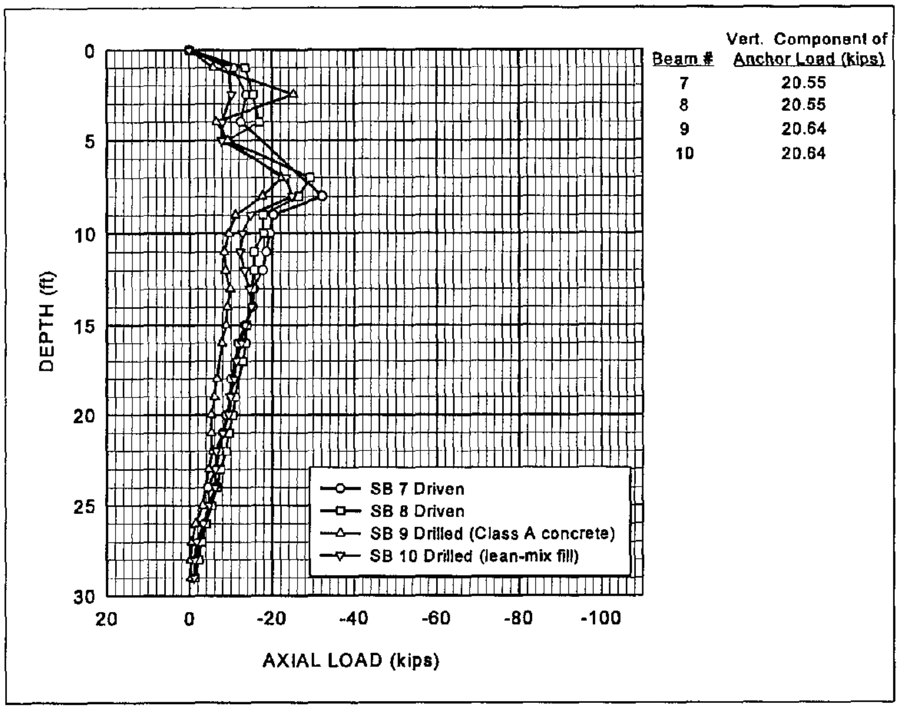

a) Beams 7 and 8

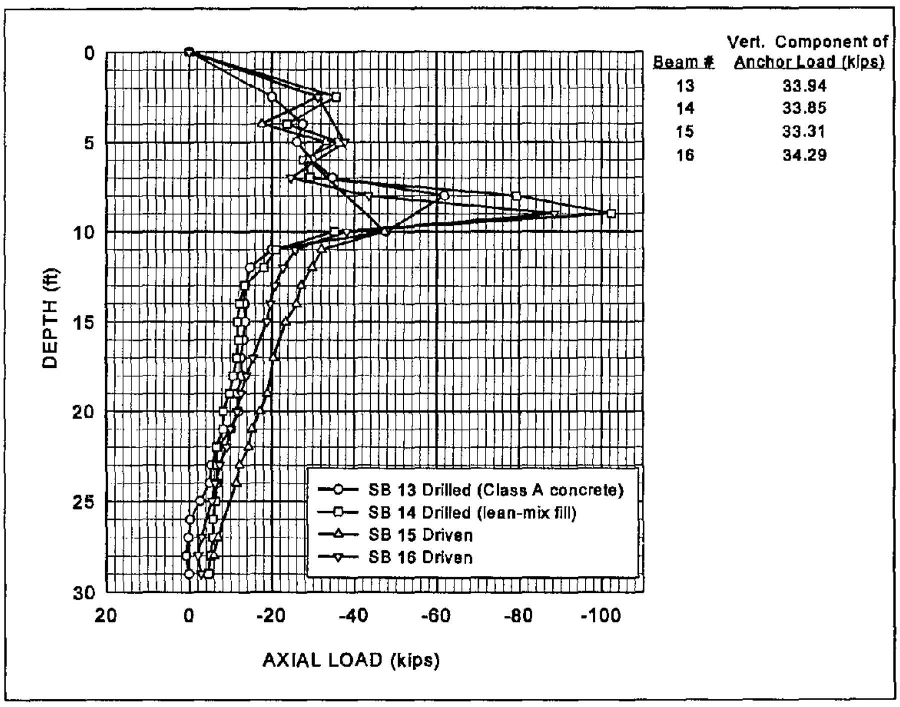

b) Beams 15 and 16

FIGURE 23
Axial Load in Driven Beams After Ground Anchors are Locked-off

TABLE 8
Calculated False Compression Loads in the Driven Soldier Beams, 8-ft Excavation[1]

SOLDIER BEAM NO.	DEPTH (ft)	MEASURED BACK FLANGE STRAINS (με)	MEASURED FRONT FLANGE STRAINS (με)	ASSUMED FRONT FLANGE BENDING STRAINS (με)	CALCULATED FRONT FLANGE COMPRESSION STRAINS (με)	CALCULATED AVERAGE COMPRESSION STRAINS (με)	CALCULATED AXIAL LOAD (kips)	AVERAGE AXIAL LOAD (kips)
7	1	-0.9	-69.1	+0.9	-70.0	-35.0	-11.4	-14.8
	2.5	8.2	-101.8	-8.2	-93.6	-46.8	-15.3	
	4	7.5	-83.3	-7.5	-75.8	-37.9	-12.4	
	5	11.6	-141.8	-11.6	-130.2	-65.1	-21.3	
	8	94.6	-177.1	-94.6	-82.5	-41.2	-13.4	
8	1	-10.0	-68.8	+10.0	-78.8	-39.4	-12.9	-14.1
	2.5	11.6	-115.2	-11.6	-103.6	-51.8	-16.9	
	4	10.1	-112.8	-10.1	-102.7	-51.4	-16.8	
	5	12.2	-104.7	-12.2	-92.5	-46.2	-15.1	
	7	60.6	-134.4	-60.6	-73.8	-36.9	-12.1	
	8	105.7	-172.3	-105.7	-66.6	-33.3	-10.9	
15	2.5	13.4	-107.5	-13.4	-94.1	-47.0	-27.8	-22.4
	4	7.5	-54.7	-7.5	-47.2	-23.6	-13.9	
	6	13.7	-100.5	-13.7	-86.8	-43.4	-25.6	
16	2.5	12.1	-108.3	-12.1	-96.2	-48.1	-28.4	-24.5
	7	16.0	-98.9	-16.0	-82.9	-41.4	-24.5	
	8	31.3	-101.6	-31.3	-70.3	-35.2	-20.8	

[1] Tensile strains (+), compression strains (-)

Temperature effects, strain gauge errors, construction damage, data acquisition and reduction errors, residual stresses, and construction operations were studied to isolate the cause of the unusual front flange compression strains. After careful evaluation, it was hypothesized that the front flange strains were caused by welding 0.5-in studs to the soldier beams. These studs were used to attach the wood lagging boards to the flange of the beams. To test this hypothesis, a short HP10×57 beam section similar to Beams 13 to 16 was fabricated. Three vibrating wire strain gauges were installed along the front and back flanges of the beam section. Then the beam was suspended in the air and 0.5-in lagging studs were welded to the front flange. Figure 24, an elevation view of the beam section, shows the location of the stain gauges and the studs. Fifteen hours after the studs were welded, the front flange gauges showed an average compressive strain of 35.7 $\mu\epsilon$. This was less than the compressive strains measured in the field, but confirmed that the welding of the studs introduced significant compressive strains in the front flange of the beams.

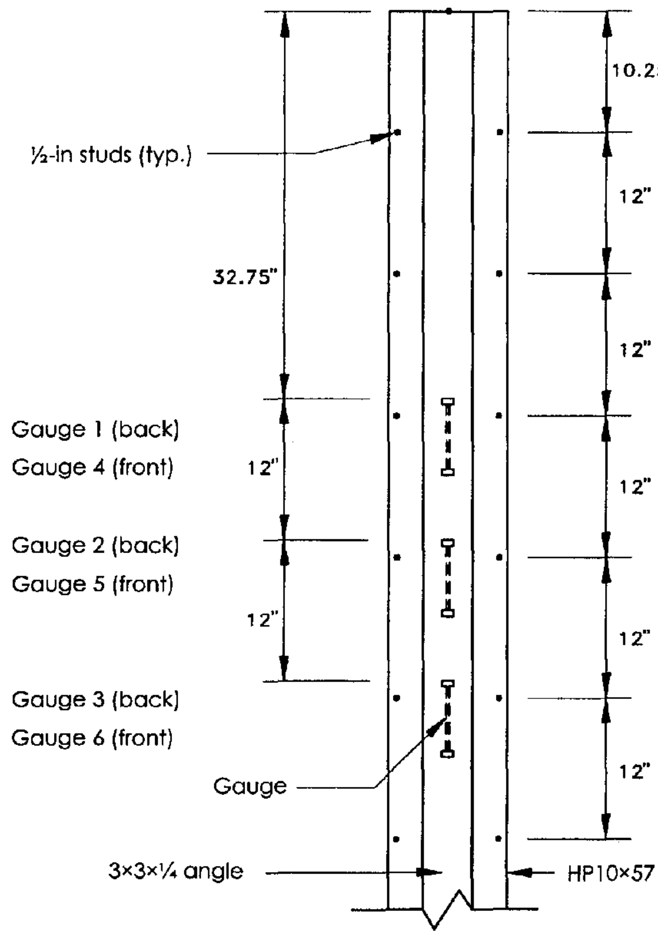

FIGURE 24
Elevation View (Front Flange) of an Instrumented HP10×57 Beam Section

To test this hypothesis further, an additional instrumented W6×25 soldier beam was installed on one of Schnabel Foundation Company's projects. The beam was similar to Soldier Beams 7 to 10 and it was driven into a dense silty sand and gravel deposit. Instead of attaching the wood lagging using welded studs, the lagging was placed behind the front flange. Figure 25 shows the axial load in the 23-ft-long soldier beam when the excavation was 11 ft deep. Two ground anchors on a common wale supported the instrumented soldier beam and two other piles. The wale was installed 6 ft from the top of the beam and the ground anchors were installed at 30 degrees from the horizontal. Load cells were used to measure the anchor forces. When the excavation reached 11 ft, the total anchor load supporting the three piles was 91.4 kips. Using CBEAMC (Dawkins, 1994), a general beam-column computer program, the vertical load applied to the instrumented soldier beam was estimated to be 19 kips. The axial load curve for the instrumented beam (Figure 25) does not show the high compression strains, and the pattern and values of axial loads are reasonable. Small tensile loads were present above the ground anchor, and compression loads approximately equal to the vertical component of the ground anchor force were measured below the anchor elevation.

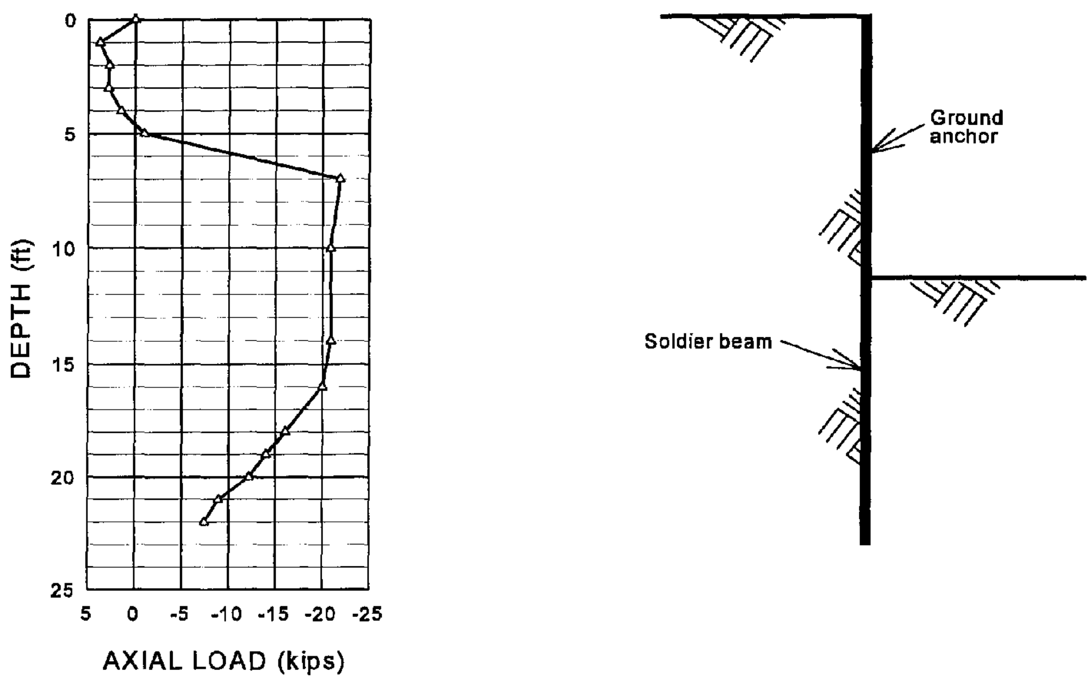

FIGURE 25
Axial Load in Driven W6×25 Soldier Beam at National Airport

Based on the above evaluation, it appears that false compression strains were present in the exposed portions of the front flanges of the instrumented beams at Texas A&M. These strains were caused by welding required to attach the lagging boards to the soldier piles. The false front flange compression strains were estimated to be 88.2 $\mu\epsilon$ in the W6×25 soldier beams, Beams 7 to 10, and 79.6 $\mu\epsilon$ in the HP10×57 soldier beams, Beams 13 to 16.

The computed axial loads and bending moments for the portions of the beams exposed during excavation were affected by the shift in the front flange compression strains. Table 9 gives the axial load and bending moment corrections associated with the shift. To correct the axial loads above the excavation levels in the figures in Appendix A and Tables 6 and 7, add the appropriate correction to the loads shown. Since the compression loads in the figures are negative, the correction will reduce the axial loads. To correct the moments above the excavation level in the figures, subtract the corrections from the moments shown. The moment correction will increase the negative moments and decrease the positive moment. Moment corrections should not be applied to moments at the ground anchor locations. Front flange strain gauge readings were not used to determine the moments at the ground anchor locations (see Section 2.3.1.3).

TABLE 9
Axial Load and Bending Moment Corrections[(1)]

SOLDIER BEAM NO.	AXIAL LOAD CORRECTION (kips)	BENDING MOMENT CORRECTION (kip-ft)
7–10	14.4	4.11
13–16	23.5	7.74

(1) Corrections apply to axial loads and bending moments above the bottom of the excavation.

2.5.2 Composite Behavior

Drilled-in soldier beam holes are backfilled with lean-mix fill over the portion of the beam that will be exposed during excavation. In practice, lean-mix fill or structural concrete is used to backfill the embedded portion of the soldier beam, the toe. The toes of Soldier Beams 9 and 13 were backfilled with structural concrete and the toes of Soldier Beams 10 and 14 were backfilled with lean-mix fill. The strains in the steel beams and the backfill were studied to determine if or where the drilled-in soldier beams behaved as a steel-backfill composite section. Behavior of beams backfilled with lean-mix fill, beams backfilled with structural concrete, and the driven beams were compared.

The concrete embedment gauges described in Section 2.2.3 were installed to measure the strains in the backfill at depths of 25, 26, 27, 28, and 29 ft. Strains in the beams and the embedment gauges and the computed bending moments and axial loads were analyzed to determine if or where each drilled-in soldier beam behaved as a composite section. Composite behavior was considered possible at locations where two of the following three criteria were satisfied:

- Lean-mix fill did not crack.
- Strains in the steel and the concrete at a given cross-section were proportional to their distance from the axis of bending.
- Bending moments and axial loads computed using composite section properties were realistic, and approximated the computed moments and axial loads for adjacent driven soldier beams.

Soldier beams cannot behave as a composite section where the lean-mix fill cracks. The lean-mix concrete used to backfill the drill holes had an average 28-day compression strength of 87 psi. Using equation 2.8, Young's Modulus for the fill was estimated to be 5.31×10^5 psi.

If the cracking stress was approximately 0.1 the compressive strength of the fill, then the cracking strain for the lean-mix fill was estimated to be 16 microstrains.

Figure 26 shows the measured strains along the back flange of each drilled-in beam before installing the ground anchors. This figure shows that the tensile strains in Soldier Beams 9 and 10 exceeded the cracking strain, 16 microstrains, down to a depth of about 16 ft, and the strains along Soldier Beams 13 and 14 exceeded the cracking strain down to a depth of about 20 ft. Figure 27 shows the measured strains along the back flanges of Soldier Beams 9 and 10 after the lower ground anchor was locked-off. At this stage of construction, the strains at the 15-, 16-, and 17-ft depths exceeded the cracking strain significantly. Based on this analysis, Soldier Beams 9 and 10 could not behave as a composite section above 17 ft, but they may behave as a composite section below that depth. Similarly, Soldier Beams 13 and 14 could not behave as a composite section above 20 ft, but they may behave as a composite section below that depth.

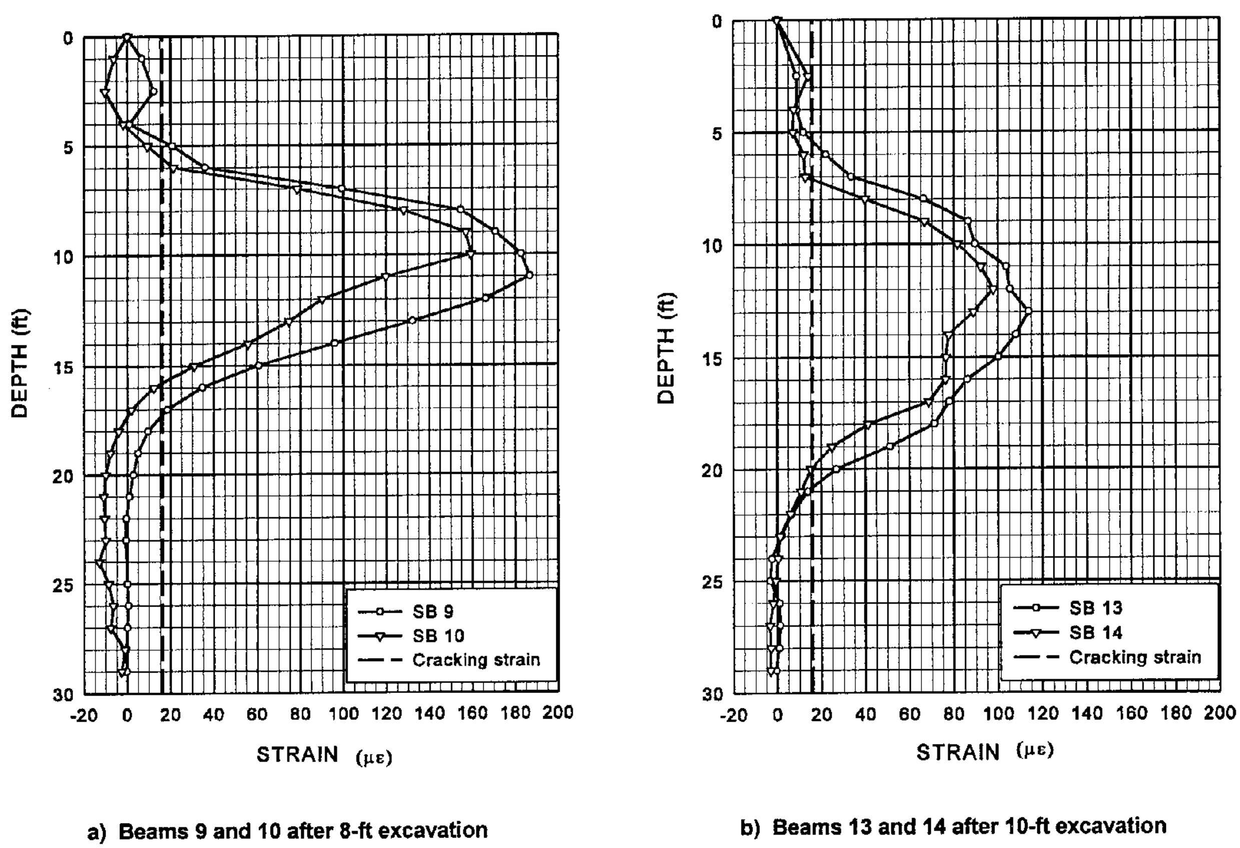

FIGURE 26
Measured Back Flange Strains in the Drilled-in Soldier Beams Before Installing Ground Anchors

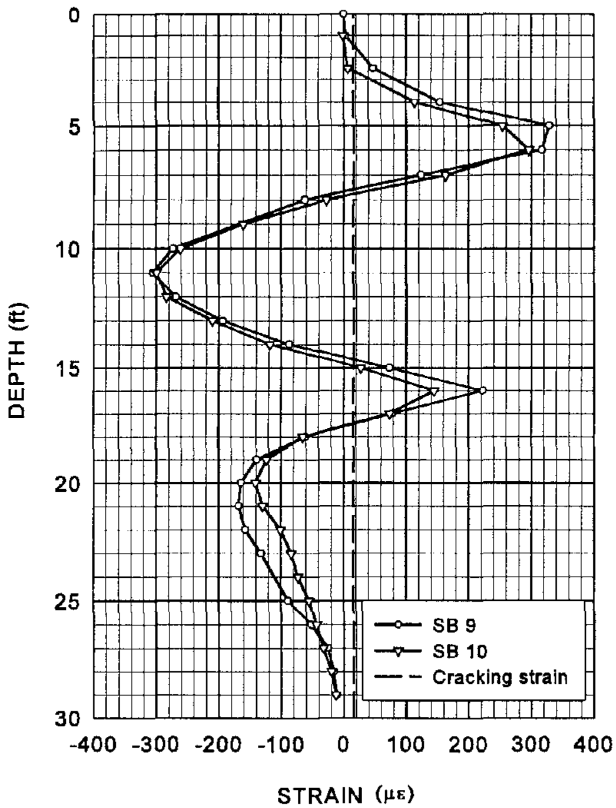

FIGURE 27
Measured Back Flange Strains of Soldier Beams 9 and 10
After Lower Ground Anchors are Locked-off

Figures 28 and 29 show the measured strains in the steel and backfill of Soldier Beams 9, 10, 13, and 14 at depths of 25 through 29 ft. For Beams 9 and 10 the strains in the steel beams are plotted at the flange strain gauge locations, ±3.375 in from the center of the beams, and the concrete strains are plotted at the embedment gauge locations, ±7.5 in from the center. Steel and backfill strains for Soldier Beams 13 and 14 are plotted ±5.375 in and ±9.5 in, respectively, from the center of the beam. Where the strains in Figures 28 and 29 are proportional to the distances from the axis of bending, the center of the beams, the soldier beams appear to behave as a composite section.

In Figure 28, the measured strains in the steel and concrete of Soldier Beam 9 were approximately proportional to their distances from the axis of bending at depths of 28 and 29 ft. Figure 28 also shows that Soldier Beam 10 did not behave as a composite section at any location along the toe. Figure 29 shows that the strains in the steel and concrete of Soldier Beam 13 were approximately proportional to their distances from the axis of bending at a depth of 27 ft and below. Beam 14 appears to behave as a composite section at a depth of 28 ft and below.

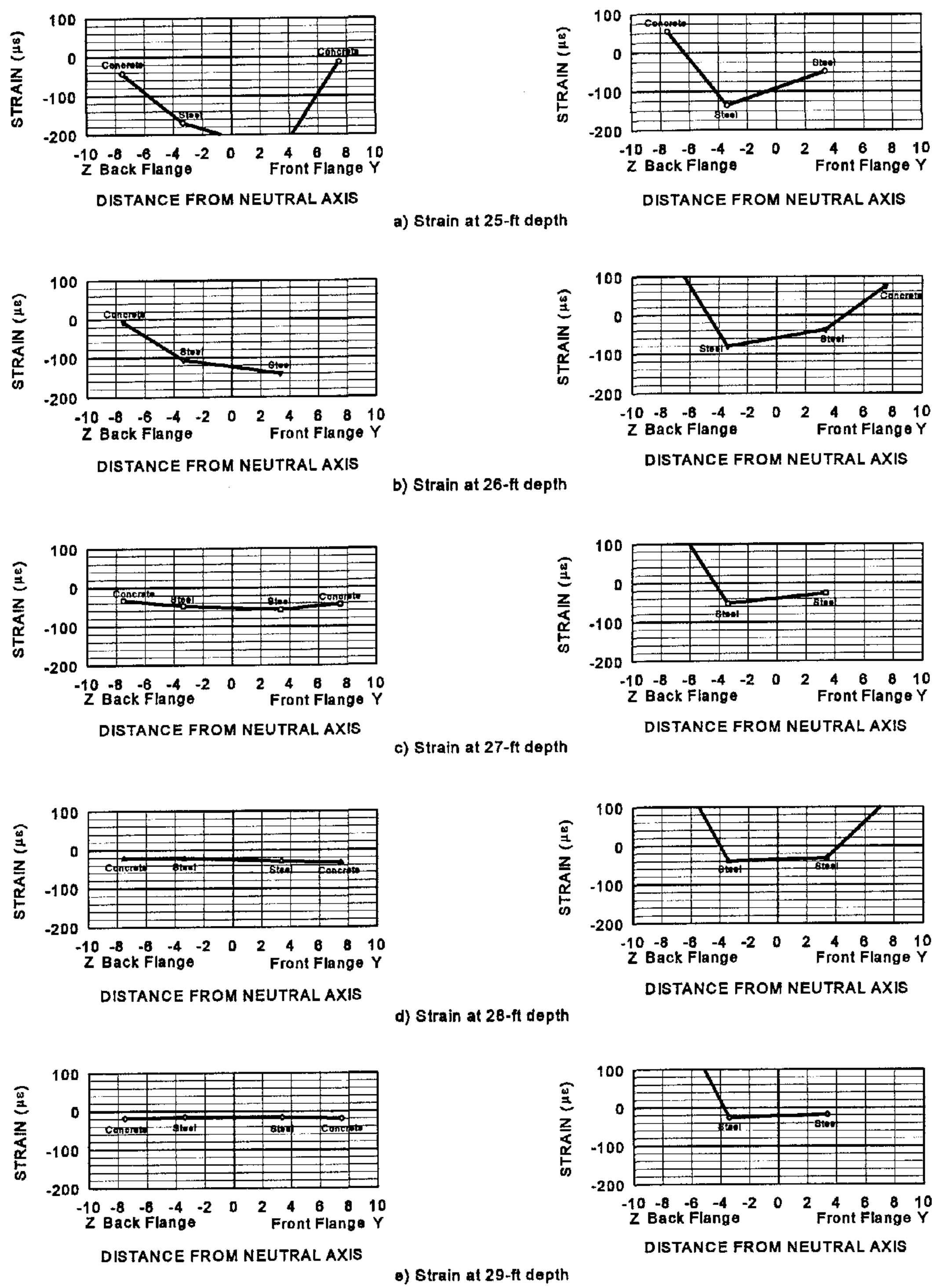

BEAM 9 (structural concrete)

BEAM 10 (lean-mix concrete)

FIGURE 28
Measured Strains in the Toes of Beams 9 and 10 at the Completion of Construction

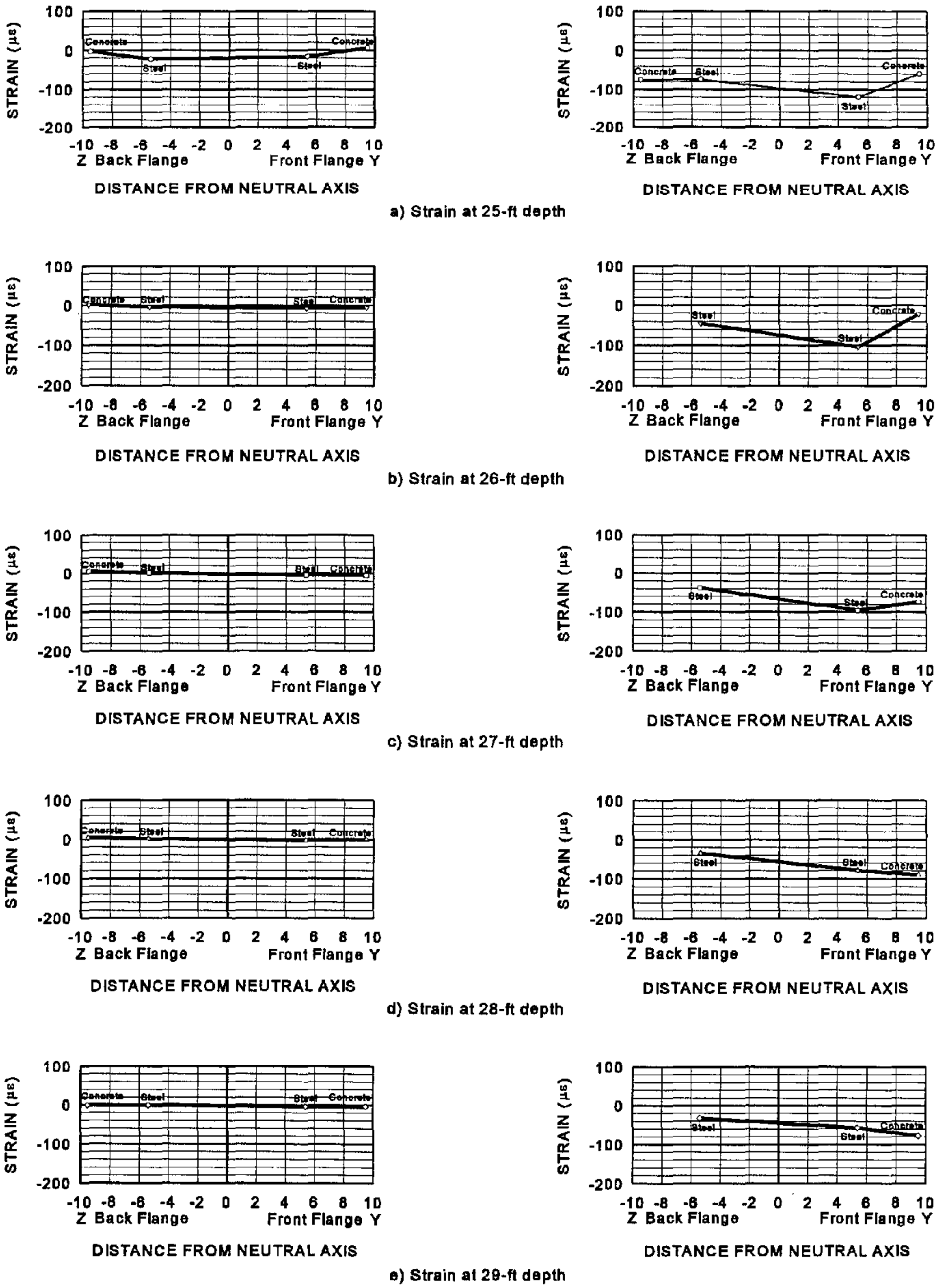

BEAM 13 (structural concrete) BEAM 14 (lean-mix concrete)

FIGURE 29
Measured Strains in the Toes of Beams 13 and 14 at the Completion of Construction

The bending moments and axial loads calculated assuming composite section properties should be similar to the calculated moments and axial loads for the driven beams if the beams behaved as a composite section. Figure 30 shows the bending moment curves and Figure 31 shows the axial load curves for the soldier beams at the conclusion of construction. Open symbols represent the bending moments and axial loads calculated using section properties for the steel beams. Filled symbols indicate the moments and axial loads calculated using section properties for the transformed composite sections in Table 4.

Figure 30 shows that the bending moments did not change significantly when the transformed composite section properties were used to compute the moments. However, Figure 31 shows that the axial loads changed significantly when transformed composite section properties were used in the calculations. Except in the toes of the beams, the steel section axial load curves are the most reasonable for Soldier Beams 9, 10, 13, and 14. In the toes, the axial load curve for Soldier Beam 9 would be more realistic if the beam behaved as a steel section above 28 ft and as a composite section at 28 ft and below. Axial strains in the toes of Soldier Beams 10 and 13 were so small that either composite or steel section properties would predict reasonable axial loads. Along the toe of Beam 14, the axial load curve computed using steel section properties was the most realistic.

Based on the criterion outlined above, the drilled-in beams did not behave as a composite section except in the lower portion of the toe of the beams backfilled with structural concrete. Composite behavior appears to have existed in Soldier Beam 9 at a depth of 28 ft and below and in Soldier Beam 13 at a depth of 27 ft and below. Figures 32 and 33 show axial load and bending moment curves for Soldier Beams 7 to 10 and 13 to 16 using appropriate section properties. Solid data points represent locations where transformed composite section properties were used. Steel section properties were used to compute the axial loads and moments at all other locations.

Composite behavior did not exist where the soldier beams were backfilled with lean-mix fill. Where lean-mix fill is used, design procedures should assume that all the load is carried by the steel section. The steel soldier beam and the structural concrete may have behaved as a composite near the bottom of the toes. When structural concrete is used to backfill the toe of a soldier beam, design procedures that determine where the section will behave as a cracked and uncracked section can be used. Assuming that the load is carried by the steel soldier beam is conservative if structural concrete is used to backfill the drilled shaft. Satisfactory behavior was obtained when the toe was backfilled with lean-mix fill.

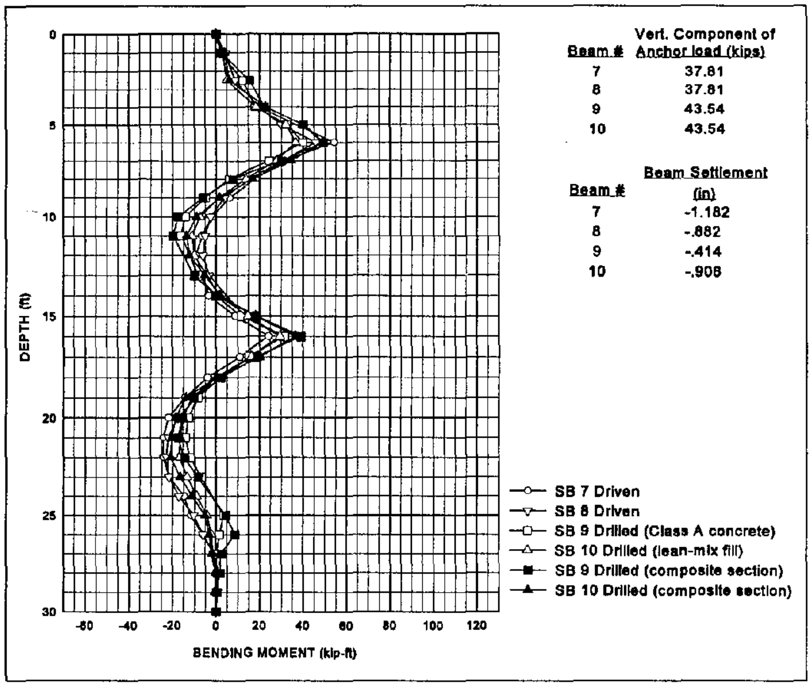

a) Beams 7 to 10

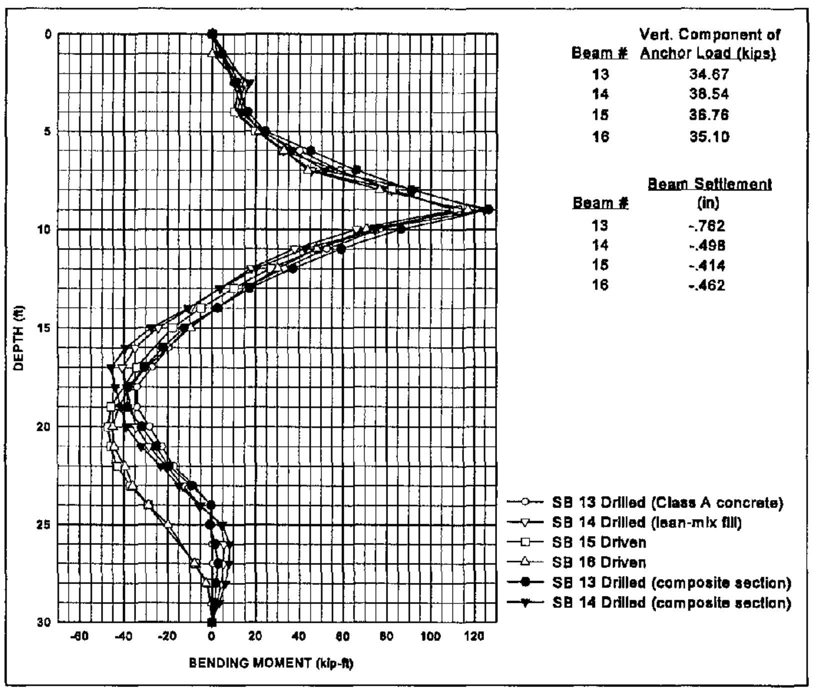

b) Beams 13 to 16

FIGURE 30
Bending Moments in Soldier Beams at the Completion of Construction Assuming Steel and Composite Section Properties

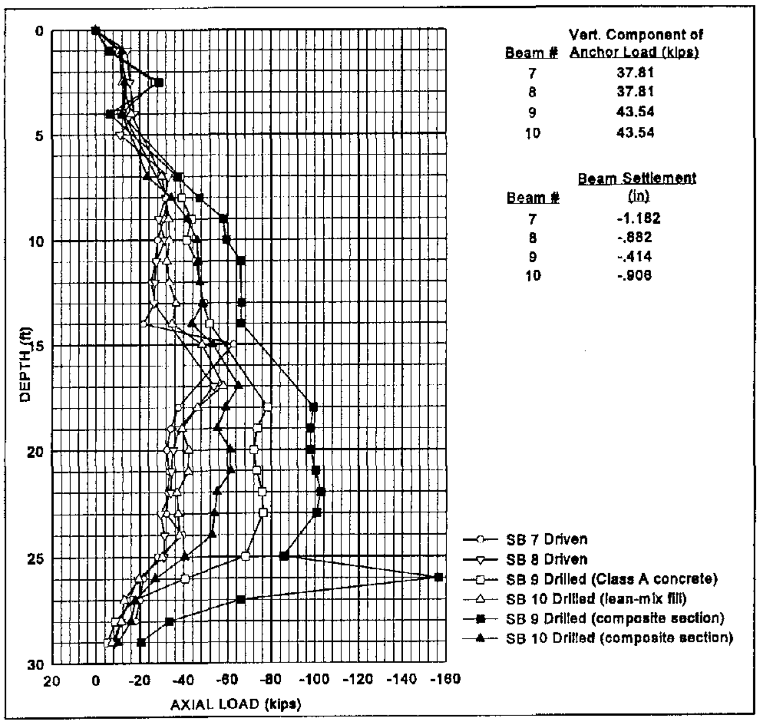

a) Beams 7 to 10

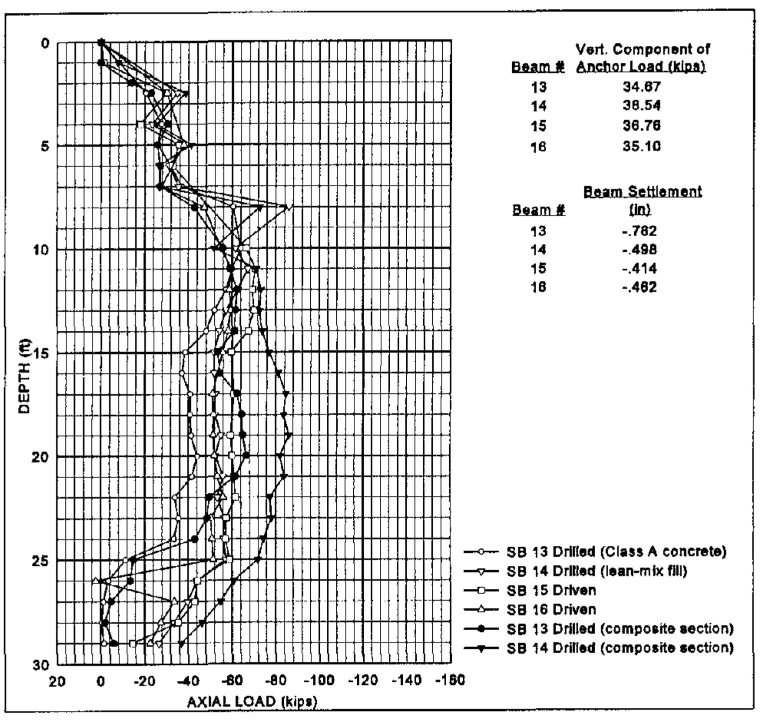

b) Beams 13 to 16

FIGURE 31
Axial Loads in Soldier Beams at the Completion of Construction Assuming Steel and Composite Section Properties

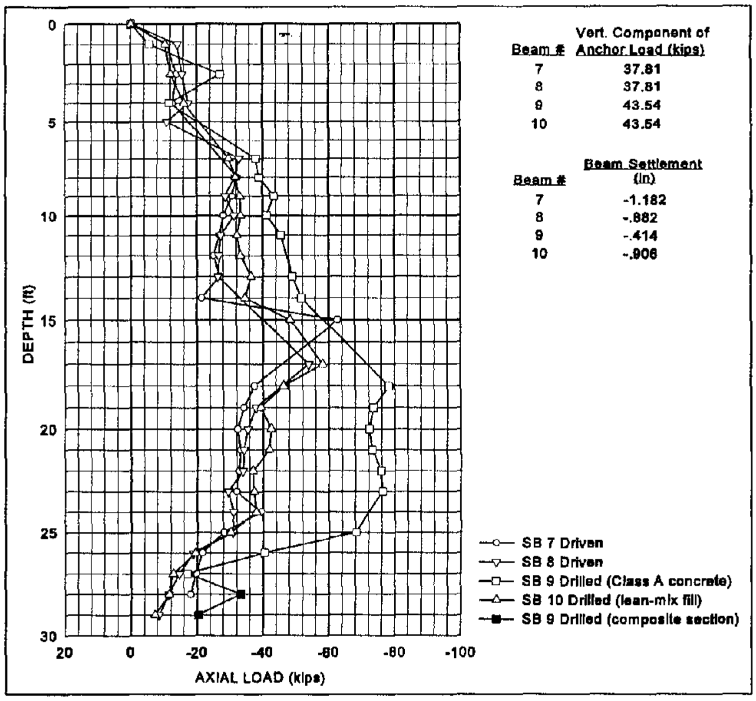

a) Beams 7 to 10

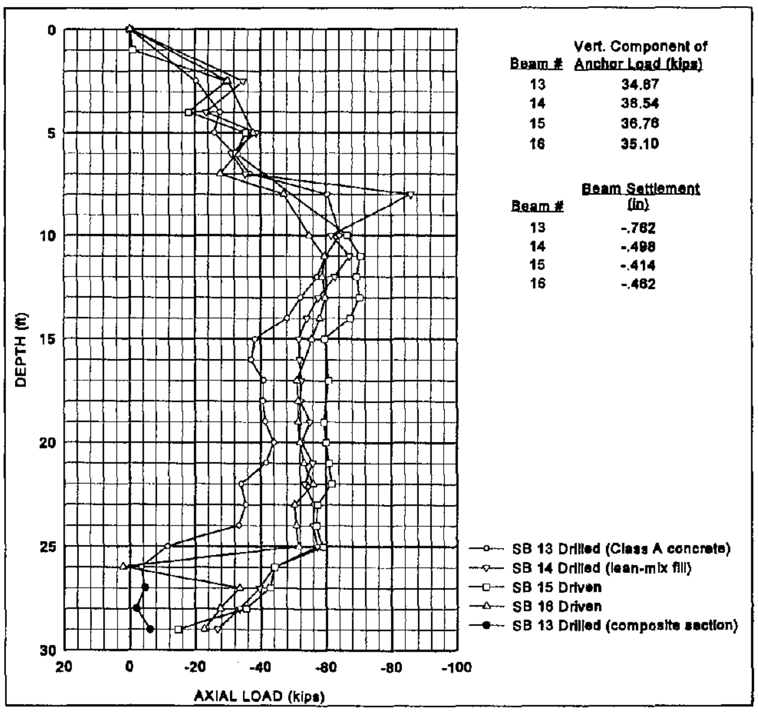

b) Beams 13 to 16

FIGURE 32
Axial Loads in Soldier Beams at the Completion of Construction Assuming Composite Behavior Where Appropriate

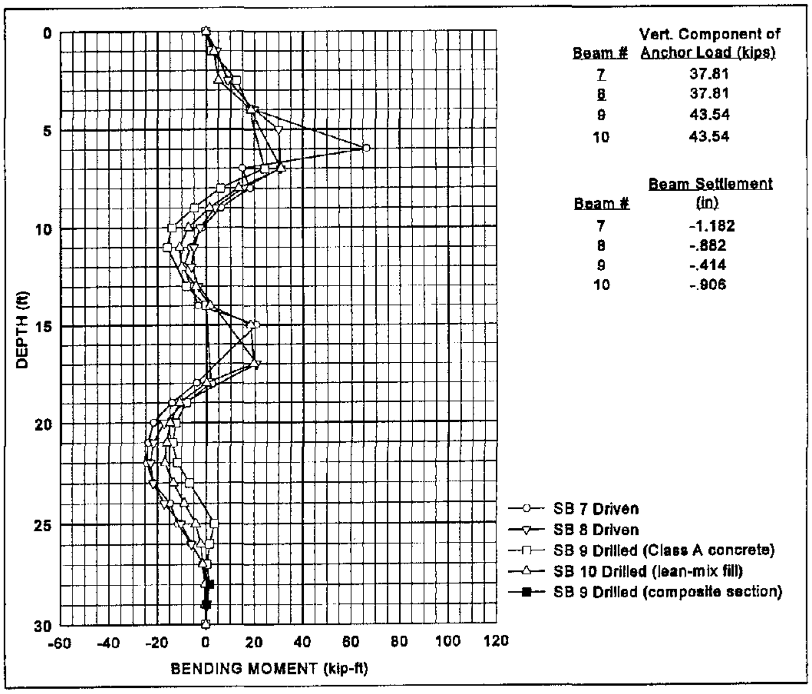

a) Beams 7 to 10

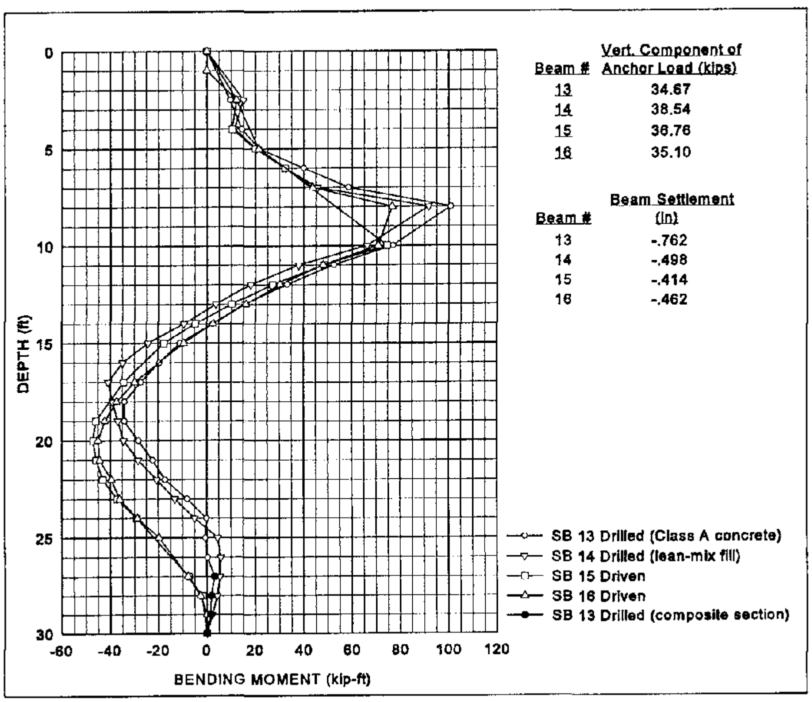

b) Beams 13 to 16

FIGURE 33

Bending Moments in Soldier Beams at the Completion of Construction Assuming Composite Behavior Where Appropriate

2.5.3 Axial Loads

2.5.3.1 Texas A&M Wall

Axial loads in Soldier Beams 7 to 10 and 13 to 16 depend on the vertical component of the ground anchor force and the relative movement of the beams with respect to the supported ground. The load is greater than the ground anchor induced force when the ground settles relative to the soldier beam, and less than the ground anchor induced force when the beam settles more than the ground.

Axial loads applied to the wall at Texas A&M were determined by measuring the load in the driven beams 1 ft below the bottom of the excavation level. Driven beams were studied to eliminate composite behavior. Measuring the loads 1 ft below the bottom of the excavation removed the false axial load readings above the bottom of the excavations (see Section 2.5.1).

Figure 34 shows the average axial loads in Beams 7 and 8 as a function of excavation depth or time. Similar data for Beams 15 and 16 are shown in Figure 35 The open squares represent the average vertical component of the measured ground anchor loads. The open circles represent the average axial load in the soldier beams 1-ft below the excavation level at each stage of construction and during the 84-day observation period. Average soldier beam settlements and the volume of lateral wall movement per inch of wall are shown in the figure.

Small compression loads were measured in the soldier beams before installing the ground anchors. Figure 34 shows a compression load of about 2 kips in Beams 7 and 8 with the excavation 8 ft deep. Figure 35 shows a 6-kip compression load in Beams 15 and 16 with the excavation 10 ft deep. These axial loads appear to be the result of "downdrag." Downdrag occurred when the soldier beam moved out, allowing the supported soil to move down relative to the beam.

After the ground anchors were stressed, the axial load in the soldier beams was less than the vertical component of the ground anchor force. A single ground anchor, located in the center of a wale, supported the upper portions of Beams 7 and 8. After stressing the anchor, the average compression load in Beams 7 and 8 at 9 ft was 19.0 kips, while the average vertical component of the ground anchor force was 20.7 kips. Beams 15 and 16 were supported by two ground anchors installed in a common wale. The average axial load in Beams 15 and 16 at 11 ft was 28.9 kips, while the average vertical component of the ground anchor force was 33.7 kips.

When the ground anchors were stressed, the beams were pulled into the ground behind the wall. As the beams moved laterally into the ground, the normal stress between the beams and the soil in the vicinity of the ground anchors increased. Under these conditions, axial load could be transferred from the beams to soil over short distances. Therefore, the axial load in the beams 1 ft below the bottom of the excavation could be less than the load applied by the ground anchors and soil downdrag.

As the excavation deepened to 14 ft and then to 17 ft, the axial load in the beams increased above the vertical component of the ground anchor force. This indicates that the ground moved down relative to the soldier beam as the excavation was deepened. Figure 34 shows that the average axial load in Beams 7 and 8 was approximately 6.3 kips greater than the vertical component of the anchor force, and Figure 35 shows that the average axial load in Beams 15 and 16 was about 2.9 kips greater than the applied force after the 14-ft excavation was made. When the excavation was completed to the 17-ft level, the average excess axial load was 12.0 kips in Beam 7 and 8, and 11.6 kips in Beams 15 and 16. The excess axial loads and the volume of lateral movement were approximately the same for all the beams when the excavation was 17 ft deep. At these construction stages soldier beam settlement was negligible.

A second row of ground anchors was installed to support Beams 7 to 10 while the excavation remained 17 ft deep. The effect of locking-off these anchors is shown in Figure 34. The increase in the axial load in Beams 7 and 8 was about the same amount as the vertical component of the second row ground anchor force. This indicates that the beams did not settle significantly as the second row anchor was stressed.

When the excavation reached 21 ft deep, the axial loads in Beams 7 and 8 decreased to approximately equal the vertical component of the ground anchor force. At this time Beam 7 settled 0.276 in and Beam 8 settled 0.192 in. When the excavation in front of Beams 15 and 16 reached the 21-ft depth, the axial loads in these beams increased slightly. With the excavation 21 ft deep, Beam 15 settled 0.096 in and Beam 16 settled 0.108 in. The behavior of the beams at the 21-ft-deep excavation supports the observation that the relative movement of the beams with respect to the ground affects the magnitude of the axial load in the beams. The vertical component of the ground anchor force in each beam was about the same for Beams 7, 8, 15, and 16. However, Beams 7 and 8 settled an average of 0.132 in more than Beams 15 and 16, and the average axial load in Beams 7 and 8 was 13.5 kips less than the average axial load in Beams 15 and 16. These differences suggest that the downdrag load in Beams 7 and 8 was transferred to the ground as the beams settled about a 1/10 in. At the 21-ft depth, the total settlement of Beams 7 and 8 equaled $0.0009H$, and the maximum lateral movement equaled $0.0026H$. Settlements and lateral movements of this magnitude are in the middle of the normal range reported by Clough and O'Rourke (1990).

Upon excavating from 21 to 25 ft, the total settlement of Beams 7 and 8 became greater than 1 in, and the axial load in these beams dropped below the vertical component of the ground anchor force. Figure 34 shows that most of the lateral movement of the wall occurred as the beams settled. At the 25-ft excavation, Beams 15 and 16 settled about 0.45 in and the axial load dropped from the value measured when the excavation was 21 ft deep. The average excess axial load in Beams 15 and 16 was 9 kips greater than the vertical component of the ground anchor force. At the end of the 84-day observation period, Beams 15 and 16 settled $0.0015H$ and moved laterally $0.0026H$. Movements of this magnitude also are within the mid-range of the typical movements reported by Clough and O'Rourke (1990). Figure 35 shows that the lateral movement of Beams 15 and 16 was about half that of Beams 7 and 8. Figures 34 and 35 show that most of the lateral movement occurred while the beams settled.

During the long-term monitoring of the wall, axial loads, ground anchor loads, lateral wall movements and settlements of Beams 15 and 16 remained unchanged. However, Beams 7 and 8 continued to settle, causing the lateral movements to increase. As Beams 7 and 8 settled, the ground anchor loads and the axial loads in the beams dropped.

Downdrag caused the axial loads in the soldier beams to be greater than the vertical components of the ground anchor loads. Downdrag load was transferred to the beams by wall friction. The tangent of the wall friction angle was assumed to be equal to the excess axial load in the beams divided by the total earth load associated with the excavation depth. The angle of wall friction for Beams 7 and 8 was determined to be 16.4° for the 17-ft-deep excavation. Beams 15 and 16 had an angle of wall friction of 12.7° when the excavation was 21 ft deep.

The beams at Texas A&M were installed into an alluvial deposit consisting of loose clayey sand overlying medium dense sand. The relative density of the deposit was estimated to be between 40 and 55 percent. Axial load behavior of the driven beams at Texas A&M is summarized below:

- Axial loads in the beams depended upon the relative movement of the ground to the beams and the vertical component of the ground anchor force.
- When the ground settled relative to the soldier beams, the axial load was greater than the vertical component of the ground anchor force.
- Once the beams settled relative to the ground, axial load was transferred from the beams to the ground.
- The maximum axial load was equal to the vertical component of the ground anchor force plus a downdrag force associated with an angle of wall friction equal to $0.512\,\phi$.
- When the beam settlements reached 0.0009 to $0.0017H$ (typical settlements for anchored soldier beam walls reported by Clough and O'Rourke, 1990), the axial load in the beams at the bottom of the excavation equaled the vertical component of the ground anchor force.
- When settlements increased above 0.002H (settlements still within the typical range reported by Clough and O'Rourke, 1990), the axial load was less than the vertical component of the ground anchor force.
- Side friction was fully mobilized on Soldier Beams 7, 8, 15, and 16.
- End bearing was fully mobilized on Soldier Beams 7 and 8. Ending bearing was not fully mobilized on Soldier Beams 15 and 16.

- Lateral movements increased as the soldier beams settled.

Schnabel Foundation Company has designed and built thousands of anchored walls with 5-ft toe embedment depths. Usually, the anchors were installed at inclinations less than or equal to $\phi/2$, and the design assumed that the vertical component of the ground anchor load was transferred to the ground above the bottom of the excavation. Settlement and lateral movement of these walls was less than half that measured at the full-scale test wall. Ground anchors for the Texas A&M wall were installed at an angle approximately equal to the friction angle of the soil. The behavior of the wall at Texas A&M was not expected. Additional case histories were studied in an attempt to understand the axial load behavior of anchored soldier beam walls.

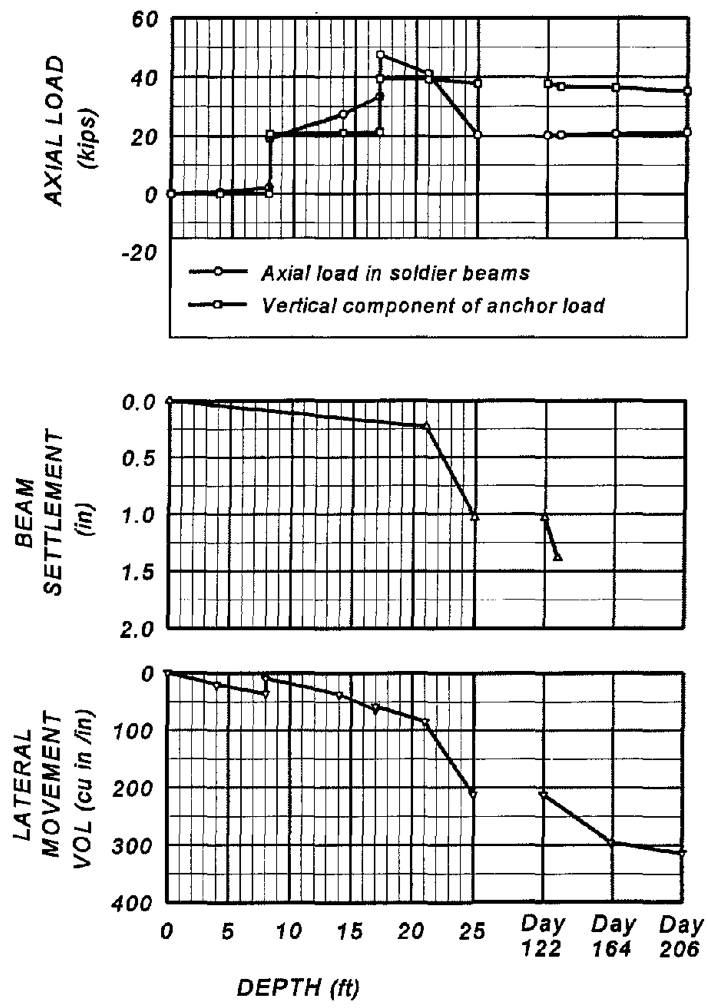

FIGURE 34
Average Axial Load, Beam Settlements, and Lateral Movement Volume for Beams 7 and 8

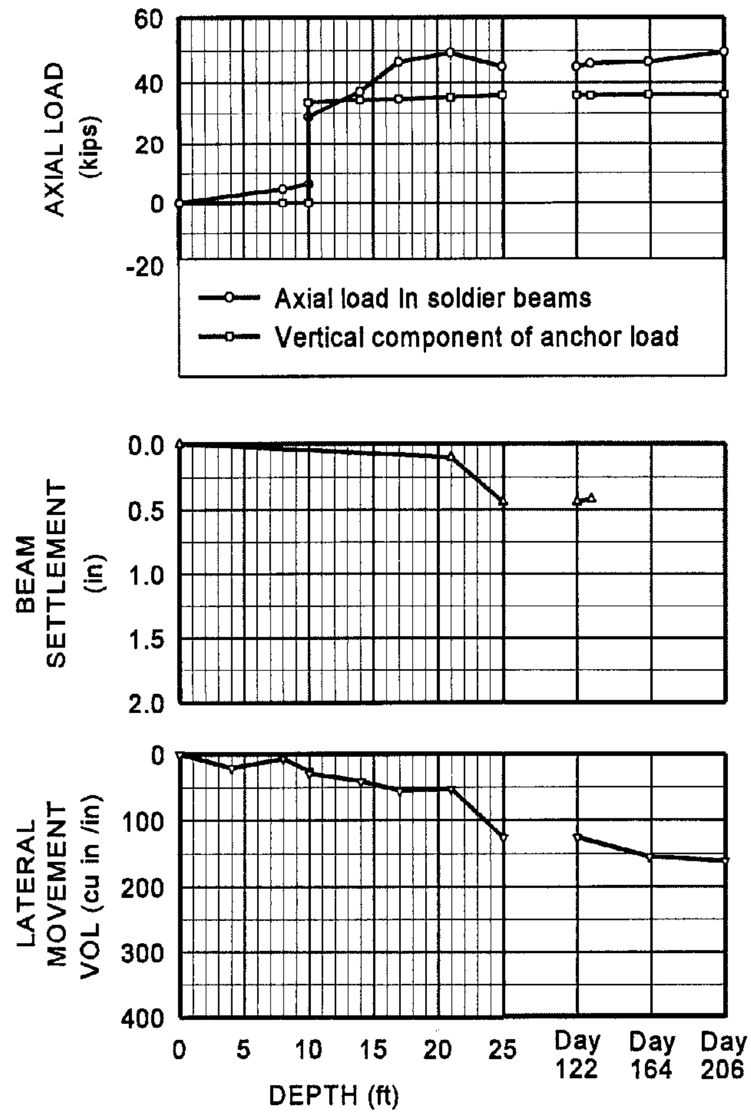

FIGURE 35
Averal Axial Load, Beam Settlements, and Lateral Movement Volume for Beams 15 and 16

2.5.3.2 125 High Street, Boston, Massachusetts

In 1988 and 1989, Schnabel Foundation Company installed and monitored the behavior of instrumented, drilled-in soldier beams at 125 High Street, Boston. Houghton and Dietz (1990) described the installation. Pairs of W12×30 beams were installed in 36-in-diameter drill holes backfilled with lean-mix fill. The anchored soldier beams supported the 56-ft-deep excavation, and the beams were installed on 9.58- to 10.0-ft centers. Soldier beam toes extended 6 ft below the bottom of the excavation. Figure 36 shows a section view of instrumented Soldier Beam 49 and a nearby boring log. Figure 37 shows similar information for instrumented Soldier Beam 67. Seven rows of ground anchors supported Beam 49 and six rows of anchors supported Beam 67. Vibrating wire strain gauges were installed on each beam. The gauges were located below each row of anchors and three gauge levels were located along the toe of the beams. Inclinometer wells, extending 15 ft below the bottoms of the soldier beams, were installed through the lean-mix fill surrounding the beams. Load cells were installed on each ground anchor supporting the instrumented beams.

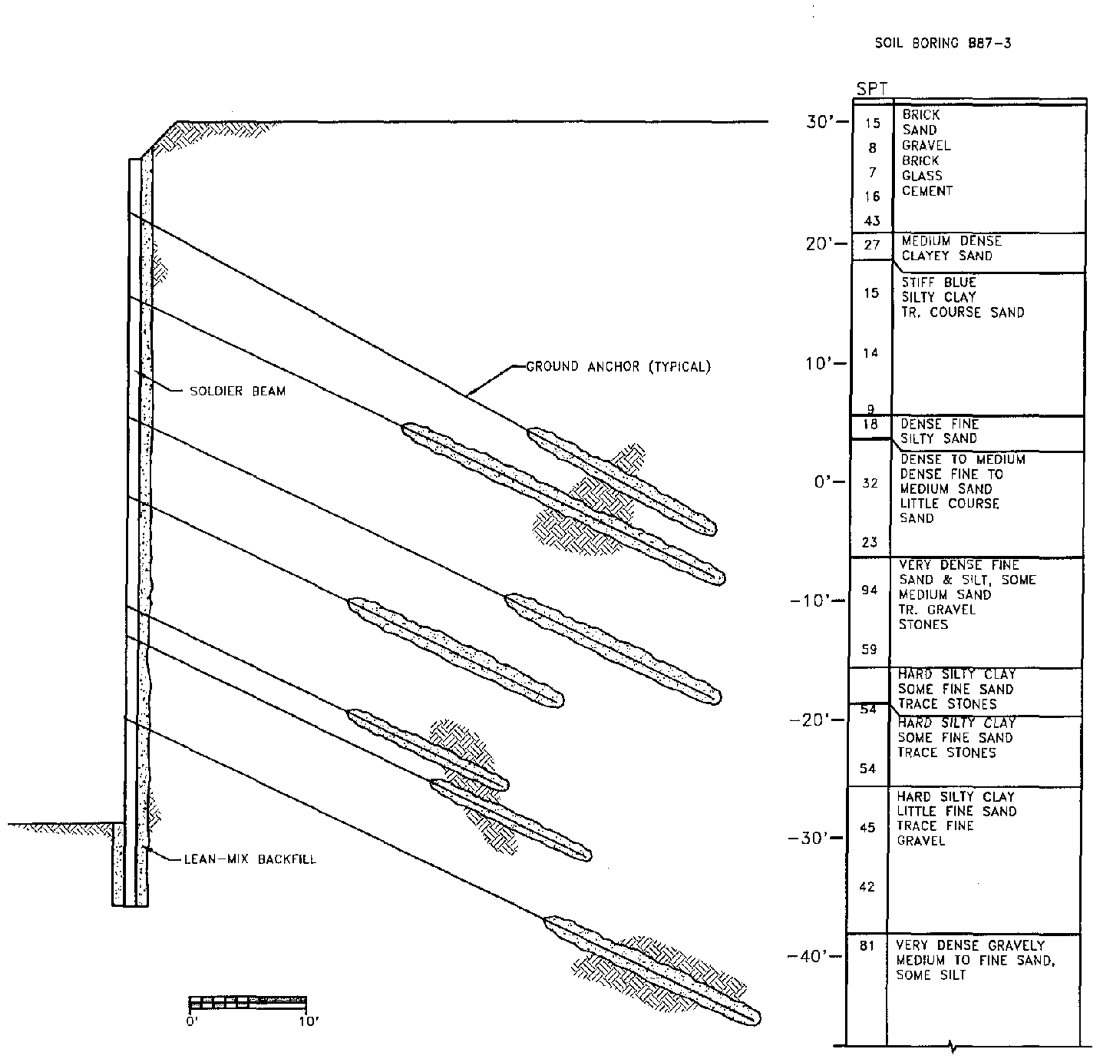

FIGURE 36
Soldier Beam 49 at 125 High Street

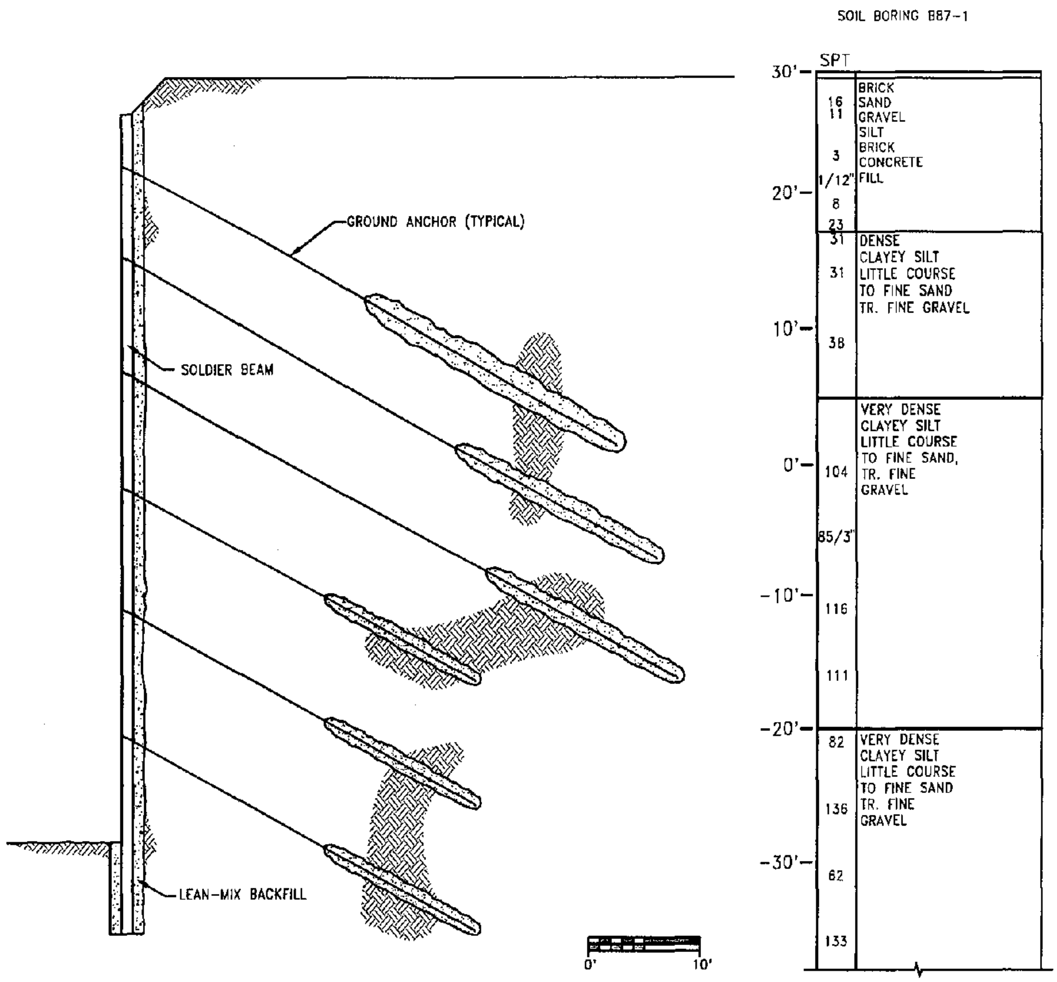

FIGURE 37
Soldier Beam 67 at 125 High Street

All the instrumentation was read regularly during the construction and for a period after the excavation was complete. Figure 38 shows the axial load in Beam 49 as a function of excavation depth or time. Similar data for Beam 67 are shown in Figure 39 The open squares represent the vertical component of the measured ground anchor loads. The open circles represent the axial load in the beam before excavating to the next ground anchor. The maximum load measured at a particular gauge location is shown by a solid circle. Lateral movement volume per inch of wall is also shown in the figures.

Figures 38 and 39 show that Soldier Beam 49 moved laterally three to four times more than Beam 67. Soldier beam settlement was not measured, but beam settlement was determined to be insignificant since the strain gauge data indicated that the axial load was taken out in shaft friction. High shaft friction was possible since the toes of the beams were installed in a hard glacial till. Maximum axial loads in both beams occurred below the fifth row of anchors. The maximum axial load in Beam 49 was 386 kips, approximately 80 kips greater than the applied vertical component of the ground anchor force at that level. The maximum axial load in Beam 67 was 192 kips, approximately 58 kips less than the applied vertical component of the ground anchor force at that level. At the second through the fifth row of anchors on Soldier Beam 49 the maximum axial load was greater than the vertical component of the applied ground anchor force. Axial load in Beam 67 never exceeded 88 percent of the applied vertical component of the ground anchor force. Vertical load in the toe of Soldier Beam 49 was 22 percent less than the vertical component of the ground anchor force. Vertical load in the toe of Beam 67 was 46 percent less than the vertical component of the ground anchor force. Beams 49 and 67 did not behave as a composite section.

Soldier Beam 49 moved laterally far enough to cause the ground behind the upper portion of the wall to settle relative to the beam and apply a downdrag load to the beam. At the same time, Beam 67 did not move laterally as far as Beam 49 and axial load was transferred from Beam 67 to the ground over its full length. Beam 49 moved laterally more than Beam 67 even during early construction stages. When the excavation was approximately 40 ft deep, additional soil borings behind the wall determined that the clay layer shown in Figure 37 extended deeper than identified during the original soil exploration. Standard penetration resistances in the clay were as low as 4 blows/ft and suggested that the deposit may have been weaker than indicated in the original soils report. The presence of the medium clay layer contributed to the movement of Beam 49 and the downdrag load. The lower 20 ft of Beam 49 was in a hard till and axial load was transferred from the beam to the ground in the till above bottom of the excavation.

Clay did not exist in the vicinity of Soldier Beam 67. Very stiff to hard glacial till was present over the bottom 45 ft of Soldier Beam 67. The lateral movements of Beam 67 were small and the soil mass did not settle relative to the beam.

The axial load behavior of Soldier Beams 49 and 67 at 125 High Street project is summarized below:

- Beam 49 moved laterally far enough to allow the ground mass above the fifth row of anchors to settle relative to the beam. Where the ground settled relative to the beams, the axial load was greater than the vertical component of the ground anchor force.
- Axial load was transferred from the soldier beams to the ground where the beams were installed into the hard glacial till.
- Seventy-eight percent of the vertical component of the ground anchor load supporting Soldier Beam 49 was transferred to the toe of the beam. The load was carried by skin friction.
- Fifty-four percent of the vertical component of the ground anchor load supporting Soldier Beam 67 was transferred to the toe of the beam. The load was carried by skin friction.
- Beams 49 and 67 did not behave as a composite section.

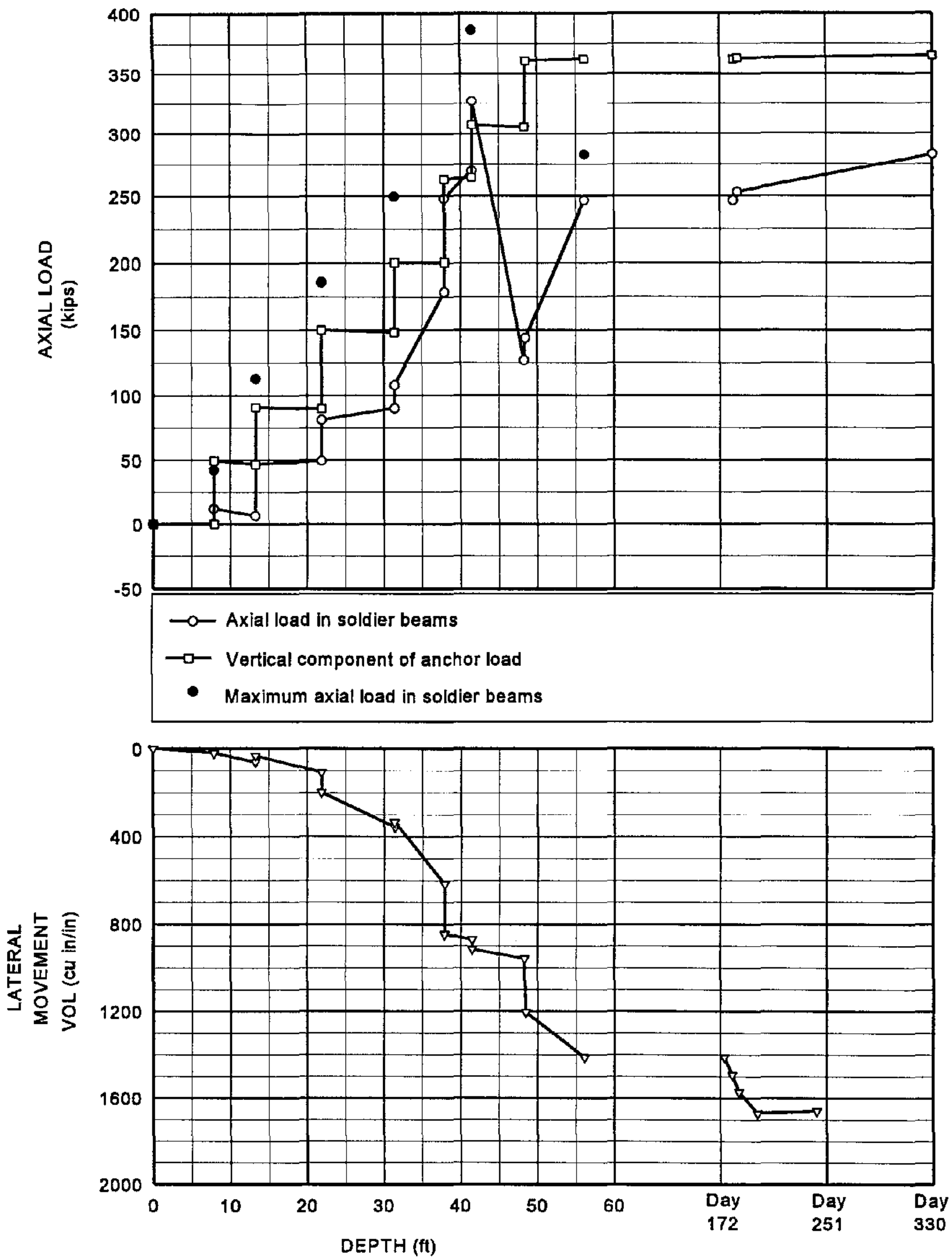

FIGURE 38
Axial Load and Lateral Movement Volume for Beam 49 at 125 High Street

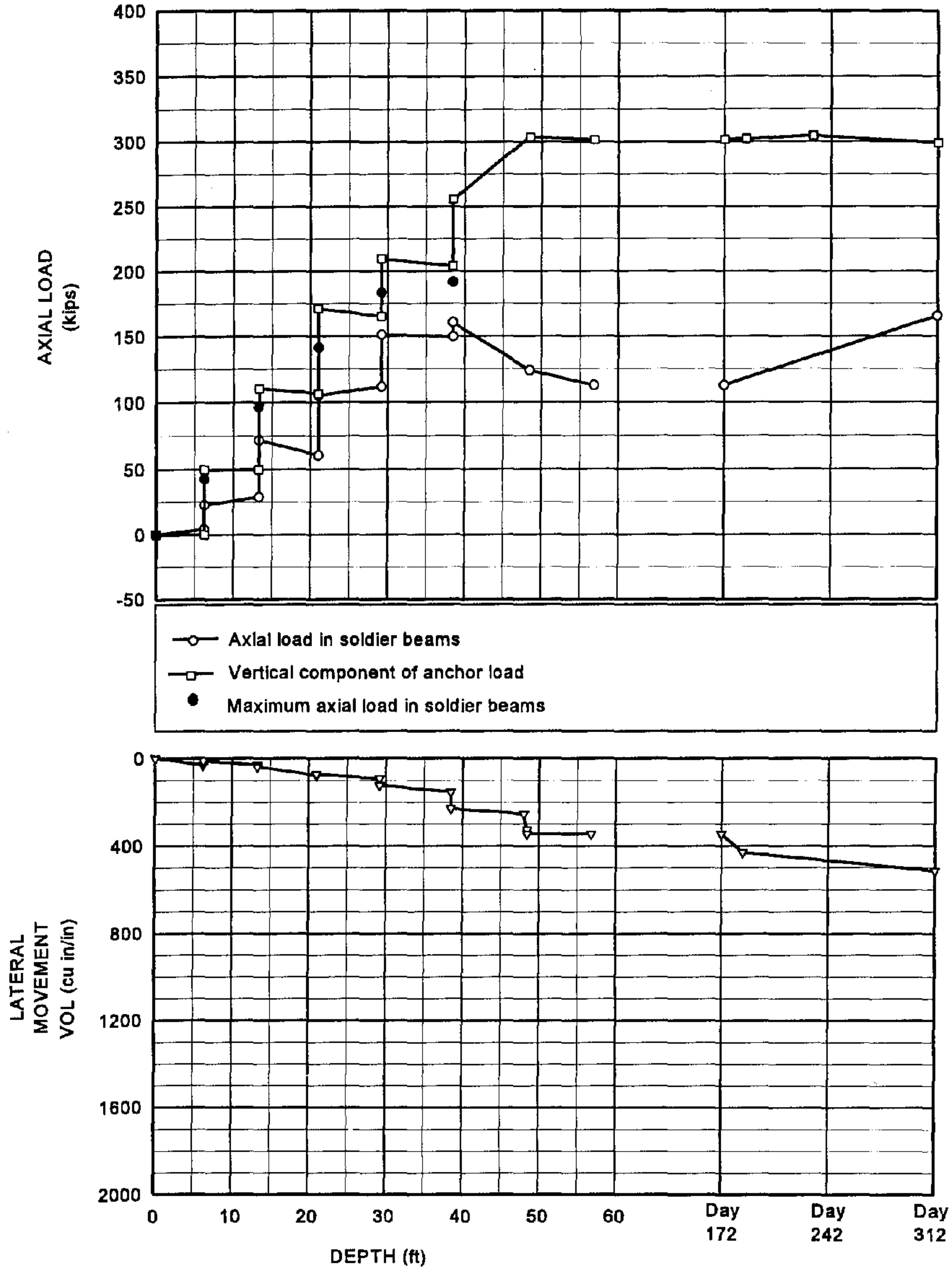

FIGURE 39
Axial Load and Lateral Movement Volume for Beam 67 at 125 High Street

2.5.3.3 North Street Grade Separation, Lima, Ohio

Two anchored retaining walls were constructed to depress North Street under the railway serving the C & O/B & O Railway Company and the N & W Railway Company. The complete installation is described by Cheney (1990). One soldier beam and two ground anchors installed for the project were instrumented. Raw instrumentation data and data interruption are contained in a report by The H. C. Nutting Company (1988). The 24.5-ft-high wall was supported by two rows of hollow-stem-auger anchors. Figure 40 shows a section through instrumented Soldier Beam 93. The 39-ft-long soldier beams were fabricated from pairs of C15 × 33.9 channels and placed in 30-in-diameter drill holes. Soldier beam toes extended 14.5 ft below the bottom of the excavation. Structural concrete was used to backfill the toe of the beams and lean-mix concrete, with a compression strength of 1000 psi, was used to backfill the exposed portion of the beams. Soldier beams were installed on 6-ft centers. Ground anchors had a design load of 80 kips and they were installed 20 degrees from the horizontal. Four levels of strain gauges were installed on the soldier beam. Gauges were located below each anchor at subgrade and in the toe of Beam 93. An inclinometer well was installed in the drill hole with the channels. Load cells were placed on the ground anchors to monitor anchor load during construction and the 731-day observation period.

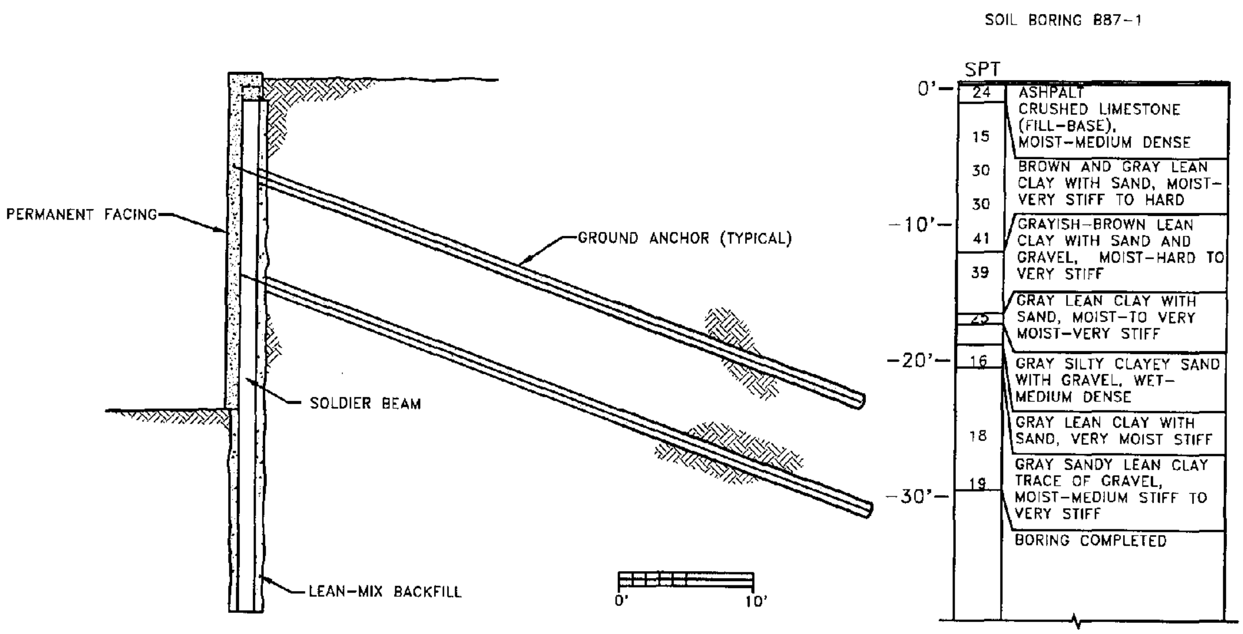

FIGURE 40
Soldier Beam 93 at Lima, Ohio

Soils at the site were a glacial ground moraine consisting of an unstratified mix of clay, silt, and sand with occasional gravel. Unconfined compressive strengths varied between 2.35 and 4.22 tsf. Effective shear strength parameters were determined by undrained triaxial compression tests with pore pressure measurements. The tests indicated that the soil had an angle of internal friction of 35 degrees and a cohesion of 340 psf.

Figure 41 shows the axial load, vertical component of the ground anchor load, and lateral movement volume for Beam 93 at each stage of construction and during the observation period. The open circles represent the vertical component of the ground anchor load. The open squares represent the axial load in the steel soldier beam below the bottom of the excavation. The open diamonds represent the axial load in the beams assuming that the beams function as a steel and concrete composite. Composite action is possible since the strains were low and the lean-mix concrete had a compression strength of 1000 psi. Figure 41 shows that the axial load transferred to the toe was less than 5 kips, assuming all the load was carried by the steel section, or less than 10 kips, assuming composite action. At least 77 percent of the vertical component of the ground anchor force was transferred to the ground above the bottom of the excavation.

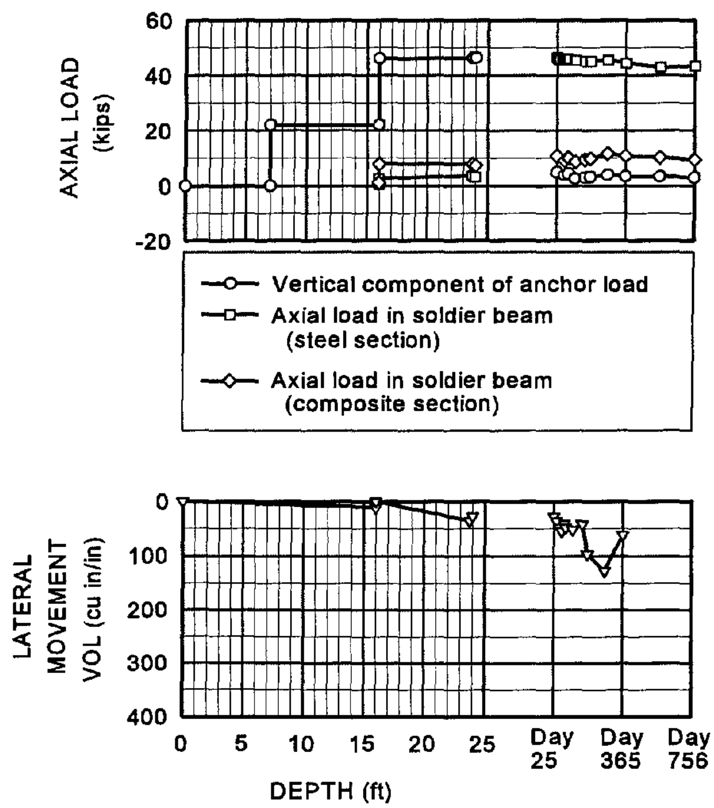

FIGURE 41
Axial Load and Lateral Movement Volume for Beam 93 at North Street Grade Separation in Lima, Ohio

The axial load behavior of Soldier Beam 93 at North Street Grade Separation, Lima, Ohio, is summarized below:

- Axial load was transferred from the soldier beams to the hard glacial till above the bottom of the excavation.
- Soldier Beam 93 did not settle significantly, and axial load was carried by skin friction.
- Steel-concrete composite behavior was possible since the measured strains were small.
- Eleven percent of the vertical component of the ground anchor load supporting Soldier Beam 93 was transferred to the toe of the beam assuming the load was carried by the steel section only.
- Twenty-two percent of the vertical component of the ground anchor load supporting Soldier Beam 93 was transferred to the toe of the beam assuming the load was carried by the steel-concrete composite section.

2.5.3.4 Retaining Wall, U.S. Route 7, Redding/Danbury, Connecticut

An anchored retaining wall was constructed as part of the relocation of U.S. Route 7. The wall was 45 ft high and supported by five rows of pressure grouted anchors. Soldier beams were fabricated from W16×89 beams installed in 30-in-diameter holes. Structural concrete was used to backfill the toe of the beams and lean-mix fill was used to backfill the exposed portion of the beams. Soldier beam toes extended 22 ft below the bottom of the excavation. Soldier beams were installed on 8.75-ft centers. Each ground anchor had a design load of 140 kips and they were installed at angles ranging from 9.5 to 28.5°. Seven levels of strain gauges were installed on Soldier Beam 77. Gauges were located below each row of anchors and two levels of gauges were located in the toe. Anchor load was assumed to be the lock-off load. The strain gauge readings and data interpretation are contained in a report by Long (1987).

The soldier beams and ground anchors for the wall were installed in a very dense silty fine sand with a trace of gravel and cobbles. Standard penetration resistances for the soil varied between 30 and 107 blows/ft with an average resistance of 65 blows/ft. The angle of internal friction was estimated to be 36°.

Figure 42 shows the axial load in the beam, and the vertical component of the ground anchor force for each stage of construction. The open circles represent the vertical component of the ground anchor force. Open squares represent the axial load in the steel soldier beam below the bottom of the excavation at each stage of construction. The open triangles represent the axial load in the beams assuming that the beam functioned as a steel and concrete composite. Composite action was not likely for any of the upper gauges because the strains exceeded the cracking strain of the lean-mix backfill. Composite action was possible in the toe, but not likely. Figure 42 shows that the axial load transferred to the toe was approximately 38 kips, assuming all the load was carried by the steel section, or 150 kips, assuming composite action. The vertical component of the ground anchor load was about 210 kips. If the load was carried by the steel section only, 81 percent of the vertical component of the ground anchor force was transferred to the ground above the bottom of the excavation.

The axial load behavior of Soldier Beam 77 in a retaining wall, U.S. Route 7, Redding/Danbury, Connecticut. is summarized below:

- Axial load was transferred from the soldier beams to the very dense silty sand above the bottom of the excavation.
- Soldier Beam 77 did not settle significantly, and axial load in the toe was carried by skin friction.
- Steel-concrete composite behavior did not occur over the upper portions of the beams since the strains exceeded the cracking strains of the lean-mix fill. In the lower portions of the beams, composite action was possible since the strains were small.
- Nineteen percent of the vertical component of the ground anchor load supporting Soldier Beam 77 was transferred to the toe of the beam assuming the load was carried by the steel section only.
- Seventy-one percent of the vertical component of the ground anchor load supporting Soldier Beam 77 was transferred to the toe of the beam assuming the load was carried by the steel-concrete composite section.

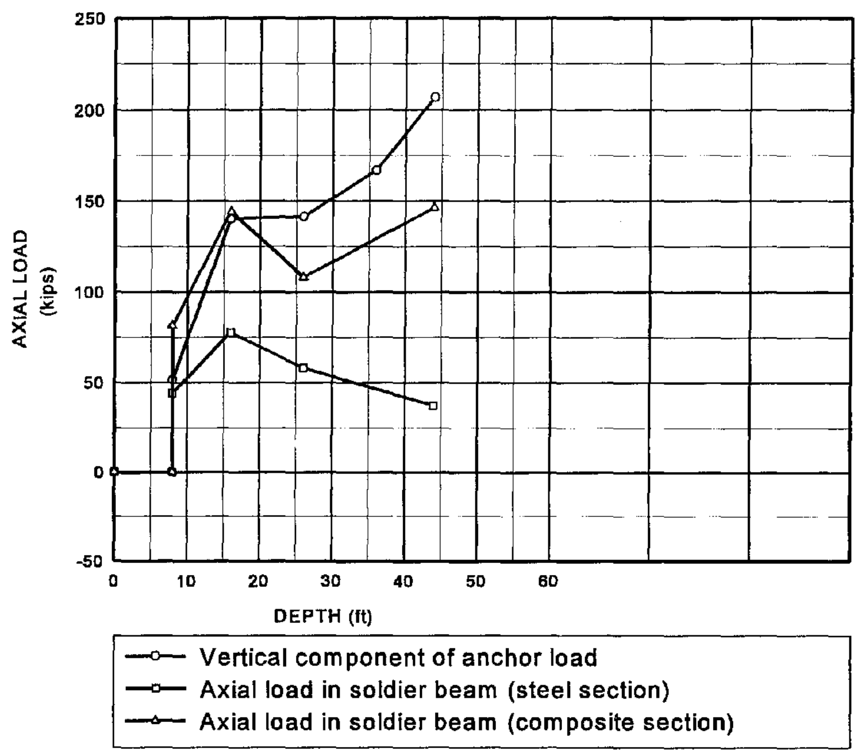

FIGURE 42
Axial Load in Soldier Beam 77 at U.S. Route 7, Danbury, Connecticut

2.5.3.5 Wall Friction

Table 10 presents a summary of the axial load transferred from the soldier beam to the ground above the bottom of the excavation, or the downdrag load transferred from the ground to the soldier beam. The tangent of the wall friction angle, δ, in the table is the load transferred from the soldier beam or the downdrag load divided by the lateral earth load applied to the beam. In the table, α is the factor used to reduce the undrained shear strength so the surface area of the beam times αs_u is equal to the downdrag force or load transferred from the beam. Positive friction angles or α's indicate downdrag load and negative friction angles or α's indicated that load was transferred from the beam to the ground.

Soldier beams at Texas A&M were installed in a loose to medium dense sand and they were subjected to downdrag loads until the beams settled. The angle of wall friction for the one-tier beams at Texas A&M is approximately 6°, 0.18ϕ. Wall friction angles for the two-tier Texas A&M beams reversed signs as the excavation was deepened from 17 to 25 ft. The change in the sign occurred as the beams settled. The soldier beams at the Danbury Wall, the Lima Wall, and Soldier Beam 67 at the Boston excavation support system were installed in dense to very dense cohesionless soils or hard glacial till. Table 10 shows that a significant portion of the vertical component of the ground anchor force in these beams was transferred to the ground above the bottom of the excavation. The load transferred from the beams at the conclusion of the monitoring period was related to an angle of wall friction ranging from -0.25 to -0.5 ϕ. Undrained shear strength for the till at the Lima, Ohio, site was determined. The α factor for the Lima wall was either -0.202 or -0.231 depending upon whether the beam was a composite section or a steel section.

Soldier Beam 49 at the Boston excavation support system behaved differently from the other beams. The upper portion of the beam supported a medium to stiff clay and the lower portion of the beam supported a hard glacial till. Section 2.5.3.2 described the behavior of Beam 49 in detail. As shown in Figure 38 and Table 10, the downdrag load was applied to the upper portion of the beam where the clay was present and extended down to the gauge level below the sixth row of anchors. Assuming an undrained shear strength of 1200 psf in the clay, the α factor was 0.621 over the upper 19 ft of the soldier beam. This value is reasonable for clays of this strength. As indicated in Table 10, 162.3 kips was transferred from the beam between the sixth row of anchors and subgrade. The angle of wall friction required for this to occur was -24.9° (-0.553ϕ).

TABLE 10
Summary of Axial and Downdrag Loads Transferred Above Subgrade

	TEXAS A&M WALL				DANBURY, CONNECTICUT WALL			LIMA, OHIO WALL		BOSTON SB 67	BOSTON SB 49	BOSTON SB 49
	One-tier 17' high	One-tier 25' high	Two-tier 17' high	Two-tier 25' high	Two-tier 18' high	Three-tier 28' high	Full Height 45' high	Full Height Steel 24.5' high	Full Height Composite 24.5' high	Full Height 56' high	Full Height (upper 3 tiers, 19' depth)	Full Height (bottom tier)
Vertical Component Anchor Load (kips)	34.7	36.0	21.3	37.8	140.3	141.4	206.7	45.7	45.7	298.7	150.5 (upper 3 tiers)	364.6 (7 tiers)
Axial Load at Subgrade (kips)	46.4	45.0	33.3	20.2	77.8	58.2	37.3	3.8	9.1	165.2	185.9 (below 3rd tier)	282.6
Downdrag Load (kips)	11.7	9.0	12.0								35.4 (below 3rd tier)	80.3 (below 6th tier)
Transferred Load Above Subgrade (kips)				17.6	62.5	82.9	169.4	41.9	36.6	133.5		162.3
Rankine Earth Load (kips)	40.8	88.3	40.8	88.3	44.5	107.8	278.3	63.4	63.4	349.7	322.6 (upper 3 tiers)	349.7 (bottom tier)
Wall Friction Angle (degrees)	+16.0	+5.8	+16.4	-19.9	-54.5	-37.6	-31.3	-33.5	-30.0	-20.9		-24.9
ϕ' (deg)	32	32	32	32	36	36	36	35	35	45		45
c' (psf)								340	340			
s_u (psf)								3300	3300		1200	
δ	0.500 ϕ	0.181 ϕ	0.512 ϕ	-0.622 ϕ	-1.514 ϕ	-1.044 ϕ	-0.869 ϕ	-0.957 ϕ	-0.857 ϕ	- 0.464 ϕ		-0.553 ϕ
α								-0.231	- 0.202		0.621	

2.5.3.6 Axial Load Observations and Recommendations

Axial load in a soldier beam depends upon: the vertical component of the ground anchor force, the strength of the supported ground, the vertical and lateral movements of the wall and axial load-carrying capacity of the toe. The following observations and recommendations are made based on the behavior of the full-scale wall and case histories.

- Lateral wall movements result when the soldier beams settle.
- The amount of lateral movement for a given soldier beam settlement depends upon the inclination of the ground anchors. Lateral movements will be small when the anchors are installed at flat angles and larger when the anchors are installed at steep angles.
- Keep the axial load to a minimum by installing the ground anchors at flat angles. For example, ground anchors installed at 15 degrees from the horizontal will apply 50 percent less vertical load to the wall than anchors installed at 30°.
- To minimize wall movements, axial capacity of the soldier beams must be adequate to support the applied vertical component of the ground anchor.
- Avoid unnecessarily high ground anchor design loads or test loads. High design loads may require long soldier beam toes in order to develop additional axial load-carrying capacity. High test loads may result in the beams settling during testing.
- Axial load will be transferred from the wall to the ground above the bottom of the excavation in dense to very dense sands or stiff to hard clays.
- Axial load will be transferred from the wall to the ground above the bottom of the excavation if the soldier beam settles relative to the ground.
- Downdrag loads will be applied to the soldier beam if the wall moves laterally more than 0.004H and the soldier beams do not settle.
- Downdrag loads are reduced to zero when the wall settles 0.1 in relative to the supported soil.
- Soldier beam toes do not have to be designed to resist downdrag loads. If downdrag loads develop, small soldier beam settlements will reduce these loads to zero.
- Axial load behavior of driven and drilled-in beams were similar.

Table 11 gives tentative recommendations for estimating axial loads transferred to a soldier beam. Limited case history data were used to develop the recommendations. They are believed to be conservative.

TABLE 11
Guidelines for Estimating the Axial Load Applied to the Toe

SANDS		CLAYS	
Medium Dense	**Dense to Very Dense**	**Soft to Medium**	**Stiff**
$10 \leq$ SPT ≤ 30	SPT > 30	$s_u \leq \gamma H/4 - 5.714H$	$s_u > \gamma H/4 - 5.714H$
I	II	I	III

I	Design toe to resist vertical components of the ground anchor loads plus applied axial loads
II	Design toe to resist vertical components of the ground anchor loads plus applied axial loads minus the horizontal components of the ground anchor loads × $\tan\delta$ (δ between $\phi/4$ and $\phi/2$)
III	Design toe to resist vertical components of the ground anchor loads plus applied axial loads minus $A_s \cdot 0.25 s_u$ (A_s = surface area of steel in contact with the ground and s_u = undrained shear strength)

2.5.4 Vertical Load-carrying Capacity of the Toe

Axial load applied to the toe of a soldier beam is resisted by skin friction and end bearing. Back-calculated load-transfer rates, end bearing values, and beam settlements for driven Soldier Beams 7, 8, 15, and 16 are shown in Figure 43. Average values for the different beam sizes are plotted for different construction stages and during the observation period.

Figure 43 shows that, during the 84-day observation period, the average load-transfer rate along the toes of Soldier Beams 7 and 8 was 4.9 kips/linear foot and the average rate for Beams 15 and 16 was 6.5 kips/linear foot. Average end bearing values were 11.5 kips and 21.3 kips for Beams 7 and 8 and Beams 15 and 16, respectively. Beams 7 and 8 settled sufficiently to fully mobilize skin friction and end bearing. Figure 43 shows that skin friction along Beams 7 and 8 was mobilized first and then end bearing was mobilized as the beams settled. Beams 15 and 16 settled enough to fully mobilize the skin friction along their lengths. However, additional end bearing capacity appears to be available. Axial load-carrying behavior of the driven soldier beams was similar to the behavior of driven bearing piles.

Figure 32 shows that Soldier Beams 10 and 14, drilled-in beams backfilled with lean-mix fill, had axial load curves and settlements similar to the driven beams. Therefore, the load-transfer rates and the end bearing values must be similar to those for the corresponding driven beams. Figure 32 shows that Soldier Beam 9, backfilled with structural concrete, settled much less than the other beams, and had higher load-transfer rates and end bearing capacity than Beams 7, 8, and 10. However, the opposite was true for Soldier Beam 13. Beam 13 also was backfilled with structural concrete, but it settled more than the adjacent beams, and it had the lowest axial load-carrying capacity of all the instrumented beams. Realistic load-transfer rates and end bearing capacities for Beams 9 and 13 could not be established from the data. The strain gauges at 26 ft indicate that the average toe capacity during the 84-day observation period was 48.7 kips for Beam 9 and 10.5 kips for Beam 13.

There was no clear cause for the differences in behavior of Beams 9 and 13. Comparing the behavior of Beams 10 and 14 with adjacent driven beams indicates that lean-mix fill can reliably be used to backfill the drill holes around the toes of soldier beams. The axial load-carrying capacity of Beams 9 and 13 indicates that structural concrete in the toes had no clear benefit. Therefore, the extra material and placement costs required for structural concrete is not warranted. Schnabel Foundation Company routinely uses lean-mix fill to backfill the toes of drilled-in soldier beams. Our experience with lean-mix fills supports the recommendation to eliminate the use of structural concrete.

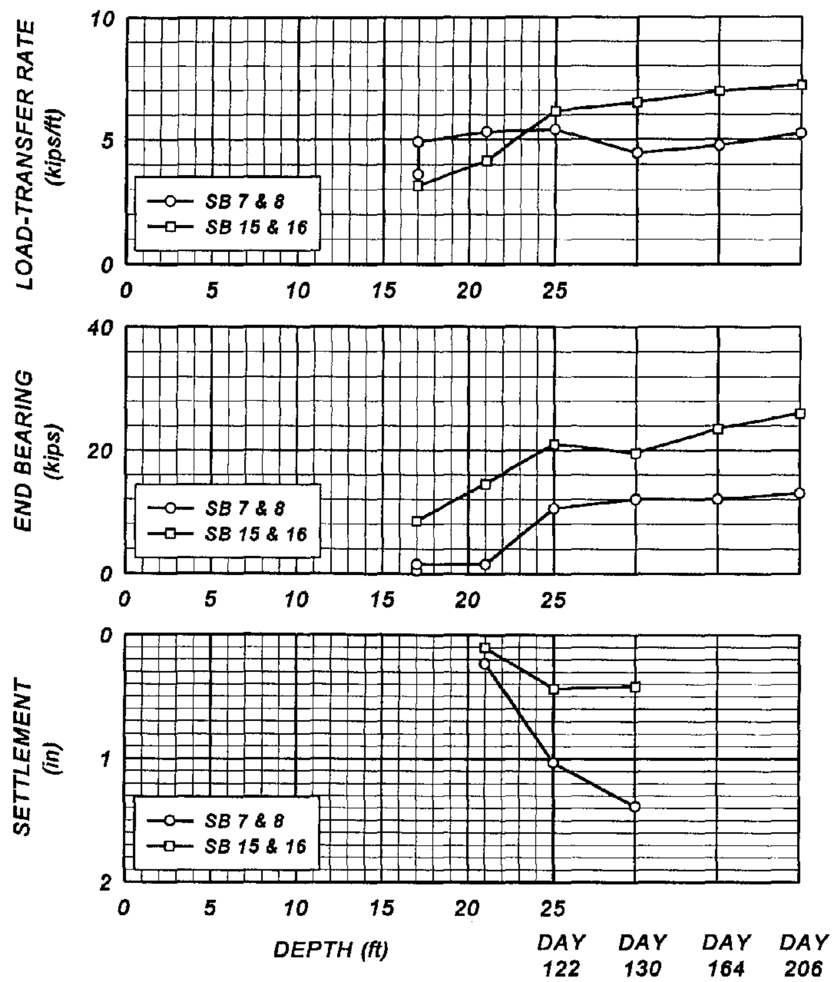

FIGURE 43
Axial Load-carrying Capacity of Soldier Beams 7, 8, 15, and 16

The ultimate axial load-carrying capacities of Soldier Beams 7, 8, 15, and 16 were determined using procedures adapted from the Army Corps of Engineers' *Design of Pile Foundations* (1993). Ultimate capacity of a driven H-beam in sands is

$$\begin{aligned} Q_{ult} &= Q_s + Q_t \\ &= f_s A_s + q A_t \end{aligned} \qquad \ldots [2.15]$$

where:

Q_{ult} = ultimate capacity

Q_s = resistance due to skin friction

Q_t = tip resistance due to end bearing

f_s = average unit skin friction resistance

A_s = block perimeter surface area of the soldier beam toe

q = unit end bearing resistance

A_t = block area of the tip

The average unit skin friction resistance, f_s, is determined using Equation 2.16.

$$f_s = K\sigma'_{v_{ave}} \tan(\delta) \qquad \ldots [2.16]$$

where:

K = lateral earth pressure coefficient (recommended range 1 to 2)

$\sigma'_{v_{ave}}$ = average effective vertical stress along the toe of the soldier beam

δ = angle of friction between soil and pile (recommended range 0.67ϕ to 0.83ϕ)

The effective vertical stress on the front of the soldier beam depends upon the depth from the bottom of the excavation. The effective vertical stress along the back of the soldier beam is greater and depends on the depth from the ground surface behind the wall. The average effective overburden stress on the toe of the soldier beam equals one-half the sum of the average effective overburden stress along the front of the soldier beam plus the average effective overburden stress along the back of the beam. If the groundwater is below the bottom of the soldier beam, the average effective vertical stress is

$$\sigma'_{v_{ave}} = \gamma(h + d)/2 \qquad \ldots [2.17]$$

where:

γ = total unit weight

h = depth of cut

d = depth of toe embedment

Unit end bearing resistance, q, is given by the equation 2.18

$$q = \sigma'_v N_q \qquad \ldots [2.18]$$

where:

σ'_v = effective vertical stress

N_q = bearing capacity factor from Figure 44

The effective vertical stress in equation 2.18 is the stress at the bottom of the soldier beam in front of the wall. The end bearing resistance depends upon the resistance along failure surfaces that would start at the bottom of the soldier beam and curve upward toward the bottom of the excavation.

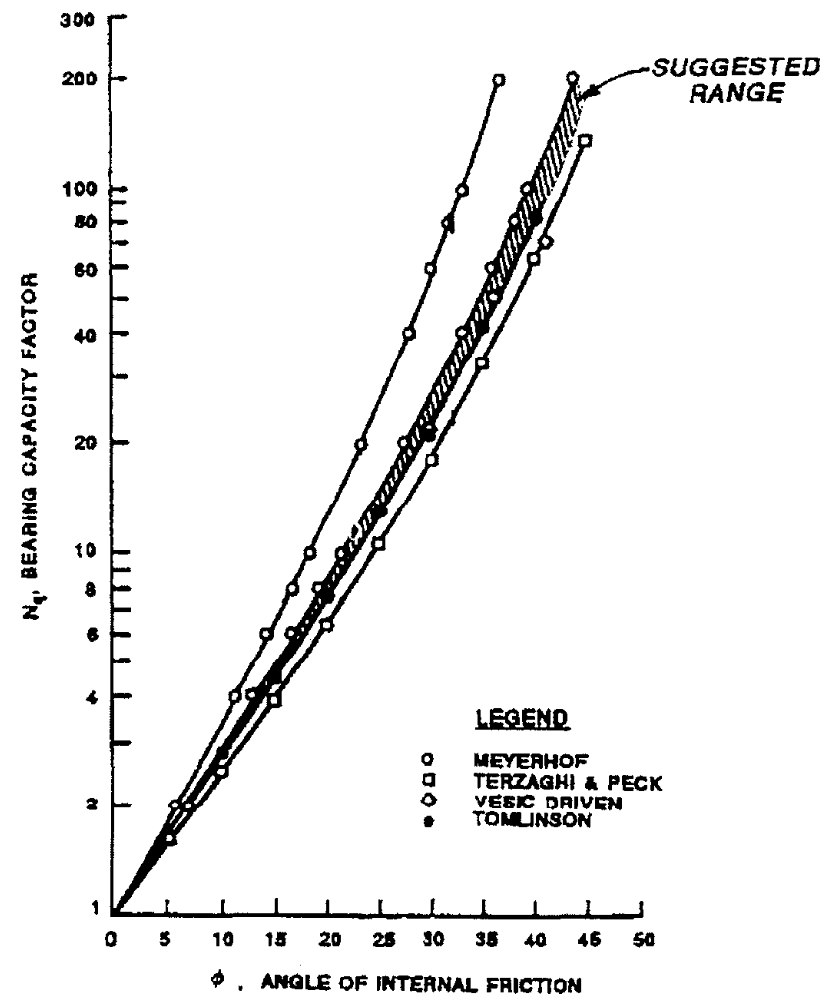

FIGURE 44
Bearing Capacity Factor, N_q
(Army Corps of Engineers, 1993)

Table 12 lists the variables used in the calculations and the computed skin friction and end bearing values for the driven soldier beams at Texas A&M. The variables, except N_q, were generally in the high end of the range recommended in the Corps' procedure. N_q was in the middle of the range recommended by Meyerhoff. The measured results for the soldier beams are included in the table for comparison. Calculated skin friction and end bearing values for the driven beams were very close to the actual values. Actual skin friction and end bearing capacities for the W6×25 beams were ultimate capacities. The actual skin friction value for the HP10×57 beams was the ultimate skin friction. The actual bearing capacity of the HP10×57 beams was less than the ultimate capacity.

TABLE 12
Calculated and Measured Skin Friction and End Bearing for Driven Beams at Texas A&M

BEAM SIZE	A_s (ft^2)	A_t (ft^2)	K	γ (pcf)	h (ft)	d (ft)	φ (deg)	δ (deg)	f_s (psf)	Q_s (kips)	Actual Skin Friction (kips)	N_q	q (psf)	Q_t (kips)	Actual End Bearing (kips)
W6×5 (SB 7&8)	11.8	0.27	2	115	25	5	32	26.6	1725	20.4	24.5	65	3.74	10.1	11.5
HP10×7 (SB 15&16)	18.3	0.71	2	115	25	5	32	26.6	1725	31.6	32.5	65	3.74	26.5	21.3

A_s is the block perimeter of the soldier beams. The block perimeter assumed that the soil between the flanges of the beam moves with the beam, creating a solid cross-section. The surface area of the soldier beams in Table 12 includes the area of the angles used to protect the strain gauges. The unit skin friction resistance, f_s, was computed using Equation 2.17.

2.5.5 Mobilized Lateral Load in the Toes of the Soldier Beams

Lateral loads in the soldier beam toes could not be measured directly. Soldier beam bending moments and lateral movements were measured below the bottom of the excavation. Bending moments and movements were used to estimate the mobilized lateral resistance along the toes of the soldier beams.

Bending moments in the portion of the soldier beams below the bottom of the excavation were small. Figure 45 shows the average bending moments in Soldier Beams 15 and 16 (one-tier section) and Figure 46 shows the average moments in Beams 7 and 8 (two-tier section) after the excavation was completed. Average bending moments at the bottom of the excavation were 20.82 kip-ft in Beams 15 and 16, and 12.14 kip-ft in Beams 7 and 8. Bending moments in the soldier beams were near zero at a depth of 28 ft. Figures 47 and 48 show that Beams 15 and 16 moved laterally between 0.25 and 0.30 in at the bottom of the excavation (25-ft depth) and between 0.05 and 0.1 in at the bottom of the beam (30-ft depth). An inclinometer between Beams 15 and 16 moved less than the soldier beams below the bottom of the excavation. The relative movement between the inclinometer and the beams was less than 0.1 in. Figure 48 shows that Beam 8 moved laterally 0.37 in at the bottom of the excavation and 0.13 in at the tip of the beam. Lateral movements of an inclinometer between Beams 7 and 8 was less than the soldier beam movement between the 25-ft and 28-ft depth. Below 28 ft, the lateral movement of the soldier beam and the inclinometer were about the same.

Development of passive resistance in front of the wall should be similar to the development of passive resistances for a sheet pile bulkhead with fixed anchorages. Rowe (1952) described the development of passive pressures along the embedded portion of sheet pile bulkheads, and showed that the mobilized pressures are different from the triangular-shaped pressure diagram assumed in the design. Rowe (1952) observed that the passive pressures developed as the wall deflects and a significant portion of the available resistance is mobilized at shallow depths while the passive resistance near the bottom of the wall is not fully mobilized. Since the passive resistance is not fully mobilized near the bottom of the toe, the result of the passive pressure will be at or above the midpoint of the toe. If the passive pressure result for Soldier Beams 7, 8, 15, and 16 was at the midpoint of the toe (2.5 ft below the bottom of the excavation), then mobilized passive resistance can be calculated by dividing the bending moment by 2.5 ft. This calculation gives a mobilized passive resistance of 4.86 kips for Beams 7 and 8, and 8.33 kips for Beams 15 and 16.

The ultimate Rankine lateral resistances were 4.6 kips for Beams 7 and 8 and 7.7 kips for Beams 15 and 16. These resistances were computed by assuming that the passive resistance developed over three times the soldier beam width. Active pressure times the soldier beam width was applied to the opposite side of the soldier beam (active load). The lateral resistance was the difference between the passive resistance and the active load. If the ultimate lateral resistance of the soldier beam toes is the Rankine capacity, then the full lateral load-carrying capacity of the soldier beams was developed in the full-scale test wall. Lateral movements of the soldier beam toes are not large enough to fully mobilize the ultimate lateral load-carrying capacities of the beams. Apparently the lateral load-carrying capacity of the soldier beam toes is greater than the capacity determined using Rankine coefficients.

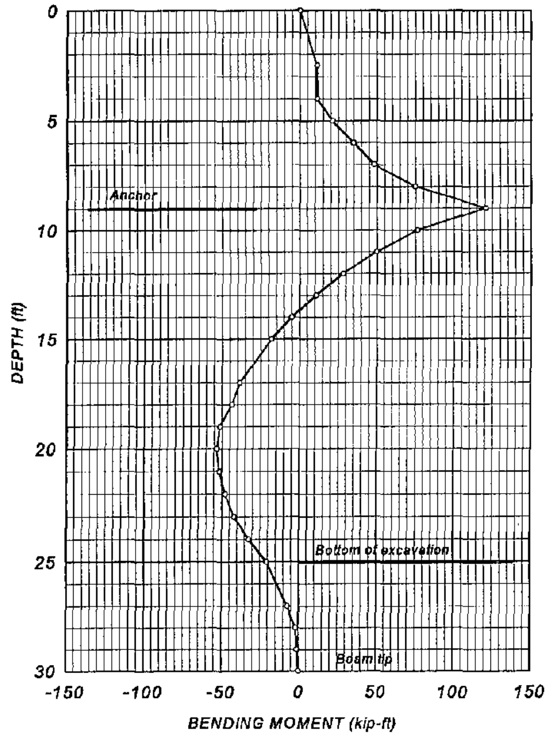

FIGURE 45
Average Bending Moment in Soldier Beams 15 and 16 — Excavation Complete

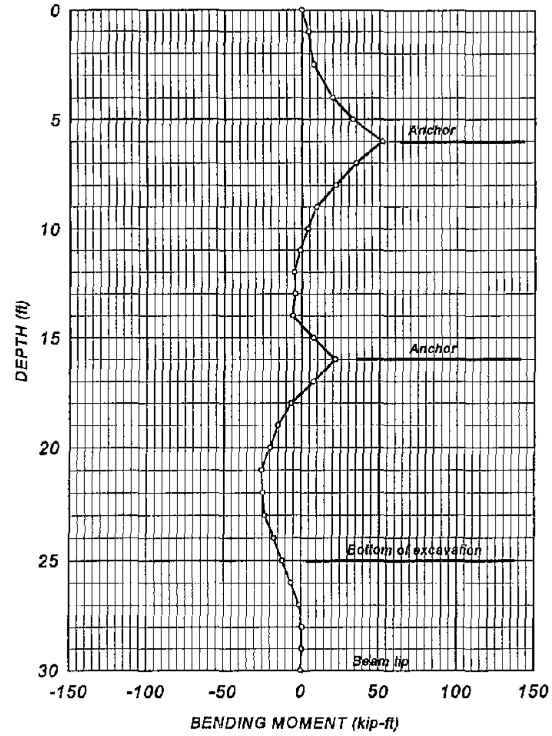

FIGURE 46
Average Bending Moment in Soldier Beams 7 and 8 — Excavation Complete

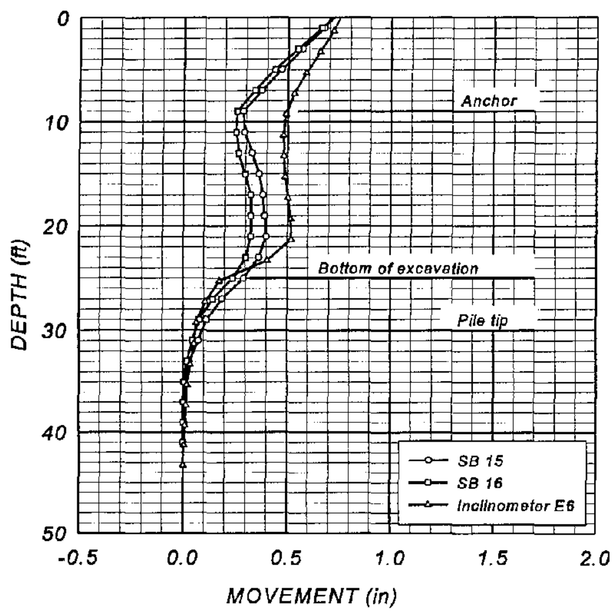

FIGURE 47
Lateral Movement of Soldier Beams 15 and 16 and Inclinometer E6 — Excavation Complete

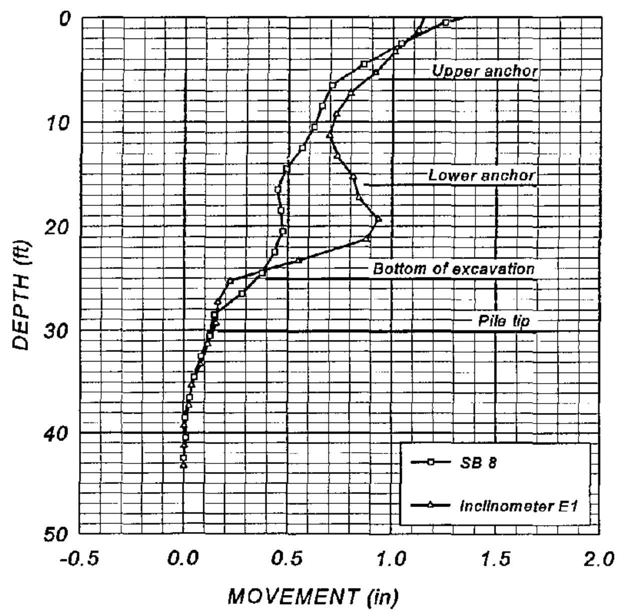

FIGURE 48
Lateral Movement of Soldier Beam 8 and Inclinometer E1 — Excavation Complete

Laterally loaded pile relationships developed by Wang and Reese (1986) for the design of cantilevered retaining walls were used to compute the ultimate lateral resistance of the soldier beams. These relationships are currently used by Texas Department of Transportation to design cantilevered drilled shaft retaining walls. Using these relationships, the computed ultimate lateral capacity was 14.2 kips for Beams 7 and 8 and 14.1 kips for Beams 15 and 16. These relationships are presented in Chapter 3. They consider four modes of failure: individual wedge failure, intersecting wedges, flow of the soil between the beams, and a continuous wall. These ultimate lateral capacities are reasonable based on the magnitude of the lateral deformations and the location where the bending moments are reduced to zero. Figure 49 shows the ultimate lateral pressure distribution based on the laterally loaded pile relationships.

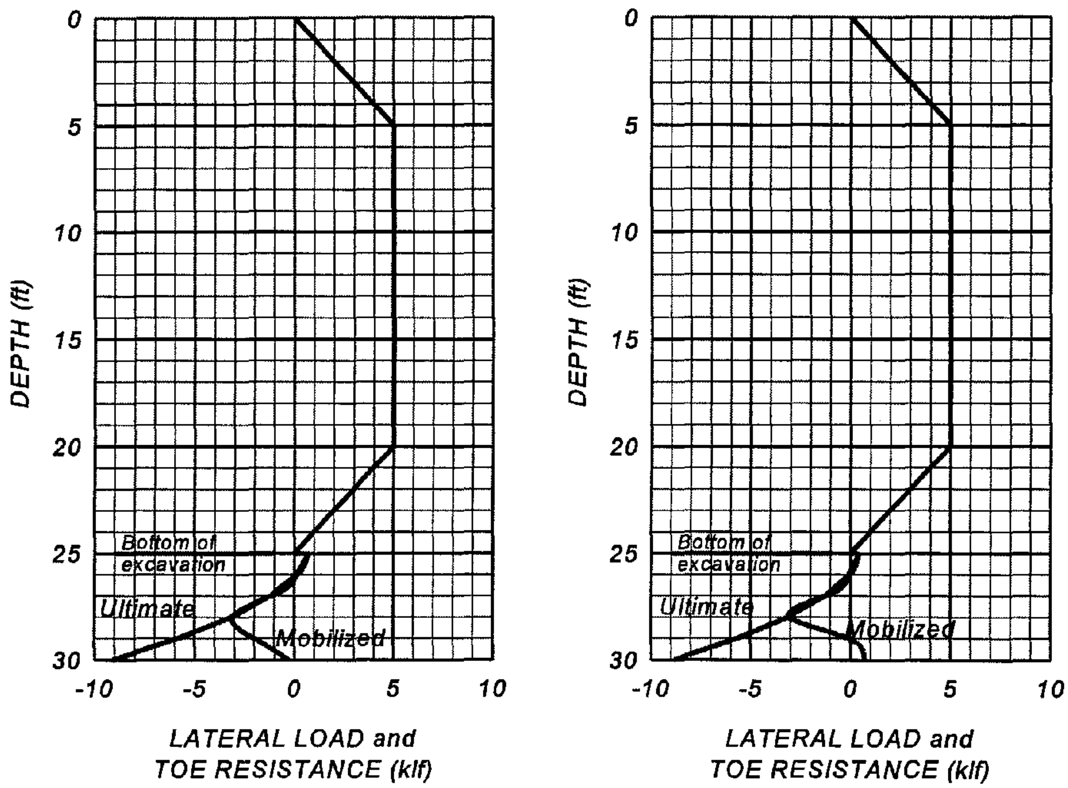

a) One-tier wall

b) Two-tier wall

FIGURE 49
Comparison of Wang-Reese Ultimate Lateral Toe Resistance with Probable Mobilized Toe Resistance for the Soldier Beams in the Full-scale Wall

Figure 49 also shows mobilized passive resistance curves for the portions of the soldier beams below the bottom of the excavations. Computed bending moments for the mobilized passive resistance curves matched the measured bending moments along the entire embedded portion of the soldier beam toe. To match the bending moments, the Wang-Reese passive resistance was fully mobilized to a depth of 28 ft. Passive resistance was 6.3 kips for the one-tier section (Beams 15 and 16) and 3.78 kips for the two-tier section (Beams 7 and 8). The resultant passive resistances for both wall sections was slightly below the 28-ft depth. The Wang-Reese relationships predicted the lateral capacity of the W6×25 and the HP10×57 soldier beams satisfactorily.

Lateral capacity of the soldier beams can be greater than that predicted by laterally loaded pile theory. In granular deposits, shear resistance will developed between the soil and the tip of the soldier beam if an axial load is transferred to the tip. This resistance will equal the mobilized end bearing resistance times the tangent of the friction angle. For an end bearing resistance of 20 kips and a friction angle of 32°, the lateral shear resistance at the tip would be 12.5 kips. Determining the axial load transferred to the tip of the soldier beam is difficult. Therefore, shear resistance at the tip of the soldier beam is not relied upon when determining the lateral capacity of a soldier beam toe.

2.5.6 Factor of Safety to Apply to the Lateral Passive Resistance of the Toe

Soil-structure interaction analyses using CBEAMC (Dawkins, 1994) were performed to guide in the selection of a factor of safety to apply to the passive resistance in the design of the embedded portion of a soldier beam. Two walls, both 25 ft high, were analyzed. A granular soil with a friction angle of 32° and a unit weight of 115 pcf was assumed. One wall consisted of HP8×36 soldier beams supported by two rows of anchors. The other wall consisted of HP12 ×53 soldier beams supported by one row of ground anchors. Soldier beams were located on 8-ft centers. Apparent earth pressures were applied to the wall. Below the bottom of the excavation, springs located every foot along the toe were used to describe the lateral resistance-deflection relationship of the soil-soldier beam system. Springs were located on the front (excavation side) and the back of the beams below the bottom of the excavation. The maximum resistance of each spring was determined using laterally loaded pile relationships developed by Wang and Reese (1986) (Chapter 3). The Wang-Reese resistances are greater than Rankine passive resistance and they have been verified for the design of cantilevered drilled shaft retaining walls. The minimum resistance of each spring equaled the Rankine active pressure over the width of the soldier beam. Spring stiffnesses were determined by assuming that the passive resistance was fully mobilized after the beam moved 0.5 in into the ground. Active pressure was assumed to be mobilized after the beam moved 0.05 in out. A detailed understanding of the Wang-Reese relationships is not necessary for determining a factor of safety to be applied to the lateral resistances. The basic principle is that the passive resistance at any depth will be fully developed when the beam moves 0.5 in into the ground.

Walls with different depths of embedment were analyzed. Mobilized passive resistance and lateral movement of the soldier beam at the bottom of the excavation were determined for depths of embedment varying from 3 to 7 ft. Table 13 presents selected results of each analyses. Available passive resistance and a factor of safety based on load are included in the table. Table 13 shows that the lateral wall movements at the bottom of the excavation were similar over a wide range of safety factors. This type of behavior is similar to that observed in sheet pile bulkheads (Rowe, 1952). Flexible sheet pile or soldier beam walls will mobilize a significant portion of the available passive resistance at shallow depths. Extending the embedment depth will not significantly reduce the lateral deflection of these types of walls.

TABLE 13
Results of Soil-structure Interaction Analyses Used to Guide the Selection of a Factor of Safety to be Applied to the Ultimate Lateral Resistance of the Embedded Portion of a Soldier Beam

WALL TYPE	EMBEDMENT DEPTH (ft)	MOBILIZED LATERAL RESISTANCE (kips)	AVAILABLE LATERAL RESISTANCE (kips)	FACTOR OF SAFETY	LATERAL MOVEMENT AT BOTTOM OF THE EXCAVATION (in)
One-tier	3	Passive resistance not adequate, no solution possible			
	4	Passive resistance not adequate, no solution possible			
	5	12.68	14.11	1.11	0.742
	6	12.41	25.22	2.03	0.638
	7	12.34	40.23	3.26	0.625
Two-tier	3	2.44	2.44	1.00	1.12
	4	4.06	6.85	1.68	0.385
	5	3.98	14.17	3.56	0.303
	6	3.90	25.00	6.41	0.286
	7	4.10	39.72	9.70	0.282

A factor of safety of 1.5 or 2.0 is applied to the passive resistance in practice today. The factor of safety is defined as the available capacity divided by the mobilized or the required capacity. The analyses show that a factor of safety of 1.5 is adequate and lateral wall movements will not be reduced significantly by increasing the factor of safety above 1.5.

2.5.7 Lateral Earth Pressures Developed at the Upper Ground Anchor

As an excavation is made to the ground anchor location, the soldier beams deflect around a point below the bottom of the excavation. When the wall deflects in this manner, active conditions are satisfied, and an active triangular distribution of pressure develops behind the wall. Ground anchor testing and stressing pulls the soldier beams into the ground, and passive pressures develop behind the beam at the anchor locations. Table 14 presents the average movement of Soldier Beams 7 to 10 and 13 to 16 into the ground during anchor testing and stressing. These movements were not large enough to fully mobilize the passive resistance of the soil behind the wall, but they were large enough to mobilize significant passive resistance.

TABLE 14
Average Wall Movements at Ground Anchor Locations After Anchor Lock-off

WALL SECTION	LOCATION	AVERAGE MOVEMENT INTO THE GROUND (in)
One-tier	Anchor	0.07
Two-tier	Upper anchor	0.12
	Lower anchor	0.10

Table 15 shows the average bending moments at the ground anchor locations after anchor lock-off and after completion of construction. These measurements show that the bending moments in the one-tier wall increased about 25 percent during construction. Smaller bending moment changes were observed in the two-tier wall during construction. The bending moment measurements at the ground anchors suggest that the moments are primarily dependent upon the applied anchor loads, and that the soldier beams distribute the anchor load to the ground. Since the beams distribute the anchor load to the ground rather than the ground loading the wall, the design earth pressure diagram must account for the development of passive pressures at the ground anchor locations.

TABLE 15
Bending Moments at the Anchor Locations After Lock-off and at the End of the Observation Period

WALL SECTION	LOCATION OF BENDING MOMENT	AVERAGE BENDING MOMENT (kip-ft)		
		After Lock-off	After Construction	Design
One-tier Wall	Anchor	95.4	120.1	110.8
Two-tier Wall	Upper anchor	46.6	47.2	35.8
	Lower anchor	30.1	26.3	45.8

Mobilized earth pressures near the upper ground anchors must exist between an active and a passive value, and give a bending moment that is equal to the measured bending moment. Figure 50 shows several earth pressure diagrams at the upper portion of the one-tier and two-tier wall sections. Active and passive earth pressures in Figure 50 are Rankine pressures times the soldier beam spacing (8 ft). (The soil has a friction angle of 32° and a unit weight of 115 pcf.) The design apparent earth pressures are the $25H$ trapezoid pressures times the beam spacing.

A triangular pressure diagram that will give a bending moment equal to the maximum measured moment is shown in each figure. The heavy curves in Figure 50 represent reasonable earth pressure distributions that will result in a bending moments equal to the maximum measured moments.

Figure 50a shows the different earth pressure diagrams for the one-tier wall. Table 15 indicates that the design bending moment is about the same as the measured bending moment. Apparently, the magnitude and the shape of the apparent earth pressure diagram predicted reasonable bending moments. Figure 50b shows the earth pressure diagrams for the two-tier wall. The design diagram for the two-tier wall was the same diagram used for the one-tier wall. Table 15 shows that the design bending moment at the upper ground anchor was less than the measured moment. Assuming the total load required to support the one- or two-tier wall sections is the same, then the shape of the diagram for the two-tier wall must be different from the diagram for the one-tier wall.

An apparent earth pressure diagram with its shape determined by the location of the supports would improve the bending moment prediction for the two-tier wall. In addition, the diagram reflects the observations that the soldier beams distribute the support loads to the ground and concentrate the pressures at the support locations. These conclusions helped guide the development of a modified trapezoidal earth pressure diagram. Earth pressures in the modified diagram increased down to a depth of two-thirds the distance to the upper anchor instead of a fixed dimension based on the height of the wall. Section 2.5.9 discusses the new diagram. Bending moments predicted using the new diagram are reasonable and appear to account for the development of the passive pressures at the ground anchor locations.

Passive earth pressures occur at the lower ground anchors too. Developing a specific pressure diagram at the lower anchor in the two-tier wall was not possible.

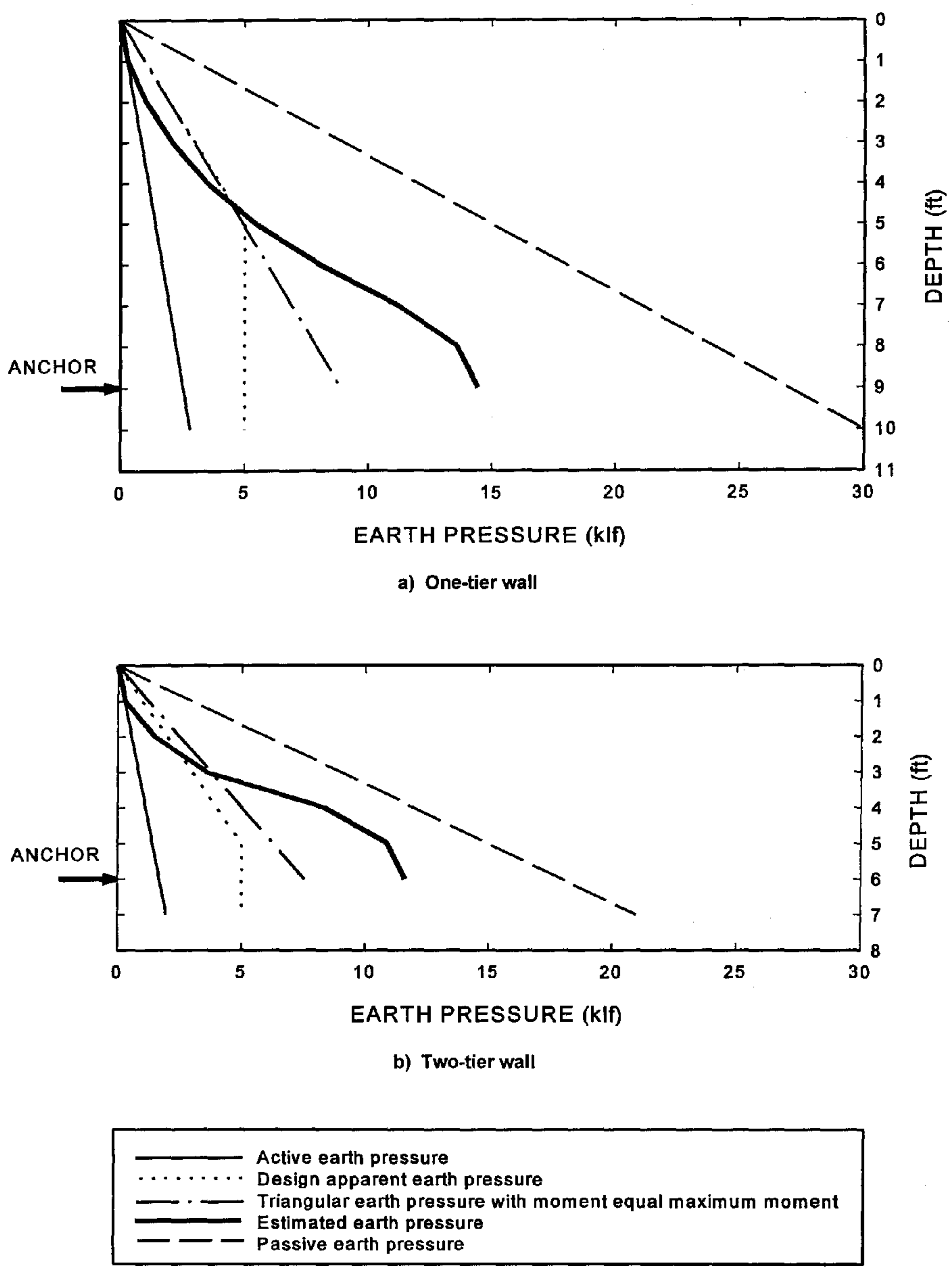

FIGURE 50
Comparison of Earth Pressure Diagrams from the Ground Surface to the Upper Anchor

Occasionally, soldier beams on a project deflect excessively back into the ground during testing of the upper ground anchor. Usually this occurs when the ground behind the upper portion of the wall has been disturbed or the ground anchor load is higher than that determined from apparent earth pressure diagrams.

Lateral movements of four soldier beams were measured during testing of the ground anchors. Drilled-in and driven HP8×36 and HP12×53 soldier beams were studied. Drilled-in beams were backfilled with a lean-mix fill. The ground anchors were at a depth of 5 ft on the HP8×36 beams and 6 ft on the HP12×53 soldier beams. Ground anchor loads were applied in six increments up to the allowable capacity of the anchor tendon. At each load increment, inclinometer reading were taken in casings installed between the flanges of the soldier beams.

Figures 51 and 52 show the net movement of the soldier beams after the full test loads were applied. Net movements were the inclinometer readings after applying the full test load minus the readings taken when the excavation was made to install the ground anchors. A maximum horizontal load of 145 kips was applied to Soldier Beam 20, the driven HP8×36 beam. A maximum load of 162 kips was applied to Soldier Beam 3 (drilled-in HP8×36), Beam 4 (drilled-in HP12×53), and Beam 19 (driven HP12×53). The HP8×36 soldier beams deflected a maximum of 0.6 in into the ground at a depth of 3 ft. The HP12×53 soldier beams deflected a maximum of 0.3 in into the ground at a depth of 5 ft. Driven and drilled-in soldier beams behaved similarly.

A soil-structure interaction analysis using CBEAMC (Dawkins, 1994) was used to predict the deflections of the soldier beams under the applied ground anchor test load. CBEAMC is a computer program that allows beams supported by a series of springs to be analyzed. In the analysis, the passive resistance behind the wall was represented by springs located every 6 in along the back of the soldier beam. The springs model the earth pressure-deflection relationship of the soil-soldier beam system. Maximum resistance of each soil spring equaled the passive resistance of the soil at each depth and the minimum resistance of the soil spring equaled the active load. Passive resistance of each spring was $K_p \gamma z s$ and the active load was $K_a \gamma z s$. K_p is a passive earth pressure coefficient, K_a is an active earth pressure coefficient, z is the depth to the spring, and s is the soldier beam spacing. Soil spring stiffnesses were determined by assuming that the passive resistance at any point was fully mobilized after the beam had deflected 0.5 in. Active load was mobilized after the beam moved out 0.05 in.

Different passive earth pressure coefficients were used in the CBEAMC analysis of the HP8×36 soldier beams in an attempt to match the measured deflections. Figure 51 shows that predicted deflections using a Rankine passive earth coefficient of 3.255 ($\phi = 32°$) were more than an order of magnitude greater than the measured deflection. The best fit between the predicted and measured deflections occurred when an earth pressure coefficient of 7.7 was used. This coefficient was selected from the plot shown in Figure 53 (NAVFAC, 1982). Deflection predictions for the HP12×53 soldier beams were made using an earth pressure coefficient of 7.7 to verify that the NAVFAC earth pressure coefficient was reasonable.

Figure 52 shows that the predicted deflections and the measured deflections for the HP12×53 beams were similar.

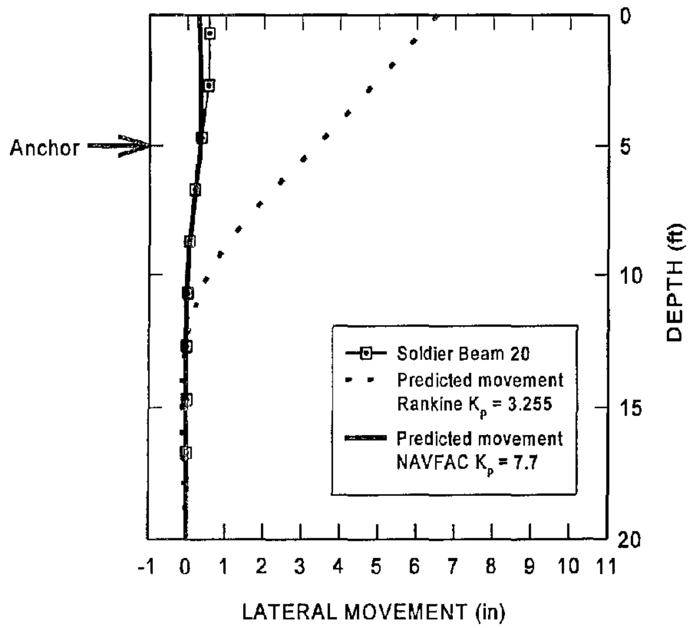

a) Horizontal load — 145 kips

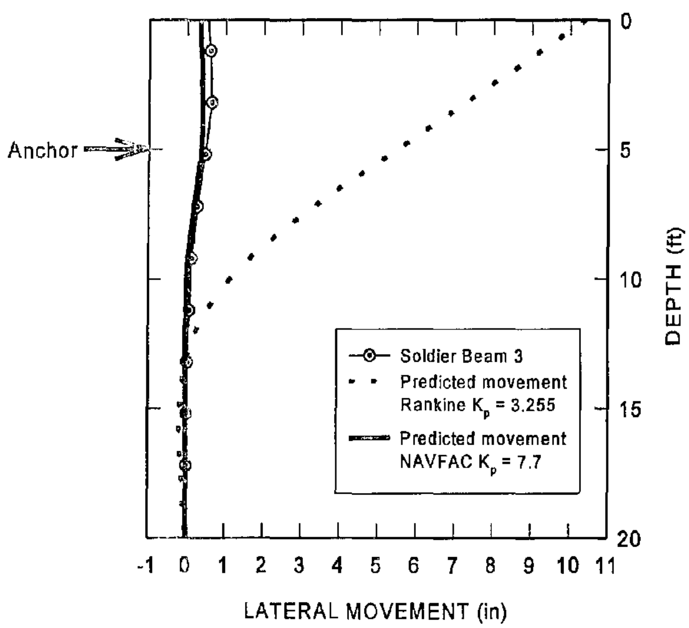

b) Horizontal load — 162 kips

FIGURE 51
Measured and Predicted Lateral Movements of the Upper Portion of Two HP8×36 Soldier Beams in Response to Ground Anchor Test Loads

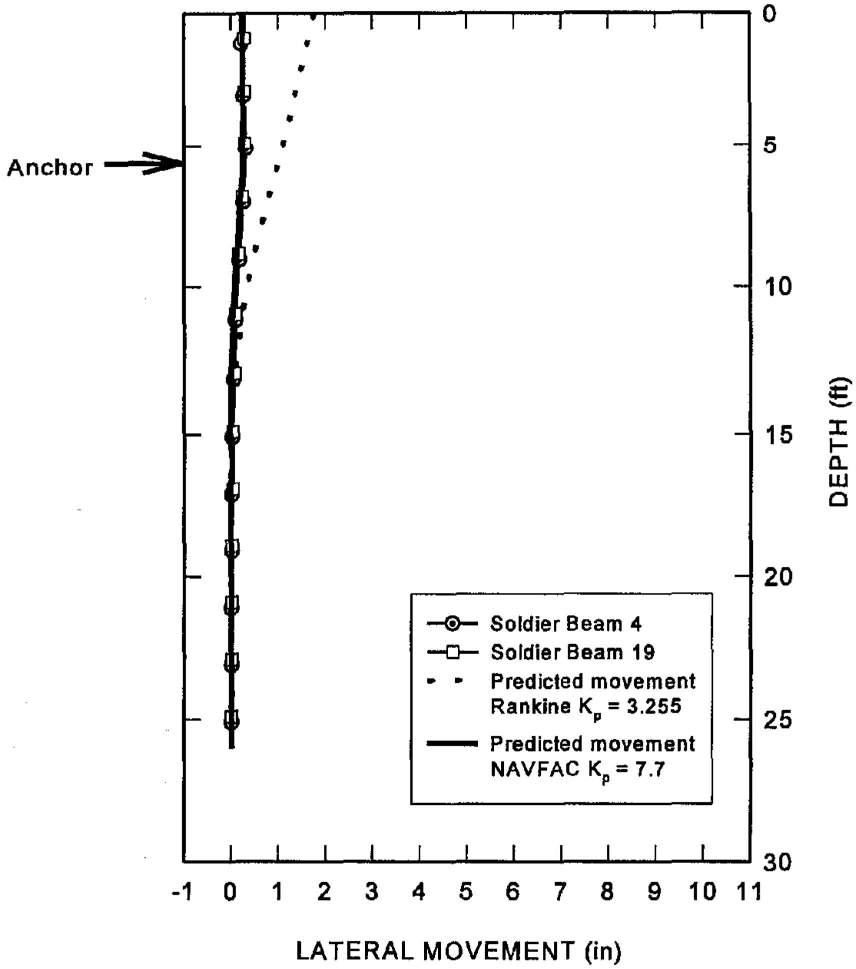

FIGURE 52
Measured and Predicted Lateral Movements of the Upper Portion of Two HP12×53 Soldier Beams in Response to Ground Anchor Test Loads

Passive resistance mobilized behind the wall during testing of the ground anchors was higher than that given by Rankine or Coulomb passive earth coefficients. Earth pressure coefficients assuming a log-spiral failure surface (NAVFAC, 1982) were appropriate for determining the lateral resistance of the soldier beams to the applied ground anchor load. Ultimate lateral resistance at any depth was the passive pressure multiplied by the soldier beam spacing.

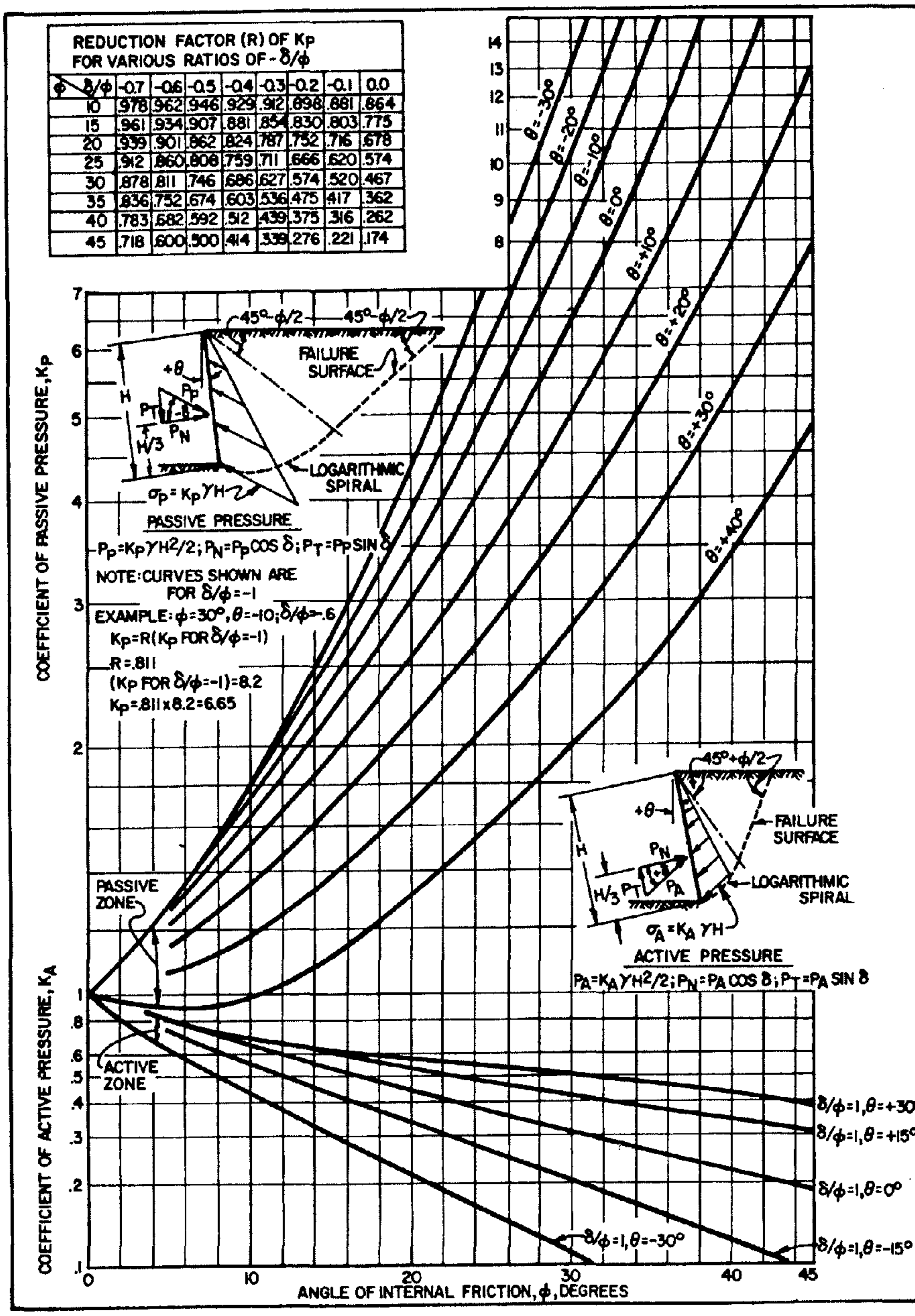

REDUCTION FACTOR (R) OF Kp FOR VARIOUS RATIOS OF -δ/φ

φ \ δ/φ	-0.7	-0.6	-0.5	-0.4	-0.3	-0.2	-0.1	0.0
10	.978	.962	.946	.929	.912	.898	.881	.864
15	.961	.934	.907	.881	.854	.830	.803	.775
20	.939	.901	.862	.824	.787	.752	.716	.678
25	.912	.860	.808	.759	.711	.666	.620	.574
30	.878	.811	.746	.686	.627	.574	.520	.467
35	.836	.752	.674	.603	.536	.475	.417	.362
40	.783	.682	.592	.512	.439	.375	.316	.262
45	.718	.600	.500	.414	.339	.276	.221	.174

FIGURE 53
Active and Passive Earth Pressure Coefficients Assuming a Logarithmic Spiral Failure Surface (NAVFAC, 1982)

Instead of using a soil-structure interaction computer solution to estimate the lateral load-carrying capacity of a soldier beam to resist the upper ground anchor load, a simple earth pressure calculation was developed. If the ultimate lateral capacity of a soldier beam is assumed to be developed over a depth of 1.5 times the distance to the upper ground anchor, then the ultimate capacity of the soldier beam would be

$$1.125 K_p \gamma H_1^2 s \qquad \ldots [2.19]$$

where K_p is given in Figure 54 and H_1 is the depth to the upper ground anchor. Equation 2.19 gives an ultimate lateral load-carrying capacity of 199 kips for the HP8×36 beams and 287 kips for the HP12×53 beams. Figure 54 shows the lateral movements predicted in CBEAMC analyses when a ground anchor load of 199 kips is applied to an HP8×36 beam and a load of 287 kips is applied to an HP12×53 beam. Maximum deflections were about 0.5 in for both beam sections. A 0.5-in deflection suggests that the passive resistance was fully mobilized. Lateral movement predictions from the soil-structure interaction analyses support the use of the earth pressure calculation for estimating the ultimate passive load-carrying capacity of a soldier beam at the upper ground anchor.

A factor of safety must be applied to the ultimate resistance to ensure that the deflections of the soldier beam are reasonable. CBEAMC analyses were used to guide the selection of the factor of safety. The ultimate lateral resistances given by Equation 2.19 were divided by different factors of safety, and CBEAMC analyses were performed using anchor loads equal to the different factored ultimate capacities. Maximum lateral movements of about 0.3 in were obtained when a factor of safety of 1.5 was used. Lateral movement curves for ground anchor loads equal to the ultimate capacities from Equation 2.19 divided by 1.5 are shown in Figure 54. Predicted lateral movements were reasonable and typical of those observed in the field.

When the sand or stiff clay apparent earth pressure diagrams are used to determine the ground anchor loads, the passive capacity of the soldier beam to resist the anchor test load does not have to be checked. However, when the ground anchor load includes surcharge, barrier, seismic, or landslide loads, then the capacity of the wall to resist the ground anchor test loads should be checked. When the ground behind the wall has been disturbed or when low-strength clays are present behind the wall, then the capacity of the wall to resist the test load should be checked. A soil-structure interaction analysis or the earth pressure calculation present in this section can be used to compute the lateral resistance of the wall to the upper ground anchor test load. When using the earth pressure calculation, the ground anchor test load should be used, and the passive resistance should be divided by a factor of safety of 1.5. When using a soil-structure interaction analysis, the fully passive resistance is used and the ground anchor test load is applied. Maximum deflections in the soil-structure interaction analysis should be less than 0.4 in to ensure an adequate factor of safety.

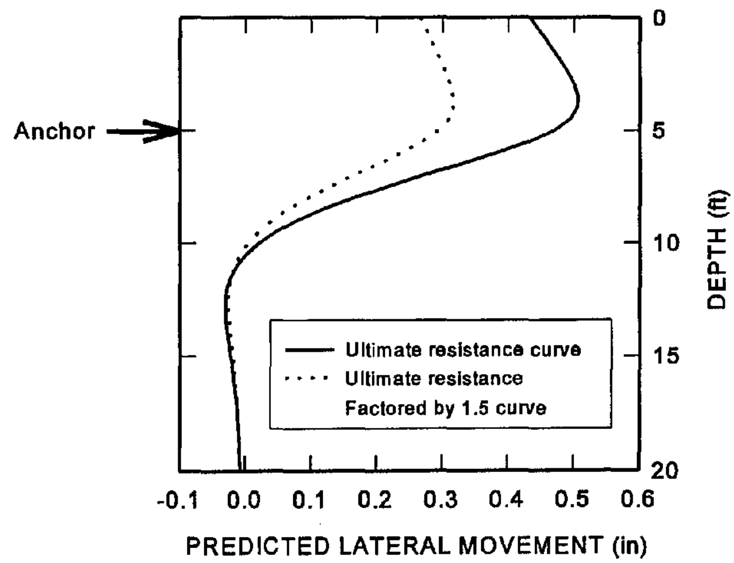

a) HP8×36 soldier beam

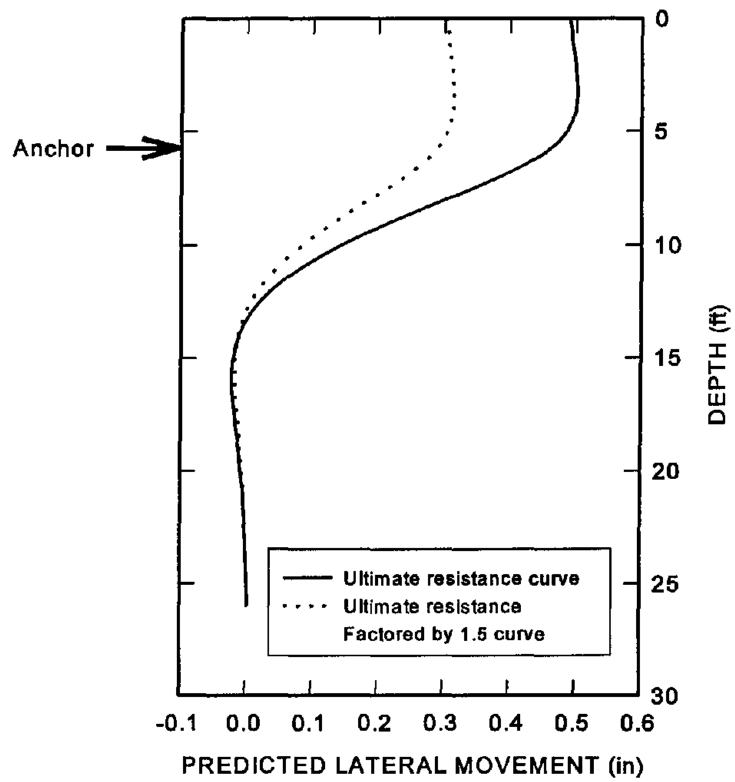

b) HP12×53 soldier beam

FIGURE 54
Predicted Lateral Movements of the Upper Portion of Two Soldier Beams in Response to Ground Anchor Loads Equal to the Ultimate Resistance from Equation 2.19 and the Ultimate Resistance Divided by a Factor of Safety of 1.5

2.5.8 Measured Bending Moments Compared with Predicted Moments

The actual bending moments in a soldier beam or wall depend upon the design earth pressures, the stiffness of the soldier beam or wall, the ground anchor load, and the strength of the supported ground. Apparent earth pressure diagrams are used to design flexible soldier beam walls supported by struts or ground anchors. Chapter 2 of *Summary Report of Research on Permanent Ground Anchor Walls*, "Volume I — Current Practice and Limiting Equilibrium Analyses" (Long, et al., 1998) discusses apparent earth pressure diagrams in detail. These diagrams were derived from measured strut loads and they are envelopes that include all the measured loads. Support forces and bending moments determined from apparent earth pressure diagrams include a factor of safety. The factor of safety inherent in the apparent earth pressure diagrams is discussed in Chapter 3 of the *Summary Report of Research on Permanent Ground Anchor Walls*, "Volume I — Current Practice and Limiting Equilibrium Analyses" (Long, et al., 1998).

Apparent earth pressure diagrams predict the location and the magnitude of the support forces because the diagrams were derived from measured strut loads. Figure 55 shows the two methods used to estimate the support loads. The "tributary area method" assumes that the support force is equal to the area of the wall supported by the ground anchor times the earth pressure. The "hinge method" places hinges at lower supports and subgrade. Then the simple beams are analyzed to determine the support loads.

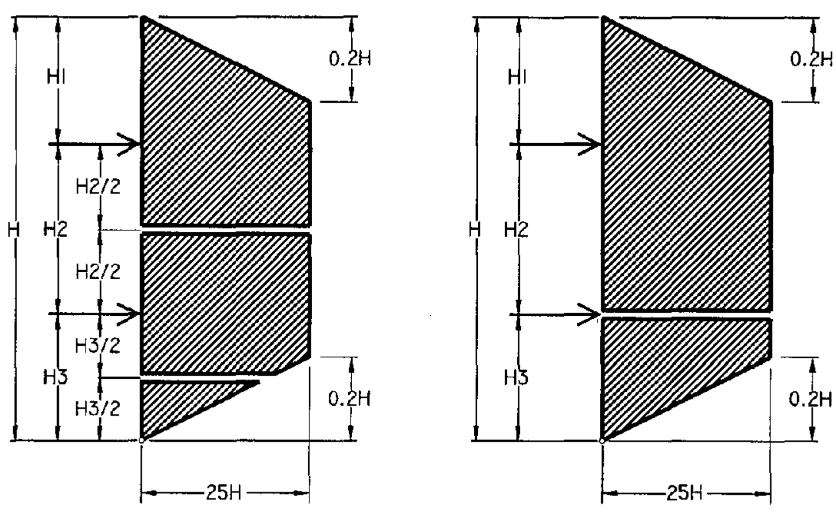

a) Tributary area method

b) Hinge method

FIGURE 55
Methods Used to Calculate Ground Anchor Loads from Apparent Earth Pressure Diagrams

Apparent earth pressure diagrams are used to estimate the magnitude of the cantilever moment, the moment at the upper support. They also predict the magnitude of the maximum bending moments below the upper support, but they may not predict the locations of the maximum bending moments below the upper support. Peck, et al. (1974) recommended that the maximum bending moment below the cantilever equal 0.1 wl^2, where w is the intensity of the earth pressure diagram and l is the spacing between the supports. Peck, et. al. (1974) also state that the wall or soldier beams may be designed to resist moments equal to two-thirds the moments calculated from the apparent earth pressure diagrams. Schnabel (1982) uses a trapezoidal apparent earth pressure diagram with the intensity of the earth pressure equal to $25H$. Schnabel uses the hinge method to determine support loads and estimate the magnitude of the maximum bending moments. Tschebotarioff (1979) uses a trapezoidal apparent earth pressure diagram with an intensity of $25\gamma H$. Except in soft soils, soldier beams are assumed to be hinged at the bottom of the excavation. However, in soft clays where the failure surface extends well below the bottom of the excavation, the soldier beams are considered continuous over the supports and the moment reduction is not taken.

Bending moment diagrams for the one-tier wall at Texas A&M were developed using Terzaghi, et al. (1996), Tschebotarioff (1979), Schnabel (1982), FHWA (Cheney, 1988), and American Association of State and Highway Transportation Officials' (AASHTO, 1996) recommendations. Terzaghi, Tschebotarioff, and Schnabel's pressure diagrams are referred to as apparent earth pressure diagrams. The computed bending moment diagrams for all five diagrams are shown in Figure 56. Earth pressure diagrams for each recommendation are shown in Figure 57. Average measured bending moments for Soldier Beams 15 and 16 also are shown in Figure 56. The solid symbols in Figure 56 represent the moments calculated using the tributary area method. Table 16 compares the support loads and moments for the various pressure diagrams using the tributary area method, the hinge method, and the measured results.

The FHWA and AASHTO earth pressure diagrams for one-tier walls use triangular pressure distributions. Triangular pressure diagrams give very large bending moments between the ground anchor and subgrade. These moments are six times the measured moments, and three times the moments calculated from the apparent earth pressure diagrams. FHWA and AASHTO design procedures also assume that the beam is continuous while the apparent earth pressure diagrams assume a hinge at subgrade. Subgrade bending moments calculated using the triangular pressure distributions and a continuous beam are 11 times greater than the measured moments. Experience with anchored bulkheads with fixed supports (Rowe, 1952) and strutted excavations (Terzaghi, et al. 1996) have shown that the deformation conditions required for a triangular earth pressure distribution do not occur with walls supported by ground anchors.

The maximum bending moments predicted by the three apparent earth pressure diagrams were at the ground anchor locations. The actual maximum bending moment occurred there too. At the conclusion of the 84-day observation period, the measured bending moment was 120.73 kip-ft, while the design moment at the support was 110.83 kip-ft. Differences between the design moment and the actual moment reflect the response of the beam to the ground anchor load rather than the earth pressures applied to the wall.

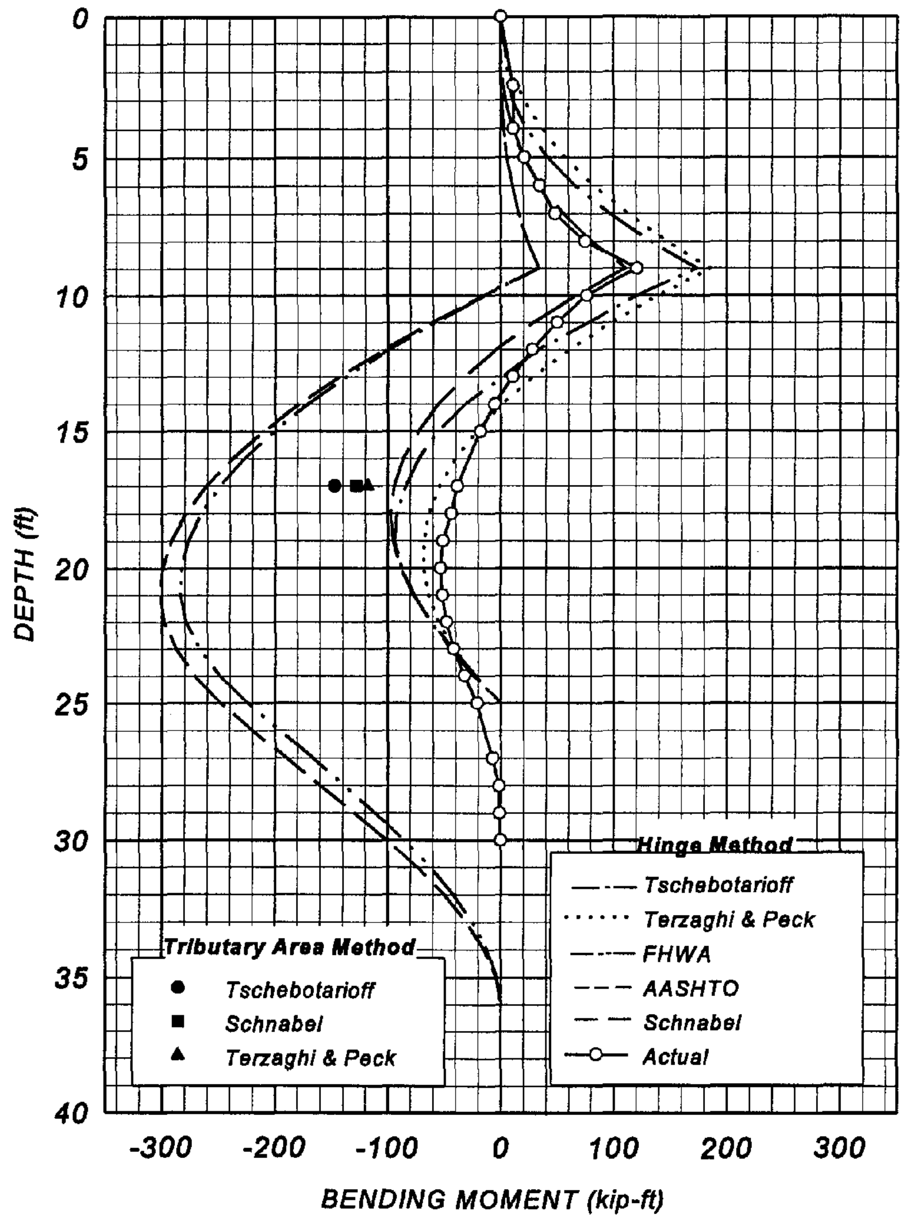

FIGURE 56
Predicted Versus Measured Moments in the One-tier Wall

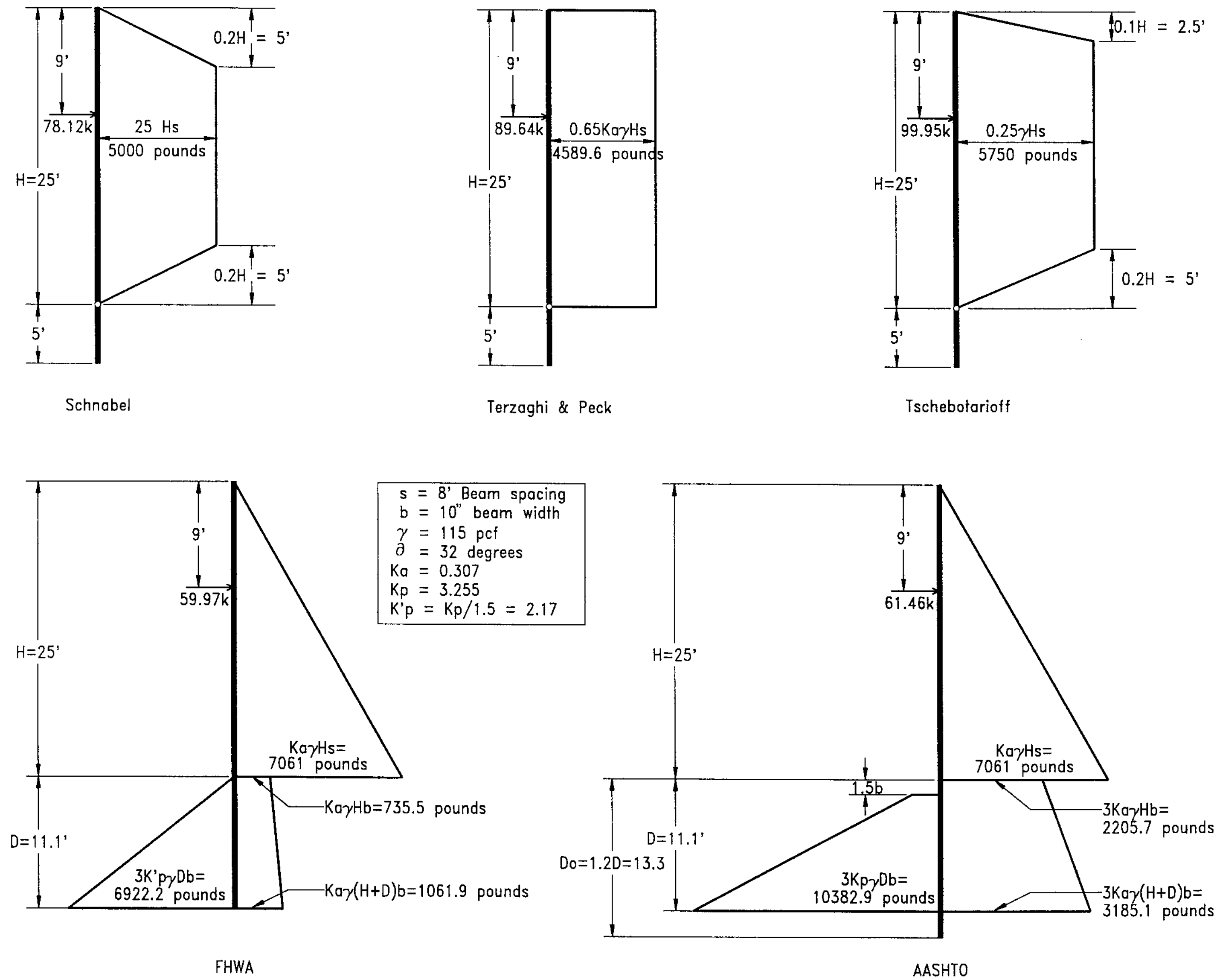

FIGURE 57
One-tier Wall Earth Pressure Diagrams

Table 16 shows that the hinge method more accurately predicts the bending moments than the tributary area method. Ground anchors supporting Beams 15 and 16 were intentionally locked-off at a load giving a horizontal result of 59 kips. This load was 75 percent of the horizontal component of the design load, 78.12 kips. The horizontal component of the ground anchor load increased to 62.69 kips (80 percent of the design load) at the conclusion of the 84-day observation period.

TABLE 16
Comparison of Anchor Loads and Bending Moments for One-tier Wall

		HORIZONTAL COMPONENT OF ANCHOR (kips)	CANTILEVER MOMENT (kip-ft)	MAXIMUM MOMENT BELOW ANCHOR (kip-ft)
Actual		62.69	120.73	-53.22
Hinge Method	Schnabel (25*H*)	78.12	110.83	-97.29
	Terzaghi & Peck ($0.65K_a\gamma H$)	89.64	185.87	-68.12
	Tschebotarioff ($0.25\gamma H$)	99.95	174.18	-94.17
	FHWA	59.97	34.32	-283.66
	AASHTO	61.46	34.32	-301.56
Tributary Area Method	Schnabel (25*H*)	72.50	110.83	-128.00
	Terzaghi & Peck ($0.65K_a\gamma H$)	78.03	185.87	-117.50
	Tschebotarioff ($0.25\gamma H$)	90.56	174.18	-147.20

The bending moment behavior of the one-tier beams at Texas A&M indicate that:

- Apparent earth pressure diagrams developed from measured strut loads satisfactorily predict the bending moments for the design of one-tier anchored walls.
- Assuming a hinge at subgrade gives a conservative prediction of the magnitude and distribution of the bending moments between the ground anchor and subgrade.
- Bending moments below the upper support are approximately two-thirds the values computed from apparent earth pressure diagrams.
- Apparent earth pressure diagrams give a reasonable distribution of the bending moments for the one-tier wall.
- Maximum bending moments occurred at the ground anchor location.
- Bending moments at the ground anchor location are a response of the soldier beam to the applied ground anchor load.
- Bending moments below the ground anchor location are a result of the applied earth pressures.
- The hinge method predicts the bending moments and anchor load satisfactorily.
- Bending moments in the toe are small.

Bending moment diagrams for the two-tier wall at Texas A&M were computed using Terzaghi, et al. (1996), Tschebotarioff (1979), Schnabel (1982), FHWA (Cheney, 1988), and AASHTO's (1996) recommendations. The computed bending moments for all five earth pressure diagrams are shown in Figure 58. Earth pressure diagrams for each of the pressure recommendations are shown in Figure 59 Average measured bending moments for Soldier Beams 7 and 8 also are shown in Figure 58. The solid symbols in Figure 58 represent the lower moments calculated using the tributary area method. Table 17 compares the support loads and moments determined using the tributary area method, and the hinge method with the measured results.

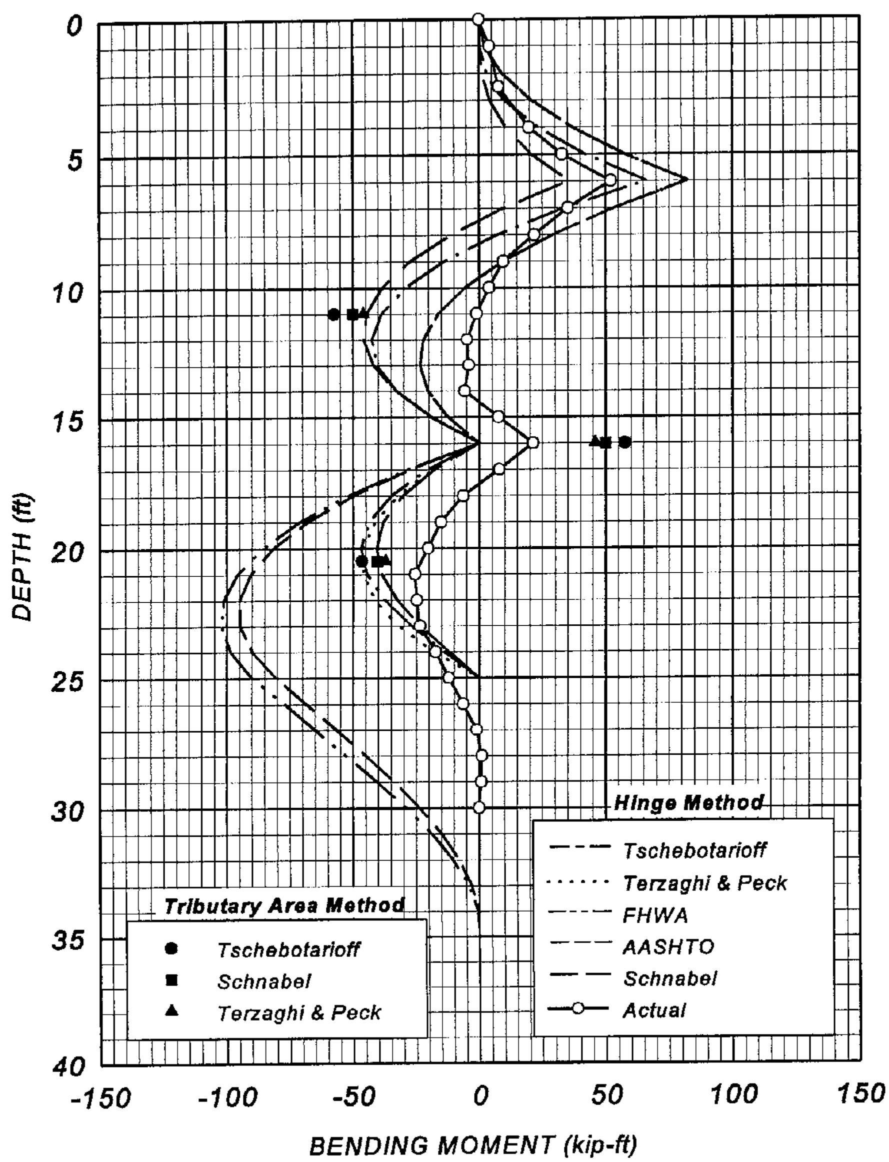

FIGURE 58
Predicted Versus Measured Moments in the Two-tier Wall

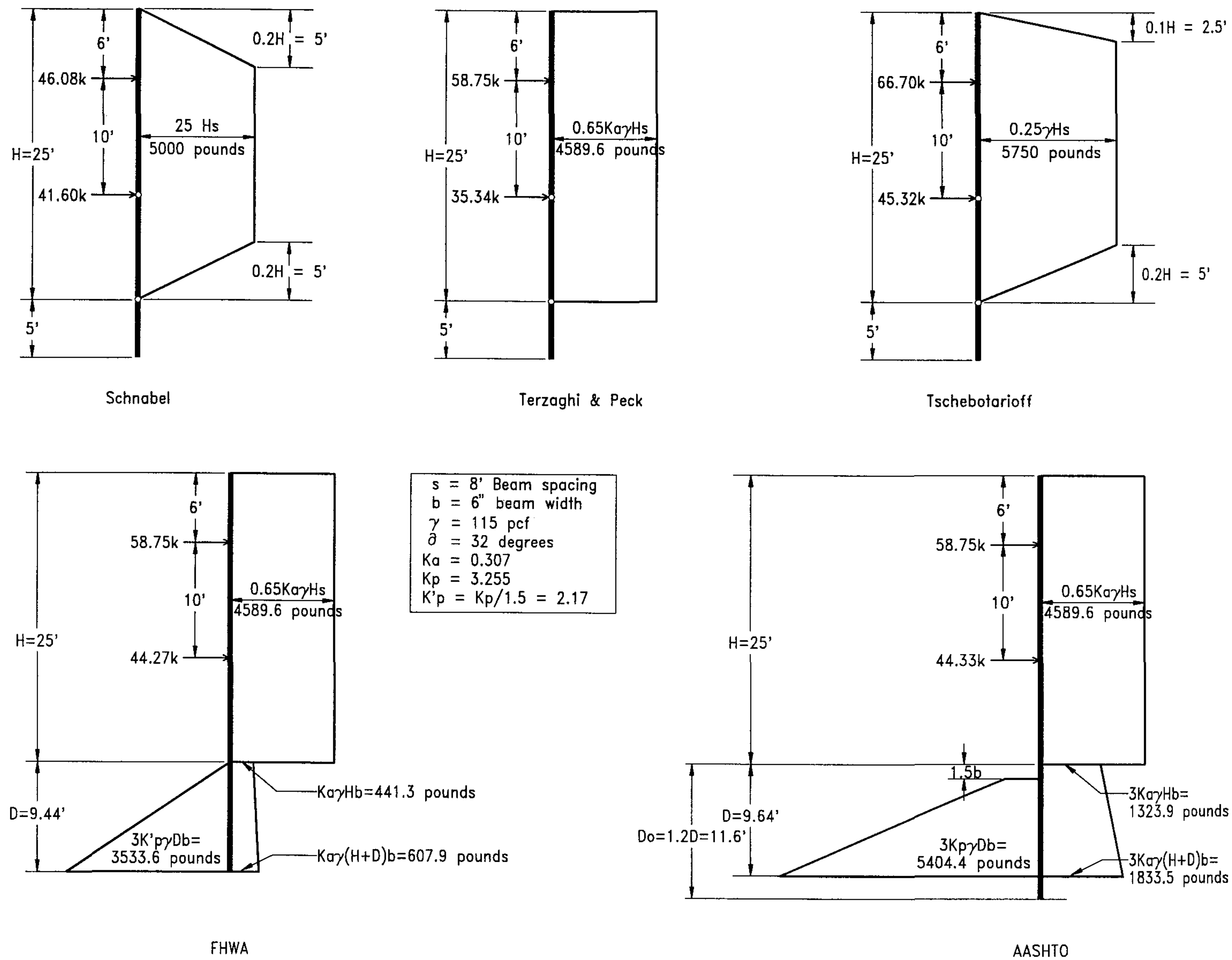

FIGURE 59
Two-tier Wall Earth Pressure Diagrams

The FHWA and AASHTO earth pressure diagrams for multi-tier walls use the Terzaghi and Peck apparent earth pressure diagram above subgrade. They also assume that the beam is continuous, rather than hinged, at subgrade. The apparent earth pressure diagrams for two-tier walls are identical to the diagrams used for one-tier walls. The bending moment curves for the apparent earth pressure diagrams were developed using the hinge method. The hinge method was used to develop the moment diagrams since each segment of the soldier beam satisfies force and moment equilibrium. As described above, the soldier beam is broken up into simple beams segments with hinges at the lower anchor and at subgrade. In Figure 58, the solid symbols represent the maximum moments calculated using the tributary area method. When using the tributary area method the maximum positive and negative moments are equal to $0.1wl^2$.

Bending moment curves developed for the two-tier wall using FHWA and AASHTO recommendations show large moments between the lower ground anchor and subgrade. These moments are approximately four times the maximum measured moments in the beams at that location, and twice the moments predicted by the apparent earth pressure diagrams. FHWA and AASHTO design procedures predict large moments because the soldier beam is analyzed as a continuous beam at the toe. Bending moments calculated using the apparent earth pressure diagrams assume a hinge at subgrade. This assumption reduces bending moments and forces the moments to more closely model the measured moments. The maximum measured moment below the upper ground anchor was 25.48 kip-ft. This moment was approximately two-thirds the maximum moment predicted by the apparent earth pressure diagrams.

The maximum measured bending moment occurred at the upper support. At the conclusion of the 84-day observation period, the measured bending moment was 52.09 kip-ft, while the design moment at the upper support was 35.83 kip-ft. As indicated above, the difference between the design moment and the actual moment reflect the response of the beam to the ground anchor load rather than the earth pressures applied to the wall.

Table 17 shows that the hinge method or the tributary area method predicted similar bending moments. However, the bending moment at the lower anchor is zero for the hinge method. The upper ground anchor supporting Beams 7 and 8 was intentionally locked-off at a load giving a horizontal resultant of 34.6 kips. This load was 75 percent of the horizontal component of the design load, 46.08 kips. The horizontal component of the upper ground anchor load increased to 35.39 kips (76.8 percent of the design load) at the conclusion of the 84-day observation period. The lower row anchor supporting Beams 7 and 8 was locked-off at a load with a horizontal component of 31.2 kips. This load was 75 percent of the horizontal component of the design load, 41.6 kips. At the end of the observation period the horizontal component of the ground anchor force had dropped to 25.53 kips (61 percent of the design load).

The bending moment behavior of the two-tier beams at Texas A&M indicate that:

- Apparent earth pressure diagrams developed from measured strut loads satisfactorily predict the bending moments for the design of two-tier anchored walls.

- Assuming a hinge at subgrade gives a conservative prediction of the magnitude and distribution of the bending moments between the ground anchor and subgrade.
- Bending moments below the upper support are approximately two-thirds the values computed from apparent earth pressure diagrams.
- Apparent earth pressure diagrams predict reasonable maximum bending moments for a two-tier wall.
- Maximum bending moments occurred at the upper ground anchor location.
- Bending moments at the ground anchors are the responses of the soldier beams to the applied ground anchor loads.
- Bending moments between the ground anchors are the result of the applied earth pressures.
- The hinge method or the tributary area method will satisfactorily predict the anchor loads and the bending moments.
- Bending moments in the toe are small.

TABLE 17
Comparison of Anchor Loads and Bending Moments for Two-tier Wall

		HORIZONTAL COMPONENT OF UPPER ANCHOR FORCE (kips)	CANTILEVER MOMENT (kip-ft)	MAXIMUM MOMENT BETWEEN ANCHORS (kip-ft)	HORIZONTAL COMPONENT OF LOWER ANCHOR FORCE (kips)	MOMENT AT LOWER ANCHOR (kip-ft)	MAXIMUM MOMENT BETWEEN LOWER ANCHOR & SUBGRADE (kip-ft)
Actual		70.79/2 = 35.39	52.09	-5.76	51.07/2 = 25.53	21.33	-25.48
Hinge Method	Schnabel (25*H*)	46.08	35.83	-45.67	41.60	0.00	-40.74
	Terzaghi & Peck ($0.65K_a\gamma H$)	58.75	82.61	-23.41	35.34	0.00	-45.90
	Tschebotarioff ($0.25\gamma H$)	66.70	66.36	-42.46	45.32	0.00	-46.85
	FHWA	58.75	82.61	-23.41	44.27	0.00	-94.87
	AASHTO	58.75	82.61	-23.41	45.33	0.00	-102.02
Tributary Method	Schnabel (25*H*)	42.50	35.83	-50.00	47.38	50.00	-40.50
	Terzaghi & Peck ($0.65K_a\gamma H$)	50.49	82.61	-45.90	43.60	45.90	-37.18
	Tschebotarioff ($0.25\gamma H$)	56.06	66.32	-57.50	54.48	57.50	-46.58

2.5.9 The Shape of the Apparent Earth Pressure Diagrams

Results from the analyses presented in Sections 2.5.7 and 2.5.8 suggest that the apparent earth pressure diagram should be trapezoidal in shape. Section 2.5.7 showed that the earth pressures start at zero at the ground surface and increase to a point above the upper ground anchor. Section 2.5.8 showed that the bending moments predicted by the trapezoidal diagrams were the most realistic. Section 2.5.8 also showed that the predicted bending moments from the design diagram (25*H* trapezoid) at the upper anchor in the two-tier wall were less than the measured moments. Measured bending moments were less than the predicted moments because the shape of the design earth pressure diagram was determined by the height of the cut rather than the location of the ground anchors. If the shape of the apparent earth pressure diagram had been determined by the ground anchor locations rather than the height of the wall, the predicted bending moments would have been closer to the measured moments. Several different trapezoidal diagrams were investigated. The total load for each diagram was the same as that given by the design diagram. The apparent earth pressure diagrams shown in Figure 60 gave bending moment predictions close to the measured moments and predicted ground anchor load similar to the design anchor loads for both the one-tier and the two-tier wall.

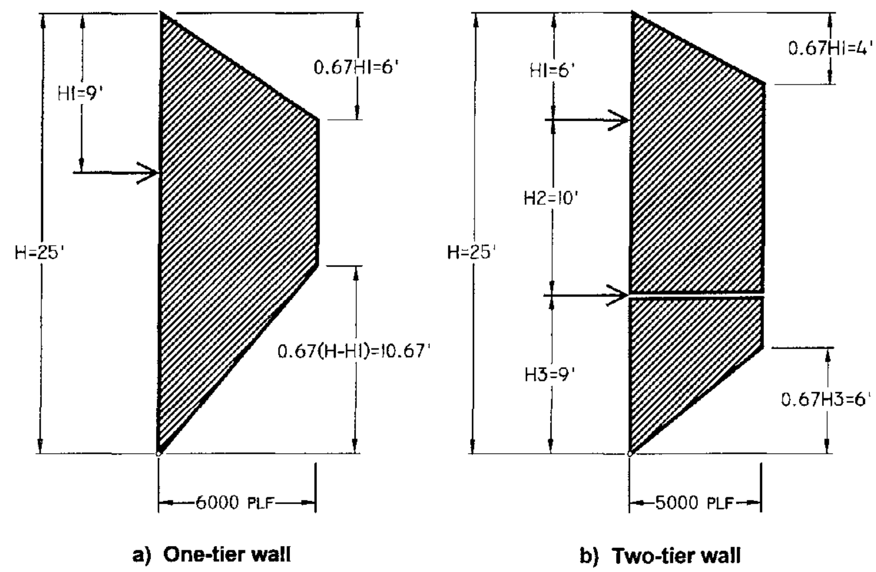

FIGURE 60
Trapezoidal Apparent Earth Pressure Diagram with Shape Determined by Anchor Locations

Earth pressures in the diagrams shown in Figure 60 increase to a maximum at a depth equal to two-thirds the distance to the upper ground anchor. For a wall supported by one row of anchors, the maximum pressure continues downward for a distance equal to one-third the height of the wall. Below that depth, the pressure decreases linearly to zero at the bottom of the excavation. For a wall supported by two or more rows of ground anchors, the maximum earth pressure continues to a point below the lowest support equal to one-third the distance from the lowest support to the bottom of the excavation. From there the pressure decreases linearly to zero at the bottom of the excavation. The total load in both earth pressure diagrams is the same.

Figure 61 shows the design bending moment diagram, the bending moment diagram for the new apparent earth pressure diagram, and the average measured bending moments in Soldier Beams 15 and 16. The figure shows that the bending moments predicted from the new diagram matched the measured bending moments better than the design diagram. Table 18 shows the actual ground anchor load, the design ground anchor load, and the anchor load from the new diagram. Table 18 shows that both diagrams give reasonable ground anchor load predictions.

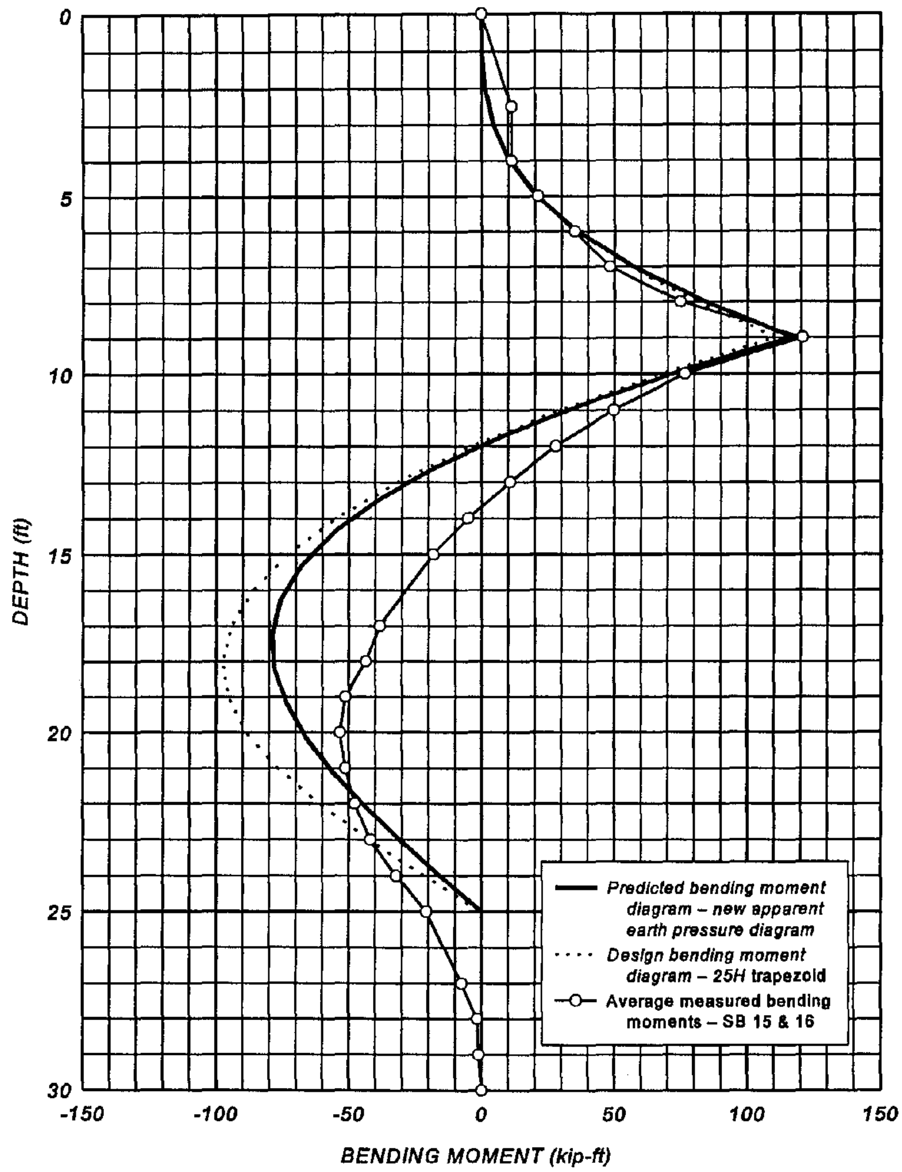

FIGURE 61
Comparison of the Average Bending Moments in Soldier Beams 15 and 16 with the Design Moment Diagram and the Moment Diagram Predicted from the Modified Trapezoidal Apparent Earth Pressure Diagram

TABLE 18
Comparison of the Average Horizontal Component of the Ground Anchor Load for Soldier Beams 15 and 16 with the Design Anchor Load and the Anchor Load Predicted from the Modified Trapezoidal Apparent Earth Pressure Diagram

	ANCHOR LOAD (kips)
Actual	62.69
Design Pressure Diagram	78.12
New Apparent Earth Pressure Diagram	84.20

Figure 62 shows the design bending moment diagram, the bending moment diagram for the new apparent earth pressure diagram, and the average measured bending moments for Soldier Beams 7 and 8. Table 19 shows the actual ground anchor loads, the design ground anchor loads, and the anchor loads from the new apparent earth pressure diagram. Bending moment diagrams and anchor loads were developed using the hinge method. Figure 62 shows that the new apparent earth pressure diagram predicts a higher bending moment at the upper ground anchor than the design pressure diagram (25*H* trapezoid). The predicted bending moment at the upper ground anchor was 43.33 kip-ft for the new diagram and 35.83 kip-ft for the design diagram (25*H* trapezoid). Maximum predicted bending moment below the upper anchor was 42.66 kip-ft for the new pressure diagram compared with 45.66 kip-ft for the design pressure diagram (25*H* trapezoid). Table 19 shows that both the design diagram and the new apparent earth pressure diagram would be satisfactory for determining the ground anchor loads.

TABLE 19
Comparison of the Average Horizontal Component of the Ground Anchor Loads for Soldier Beams 7 and 8 with the Design Anchor Loads and the Anchor Loads Predicted from the Modified Trapezoidal Apparent Earth Pressure Diagram

	ANCHOR LOAD (kips)	
	Upper Anchor	Lower Anchor
Actual	35.40	25.56
Design Pressure Diagram	46.08	41.60
New Apparent Earth Pressure Diagram	49.33	39.84

Bending moments and ground anchor loads determined from a trapezoidal earth pressure diagram with the shape determined by the location of the ground anchors reflects the behavior of flexible soldier beam walls. This diagram will give reasonable bending moment and ground anchor load predictions.

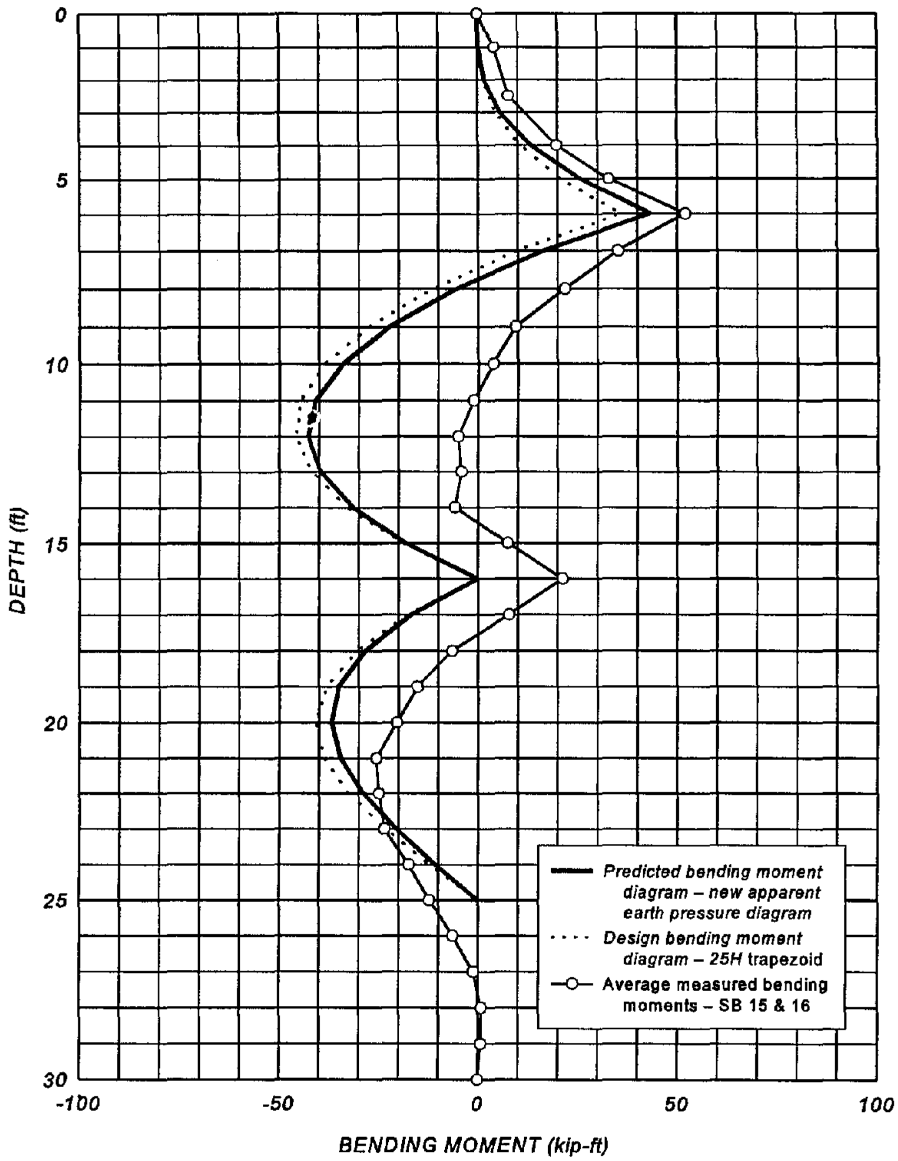

FIGURE 62
Comparison of the Average Bending Moments for Soldier Beams 7 and 8 with the Design Moment Diagram and the Moment Diagram Predicted from the Modified Trapezoidal Apparent Earth Pressure Diagram

2.5.10 Eccentric Ground Anchor Connections (Sidewinder Connections)

Ground anchor to soldier beam connections have been made where the ground anchor load is installed eccentrically to the soldier beam. These connections are called "sidewinder connections" because they can twist the soldier beam. A sidewinder connection was installed in Soldier Beam 21, an HP10×42 section. The ground anchor connection was fabricated so the ground anchor load would be applied a distance of 2 in from the web of the beam. The connection was 5 ft down from the top of the soldier beam.

The ground anchor was loaded in six increments up to 133 kips. Rotation of the soldier beam at the anchor location was measured using a pair of dial gauges. Table 20 gives the angular rotation of the soldier beam at each load increment.

TABLE 20
Rotation of an HP10×42 Soldier Beam During Testing of an Eccentric Ground Anchor

TEST LOAD (kips)	ROTATION (deg)
25	0.07
50	0.22
75	0.50
100	0.93
120	1.38
133	2.16

Rotation of the soldier beam causes torsional stresses to develop, and the extreme fiber stress in the flanges of the soldier beams will be the sum of the torsional stress plus the bending stress. Since the bending stresses are high at the ground anchor locations, the torsional stresses can be important.

Torsional stresses were determined assuming that the soldier beam is fixed at some depth below the eccentric connection. The torque caused by the eccentric, ground anchor load was computed from the measured rotation angle using

$$T = \frac{\Theta J G}{l - a \tanh\left(\frac{l}{a}\right)} \qquad \text{. . . [2.20]}$$

where:

T = torque
Θ = rotation angle in radian
J = polar moment of inertia
G = shear modulus of elasticity
l = distance from ground anchor to point of fixity
$a = \frac{h}{2}\sqrt{\frac{EI_{yy}}{JG}}$
h = beam depth less flange thickness
E = modulus elasticity
I_{yy} = moment of inertia around y-y axis

The couple, due to the eccentric ground anchor load, creates a moment in each flange of the soldier beam. The moment is

$$M_{max} = \left(\frac{T}{h}\right) a \tanh\left(\frac{l}{a}\right) \qquad \ldots [2.21]$$

The tensile and compressive stresses developed in each flange by the moment are

$$\sigma = \frac{M_{max}\frac{b}{2}}{\frac{1}{12} t b^3} \qquad \ldots [2.22]$$

where:

b = flange width
t = flange thickness

Equations 2.20 through 2.22 were used to determine the stresses that developed when a 100-kip ground anchor load was applied. Figure 63 shows the variations in torsional stresses depending upon the point of fixity. Bending moment measurements on Soldier Beams 7 to 10 and 13 to 16 indicate that the bending moments were approaching zero between 5 and 6 ft below the ground anchor elevation when the ground anchor was loaded. Assuming the soldier beam was fixed at a location of 5 ft, then the extreme fiber stress would be about 10 ksi. The actual point of fixity is unknown. This stress is 50 percent of the allowable extreme fiber stress on a Grade 36 soldier beam and 37 percent of the allowable extreme fiber stress on a Grade 50 soldier beam.

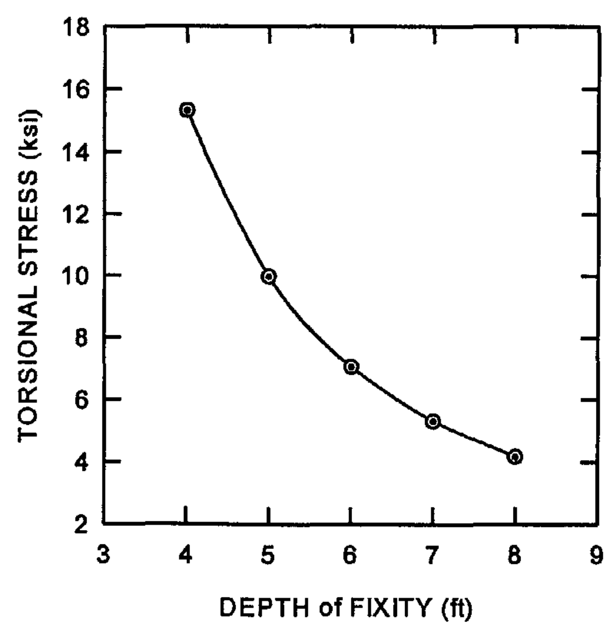

FIGURE 63
Predicted Torsional Stresses in an HP10×42 Soldier Beam with a Sidewinder Ground Anchor Connection

This analysis shows why eccentric ground anchor connections have performed poorly on some projects. Details to resist these torsional stresses may be developed so sidewinder connections can be used in the future. Until then they should be avoided. Eccentric connections would be advantageous for projects where large-diameter ground anchors are used or when additional ground anchors have to be installed.

2.5.11 Effect of Reducing the Load in Two Ground Anchors

The load was reduced on the upper ground anchor supporting Soldier Beams 7 and 8, and the ground anchor supporting Soldier Beam 15. Instrumentation readings were taken just before reducing the load, just after the load was reduced, and 347 days after the load was reduced.

2.5.11.1 Two-tier Wall

The load on the upper ground anchor supporting Soldier Beams 7 and 8 was reduced from 81.8 kips to 34.8 kips. Figure 64 shows the bending moments in Soldier Beams 7 and 8 and the moments in Soldier Beam 9. Bending moments in Soldier Beams 7 and 8 changed in response to the load reduction, but the moments in Beam 9 did not change. The moments at the upper and lower ground anchors on Beams 7 and 8 decreased in response to the load reduction. Bending moments in the span between the upper and lower anchor on Soldier Beams 7 and 8 increased.

Figure 65 shows the lateral movement of Soldier Beams 8 and 9 in response to the load reduction. Inclinometer readings could not be obtained for Soldier Beam 7. Lateral movement patterns for Soldier Beams 8 and 9 were similar. Lateral movements for Beam and 8 increased 7 percent when the load was reduced. After 347 days, the lateral wall movements had increased a total of 22 percent. Beam 9 moved a smaller amount.

Table 21 presents the ground anchor loads on Soldier Beams 7, 8, and 9. It shows that the load in the lower ground anchor supporting Soldier Beams 7 and 8 changed very little as the load in the upper anchor was reduced. The table also shows that the load in the ground anchors supporting Soldier Beam 9 was not affected by reducing the load in the upper anchor supporting Beams 7 and 8. The total lateral load in the anchors supporting Soldier Beams 7 to 9 was about 18 percent less after the 347-day period than it was before the load reduction.

Table 22 shows the axial load in Soldier Beams 7, 8, and 9 below the bottom of the excavation. Axial load in Soldier Beams 7 and 8 decreased as the load in the anchor was released. The reduction in the axial load was less than the reduction in the vertical component of the ground anchor load. Axial load in Beam 9 increased about 15 percent as the load was reduced.

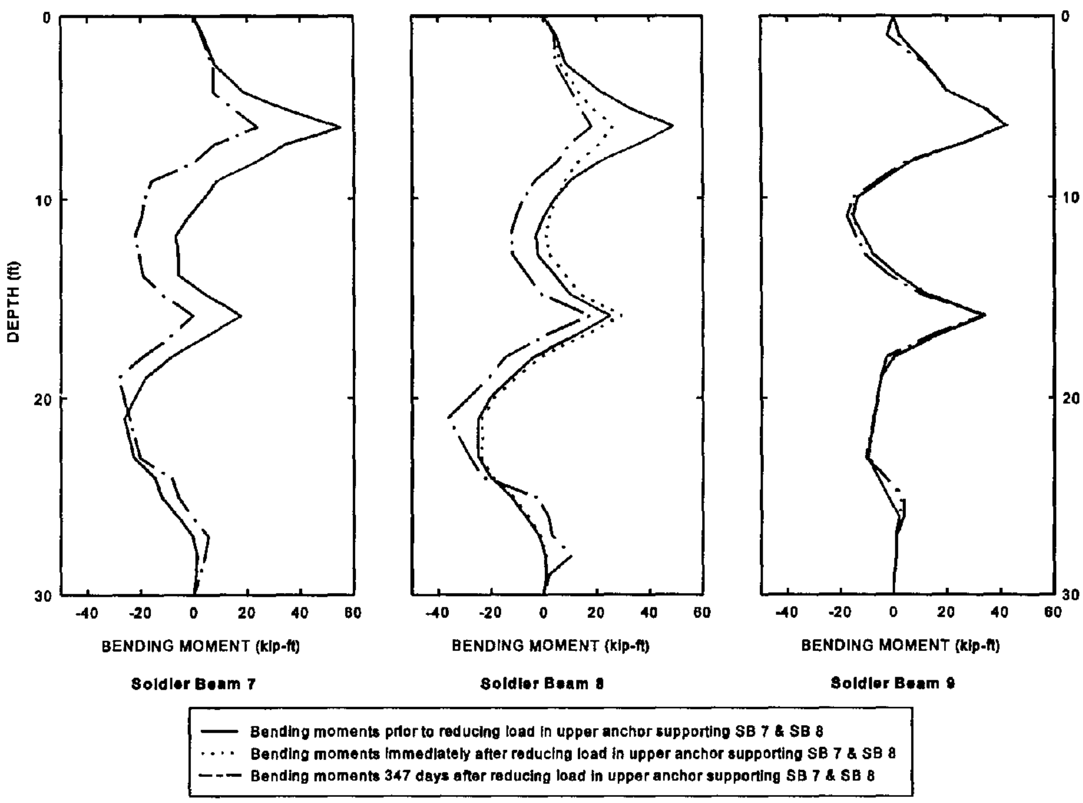

FIGURE 64
Bending Moment in Soldier Beams 7, 8, and 9 Before and After the Load in the Upper Ground Anchor Supporting Soldier Beams 7 and 8 Was Reduced

TABLE 21
Ground Anchor Loads on Soldier Beams 7, 8, 9, 14, 15, and 16 After Reducing the Load in Two Ground Anchors

SOLDIER BEAM NO.	ANCHOR LOCATION	ANCHOR LOAD (kips)		
		Before Load Reduction	After Load Reduction	347 Days After Load Reduction
7	Upper	40.9	17.4	19.2
	Lower	29.5	31.0	29.8
8	Upper	40.9	17.4	19.2
	Lower	29.5	31.0	29.8
9	Upper	49.7	50.7	50.0
	Lower	39.6	39.5	39.7
14	—	80.9	82.2	85.6
15	—	74.5	30.0	41.8
16	—	70.3	77.0	77.4

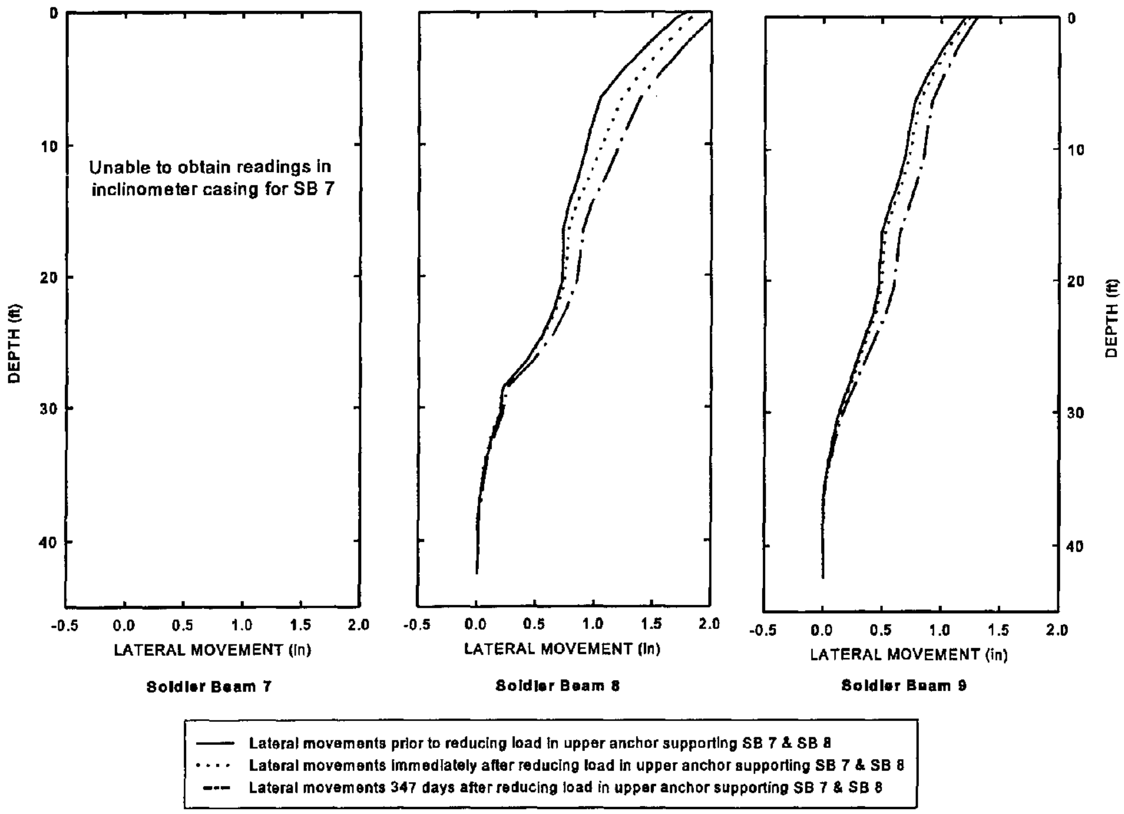

FIGURE 65
Lateral Movement in Soldier Beams 8 and 9 Before and After the Load in the Upper Ground Anchor Supporting Soldier Beams 7 and 8 Was Reduced

TABLE 22
Axial Load in Soldier Beams 7, 8, 9, 14, 15, and 16 After Reducing the Load in Two Ground Anchors

SOLDIER BEAM NO.	AXIAL LOAD (kips)		
	Before Load Reduction	After Load Reduction	347 Days After Load Reduction
7	22.71	13.47	30.75
8	19.91	21.61	45.32
9	52.47	54.67	60.74
14	54.76	56.80	61.70
15	44.78	33.00	39.94
16	38.20	40.89	41.68

2.5.11.2 One-tier Wall

The load in the ground anchor supporting Soldier Beam 15 was reduced from 74.5 kips to 30.0 kips. Figure 66 shows the bending moments in Soldier Beam 15 and the moments in adjacent Soldier Beams 14 and 16. Bending moments in Soldier Beam 15 changed in response to the load reduction, but the moments in Beams 14 and 16 did not change significantly. The moment at the upper ground anchor on Beam 15 decreased by 46 percent as the load was reduced.

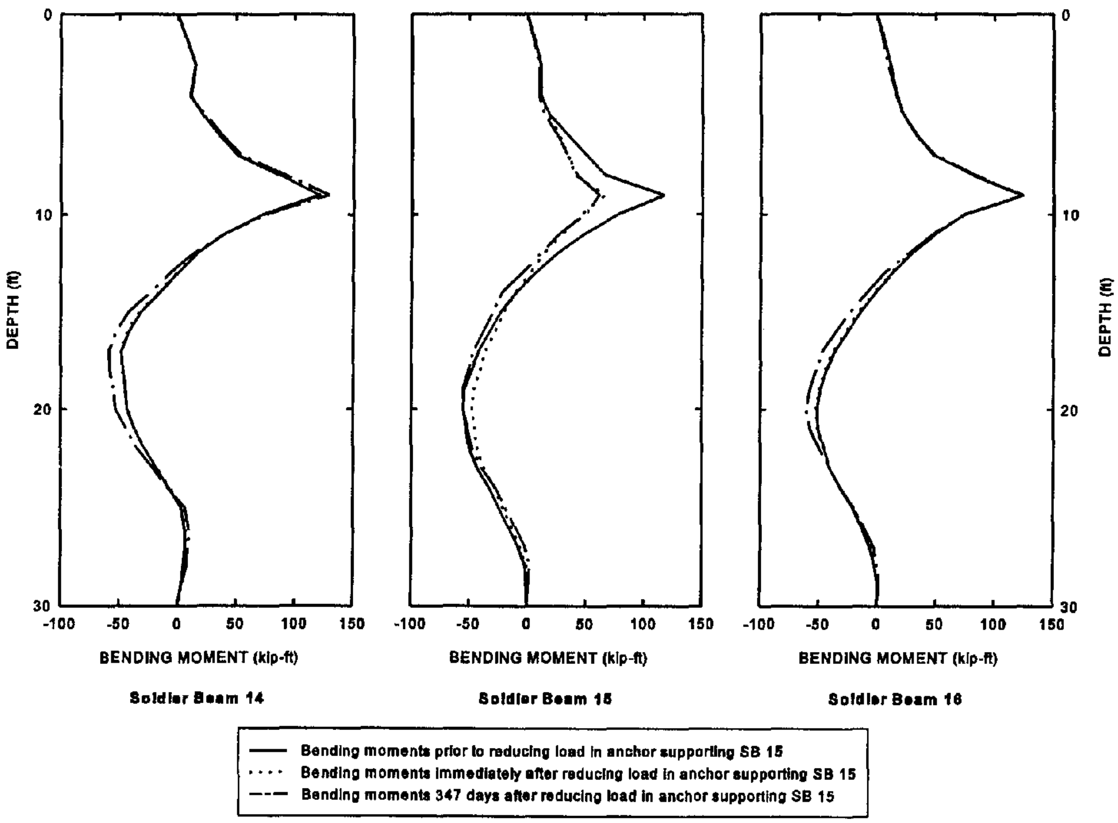

FIGURE 66
Bending Moment in Soldier Beams 14, 15, and 16 Before and After the Load in the Anchor Supporting Soldier Beam 15 Was Reduced

Figure 67 shows the lateral movement of Soldier Beams 14 to 16 in response to the load reduction. Movements of Soldier Beam 15 increased 13 percent when the load was reduced. After 347 days, the movements had increased a total of 173 percent from those measured before reducing the load. Lateral movements of adjacent Soldier Beams 14 and 16 were similar. Movements of Beams 14 and 16 increased an average 3 percent when the load was reduced. After 347 days, the lateral movements of Beams 14 and 16 had increased a total of 30 percent.

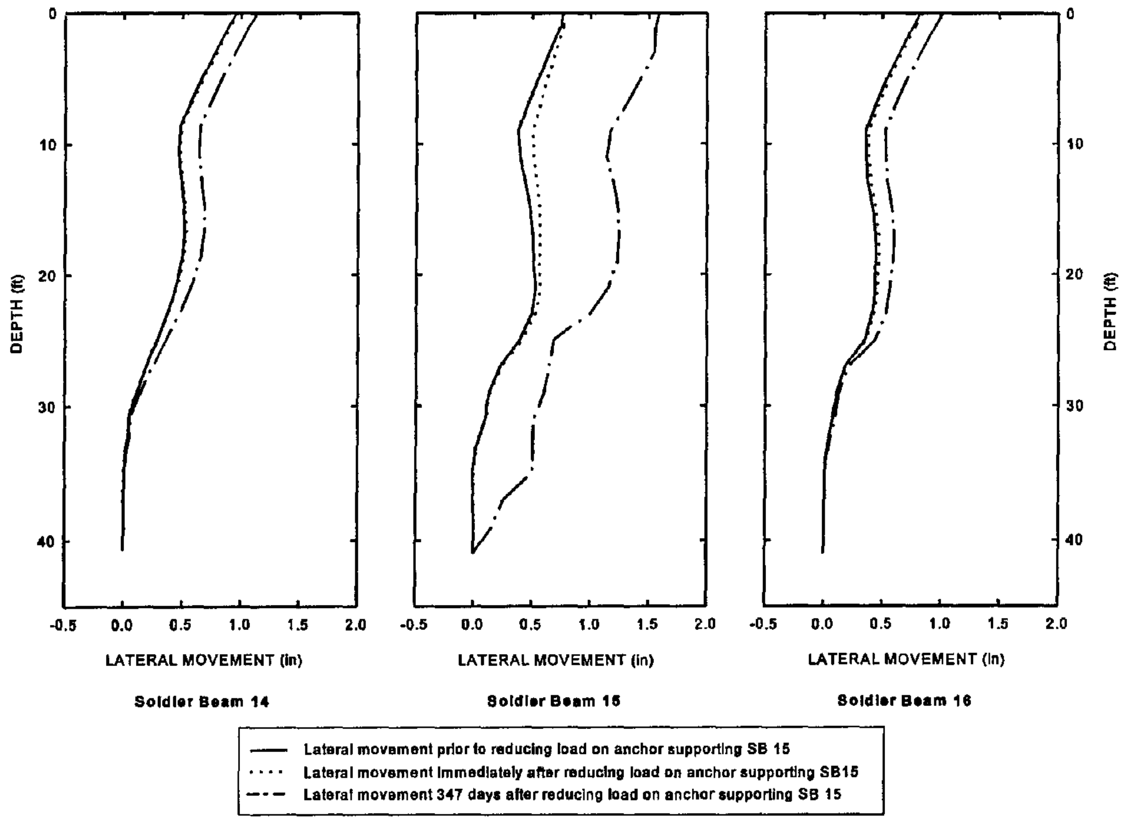

FIGURE 67
Lateral Movement of Soldier Beams 14, 15, and 16 Before and After the Load in the Ground Anchor Supporting Soldier Beam 15 Was Reduced

Table 21 presents the ground anchor loads for Soldier Beams 14 to 16. Load in the anchor supporting Soldier Beam 15 increased from 30 to 41.8 kips during the 347-day observation period. Load in the anchors supporting Soldier Beams 14 and 16 increased 6 and 10 percent, respectively during the observation period. The total lateral load in the anchors supporting Soldier Beams 14 to 16 was about 10 percent less after the 347-day period than it was before the load reduction.

Table 22 shows the axial load in Soldier Beams 14 to 16 below the bottom of the excavation. Axial load in Soldier Beams 15 decreased as the load in the anchor was released. The reduction in the axial load was less than the reduction in the vertical component of the ground anchor load. Axial load in Beam 14 and 16 increased about 10 percent as the load was reduced.

2.5.11.3 Observations

Visual observations and measurements showed that the wall remained serviceable after the load was reduced. Lateral wall movements increased in response to reducing the load on the ground anchors. Bending moments in the soldier beams supported by the ground anchors whose load was reduced decreased. Bending moments in adjacent soldier beams remained essentially unchanged as the load on anchors supporting adjacent soldier beams was reduced. The maximum bending moments after the load reductions were smaller than the maximum moments before the load reduction. Bending moment changes would not require the soldier beam to be redesigned. Bending moment, lateral wall movement, and ground anchor load changes in response to unloading the two ground anchors indicate that the wall would be serviceable if an anchor failed to carry the design load.

CHAPTER 3
SIMPLE SOIL-STRUCTURE ANALYSES FOR WALLS

Anchored walls distribute the ground anchor load(s) to the ground. The maximum bending moments in these flexible walls depend more upon the magnitude of the anchor loads than the intensity of the earth pressures. Current practice is to use apparent earth pressure diagrams to determine the ground anchor loads required to support the wall. The full-scale wall results (Chapter 2) and the limiting equilibrium studies (Chapters 3) of *Summary Report of Research on Permanent Ground Anchor Walls*, "Volume I — Current Practice and Limiting Equilibrium Analyses" (Long, et al., 1998) show that anchor forces determined from apparent earth pressure diagrams are sufficient to support the wall and contain an adequate factor of safety. Chapter 2 showed that the design procedures that used triangular earth pressures nderestimated the bending moments at the upper ground anchor location, and apparent earth pressure methods that incorporate a hinge at subgrade predicted the bending moments more accurately.

A soil-structure numerical method for anchored wall analysis/design should: model the response of the wall-soil system to the applied ground anchor forces; model the development of lateral resistance along the embedded portion of the wall; eliminate the need for incorporating hinges in the wall or soldier beam; and predict the bending moments accurately. As part of this research a soil-structure interaction numerical method for anchored wall design was developed at Texas A&M University and modified by Schnabel Foundation Company and Prototype Engineering. The work at Texas A&M used the computer code BMCOL76 (Matlock, et al., 1981). Back-calculated earth pressure-deflection curves above the bottom of the excavation, and single pile p-y curves for the soldier beam toe were used in BMCOL76. The work by Schnabel Foundation Company and Prototype Engineering used the computer program CBEAMC (Dawkins, 1994), and combined apparent earth pressure diagrams and earth pressure-deflection curves.

3.1 OBJECTIVES

Texas A&M developed a beam-column method for anchored wall analysis. The work included:

- Selection of a beam-column computer code for the analysis of anchored walls.
- Development of earth pressure-deflection relationships (soil response curves) that attempted to model the behavior of the full-scale wall described in Chapter 2.
- Modification of the beam-column code to enable construction stages to be modeled.
- Comparison of predictions for the full-scale wall and case histories with measurements.

The work done by Schnabel Foundation Company and Prototype Engineering involved the development of a user-friendly computer program for the analysis/design of anchored walls. The computer code implements apparent earth pressure diagrams and soil-structure interaction modeling along the toe. The computer code was developed to model continuous flexible walls (sheet pile walls) or discontinuous walls (soldier beam walls). The code and documentation are contained in *TB Wall — Anchored Wall Design and Analysis Program for Personal Computers* (Urzua and Weatherby, 1998). CBEAMC, a documented and proven public domain program developed for the United States Army Corps of Engineers, was adapted for use in the computer program. BMCOL76 was not used in the development of the computer code since the original developers retained the rights to the code.

3.2 SOIL-STRUCTURE INTERACTION MODELING

Soil-structure interaction computer codes based on finite difference methods or simple finite element methods are used to analyze structural beam-columns, laterally loaded piles, and beams supported by linear and non-linear elastic supports. These computer codes are called beam-column programs. BMCOL76, a finite difference program, and CBEAMC, a finite element program, are two widely used beam-column computer programs. Both programs model the earth pressure-deflection behavior of the system identically and give the same results for similar problems.

3.2.1 Early Earth Pressure-deflection Relationships

Beam-column programs have been used to analyze retaining walls by Haliburton (1968), Bowles (1974), Pfister, et al. (1982), Munger, et al. (1990), and Dawkins (1994). The earth pressure-deflection relationships in these analyses are idealized elasto-plastic curves, where p is the horizontal earth pressure acting on the wall and y is the deflection of the wall. Figure 68 shows a typical earth pressure-deflection curve for a continuous wall. The minimum and maximum pressures on the wall are assumed to be the Rankine active and passive pressures, respectively. The minimum and maximum pressures are reached after the wall has moved sufficiently to mobilize the active or passive states of stress. A modulus, E_s, or reference deflections, y_a and y_p, are necessary to construct the earth pressure-deflection curves.

Haliburton (1968) used a soil modulus E_s in compression, and a modulus E_s' in extension to develop earth pressure-deflection curves for walls. These moduli were obtained from triaxial tests. They were used to construct elasto-plastic earth pressure-deflection curves similar to the one shown in Figure 69 After determining the at-rest pressure, the ultimate active and passive pressures, and the moduli, the deflections required to mobilize the active and passive states of stress were known.

Pfister, et al. (1982) recommended a non-linear earth pressure-deflection curve for anchored wall design and analysis (Figure 70). Based on Soletanche's structural diaphragm wall experience, he used a horizontal subgrade moduli that depended on the shear strength of the soil (Figure 71). The horizontal subgrade moduli in Figure 71 were developed for stiff continuous diaphragm walls where water pressures often were significantly greater than the earth pressures. When water pressure is applied to the wall, the value of the subgrade moduli may not be critical, since the load on the wall is primarily due to the water pressure.

Wang and Reese (1986) presented a method to design cantilevered drilled shaft retaining walls. Their method used active earth pressures above the bottom of the excavation, and P-y curves for calculating the resistance of the soldier beam toe. The P-y curves used to predict the passive resistance of the soldier beams were similar to those used for laterally loaded piles (COM 624P (Wang and Reese, 1992)). In their method, the P-y curves for the drilled shaft walls were modified to account for group effect (interaction between closely spaced drilled shafts).

Earth pressure-deflection curves for anchored soldier beam walls may be different from those developed for other applications. Soldier beam walls are flexible and free draining. As a result, the earth pressure-deflection relationships may be affected by:

- Construction sequence.
- Flexibility of the wall.
- Discontinuous nature of the wall.
- Simplifications in modeling three-dimensional behavior using a two-dimensional model.

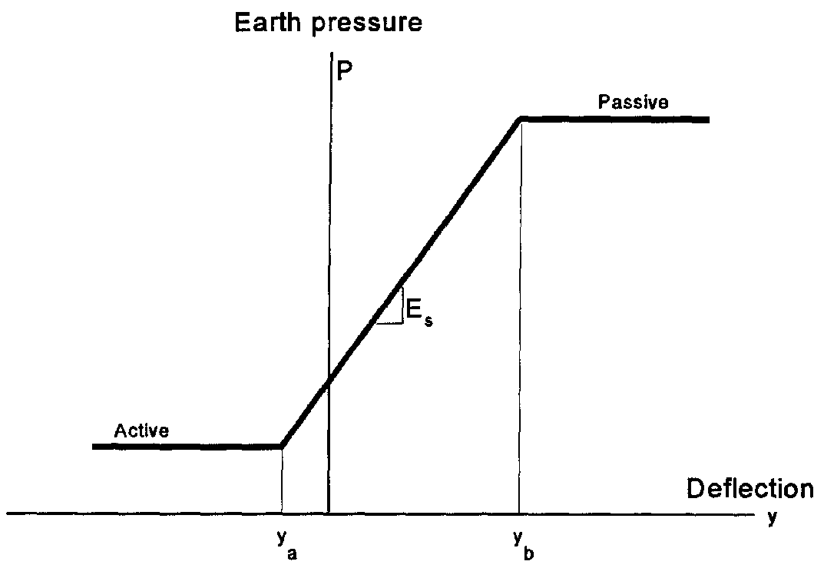

FIGURE 68
Idealized Earth Pressure-deflection Curve

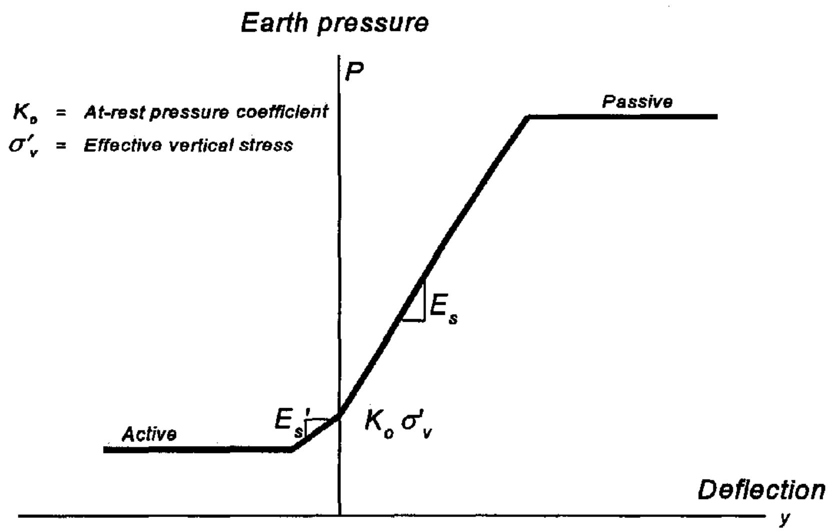

FIGURE 69
Soil Moduli Defined Non-linear *P-y* Curve for Anchored Wall Analysis (Haliburton, 1968)

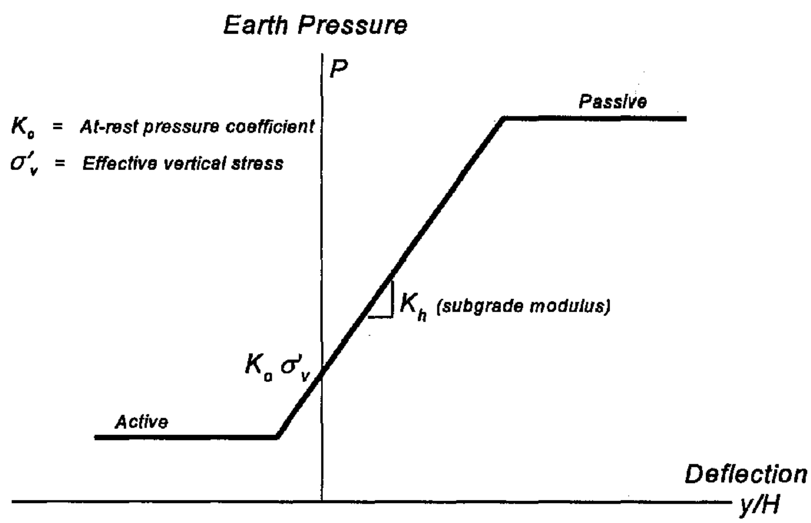

FIGURE 70
Horizontal Subgrade Moduli Defined Non-linear *P-y* Curve for Anchored Wall Analysis (Pfister, et al., 1982)

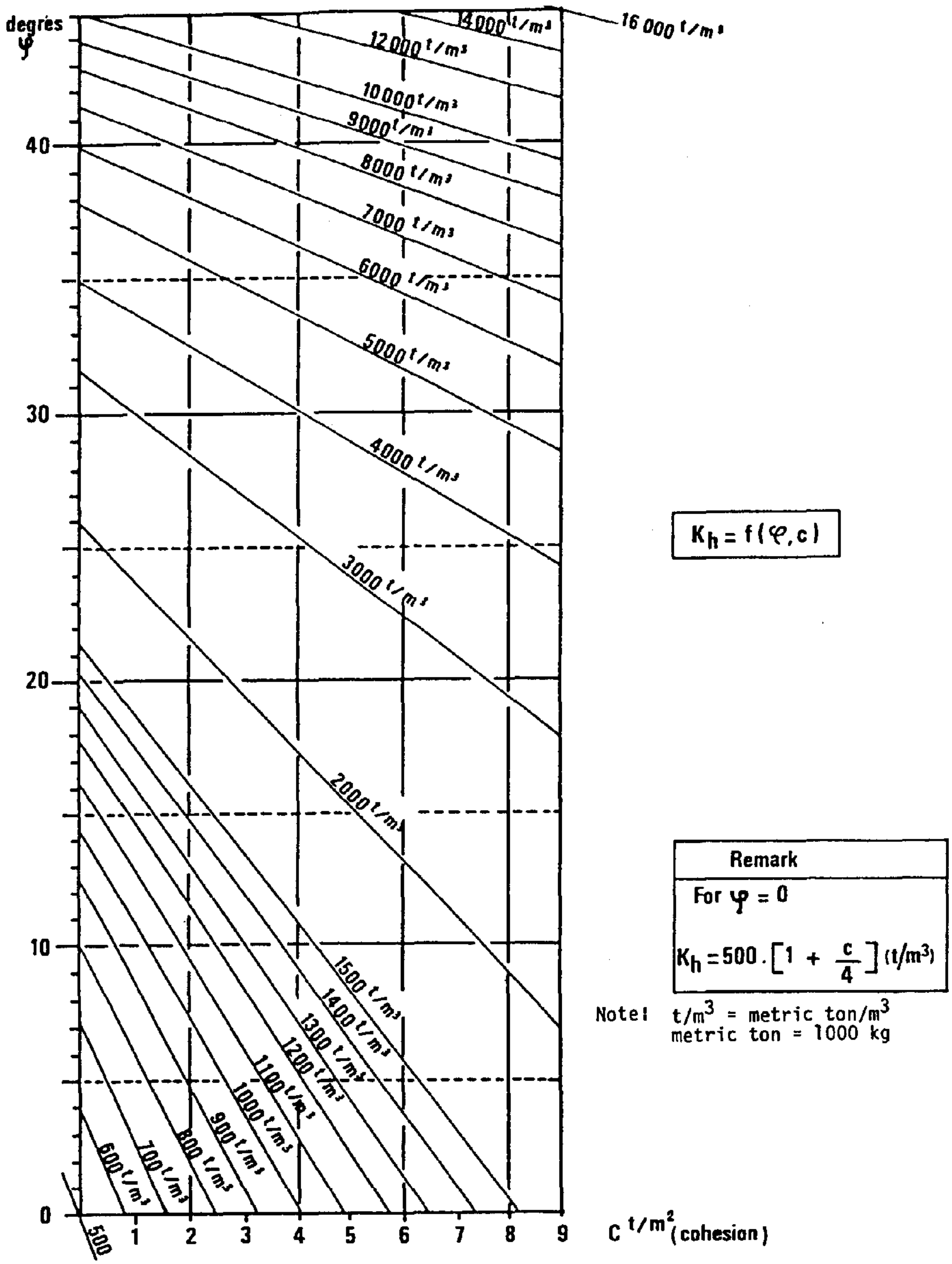

FIGURE 71
Horizontal Subgrade Moduli, K_h (Pfister, et al., 1982)

3.2.2 Back-calculation of Earth Pressure-deflection Curve for Texas A&M Walls

Earth pressures behind anchored walls change in response to excavation and anchor stressing. The earth pressures acting on the wall are redistributed depending upon wall movement, anchor load, and the wall stiffness. Typical earth pressure distributions for the different stages of a construction are shown in Figure 72.

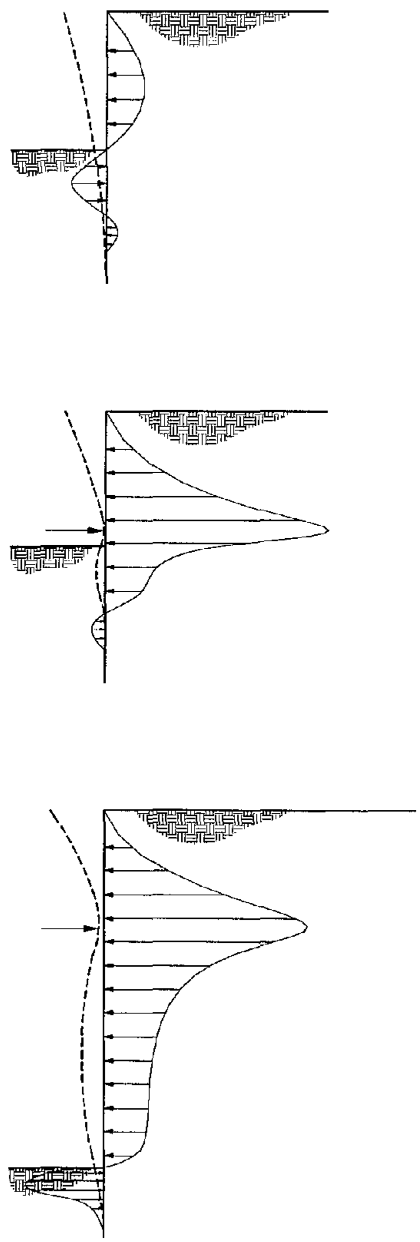

a) Excavate to anchor level

b) Stress anchor

c) Construction completed

FIGURE 72
Idealized Earth Pressure Distributions on an Anchored Wall

Earth pressures acting on Soldier Beam 16 installed at Texas A&M were calculated by double differentiation of the measured bending moment diagram. (Bending moment diagrams for Beam 16 are contained in Appendix A.) Bending moment diagrams with continuous first and second derivatives are necessary to determine the earth pressures. A cubic spline interpolation technique was used to develop bending moment diagrams that were continuous and differentiable. A cubic polynomial spline function is represented by Equation 3.1 and Figure 73.

$$S_j = a_j + b_j(x-x_j) + c_j(x-x_j)^2 + d_j(x-x_j)^3 \qquad \ldots [3.1]$$

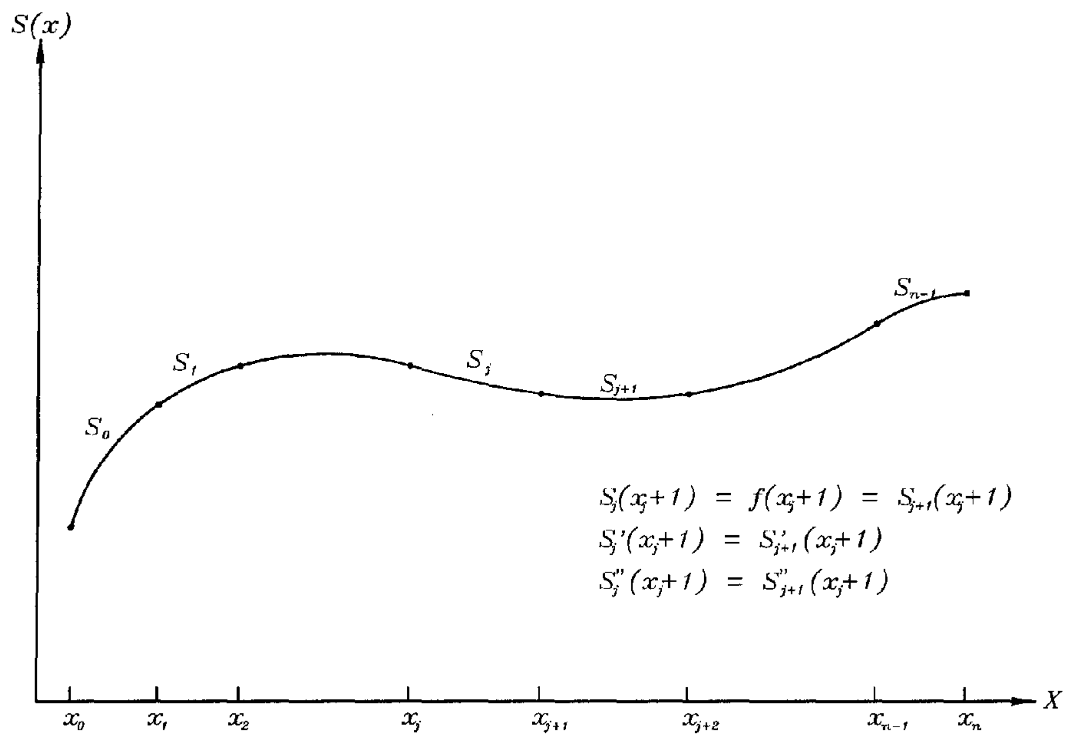

FIGURE 73
Illustration of a Cubic Spline Function

The cubic spline interpolant S for a given function f satisfies the conditions given in Equations 3.2 to 3.9:

1) S is a cubic polynominal, denoted S_j, on the interval $[x_j, x_{j+1}]$ j . . . [3.2]

2) $S_j(x_j) = f(x_j)$, $j = 0, 1, \ldots, n$ . . . [3.3]

3) $S_{j+1}(x_{j+1}) = S_j(x_{j+1})$, $j = 0, 1, \ldots, n-2$ . . . [3.4]

4) $S'_{j+1}(x_{j+1}) = S'_j(x_{j+1}),\ j = 0, 1, \ldots, n-2$ . . . [3.5]

5) $S''_{j+1}(x_{j+1}) = S''_j(x_{j+1}),\ j = 0, 1, \ldots, n-2$ . . . [3.6]

6) one of the following set of boundary conditions is satisfied

a) $S''(x_o) = S''(x_n) = 0$ . . . [3.7]

b) $S'(x_o) = f'(x_o)$ and $S'(x_n) = f'(x_n)$ . . .[3.8]

c) $S''(x_o) = f''(x_o)$ and $S''(x_n) = f''(x_n)$ . . .[3.9]

The cubic spline interpolation and double differentiation were done on the mainframe computer at Texas A&M. The measured bending moment profile for Soldier Beam 16 at the completion of construction and the interpolated bending moment diagram are shown in Figure 74. Double differentiation of the interpolant for different stages of construction gave the earth pressures at that stage of construction multiplied by the beam spacing. Figure 75 shows the computed earth pressure diagram for the cantilever excavation stage (excavation at 10 ft, anchor not installed). Figure 76 shows the computed earth pressure diagram after the ground anchor had been tested and locked-off (10-ft excavation). The computed earth pressure diagram for the completed wall is shown in Figure 77.

Figure 77 compares the back-calculated earth pressures with Rankine earth pressures, and $25H$ trapezoidal and Terzaghi and Peck apparent earth pressures. Computed earth pressures down to a depth of 5 ft were approximately equal to the Rankine active pressures. Below 5 ft, the earth pressure increased to approximately the Rankine passive pressure at a depth of 9 ft. The dotted portion of the earth pressure diagram between 7 and 10 ft was estimated and not computed by double differentiation of the bending moment interpolant. Between the 9-ft and the 11-ft depth, the earth pressures decreased to the Rankine active pressure. Calculated earth pressures between 11 ft and the bottom of the excavation were lower than the Rankine active pressures and the apparent earth pressures. Between the 11-ft and the 26-ft depth the average back-calculated earth pressure was 2,530 lb/linear ft. Over this height the average back-calculated earth pressure was 55 percent of Terzaghi and Peck pressure and 51 percent of the $25H$ apparent earth pressure. The total back-calculated load between the 11-ft and the 26-ft depth was 37,950 lb. Low earth pressures between the ground anchor and the bottom of the excavation reflect the redistribution of load to the ground anchor location. Figure 77 also shows that the earth pressures between the anchor and the bottom of the excavation are lower than the Rankine active pressures. The mobilized passive capacity of the toe was computed to be approximately 8 kips. Mobilized passive capacity of the toe was 68 percent of the Rankine passive capacity (1.5 $(K_p \gamma H^2 b)$.

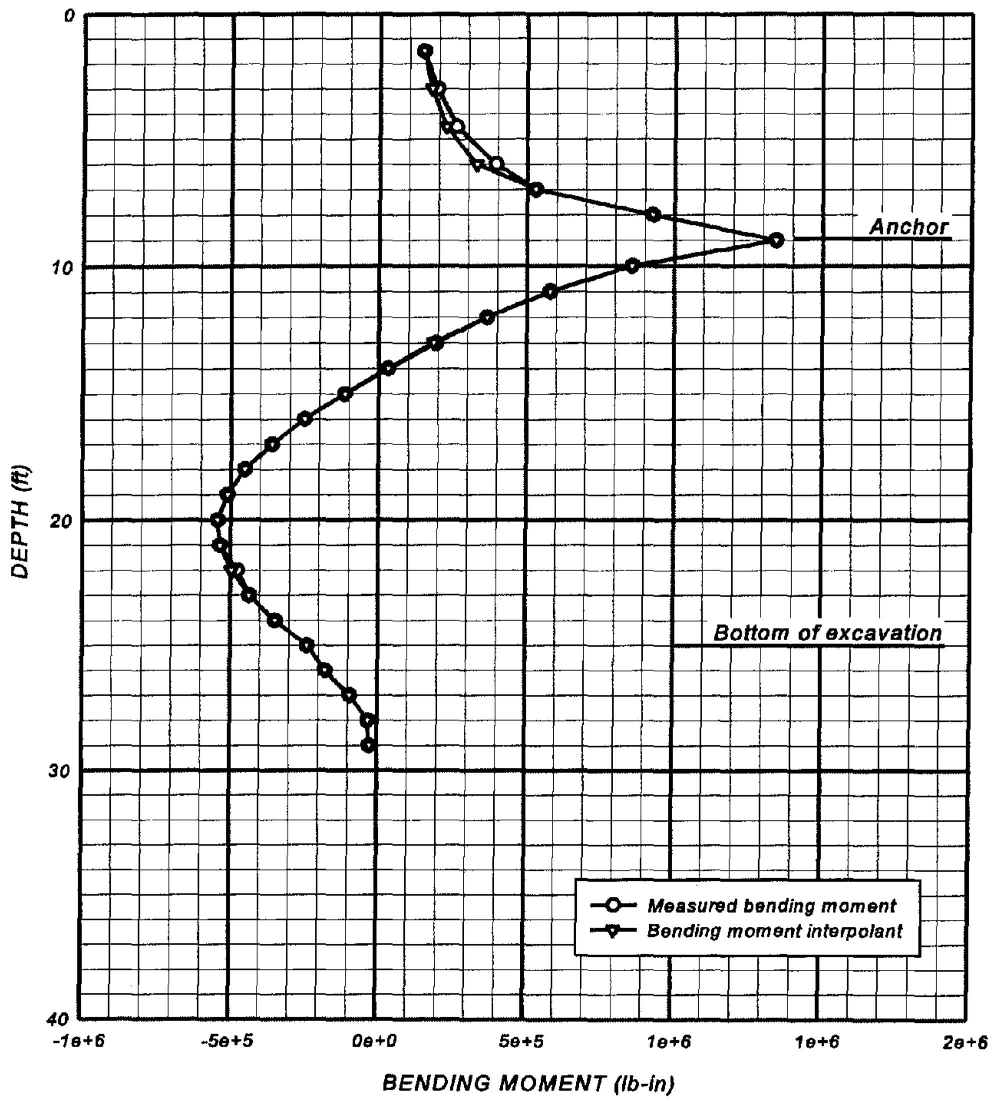

FIGURE 74
Measured Bending Moment and Cubic Spline Bending Moment Interpolant for Soldier Beam 16, Completion of Construction

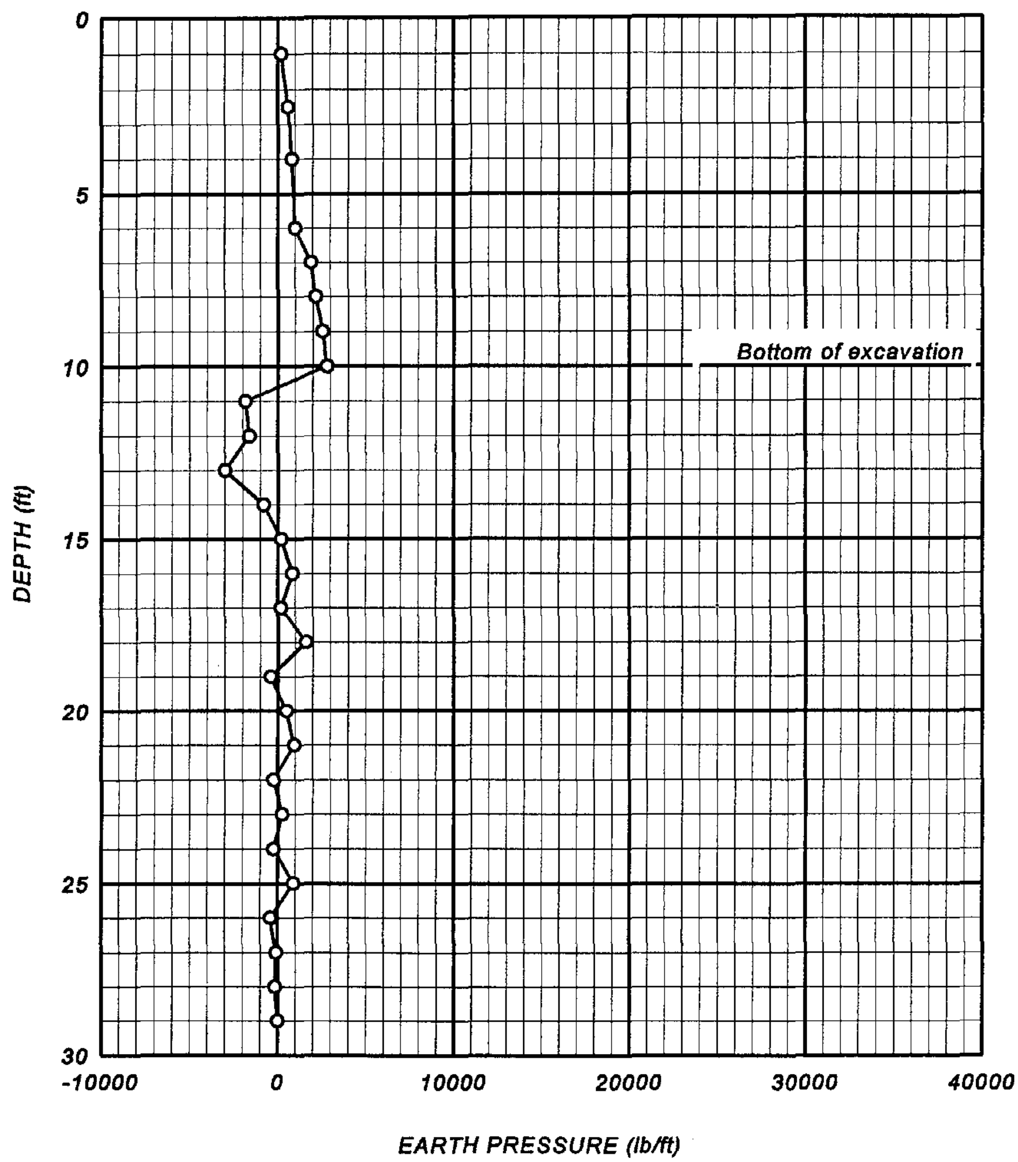

FIGURE 75
Earth Pressures Computed by Double Differentiation of the Cubic Spline Bending Moment Interpolant for Soldier Beam 16, 10-ft Excavation

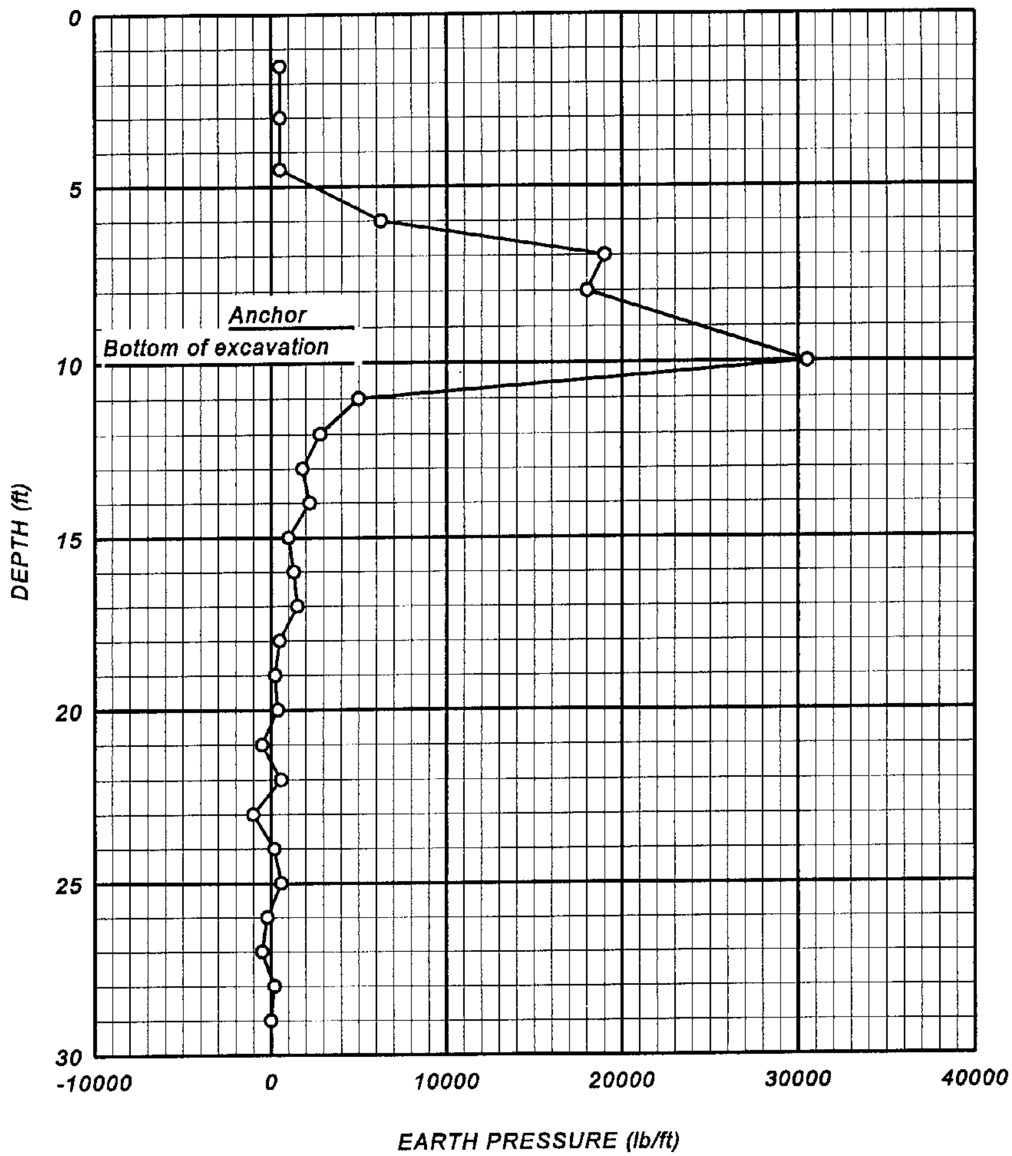

FIGURE 76
Earth Pressures Computed by Double Differentiation of the Cubic Spline Bending Moment Interpolant for Soldier Beam 16, Ground Anchor Locked-off

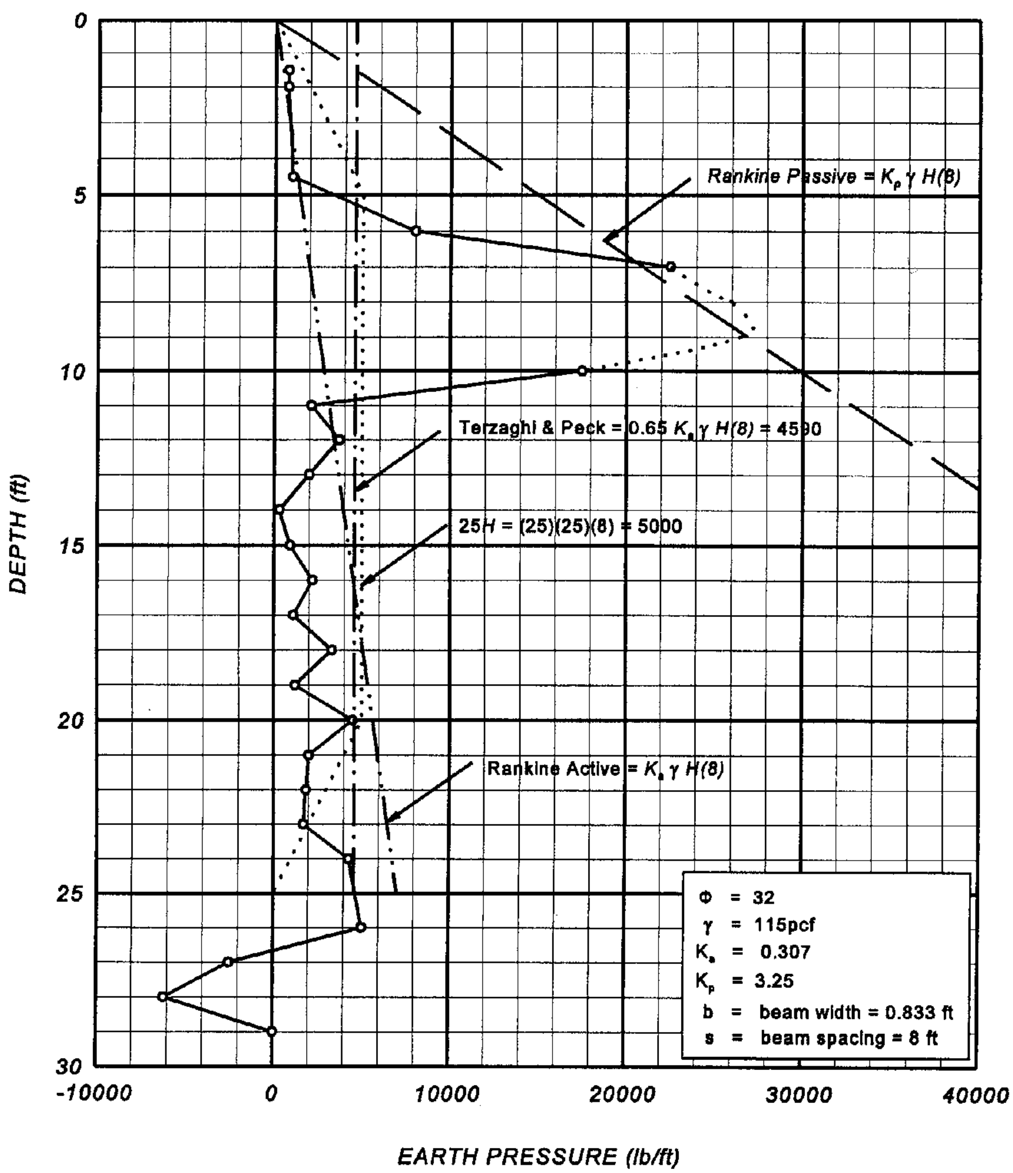

FIGURE 77
Earth Pressures Computed by Double Differentiation of the Cubic Spline Bending Moment Interpolant for Soldier Beam 16, Construction Completed

To develop an earth pressure-deflection curve for the soldier beams installed at Texas A&M, it was necessary to determine the beam deflections and earth pressures associated with the different stages of construction. An earth pressure coefficient for the back-calculated earth pressures was determined by dividing the earth pressure by the vertical effective stress and the soldier beam spacing. Measured beam deflections were determined from the inclinometer reading and adjusted to account for plastic movement (non-recoverable) movement of the soldier beam. Figure 78 shows how the soldier beam movements for the earth pressure-deflection curves were developed. For the cantilevered excavation stage, the deflection (y_1, y_2, and y_3) occurred as the beam moved out in response to the excavation. The calculated earth pressure coefficients corresponding to the measured deflections are plotted on the earth pressure coefficient-deflection curve as shown. As the ground anchor is stressed, the soldier beam moves back into the soil and deflects y_4, y_5, and y_6 at the three locations shown. The passive earth pressures that develop as the beam is pulled back into the ground are related to the change in deflection between the two stages shown in Figure 78. The calculated passive earth pressure coefficients corresponding to the measured deflections are plotted as shown in Figure 78.

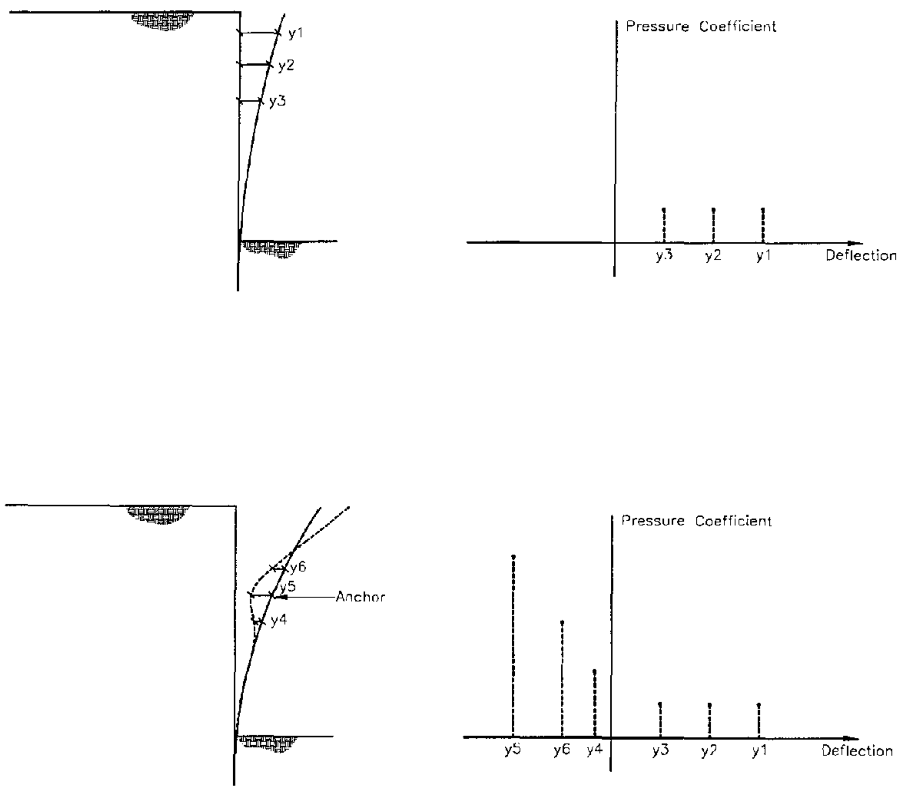

FIGURE 78
Illustration Showing How the Deflections for the Experimental Earth Pressure-deflection Curve are Developed

Earth pressure coefficients and relative deflections for Soldier Beam 16 are shown in Figure 79. At a defection of 0.05 in the average active earth pressure coefficient was 0.15. The low active earth pressure coefficient was probably a result of pressure redistribution caused by arching. The at-rest earth pressure coefficient (zero deflection) was 1.0. Since the passive capacity of the soldier beams was not reached during anchor stressing, a passive earth pressure coefficient for the experimental earth pressure-deflection curve was not determined. The passive pressure coefficient, K_p was estimated to be equal to the inverse of the active coefficient (K_p = 6.6). The deflection required to fully mobilize the passive earth pressure was assumed to be 0.5 in. Figure 80 gives the experimental earth pressure-deflection curve developed for Soldier Beam 16 in the full-scale wall at Texas A&M.

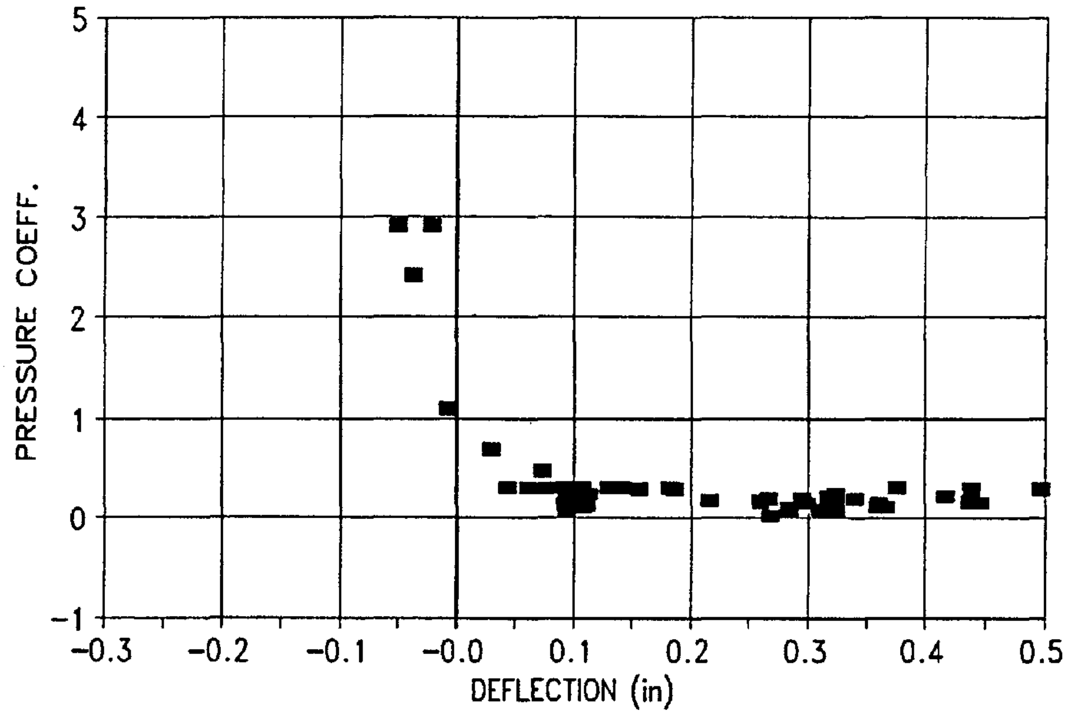

FIGURE 79
Earth Pressure Coefficient-deflection Curve for Soldier Beam 16

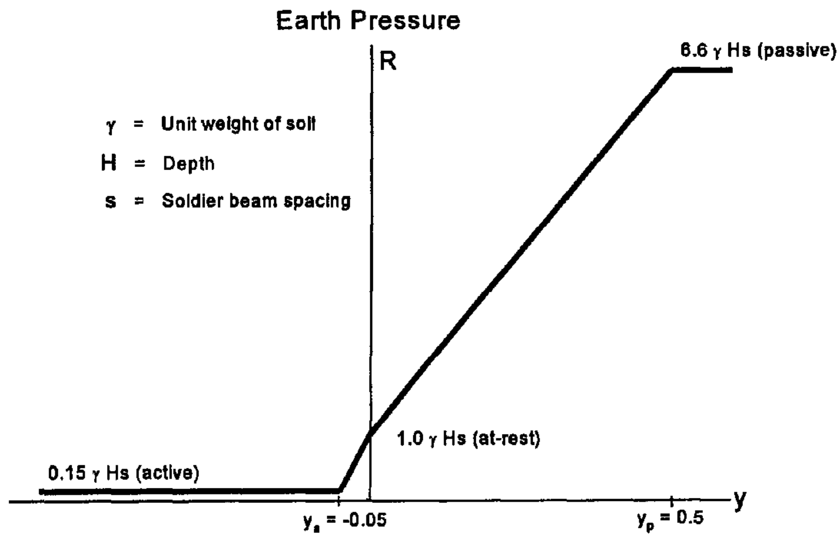

FIGURE 80
Experimental Earth Pressure-deflection Curve for Soldier Beam 16

3.3 BEAM-COLUMN METHOD FOR ANCHORED WALLS

3.3.1 Fundamental Concepts

3.3.1.1 Modeling the Anchored Wall

An anchored wall can be modeled as a beam supported by non-linear springs, as shown in Figure 81. The wall is modeled as a beam with bending stiffness, EI. Non-linear springs are used to model the earth pressure-deflection relationships for the system. Concentrated non-linear springs are used to model the ground anchors.

Two types of anchored walls are common. The first type of wall is a continuous wall such as a diaphragm wall or a sheet piling wall, and the other is a discontinuous wall such as a soldier beam and wood lagging wall (Figure 82). In a discontinuous wall, only the soldier beam is present below the bottom of an excavation. Therefore, the earth pressure-deflection relationship for each type of wall must differ below the bottom of the excavation.

In a continuous wall, a unit width of the wall is modeled as a structural member having a lateral bending stiffness, EI. Non-linear earth pressure-deflection springs represent the earth pressure acting on a unit width of the wall. The ground anchor force divided by the horizontal anchor spacing is used in the development of a concentrated non-linear spring to model the ground anchor.

In a soldier beam and wood lagging wall, the section of wall to be modeled has a width corresponding to the spacing between soldier piles and is centered around the soldier beam (Figure 82). The bending stiffness of the soldier beam, EI, is used to model the soldier beam and wood lagging wall. Earth pressure-deflection springs above the bottom of the excavation represent the total earth pressure acting on the wall between soldier beams. The horizontal component of the actual anchor loads are used in the development of concentrated non-linear anchor spring. Earth pressure-deflection springs below the excavation level are different from the earth pressure-deflection springs for a continuous wall. These springs must include three-dimensional effects, similar to a laterally loaded pile.

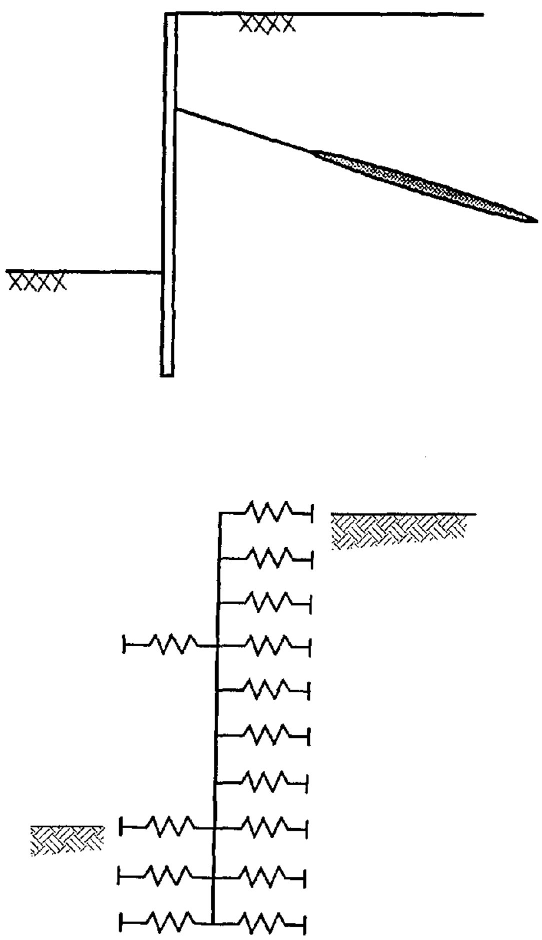

a) Cross-section

b) Non-linear Springs

FIGURE 81
Idealized Ground Anchor Wall Model for Soil-structure Interaction Analysis

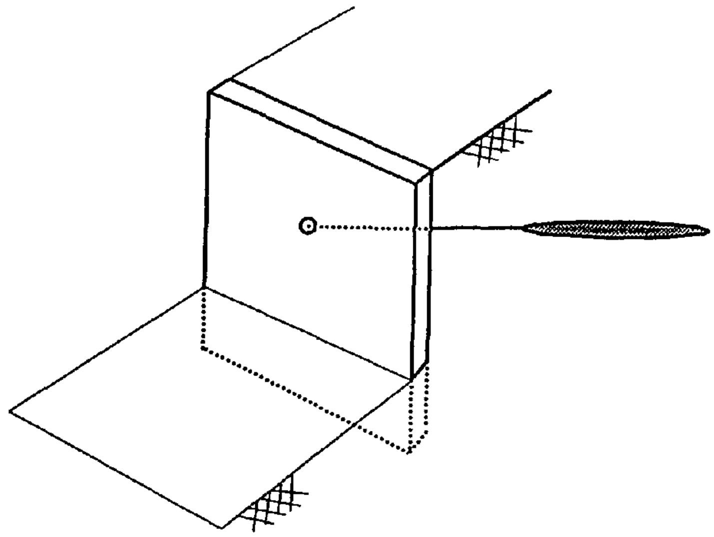

a) Continuous Wall (slurry wall or sheet pile wall)

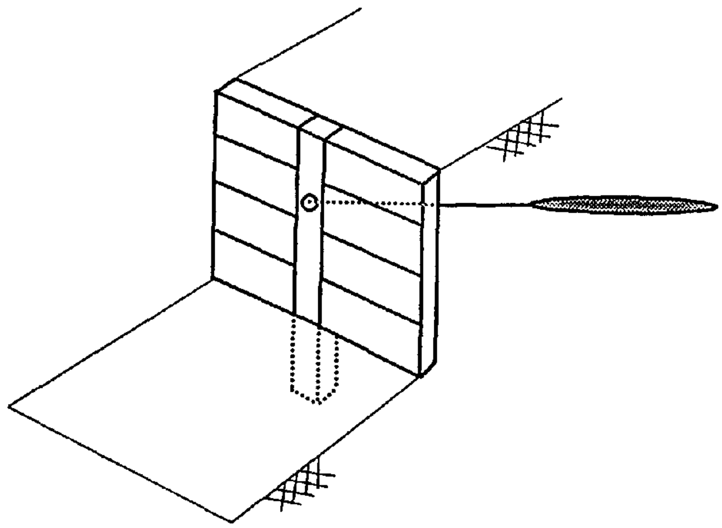

b) Discontinuous Wall (soldier beam and wood lagging wall)

FIGURE 82
Wall Types in Soil-structure Interaction Analyses

3.3.1.2 Modeling of the Excavation Sequence

Construction activities may influence wall and soil behavior. Excavation stages, dewatering, installation and loading the ground anchors, workmanship, and the time the excavation remains open can affect the behavior of an anchored earth retaining wall.

Simulating the construction sequences for an anchored wall involves modeling a series of loading and unloading stages (Figure 83). Surcharge loads, if applied, can be considered as a separate construction stage in the analysis.

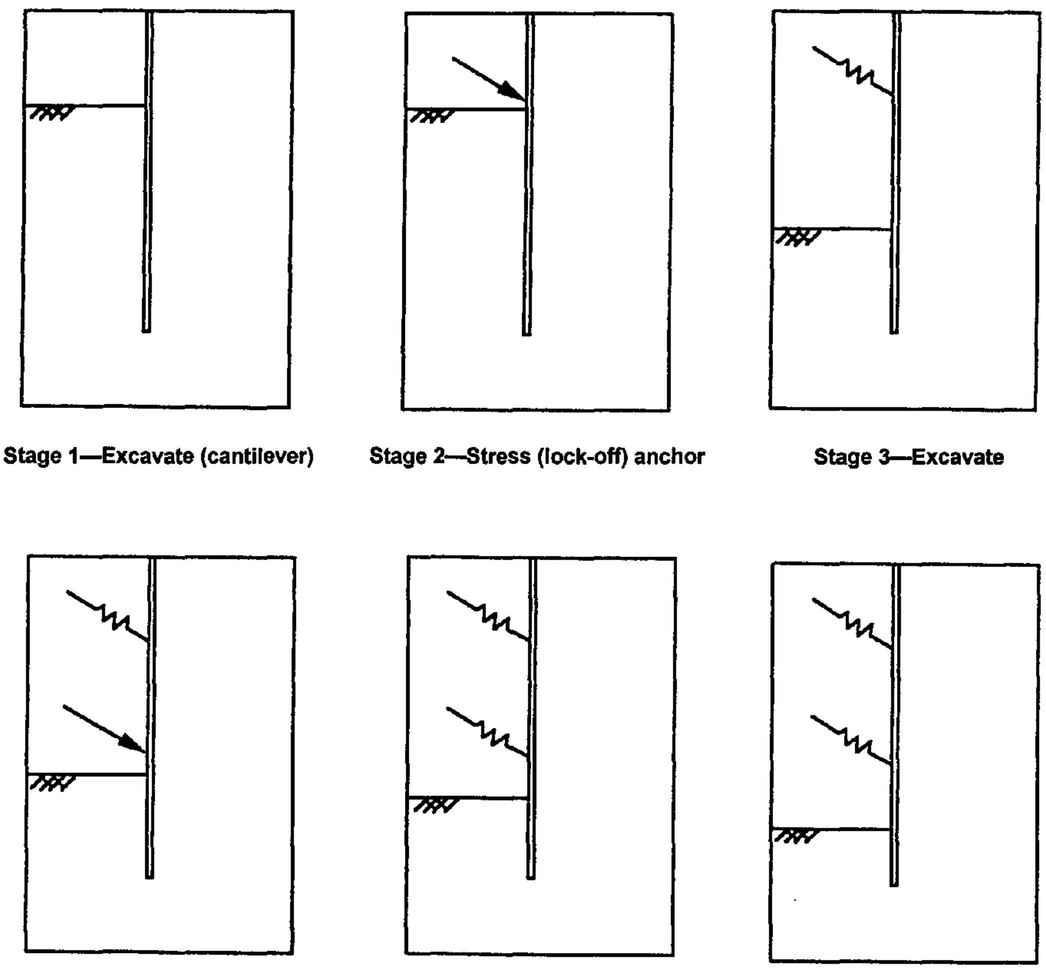

Stage 1—Excavate (cantilever) Stage 2—Stress (lock-off) anchor Stage 3—Excavate

Stage 4—Stress (lock-off) second anchor Stage 5—Excavate Stage 6—Repeat stages until excavation completed

FIGURE 83
Typical Construction Stages Considered in a Soil-structure Interaction Analysis

Ground behind the wall is unloaded as the wall deflects in response to excavating to the ground anchor level (cantilever stage). Deflections at some locations will be large enough to mobilize the active state of stress. Figure 84 shows idealized wall and soil response curves at three locations (R_1, R_2, and R_3). In this report the wall and soil response curves are called R-y curves to distinguish them from P-y curves. At R_1 the wall moved laterally a distance represented by the deflection, y_1. This deflection is shown in the deflection profile for the wall and the R-y curve for location R_1 (Figure 84). The R-y curve shows that the deflection exceeded the deflection necessary to mobilize the active state of stress (earth pressures remained constant with additional movement). Deflections greater than the reference deflections are plastic (non-recoverable) movements. Below the bottom of the excavation, the wall moved outward to mobilize passive resistance. Behind the wall, the force applied to the wall decreased as the wall moved outward. The response of the wall soil system below the bottom of the excavation can be represented by a combined R-y curve. The combined R-y curve is the sum of the R_2 and the R_3 curves.

When the ground anchor is stressed, the wall is pulled back into the ground and the soil is loaded by the wall. Figure 85 shows idealized soil response curves for this stage of construction at the same location as those shown in Figure 84. At this stage of construction, the ground anchor is modeled as a concentrated load. The R_1 curve in Figure 85 is shifted from the position shown in Figure 84 to account for the plastic movement that occurred at that location during the cantilever excavation stage. Figure 86 shows how the shifted R_1 curve was developed. In Figure 86 the R-y curve for the cantilever stage (Curve 1) and the shifted R-y curve for the anchor stressing stage (Curve 2) are shown. Curve 1 shows that, before any construction, the force on the wall was R_0 and the deflection was zero. As the cantilever excavation was made, the wall was unloaded. This step is represented by the cantilever excavation path in Figure 86. At the conclusion of the cantilever excavation, the force on the wall is R_a and the deflection of the wall is y_{a2} (Figure 86), which is equal to y_1 (Figure 84). Since plastic movements occurred at R_1 during the cantilever stage, a new R-y curve is required for the anchor stressing stage. The new R-y curve is required because reloading associated with anchor stressing does not follow the unloading curve. Instead, passive resistance is mobilized when the wall moves back into the ground. The new R-y curve (Curve 2) is developed by shifting Curve 1 an amount equal to the plastic movement from the previous stage (y_{a2}-y_{a1}). The shifted R-y curve (Curve 2) has new reference deflections, y_{a2} and y_{p2}, and models the reloading response during anchor stressing. The anchor stress path is shown on Curve 2 in Figure 86. The R_2 and R_3 curves in Figure 85 were not shifted for the anchor stressing stage since the movements for the cantilever excavation and the stressing stage were in the elastic range.

Shifted R-y curves account for the effects of construction and allow beam-column methods to model anchored wall construction sequences without storing beam deflections from each construction stage. Shifted R-y curves simulate construction activities by accumulating plastic movements from prior construction stages. When using the shifted R-y curves in a beam-column program, the beam is assumed to be in its original position (zero deflection) for each run, and the shifted curves include the effects of construction activities.

Anchor load, after lock-off, depends upon wall deflection at the anchor location. A ground anchor is modeled by a load-deflection (T-y) curve. Figure 87 shows R-y curves and a T-y curve for the ground anchor when the excavation extends below the ground anchor. The R_1 and R_2 curves from the anchor stressing stage (Figure 85) were not shifted since plastic movements did not occur during the anchor stressing stage. A new R_3 curve is shown in Figure 87 since the active and passive resistance on the left side of the wall changed in response to deepening the excavation. In developing the T-y curve for the ground anchor, horizontal components of the ground anchor deflections and loads are used. The horizontal component of the anchor lock-off load corresponds to zero deflection of the wall after stressing (Section 3.3.3). The initial slope of the T-y curve is the anchor tendon stiffness. T-y curves change slope at the yield strength of the anchor tendon. The second portion of the curve represents the ground anchor behavior between the yield and ultimate strength.

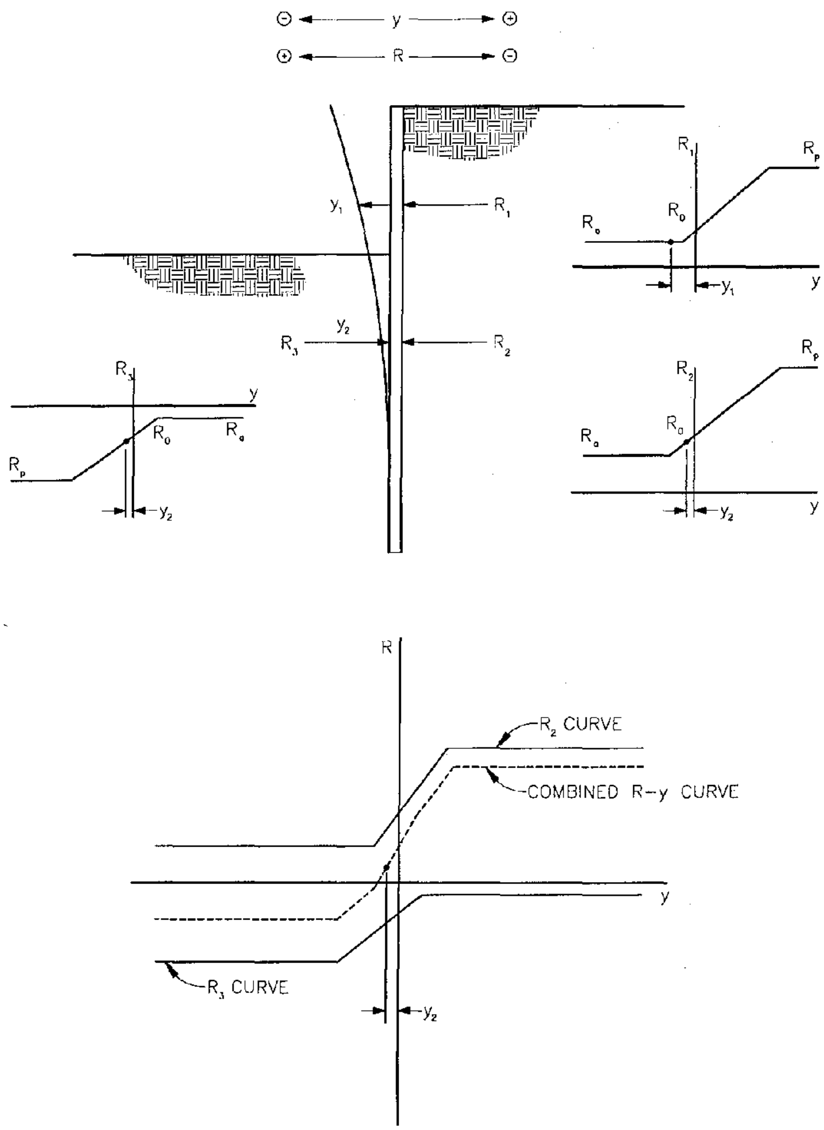

FIGURE 84
Diagram Illustrating the *R-y* Curves for the Cantilever Stage

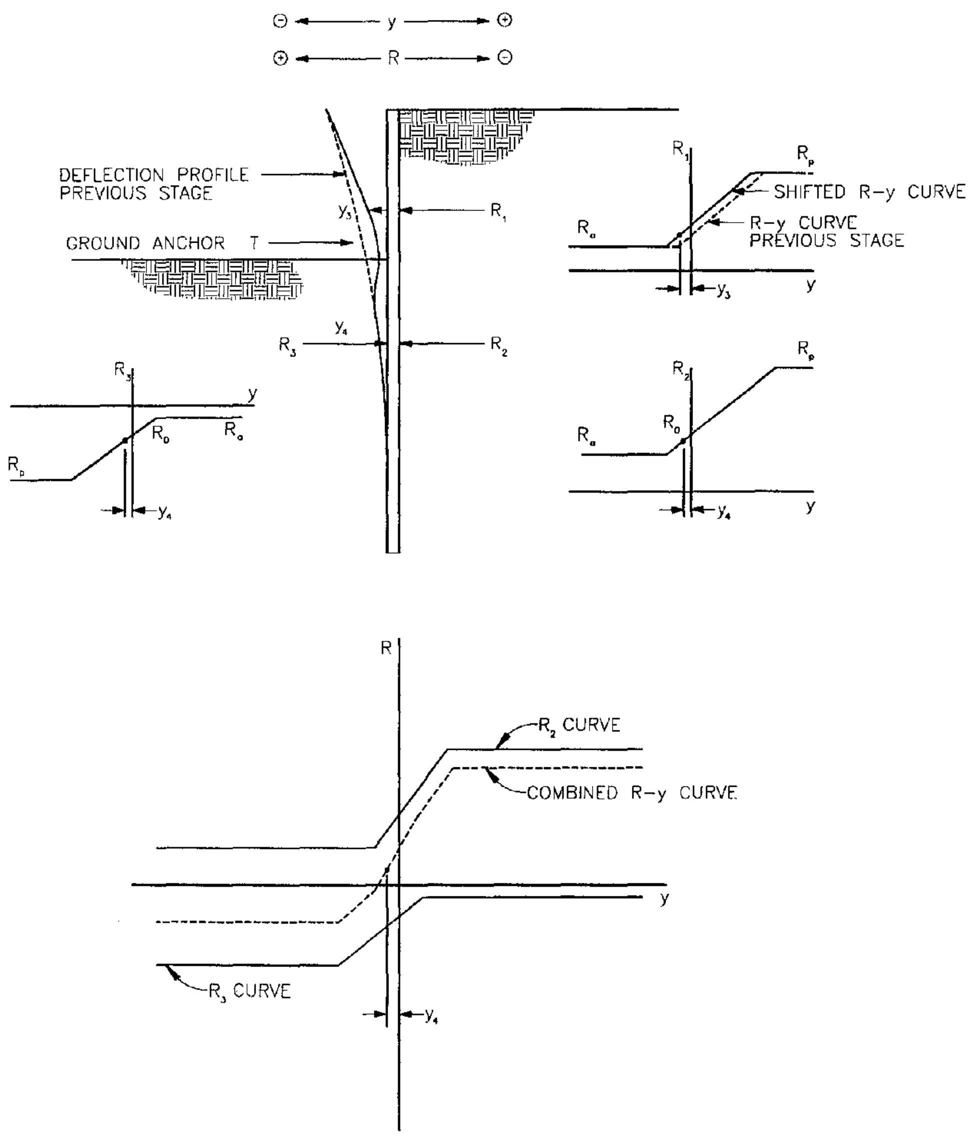

FIGURE 85
Diagram Illustrating the *R*-*y* Curves at Anchor Stressing

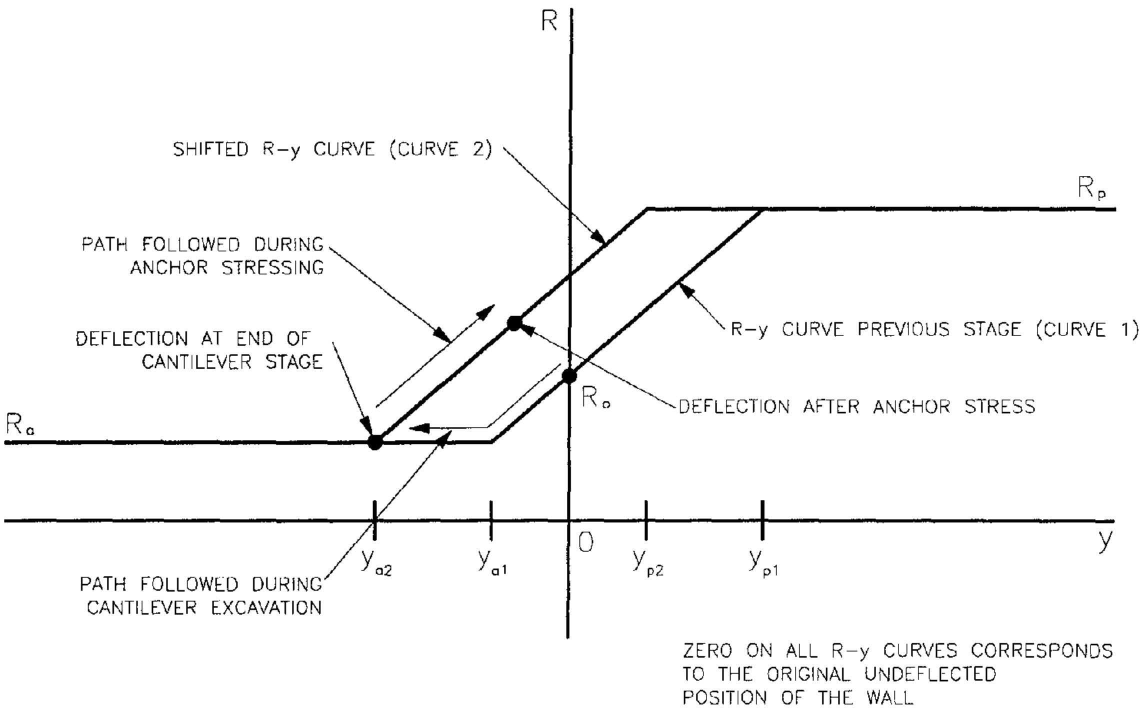

FIGURE 86
Shifted *R-y* Curve to Model Construction Stages

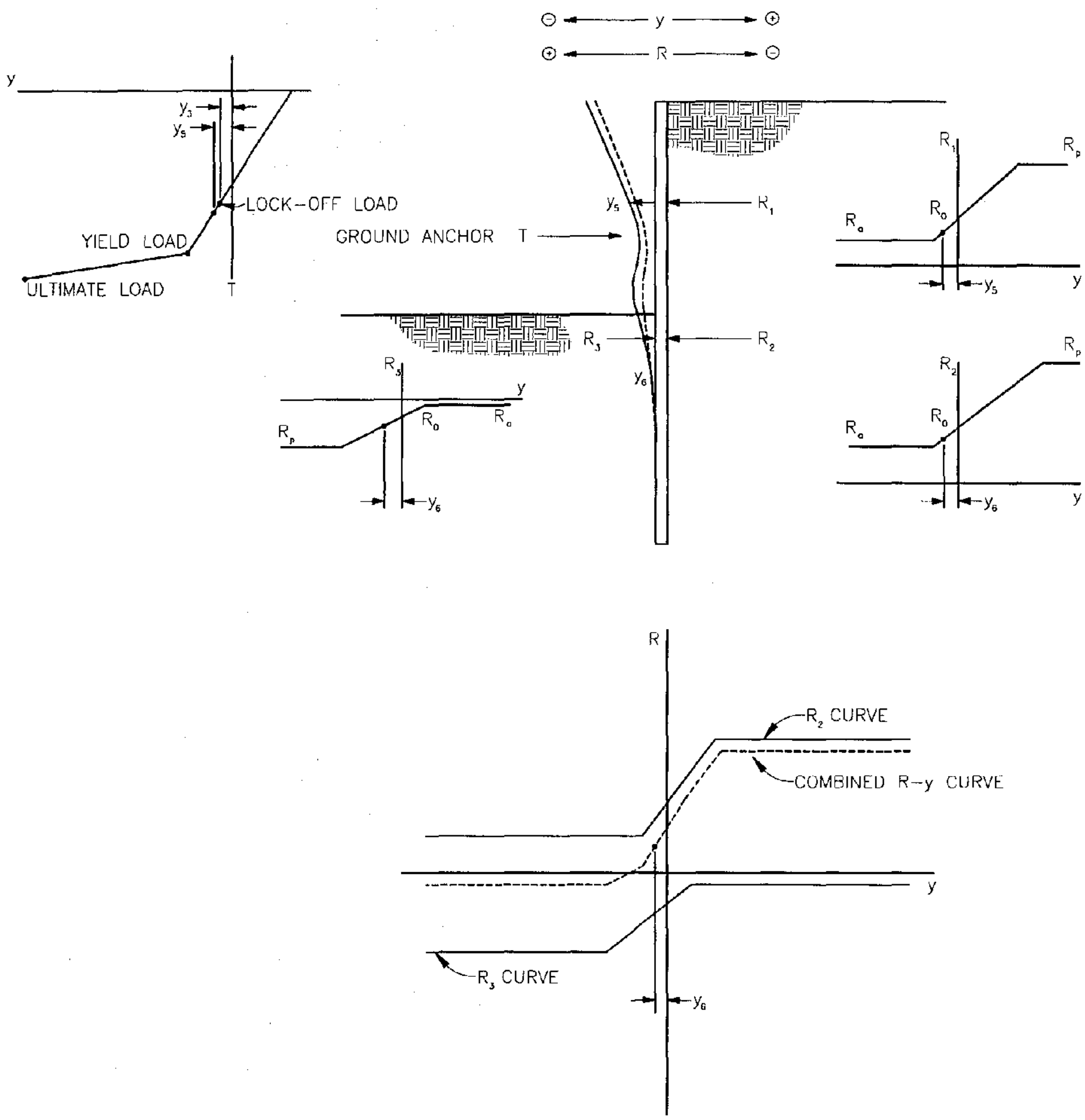

FIGURE 87
Diagram Illustrating the *R-y* Curves During Excavation Below the Ground Anchor

3.3.2 Non-linear Earth Pressure-deflection (R-y) Curves for Walls

R-y curves represent the soil mass as a series of independent non-linear springs. The non-linear springs (soil response curves) are assumed to incorporate soil behavior and the interaction between the soil and the wall.

The earth pressure and deflection relationship upon which the R-y curves are developed depends upon the following:

- Active earth pressures, based on the conventional earth pressure theory, are developed after the outward deflection of the wall exceeds an active reference deflection.
- Passive resistances, based on the conventional earth pressure theory, are developed after the wall deflection of the wall in the supported ground exceeds a passive reference deflection.
- At-rest earth pressures based on conventional earth pressure theory exist when wall deflection is zero.
- Reference deflections necessary to mobilize the active pressures and passive resistances depend on the soil type. (The reference deflections for the medium dense sand are based on measurements obtained from the Texas A&M full-scale wall (Section 3.2.2). Reference deflections for clay were assumed and verified by comparing the predicted behavior with case history results (Sections 3.4.4 and 3.4.5).

The five parameters involved in defining a non-linear R-y curve are: the active earth pressure coefficient, the at-rest earth pressure coefficient, the passive earth pressure coefficient, the reference deflection for the full active earth pressure, and the reference deflection for the full passive resistance.

3.3.2.1 Plane Strain R-y Curves for Sand

Active, passive, and at-rest earth pressures at a depth, z, for cohesionless soils are:

$$P_{at\text{-}rest} = K_o \sigma_v \qquad \text{. . . [3.10]}$$

$$P_{active} = K_a \sigma'_v \qquad \text{. . . [3.11]}$$

$$P_{passive} = K_p \sigma'_v \qquad \text{. . . [3.12]}$$

where:

K_o = at-rest earth pressure coefficient

K_a = active earth pressure coefficient

K_p = passive earth pressure coefficient

σ'_v = effective vertical stress at depth z

The at-rest earth pressure coefficient, K_o, for normally consolidated sands is given by Equation 3.13 (Jaky, 1944).

$$K_o = 1 - \sin\phi \qquad \ldots [3.13]$$

At-rest earth pressure coefficient, K_o, depends upon the stress history of the soil. Stress history for a cohesionless soil can be represented by the over consolidation ratio, OCR. For overly consolidated sands, the at-rest earth pressure coefficient is given by Equation 3.14 (Mayne and Kulhawy, 1982).

$$K_o = (1 - \sin\phi)\sqrt{OCR} \qquad \ldots [3.14]$$

Section 3.5.1 shows that the bending moments are not sensitive to values of K_o within a range of typical values.

Rankine's active and passive earth pressure coefficients for a vertical wall with a horizontal ground surface behind the wall are given by Equations 3.15 and 3.16.

$$K_a = \tan^2\left(45° - \frac{\phi}{2}\right) \qquad \ldots [3.15]$$

$$K_p = \tan^2\left(45° + \frac{\phi}{2}\right) \qquad \ldots [3.16]$$

Rankine pressures are assumed to be horizontal, and wall friction does not affect Rankine pressures.

Coulomb (1776) developed relationships for active and passive earth pressure coefficients that considered wall friction acting on a failure wedge, as shown in Figure 88. Coulomb earth pressures are inclined at an angle, δ, the angle of wall friction. For a vertical wall and a horizontal ground surface the Coulomb active and passive earth pressure coefficients are given by Equations 3.17 and 3.18.

$$K_a = \frac{\cos^2\phi}{\cos\delta\left[1 + \sqrt{\dfrac{\sin(\phi+\delta)\sin\phi}{\cos\delta}}\right]^2} = \frac{1}{\cos\delta\left[\dfrac{1}{\cos\phi} + \sqrt{\tan^2\phi + \tan\phi\tan\delta}\right]^2} \qquad \ldots [3.17]$$

$$K_p = \frac{\cos^2\phi}{\cos\delta\left[1 - \sqrt{\dfrac{\sin(\phi+\delta)\sin\phi}{\cos\delta}}\right]^2}$$

$$= \frac{1}{\cos\delta\left[\dfrac{1}{\cos\phi} - \sqrt{\tan^2\phi + \tan\phi\tan\delta}\right]^2} \qquad \text{. . . [3.18]}$$

where:

ϕ = angle of internal friction of the soil
δ = wall friction angle as defined in Figure 88

Active and passive Coulomb earth pressures on a vertical wall are given by Equations 3.19 and 3.20. Coulomb earth pressures are inclined at the angle of wall friction, δ, as shown in Figure 88.

$$P_{active} = (K_a \sigma'_v)\cos\delta \qquad \text{. . . [3.19]}$$

$$P_{passive} = (K_p \sigma'_v)\cos\delta \qquad \text{. . . [3.20]}$$

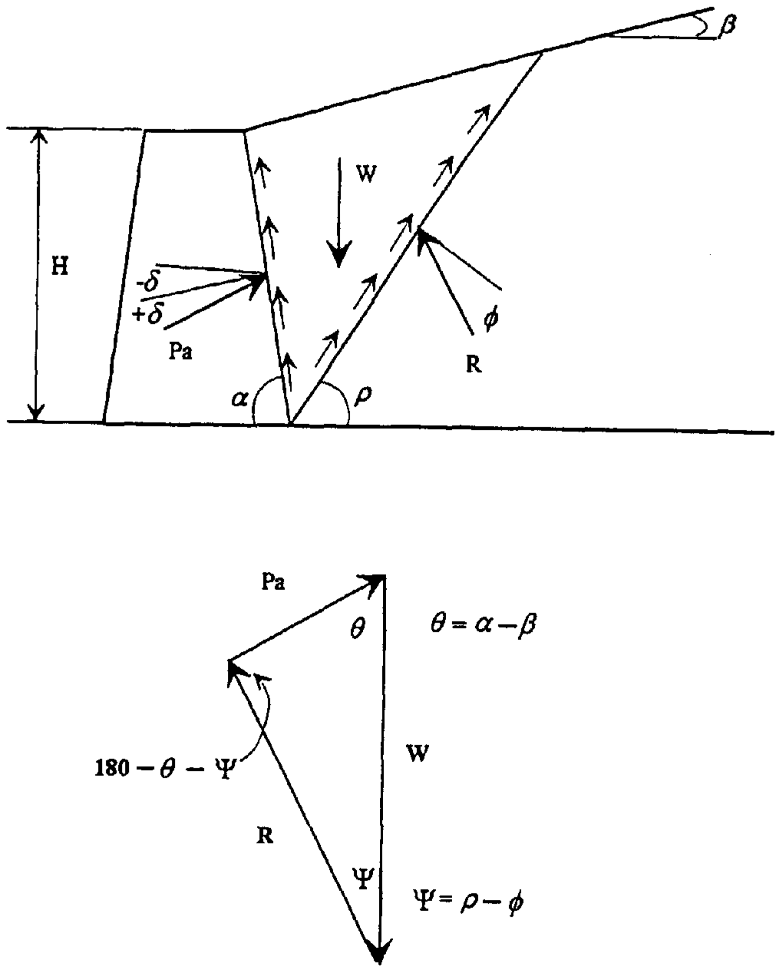

FIGURE 88
Coulomb Earth Pressures with Wall Friction

Figure 80 shows the experimental R-y curve developed from the back-calculated earth pressures for the Texas A&M wall. R-y curves for continuous walls and the above-ground portion of soldier beam walls are similar to the experimental curve for the Texas A&M wall. Figure 89 shows typical R-y curves for anchored soldier beam and continuous walls in sand. Rankine or Coulomb earth pressure coefficients are used to determine the maximum and minimum loads applied to the wall over a unit depth. An active reference deflection of 0.05 in and a passive reference deflection of 0.5 in are used in the development of the R-y curves for cohesionless soils. The slope of the elastic portion of the R-y curve is assumed to be established by the active and passive limit loads and the reference deflections. Sensitivity analyses in Section 3.5.1 showed that bending moments are not sensitive to the value of the at-rest earth pressure coefficient. Therefore, a straight line is used to describe the elastic behavior of the wall between the active and the passive response of the wall. As Figure 89 shows, the active and passive loads used to develop the R-y curves for a soldier beam wall use active and passive pressures multiplied by the soldier beam spacing. Active and passive loads for continuous wall, R-y curves use active and passive pressures over a unit width.

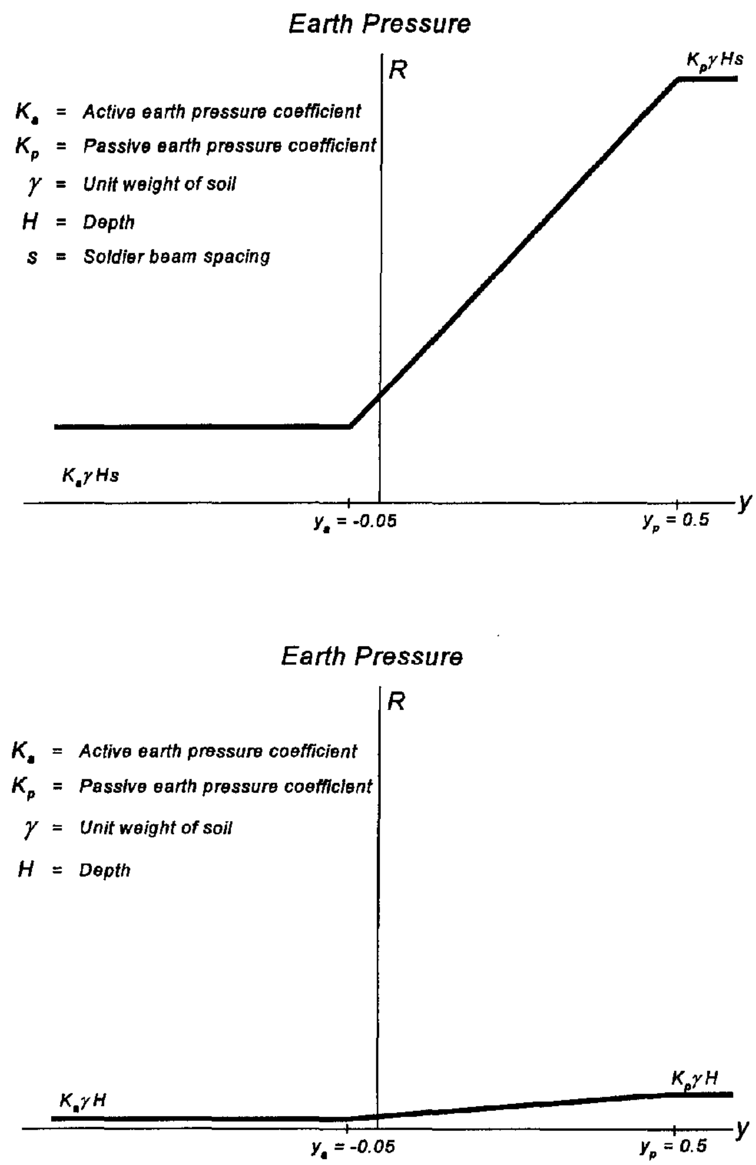

FIGURE 89
Diagram Illustrating a Plane Strain R-y Curve for an Anchored Wall in Sand

3.3.2.2 R-y Curve for a Single Soldier Beam in Sand

Soil resistance-deflection (R-y) curves for the portion of a soldier beam below the bottom of the excavation are different from the plain strain R-y curves for a continuous wall or a soldier beam wall above the bottom of the excavation. R-y curves for the soldier beam toe should include three-dimensional effects. Since soldier beam toes are similar to laterally loaded piles, they will develop their load-carrying capacity similarly. American Petroleum Institute (API) soil response curves (P-y curves) developed from full-scale load tests on laterally loaded piles in sand (O'Neill and Murchison, 1983) were selected by Texas A&M to model the embedded portion of a soldier beam (toe). Murchison and O'Neill (1984) showed that these curves accurately predicted the response of piles to lateral loads. Equation 3.21 describes the response of the API single pile shown in Figure 90.

$$P = AP_u \tanh\left(\frac{kz}{AP_u}y\right) \qquad \text{. . . [3.21]}$$

$$A = 3 - 0.8\frac{z}{b} \geq 0.9 \qquad \text{. . . [3.22]}$$

where:

P_u = ultimate lateral resistance at depth, z (lb/in)

k = initial modulus of subgrade reation, (lb/in^3) from Figure 91

b = soldier beam diameter or width (in)

z = depth considered (in)

In Equation 3.21, the ultimate lateral resistance for sand, P_u, varies from a value of P_{us} at shallow depths to a value of P_{ud} below (O'Neill and Murchison, 1983). P_{us} is the resistance of a shallow three-dimensional wedge of soil, and P_{ud} is the resistance determined by plastic flow of the soil around the pile. To determine P_u at a given depth, calculate P_{us} and P_{ud} using Equations 3.23 and 3.24, and select the smaller of the two values. Then, P_u is substituted in Equation 3.21 to calculate the lateral resistance at that depth for a given deflection.

$$P_{us} = \left(C_1 z + C_2 b\right)\sigma'_v \qquad \text{. . . [3.23]}$$

$$P_{ud} = C_3 b \sigma'_v \qquad \text{. . . [3.24]}$$

where

σ'_v = effective vertical stress at depth z (psi)

C_1, C_2, C_3 are coefficients from Figure 91

b = average pile diameter (in)

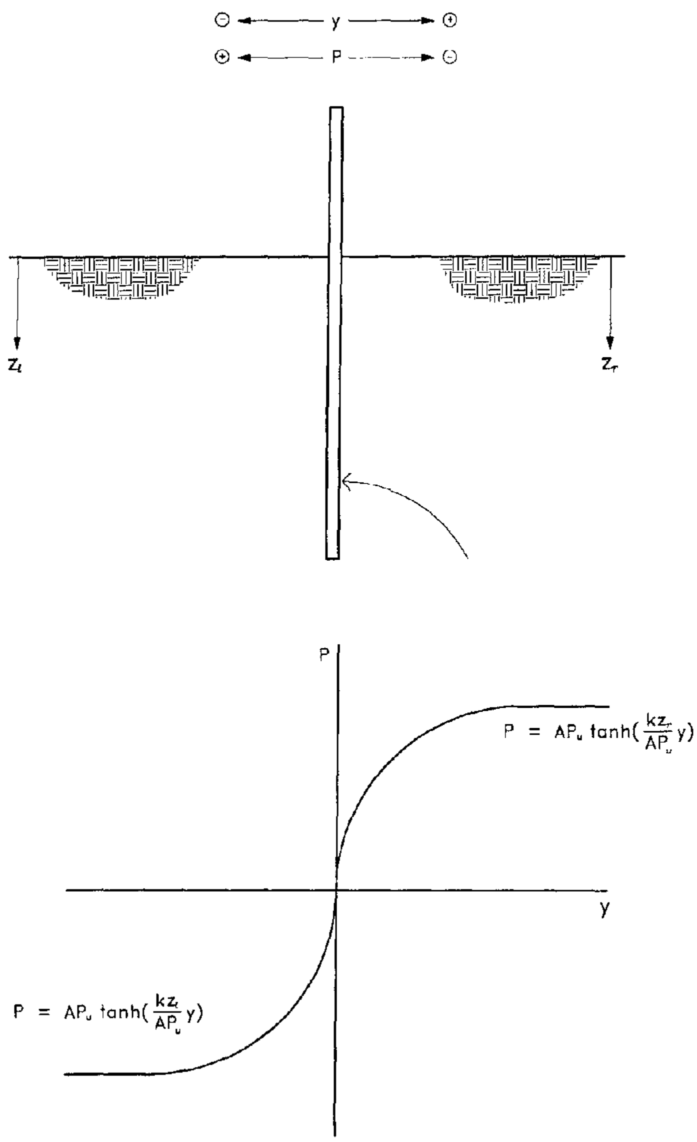

FIGURE 90
Diagram Illustrating a Non-linear API *P-y* Curve for a Single Pile in Sand

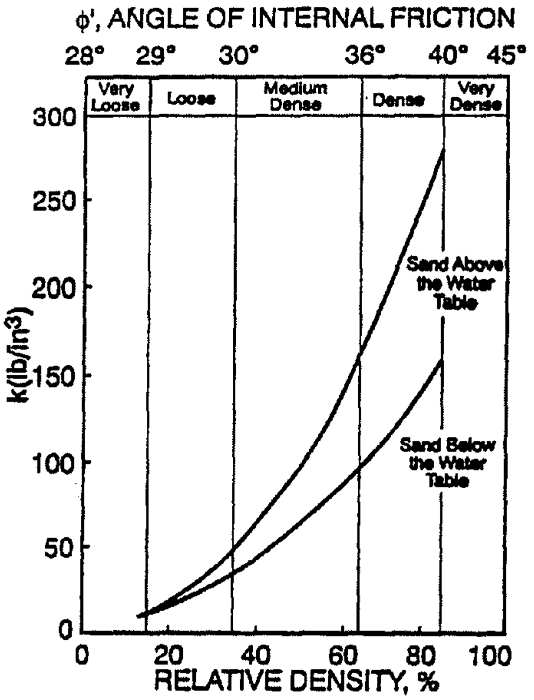

a) Coefficients C_1, C_2, and C_3

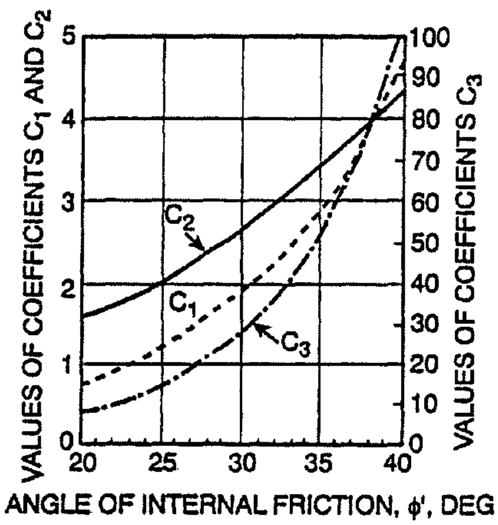

b) Initial modulus of subgrade reaction, k

FIGURE 91
Coefficients and k for API Single Pile P-y Curves in Sand
(Murchison & O'Neill, 1983)

API P-y curves for single piles in sand were developed from load tests on piles with a horizontal ground surface. Therefore, the P-y curve is symmetrical and represents the pressure difference between the active earth pressures on one side of the pile and passive pressures on the other side. Excavation for an anchored wall causes the ground surface in front of the wall to be lower than the ground surface behind the wall. This imbalance must be considered when adapting the API P-y curves to predict the response of an anchored soldier beam (R-y curves). Figure 92 shows how a typical API curve is modified to account for the excavation in front of the wall.

In Figure 92, the solid curve for the left side of the soldier beam is the API P-y curve, assuming that the ground surface surrounding the soldier beam is at the bottom of the excavation. The solid P-y curve for the right side of the soldier beam assumes that the ground surface is at the level behind the wall. These two curves have to be shifted to account for the differences in the active pressure components in the curves. Since the active thrust on the back of the wall is $K_a \gamma H b$ greater than the active thrust incorporated in Equation 3.21 for the left side of the beam, then the ultimate resistance for the left side must be decreased by $K_a \gamma H b$. In addition, the active thrust on the front of the wall is $K_a \gamma H b$ less than the active thrust component incorporated in Equation 3.21 for the right side of the beam. Therefore, the ultimate resistance for the right side of the wall is increased by $K_a \gamma H b$. The dotted curve in Figure 92 represents a typical combined R-y curve that would be used to describe the soil response-deflection behavior of a soldier beam's toe.

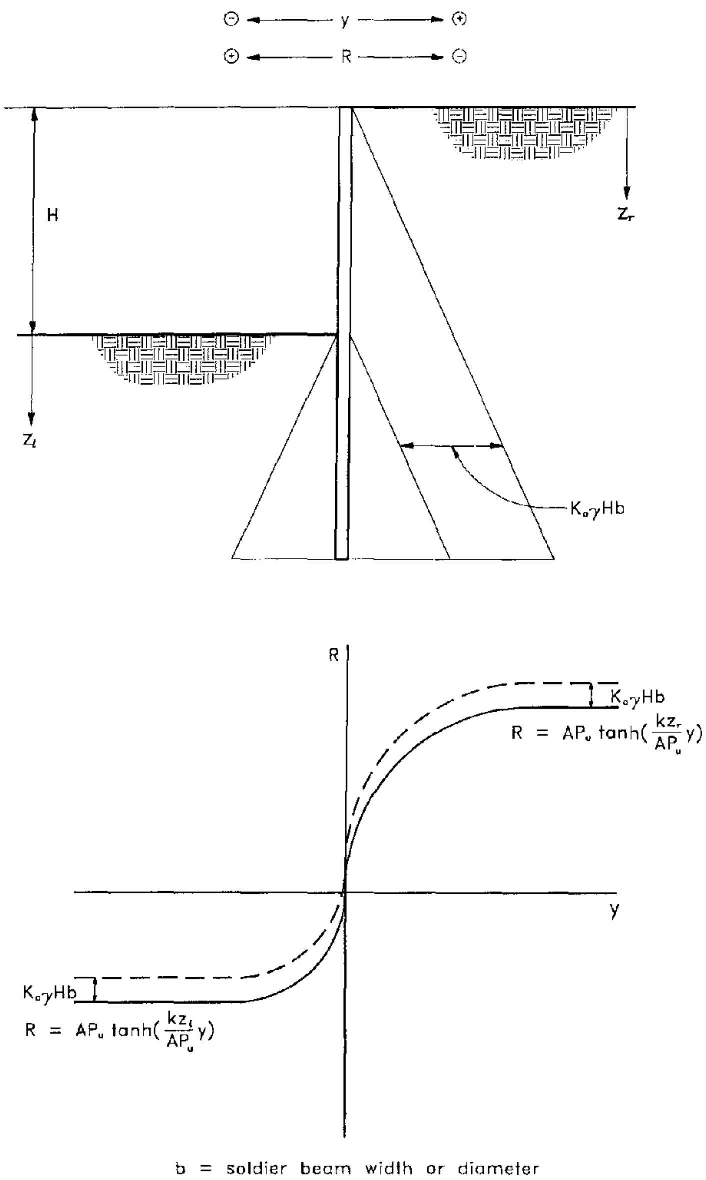

FIGURE 92
Diagram Illustrating an *R*-*y* Curve for the Toe of a Soldier Beam in Sand

3.3.2.3 Plane Strain R-y Curves for Clay

Anchored walls are frequently constructed in a short time and the porewater pressures in a clay supported by the wall do not change significantly for an extended period after the wall is completed. In this case, undrained (total stress) shear strengths are used to develop the R-y curves. If the porewater pressures dissipate with time, then drained (effective stress) shear strengths are used to develop the plane strain R-y curves. Porewater pressures in the clay below the bottom of the excavation are unlike to change from those assumed during design. Therefore, undrained strengths are used to develop the R-y curves for clays below the bottom of the excavation.

Figure 93 shows typical R-y curves for different portions of a continuous anchored wall supporting a cohesive soil. For the undrained (total stress) case, the active, passive and at-rest earth pressures in a clay at a depth, z, are given by Equations 3.25, 3.26 and 3.27, respectively. Computed earth pressures for each depth and the reference deflections given in Table 23 are used to develop the total stress R-y curves as a function of depth for the anchored wall. For a soldier beam wall, the pressures are multiplied by the soldier beam spacing.

Active earth pressures in clay can be negative (tension) from the ground surface to some depth depending upon soil strength. In a total stress analysis, the active earth pressures are negative to a critical depth, H_c, given by Equation 3.28. Since the soil wall interface cannot develop tension, the active earth pressures are considered zero above the critical depth. A typical R-y curve above the critical depth is shown in Figure 93.

$$P_{active} = \sigma_v - 2s_u \qquad \text{. . . [3.25]}$$

$$P_{passive} = \sigma_v + 2s_u \qquad \text{. . . [3.26]}$$

$$P_{at\text{-}rest} = \sigma_v \qquad \text{. . . [3.27]}$$

$$H_c = 2\frac{s_u}{\gamma} \qquad \text{. . . [3.28]}$$

where:

s_u = undrained shear strength of the clay

γ = total unit weight

σ_v = total vertical stress at depth z

TABLE 23
Reference Deflections for Plane Strain R-y Curves for Clay

	$s_u < 2tsf$	$2tsf < s_u < 4tsf$	$s_u > 4tsf$
y_a	-0.20 in	-0.15 in	-0.12 in
y_p	+1.0 in	+0.8 in	+0.4 in

For the drained (effective stress) case, the active, passive, and at-rest earth pressures in a clay at a depth, z, are given by Equations 3.29, 3.30, and 3.31, respectively.

$$P_{active} = K_a \sigma'_v - 2c\sqrt{K_a} \quad \ldots [3.29]$$

$$P_{passive} = K_p \sigma'_v + 2c\sqrt{K_p} \quad \ldots [3.30]$$

$$P_{at\text{-}rest} = K_o \sigma'_v \quad \ldots [3.31]$$

where:

K_a = active earth pressure coefficient
K_p = passive earth pressure coefficient
K_o = at-rest earth pressure coefficient
σ'_v = vertical effective stress at depth z
c = drained cohesion of the soil

Equations 3.14, 3.15, and 3.16 are used to calculate the drained case earth pressure coefficients for a cohesive soil. Accurately estimating the porewater pressures is necessary to determine the vertical effective stress to be used in an effective stress analysis.

In an effective stress analysis the active earth pressures can be negative (tension) from the ground surface to some depth. The critical depth for effective stress R-y curves is given by Equation 3.32. Critical depth for effective stress R-y curves is different from the critical depth for total stress R-y curves. However, effective and total stress R-y curves above the critical depth are constructed similarly. Figure 93 shows a typical effective stress R-y curve above the critical depth H_c.

$$H_c = \frac{2c}{\gamma\sqrt{K_a}} + \frac{u}{\gamma} \quad \ldots [3.32]$$

where:

γ = total unit weight
u = porewater pressure
c = cohesion intercept
K_a = active earth pressure coefficient

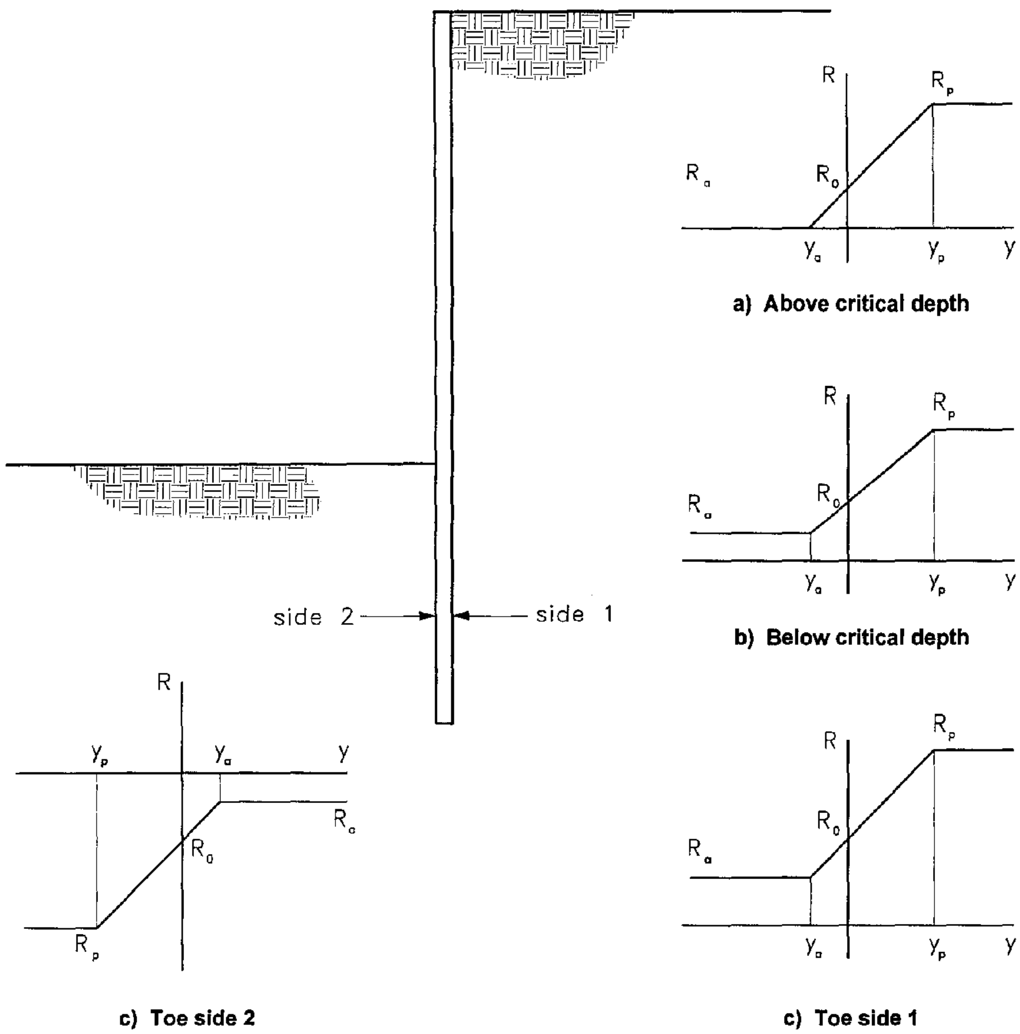

FIGURE 93
Diagram Illustrating Non-linear Plane Strain *R-y* Curves for a Retaining Wall in Clay

3.3.2.4 R-y Curves for a Single Soldier Beam in Clay

The soil resistance-deflection (R-y) curves for the toe of a soldier beam in clay are different from the plane strain R-y curves for a continuous wall or a soldier beam wall above the bottom of the excavation. R-y curves for soldier beam toes in clays are based on laterally loaded pile tests performed by Reese, et al. (1975). In a stiff clay, Reese found the ultimate resistance, P_u, at depth, z, is given by Equation 3.33.

$$P_u = A\,[2 s_u b + \sigma_v b + 2.83\, s_u z] \le 11 A\, s_u b \qquad \ldots [3.33]$$

where:

A = reduction factor that depends on the depth considered (Table 24)
b = soldier beam diameter width
s_u = undrained shear strength of the soil
σ_v = total vertical stress at depth z

TABLE 24
Factor *A* for Equation 3.33

A	DEPTH
0.2	z = 1
0.5	0 < z < 2b
1.0	z > 2b

A typical lateral resistance-deflection curve for a single pile in stiff clay using Equation 3.33 is shown in Figure 94. The elastic portion of the P-y curve is established by selecting reference deflections y_{cl} and y_{cr}. The P-y curve in Figure 94 is symmetrical since the ground surface is horizontal. R-y curves for the toe of a soldier beam in clay will be non-symmetrical, since two terms in Equation 3.33 depend upon the overburden depth. Figure 95 shows how an R-y curve would be developed from the P-y curve shown in Figure 94. Table 25 contains the reference deflections required to define the elastic portion of the R-y curve. These deflections were developed from laterally loaded pile practice and verified/modified after comparing predicted bending moments against measured bending moments for the case histories presented in Sections 3.4.4 and 3.4.5.

TABLE 25
Reference Deflections for Single Pile *R-y* Curves for Clay

	s_u < 2tsf	2tsf < s_u < 4tsf	s_u > 4tsf
y_{cl}	-0.7 in	-0.5 in	-0.1 in
y_{cr}	+0.7 in	+0.5 in	+0.1 in

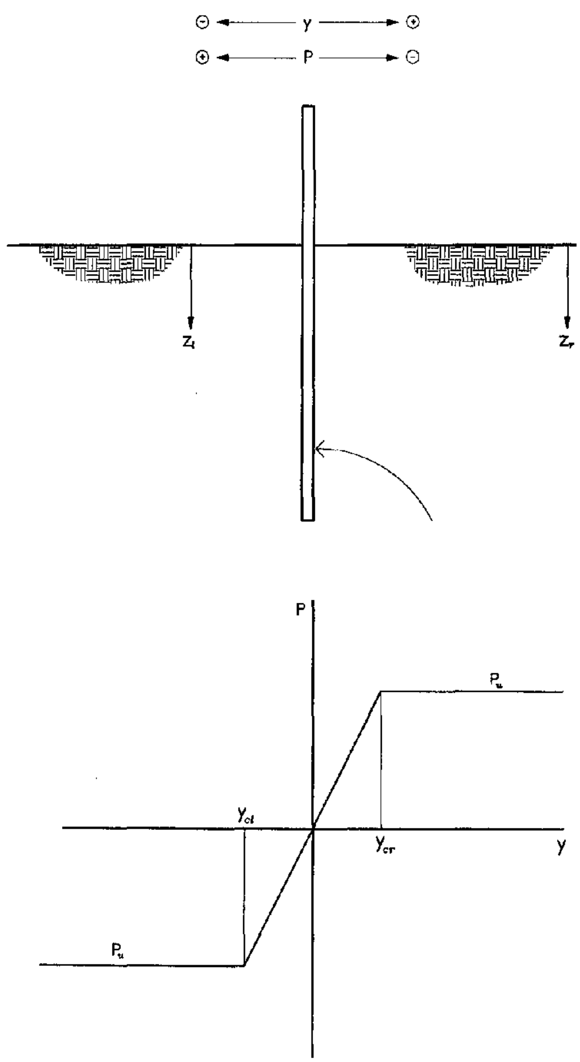

FIGURE 94
Diagram Illustrating a Non-linear *P-y* Curve for a Single Pile in Clay

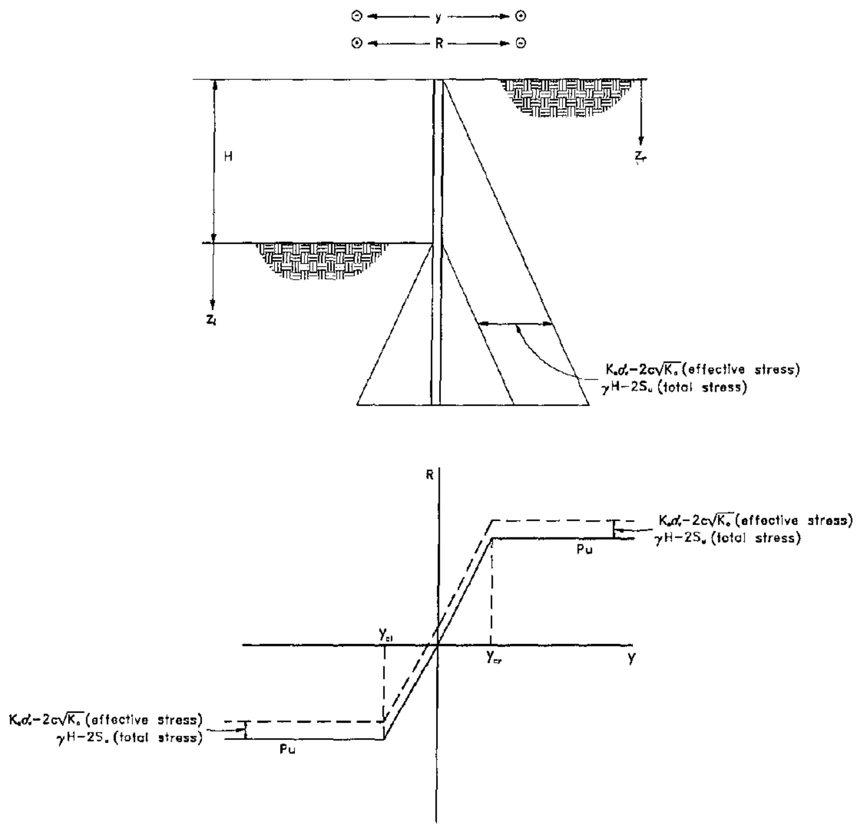

FIGURE 95
Diagram Illustrating an *R*-*y* Curve for the Toe of a Soldier Beam in Clay

3.3.3 Modeling the Ground Anchors

A ground anchor applies two types of loads to an anchored wall. Stressing of an anchor is simulated by applying a constant load on the wall (Figure 85). After the anchor is stressed and locked-off, the anchor load depends on the deflection of the wall, and the load applied by the ground anchor is simulated by an anchor load-deflection (T-y) curve (Figures 87 and 96). Since ground anchors are installed at an angle, the horizontal components of anchor load and elongation are used in developing the T-y curves. To simulate the construction sequence, the T-y curve for an anchor is developed so the lock-off load corresponds to the wall deflection from the previous construction stage (anchor stressing).

Figure 96 shows that the anchor force increases as the wall moves outward, and decreases as the wall moves into the supported ground. The initial slope of the T-y curve is the anchor tendon stiffness, and it is given by Equation 3.34.

$$k = \frac{A_s E_s}{L_u} \cos \alpha \qquad \ldots [3.34]$$

where:

k = anchor tendon stiffness
A_s = area of anchor tendon
E_s = Young's modulus for the anchor tendon
L_u = effective unbonded length
α = anchor inclination

In Equation 3.34, the effective elastic length of the anchor tendon is assumed to be the sum of the unbonded length plus half the tendon bond length. The actual effective elastic length can be determined from ground anchor tests if the beam-column program is used to analyze an actual installation. At the yield load, the T-y curve changes slope. The second portion of the anchor curve (Figure 96) represents the ground anchor behavior between the yield and ultimate tendon strength.

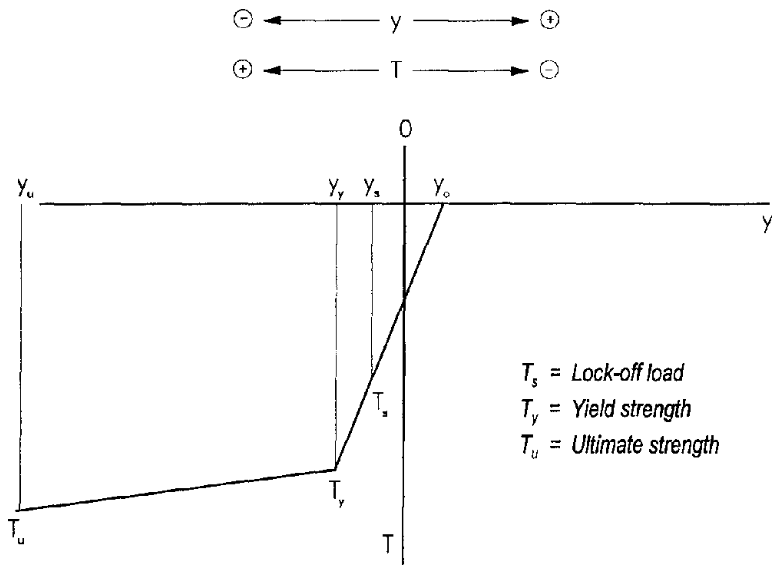

Deflections

$y = 0$ = zero deflection for T-y curve (*curve shifted*)

y_o = wall deflection when anchor load = 0

y_s = wall deflection after anchor stressing (*lock-off*)

y_y = wall deflection when anchor tendon yields

y_u = wall deflection when anchor tendon ruptures

y_s = shift in T-y curve

$y_o + |y_s|$ = (elastic elongation of tendon during stress) x (cos α)

(α = *anchor angle the horizontal*)

$y_o + |y_y|$ = horizontal component of tendon elongation @ yield strength $= \frac{f_{yield} L_u}{A_s E_s} \cos \alpha$

(f_{yield} = yield strength of the anchor tendon)

(L_u = effective elastic length of the anchor tendon)

(A_s = tendon area)

(E_s = Young's modulus of the tendon)

$y_o + |y_u|$ = horizontal component of tendon elongation @ ultimate strength $= L_u \epsilon_{rupt} \cos \alpha$

(ϵ_{rupt} = rupture strain)

FIGURE 96
Diagram Illustrating a Ground Anchor *T-y* Curve

3.3.4 Simulation of the Construction Sequence

The construction sequence can be simulated by a series of unloading and loading stages. Excavation removes overburden pressures from in front of the wall and causes horizontal unloading. Anchor stressing causes horizontal loading of the wall. The construction sequences that are modeled consist of simulating a series of excavation stages and anchor stressing stages.

Section 3.3.1.2 conceptually describes the shifting of the *R-y* curves to enable the construction stages to be modeled. *R-y* curves implemented in BMCOL76 and other beam-column computer programs have to be modified to include construction effects in a manner compatible with the program. The *R-y* curve shown in Figure 97 models the soil response at a ground anchor location as the excavation is made and the anchor is stressed. Excavation to the upper ground anchor level causes the wall to deflect outward and an unloading of the *R-y* curve from point A to point C (Figure 97). During anchor stressing, the wall is pulled back into the ground from point C toward point D (Figure 97). If the passive resistance of the wall is exceeded during anchor stressing, the deflection of the wall would move from point D toward point E. Figure 97 shows that reloading associated with anchor stressing does not follow the unload curve if plastic movements have occurred. Beam-column computer programs cannot use soil response curves with different loading and unloading curves similar to the one shown in Figure 97. These programs required that the loading and unloading of the system follow the same soil response curve. Therefore, to model the different construction stages associated with an anchored wall, it is necessary to shift the *R-y* curves to account for the plastic movement that occurs at that location.

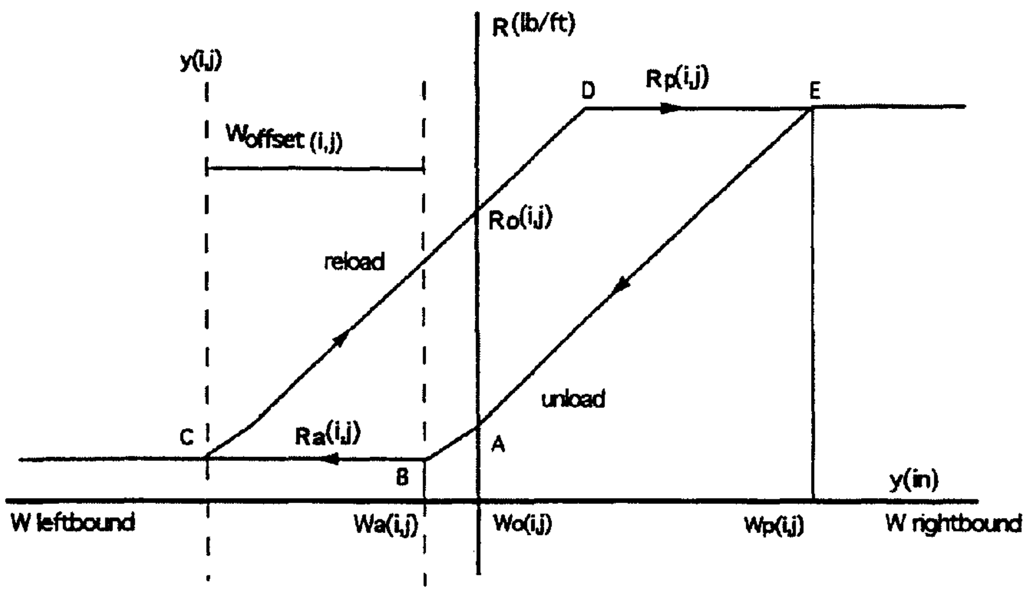

FIGURE 97
Diagram Illustrating a Yielded Non-linear *R-y* Curve at a Ground Anchor Location

Plastic movement at a locations occurs after the soil mass has been strained sufficiently to mobilize the shear strength of the soil. In Figure 97, the plastic movement is represented by the offset distance, w. This offset distance is used to shift the R-y curves using the following procedure. The offset distance for location, i, and construction stage j, is $w_{offset}(i,j)$ and it is used to prepare the R-y curves of the $(j+1)th$ construction stage.

The procedure for determining the offset distances for a construction stage uses the following definitions:

$w_a(l, j)$	=	deflection required to mobilize the active resistance of the R-y curve at node l as an input to the simulation of the jth construction stage,
$w_o(l, j)$	=	deflection corresponding to the at-rest resistance of the R-y curve at node l as an input to the simulation of the jth construction stage,
$w_p(l, j)$	=	deflection required to mobilize the passive resistance of the R-y curve at node l as an input to the simulation of the jth construction stage,
$w_{offset}(l, j)$	=	deflection at the ith node obtained at the end of the jth construction stage,
$R_a(l, j)$	=	active force per unit depth of wall in the R-y curve at node l as an input to the simulation of the jth construction stage,
$R_o(l, j)$	=	at-rest force per unit depth of wall in the R-y curve at node l as an input to the simulation of the jth construction stage, and
$R_p(l, j)$	=	passive force per unit depth of wall in the R-y curve at node l as an input to the simulation of the jth construction stage.

The calculation of the offset distance to be used in preparing the R-y curves for the $(j+1)th$ construction stage and for the portion of the wall that was above the excavation level (Zone 1 in Figure 98) varies depending upon which one of the following cases is satisfied. For a given deflection, $y(i,j)$ the offset distance, $w_{offset}(i,j)$ is

Case 1 $\quad y(i,j) > w_p(i,j)$

$$w_{offset}(i,j) = y(i,j) - w_p(i,j) \qquad \ldots [3.35]$$

Case 2 $\quad w_a(i,j) < y(i,j) < w_p(i,j)$

$$w_{offset}(i,j) = 0 \qquad \ldots [3.36]$$

Case 3 $\quad y(i,j) < w_a(i,j)$

$$w_{offset}(i,j) = y(i,j) - w_a(i,j) \qquad \ldots [3.37]$$

Note: $w_{offset}(i,j)$, 0 in Case 3

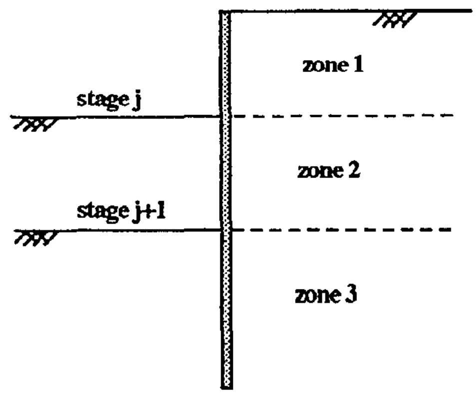

FIGURE 98
Zones for Calculating $w_{offset}(i, j)$

The offset distance for the R-y curves along the portion of the wall below the excavation level at the end of the jth construction stage, but above the excavation level for the $(j+1)th$ construction stage (Zone 2 in Figure 98) is

$$w_{offset}(i, j) = y(i, j) \qquad \text{. . . [3.38]}$$

In Zone 3 (Figure 98), for portions of the wall that will remain below the excavation level for the $(j+1)th$ construction stage, the offset distance, $w_{offset}(i, j)$ for the R-y curves is

$$w_{offset}(i, j) = 0 \qquad \text{. . . [3.39]}$$

To construct the new R-y curves for the $(j+1)th$ construction stage at node i the forces per unit depth of the wall are determined in accordance with procedures outlined in Section 3.3.2. The deflections required for the $(j+1)th$ R-y curves simulate the effects of the jth construction stages and are equal to the following

$$w_{left}(i, j+1) = w_{leftbound} \qquad \text{. . . [3.40]}$$

$$w_a(i, j+1) = w_a(i, j) + w_{offset}(i, j) \qquad \text{. . . [3.41]}$$

$$w_o(i, j+1) = w_o(i, j) + w_{offset}(i, j) \qquad \text{. . . [3.42]}$$

$$w_p(i, j+1) = w_p(i, j) + w_{offset}(i, j) \qquad \text{. . . [3.43]}$$

$$w_{right}(i, j+1) = w_{rightbound} \qquad \text{. . . [3.44]}$$

A flowchart outlining the simulations of the construction sequences in BMCOL76 is shown in Figure 99.

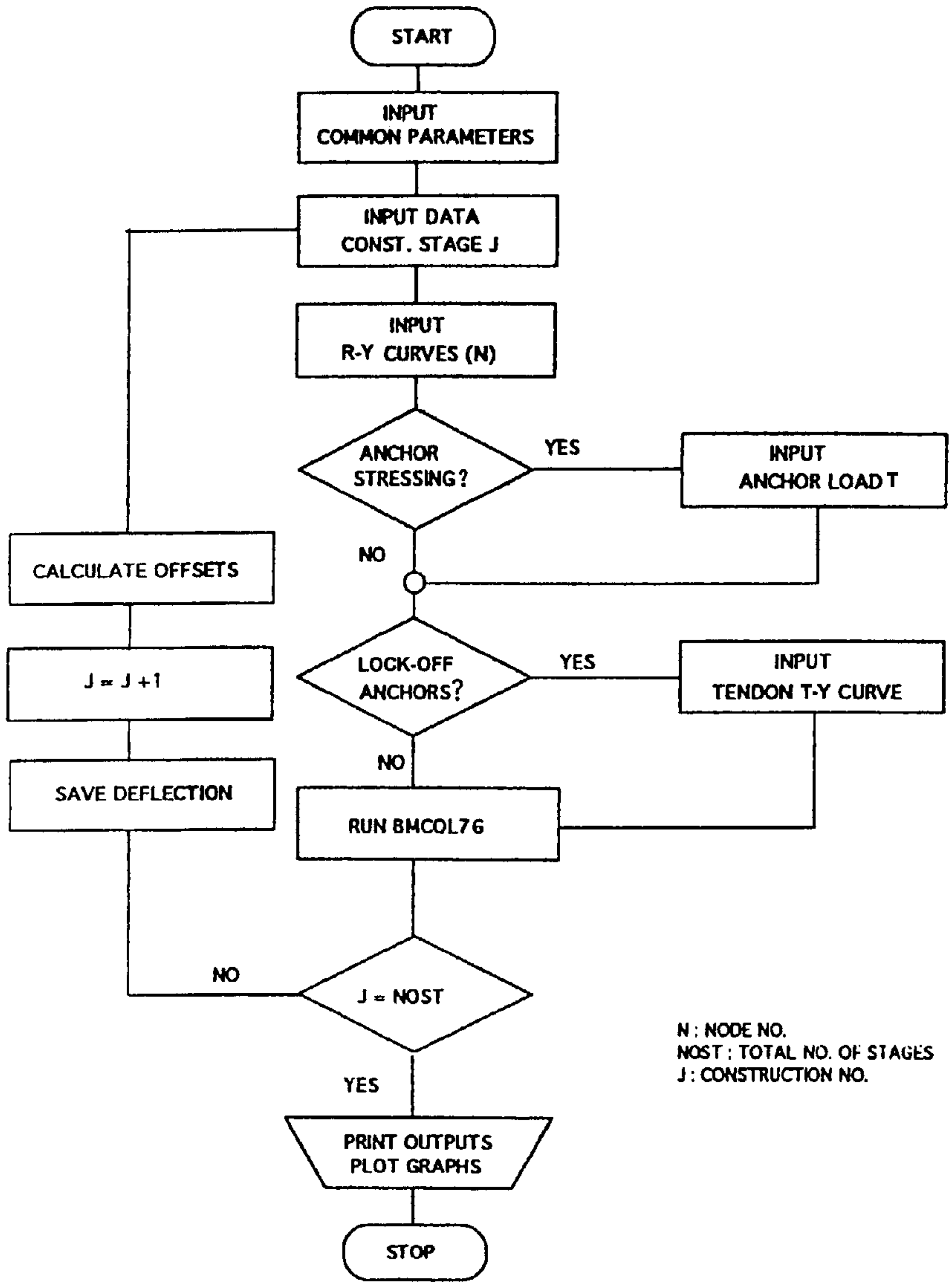

FIGURE 99
BMCOL76 Flowchart for Modeling the Construction Sequence

3.4 BEAM-COLUMN METHOD PREDICTIONS

The behavior of five anchored walls was predicted using the beam-column method and shifted R-y curves to model the construction sequence. Predictions were compared with the observed performance of the walls. First, predictions for the one-tier Texas A&M wall using back-calculated R-y curves (Section 3.3.2.1) and single soldier beam R-y curves (Section 3.3.2.2) were compared with measured results. Then, predictions were developed for the two-tier Texas A&M wall using R-y curves similar to those developed for the one-tier wall (adjustments were made for soldier beam width). Plane strain R-y curves for sand (Section 3.3.2.1) were used to predict the behavior of a structural diaphragm wall in a coarse-grained soil deposit (Bonneville Navigation Lock wall). The Bonneville wall was analyzed to evaluate whether the recommendations for plane strain R-y curves in sand were satisfactory for a continuous wall having high ground anchor loads (anchors pulled the wall back into the ground). Total and effective stress R-y curves for clays were used in the analyses of a two-tier wall in Lima, Ohio, and a six-tier wall in Boston, Massachusetts. The Lima and Boston walls were used to evaluate the reference deflections presented in Sections 3.3.2.3 and 3.3.2.4. Since the ground anchor loads for the Lima wall were high (design loads greater than loads determined from at-rest earth pressures), the predictions evaluated the passive portion of the R-y curves. Ground anchor loads for the Boston wall were determined from apparent earth pressures diagrams and the wall was not pulled back into the ground. Predictions for the Boston wall were used to evaluate the active and passive portions of the R-y curves for clays.

3.4.1 One-tier Wall at Texas A&M

BMCOL76, modified to enable the R-y curves to be shifted to account for the effects of construction, was used to predict the bending moments and the deflections for the one-tier wall built at Texas A&M. Plane strain R-y curves for sand (Section 3.3.2) were used for the portion of the wall above the bottom of the excavation. Active and passive earth pressure coefficients and reference deflections from the experimental R-y curve (Section 3.2.2) were used to develop the plane strain R-y curves for the analysis. Table 26 presents the experimental R-y curve parameters. The active earth pressure coefficient from the experimental R-y curve was about 50 percent of the Rankine active earth pressure coefficient. This low active pressure coefficient had to be used, since the wall failed in analyses when the recommended R-y curves for sand (Section 3.3.2) were used. Arching appears to cause the earth pressures to be reduced in the span between the ground anchor and the bottom of the excavation, and the experimental active earth pressure coefficient is correct. Unfortunately, a mathematical relationship for reducing the Rankine or Coulomb active coefficients could not be developed. R-y curves for a single soldier beam in sand (Section 3.3.2.2) were used for the soldier beam toe. Predictions were made for the following construction stages:

1. Excavate to 10 ft.
2. Stress the anchor at 9 ft.
3. Excavate to 25 ft.

TABLE 26
Back-calculated Parameters for Experimental Plane Strain *R-y* Curve for Texas A&M Wall

Active earth pressure coefficient	0.15
Active reference deflection	0.05 in
Passive earth pressure coefficient	6.6
Passive reference deflection	0.5 in

Calculated bending moments and deflections were compared with those measured during construction of the wall.

The one-tier wall was installed in a medium dense sand with a unit weight of 115 pcf and a friction angle of 32°. Wall data necessary for the analysis are presented in Table 27. Table 28 presents the data used to develop the *T-y* curve for the ground anchor.

TABLE 27
Data for One-tier Texas A&M Wall

Wall height	25 ft
Soldier beam toe	5 ft
Beam flange width	10.2 in
Lateral stiffness, EI	1.25 wall 10^{10} lb-in^2
Soldier beam spacing	8 ft

TABLE 28
Ground Anchor Data for One-tier Texas A&M Wall

Unbonded length	15 ft
Tendon bond length	24 ft
Lock-off load	68.6 kips
Tendon area	1.25 in^2
Young's modulus	29,000 × 10^3 psi
Rupture strain	4%
Yield strength	150 kips
Ultimate strength	187.5 kips
Anchor angle	30°

Anchor stressing was simulated by applying a constant load at the anchor location. For the final construction stage, a T-y curve (Section 3.3.3) was used to model the ground anchor. The construction sequence was simulated by shifting R-y and T-y curves as explained in Section 3.3.4. Measured deflections and bending moments for the three construction stages are compared with the predictions from the BMCOL76 analyses in Figures 100 and 101. Bending moments and deflections calculated for the final construction stage, with and without the construction sequence modeled, are shown in the figures.

Figure 100a and Figure 101a show that the predicted deflections and bending moments for the first construction stage, a 10-ft cantilever excavation, were larger than the measured ones. The predicted location of the maximum bending moment was lower than the observed location.

After anchor stressing, in the second construction stage (Figures 100b and 101b), the predicted bending moments above the ground anchor and the maximum bending moment at the ground anchor were similar to the measured moments. Below the ground anchor the predicted bending moments were larger than the actual bending moments. Deflection profiles (Figures 100a and 100b) show that anchor stressing caused the wall to move back into the ground approximately 0.05 in near the anchor. Figures 100a and 100b show that the analyses predicted that the wall would move back about 0.145 in after stressing.

For the final excavation stage, Figure 100c shows that the measured lateral movements and the deflections predicted using R-y curves that modeled the construction sequence were similar. Figure 100c also shows that the prediction assuming that the wall was "wished" into the ground underestimated the deflections. Predicted and measured bending moments for the final construction stage are shown in Figure 101c. The predicted moment diagram for the analysis that modeled the construction sequence was close to the measured moment diagram. Predicted bending moments developed without modeling the construction sequence were less than the measured moments along the upper portion of the wall and larger than the measured moments in the lower portion of the wall. Bending moments predicted by either method were reasonably close to the measured moments. However, deflections calculated without considering the construction sequence were significantly less than the measured deflections.

The following observations are made regarding the analysis of the one-tier Texas A&M wall. Deflection predictions using R-y curves that model the construction sequence cannot account for all of the sources of anchored wall movements. R-y curves do not include movements resulting from settlement of the wall or mass movements of the anchor-wall system. Therefore, movement predictions from beam-column or beam-on-elastic-foundation analyses should not be relied upon to given accurate deflection estimates. Bending moment predictions using beam-column analyses and back-calculated R-y curves predicted the bending moments satisfactorily. Moment predictions using the recommended R-y curves could not be made since the wall failed when the recommended active earth pressure coefficients were used. The use of soil-structure interaction analyses and R-y curves for flexible walls is discussed in Section 3.6.

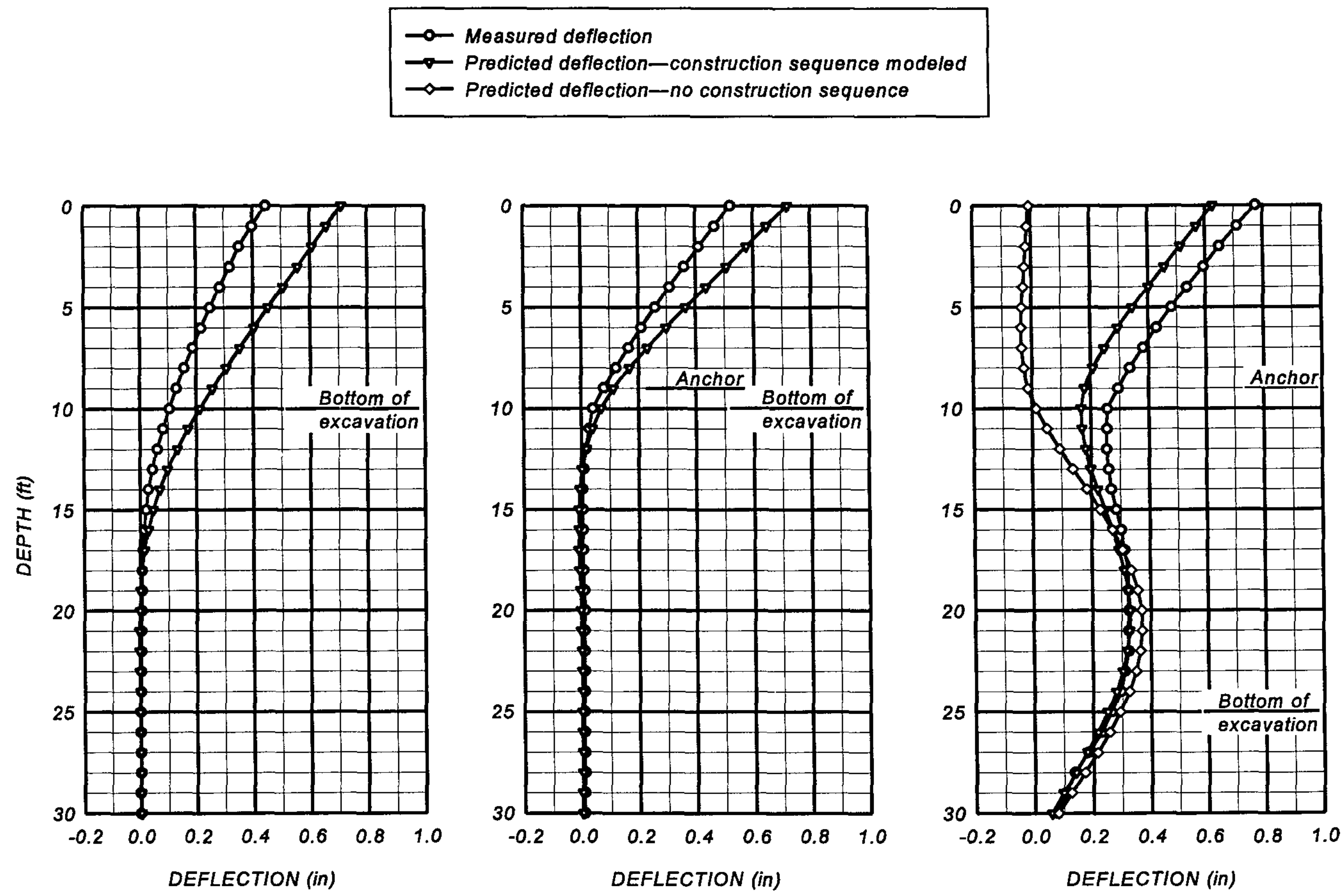

a) 10-ft Excavation

b) Anchor stressed

c) Final excavation (25 ft)

FIGURE 100
Measured and BMCOL76 Predicted Deflections for One-tier Texas A&M Wall

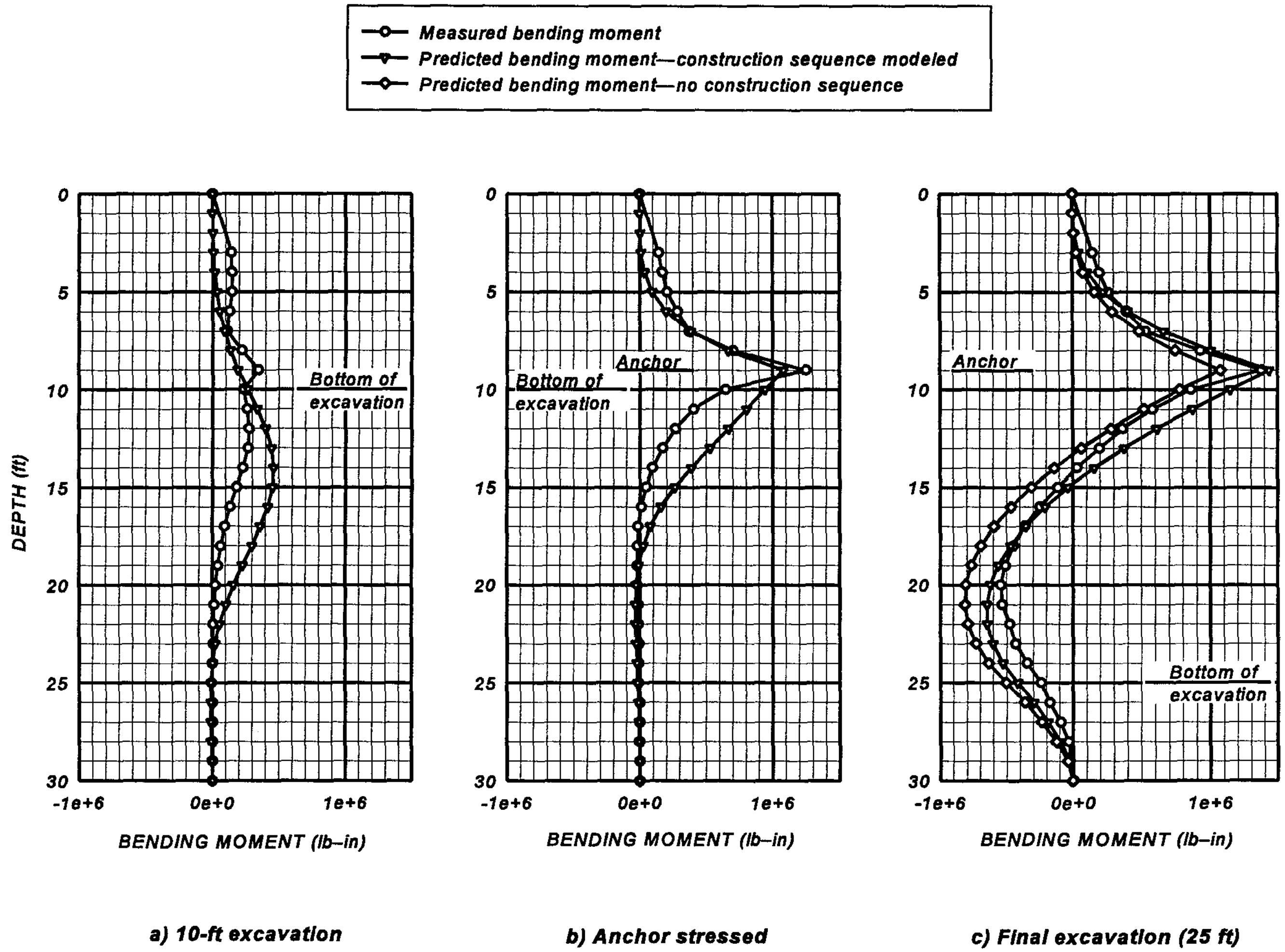

FIGURE 101
Measured and BMCOL76 Predicted Bending Moments for One-tier Texas A&M Wall

Figure 102 shows the back-calculated earth pressure diagram determined by double differentiation of the cubic spline bending moment interpolant (Section 3.2.2), and the pressures predicted by the BMCOL76 analysis. Dotted portions of these two curves were estimated. Terzaghi and Peck's apparent earth pressures for a soil having a $\phi = 32°$ and a $\gamma = 115$ pcf, $25H$ apparent earth pressures (the design diagram), and Rankine active earth pressures also are shown in Figure 102. At the ground anchor location, the predicted earth pressures were significantly greater than the Rankine pressures, 20 to 33 percent greater than the apparent earth pressures, and less than the back-calculated pressures. Above and below the ground anchor the back-calculated and predicted earth pressures were less than the apparent earth pressures. At the ground anchor location, bending moments associated with the back-calculated pressures, and moments calculated from the predicted earth pressures or the design pressure diagram were the same. Predicted and back-calculated earth pressures near the ground anchor show that, at the anchor, the wall distributes the anchor load to the soil. Below 13 ft, the wall was loaded by the ground and the predicted and back-calculated earth pressures were small. There the pressures equaled the overburden stress times an earth pressure coefficient of 0.15.

The predicted bending moments in Figure 101c were developed from the predicted earth pressures shown in Figure 102. Below 13 ft, predicted and measured bending moments were similar and the back-calculated and predicted earth pressures were similar. Figure 56 shows that the measured bending moments for the lower portion of the wall were 60 percent of the design bending moments (determined from the $25H$ pressure diagram), and 300 percent less than moments predicted by triangular pressure diagrams. These observations indicate that apparent earth pressure diagrams overestimate the bending moments for the lower portion of the wall, and support using the bending moment reduction recommended by Peck, et al. (1974) when designing single-tier anchored walls. Comparing the measured and predicted bending moments with the bending moment diagrams in Figure 56 also shows that Rankine triangular earth pressure diagrams are not appropriate for one-tier anchored walls.

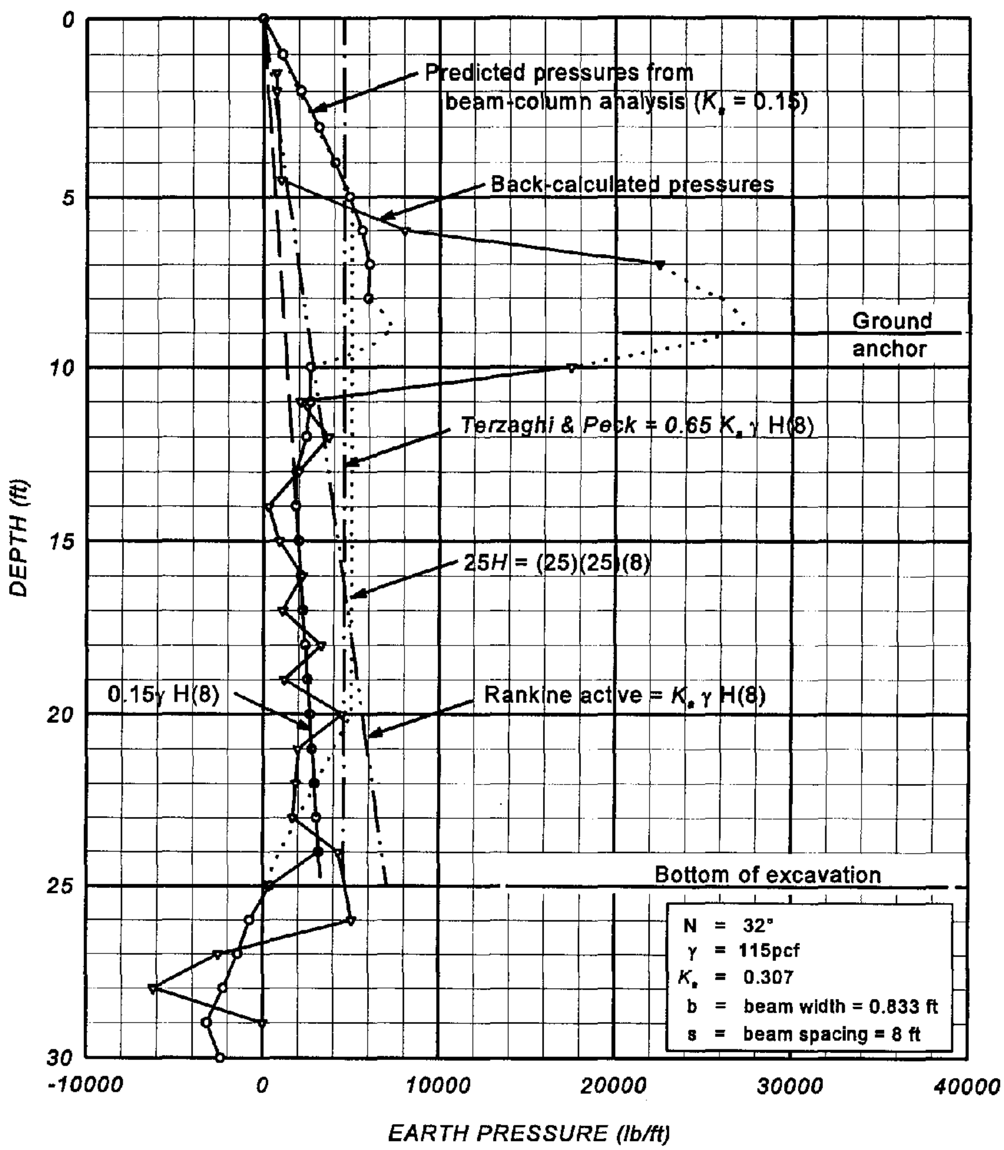

FIGURE 102
Comparison of BMCOL76 Predicted Earth Pressures with Back-calculated, Apparent and Rankine Earth Pressures for the One-tier Texas A&M Wall

3.4.2 Two-tier Wall at Texas A&M (Sand)

The two-tier wall built at Texas A&M was analyzed using BMCOL76. Experimental plane strain R-y curves using the back-calculated parameters in Table 26 were used to model the earth pressure-deflection response of the system above the bottom of the excavation. R-y curves for a single soldier beam in sand were used to predict the response of the soldier beam toe (Section 3.3.2.2). Predictions were made for the following construction stages:

1. Excavate to 8 ft.
2. Stress the anchor at 6 ft.
3. Excavate to 17 ft.
4. Stress the anchor at 16 ft.
5. Excavate to 25 ft.

Soil properties at the site are described in Section 3.4.1. Table 29 presents wall data and Table 30 presents ground anchor data used in the analyzes. In the two-tier wall section, a single ground anchor in the center of the wale supported two adjacent soldier beams. When developing the T-y curves for the ground anchors, the data in Table 30 were divided by two.

TABLE 29
Data for Two-tier Texas A&M Wall

Wall height	25 ft
Soldier beam toe	5 ft
Beam flange width	6.1 in
Lateral stiffness, EI	3.99×10^9 lb-in^2
Soldier beam spacing	8 ft

TABLE 30
Ground Anchor Data for Two-tier Texas A&M Wall

	Upper Tier	Lower Tier
Unbonded length	18 ft	15 ft
Tendon bond length	24 ft	24 ft
Lock-off load	82.2/2 = 41.1 kips	71.8/2 = 35.9 kips
Tendon area	1.25/2 = 0.625 in^2	1.25/2 = 0.625 in^2
Young's modulus	$29{,}000 \times 10^3$ psi	$29{,}000 \times 10^3$ psi
Rupture strain	4%	4%
Yield strength	150.0/2 = 75.0 kips	150.0/2 = 75.0 kips
Ultimate strength	187.5/2 = 93.75 kips	187.5/2 = 93.75 kips
Anchor angle	30°	30°

In the analyses, anchor stressing was simulated by applying a constant load at the anchor location. T-y curves were used to simulate the ground anchors after stressing (Section 3.3.3). The construction sequence was simulated by shifting the R-y curves, as explained in Section 3.3.4. Figures 103 and 104 compare the measured deflections and bending moments for the five construction stages with those predicted using the beam-column analysis. Calculated deflections and bending moments for the final construction stage, with and without simulation of the construction sequence, are shown in Figures 103e and 104e.

Figures 103a and 104a show that the predicted deflections and bending moments for the first stage of construction, an 8-ft cantilever excavation, were similar to the measured ones. The predictions for the two-tier wall after the upper anchor stressing stage are poorer than the predictions for the one-tier wall (Section 3.4.1).

Predicted deflections and bending moments after stressing the upper ground anchor are compared with the measured values in Figures 103b and 104b. Measured deflections and bending moments for this stage of construction were similar to the predicted values. Shifted R-y curves were used in the analysis at locations where the wall deflected outward more than 0.05 in, the active reference deflection.

Results for the third construction stage, excavate to 17 ft, are shown in Figures 103c and 104c. The predicted deflections were approximately two-thirds the measured deflections. Measured and predicted bending moments were similar.

Figure 103d compares the deflected shape of the soldier beam after the lower ground anchor was stressed with the deflections predicted using BMCOL76 and shifted R-y curves. The figure shows that the measured deflections above the lower ground anchor were about 50 percent greater than the predicted deflections. Predicted and measured bending moments after stressing the lower anchor are compared in Figure 104d. Figure 104d shows that the analysis predicted the size and shape of the bending moment diagram above the bottom of the excavation. Below the bottom of the excavation the measured bending moments were larger than the predicted moments.

For the final excavation stage, Figure 103e shows the measured and predicted deflections of the soldier beam. Deflection predictions using shifted R-y curves to simulate the construction effects and predictions assuming that the wall was wished into the ground are shown. Figure 103e shows that the measured deflections were much larger than the predicted deflections no matter if the construction sequence was modeled or not. The underestimation of the deflections by the amount shown confirms that R-y curves are not able to predict wall deflections satisfactorily.

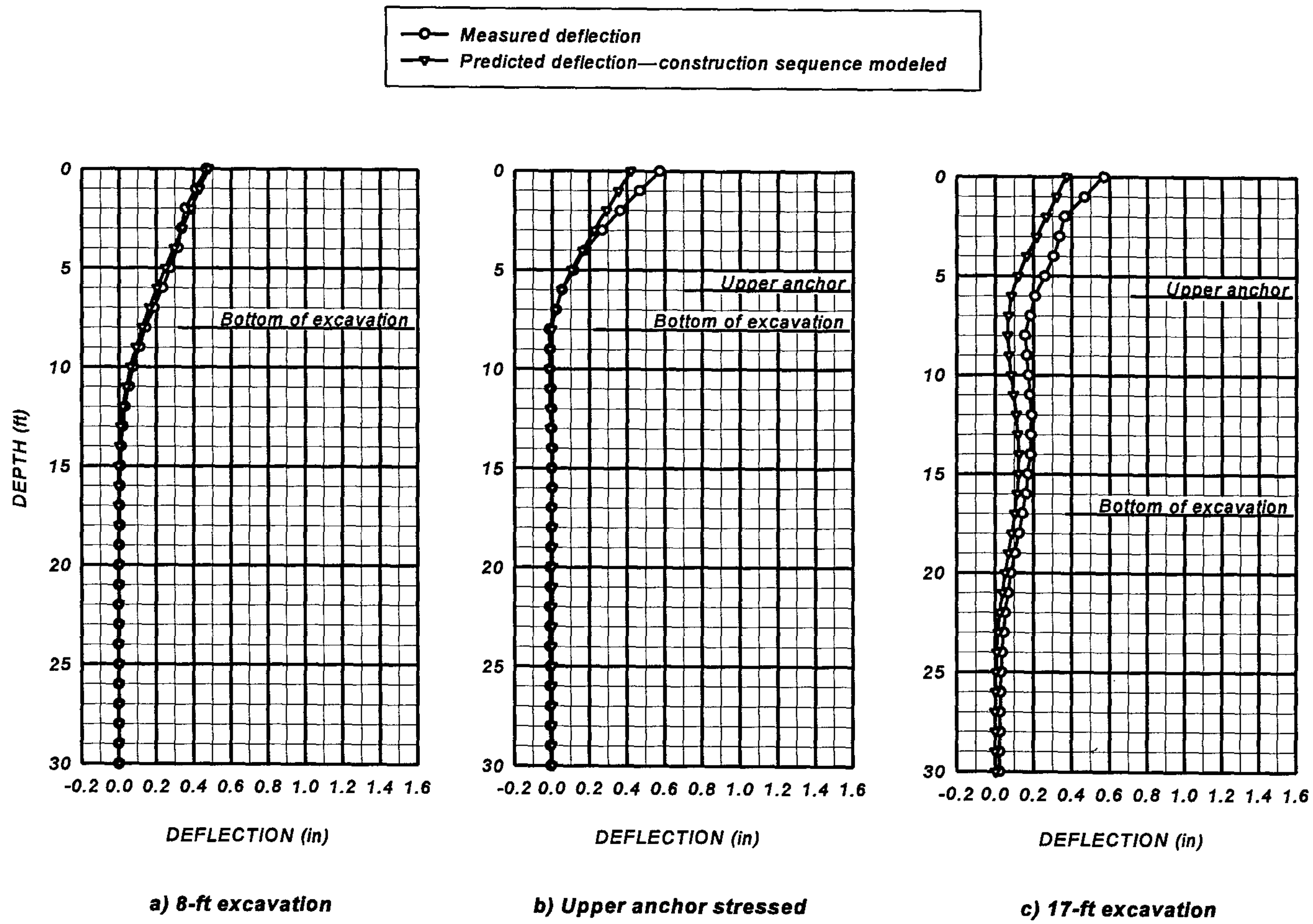

FIGURE 103
Measured and BMCOL76 Predicted Deflections for Two-tier Texas A&M Wall

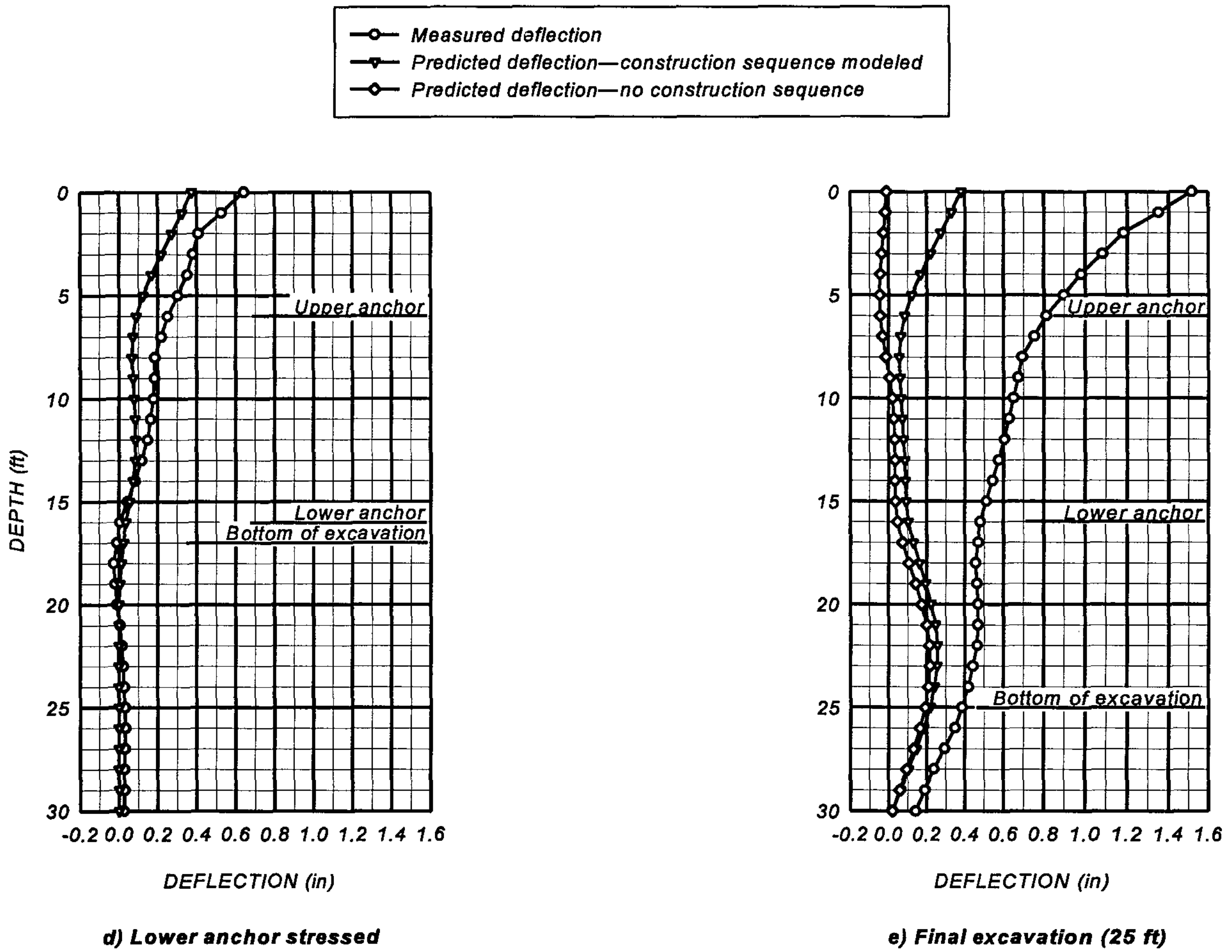

FIGURE 103
(continued)

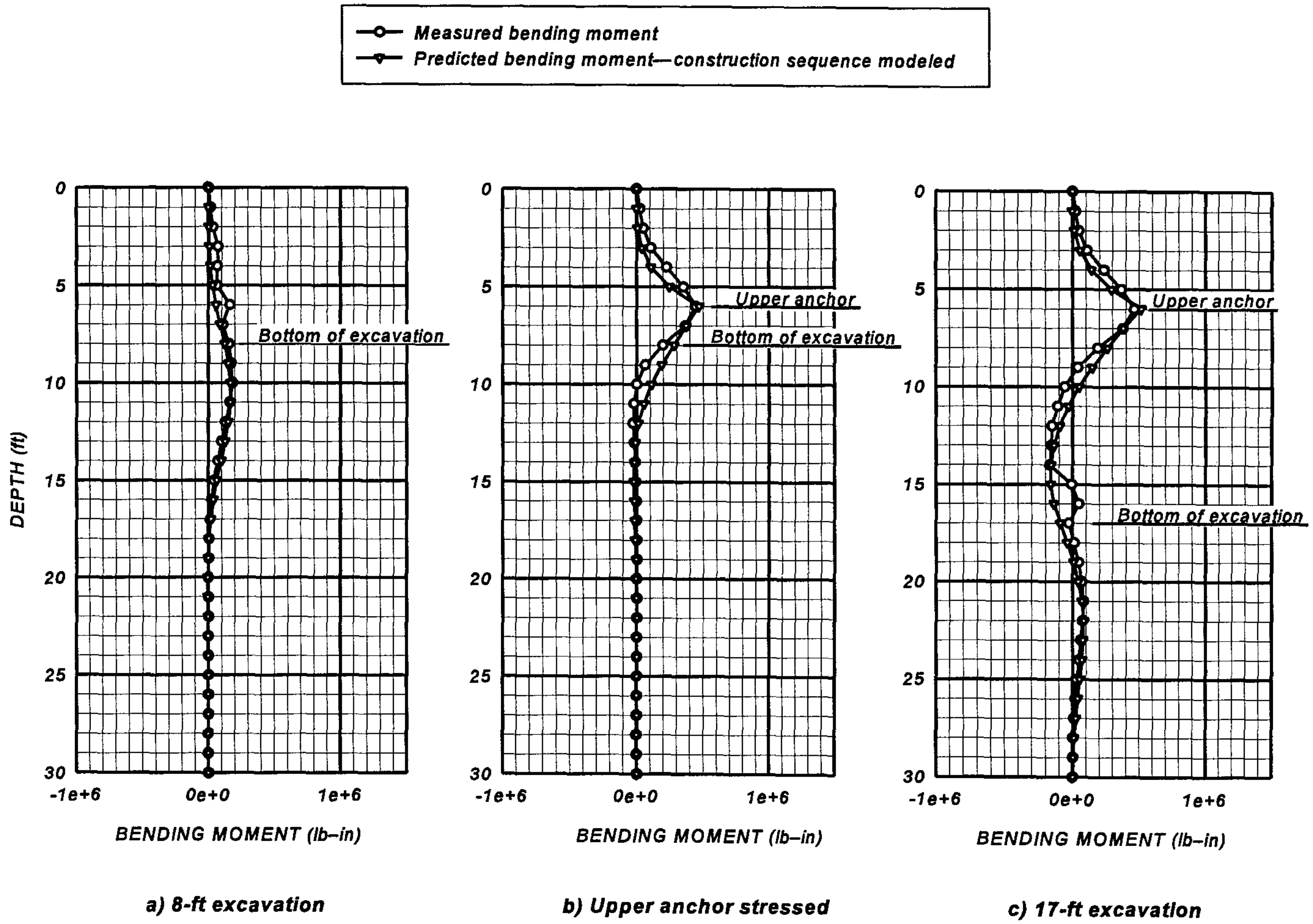

FIGURE 104
Measured and BMCOL76 Predicted Bending Moments for Two-tier Texas A&M Wall

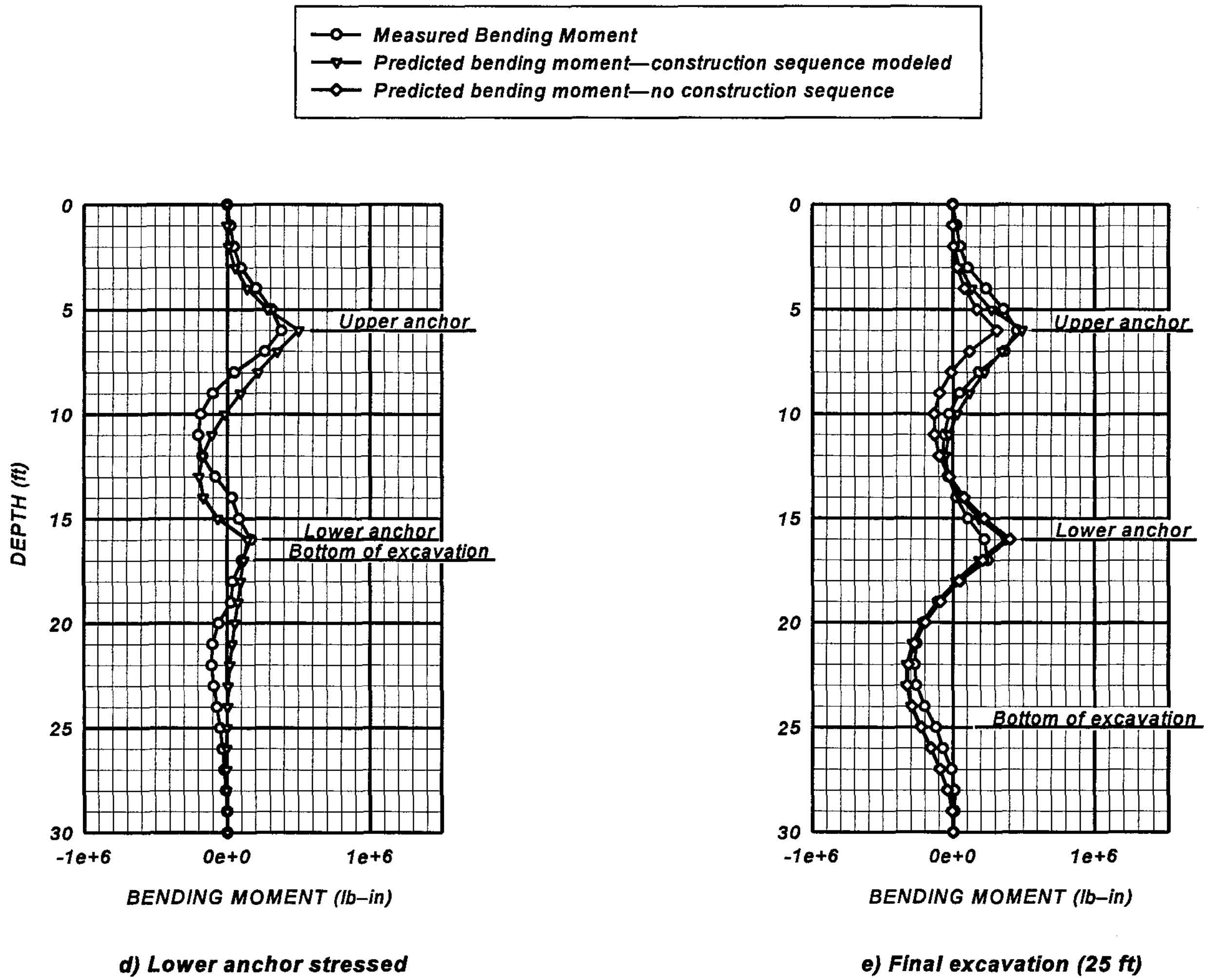

FIGURE 104
(continued)

Predicted bending moments for the final construction stage, a 25-ft excavation, are compared with the measured bending moments in Figure 104e. At the upper anchor location, the predicted bending moment determined using R-y curves that modeled the construction sequence was similar to the measured bending moment. At the upper anchor, the predicted bending moment assuming that the wall was wished into the ground was approximately 20 percent less than the measured bending moment. Below the upper ground anchor, predicted bending moments were similar no matter whether or not the construction sequence was modeled.

As discussed in Section 3.4.1 and demonstrated in this section, deflection predictions using beam-column analyses and nonlinear R-y curves cannot account for all sources of anchored wall movements. Bending moments predicted using the beam-column analyzes and R-y curves were close to the measured bending moments. Predicted and measured bending moments for the final construction stage were the maximum moments in the beam at the anchor locations and in the spans between supports. Therefore, for the design of flexible soldier beam walls, bending moments for the final construction stage can be used, and checking intermediate construction stages is unnecessary. Intermediate construction stages should be analyzed if the excavation is going to extend well below a support before installation of that support, or if supports will be removed as backfill is placed in front of a wall. Section 9.12 of the *Design Manual for Permanent Ground Anchor Walls* (Weatherby, 1997b) presents additional discussion concerning the need to analyze intermediate construction stages.

Figure 105 shows the earth pressure diagram predicted by the beam-column analysis and compares that diagram with Rankine active pressures and typical apparent earth pressure diagrams. A triangular pressure diagram for an active earth pressure coefficient of 0.15 also is shown in Figure 105. Predicted earth pressures at the ground anchor locations indicate that analysis predicts that the wall will be pulled into the soil at the ground anchor locations. Above 17 ft, the predicted earth pressures were greater than the pressures corresponding to an earth coefficient of 0.15 (the active earth pressure coefficient used to develop the R-y curves). Below 17 ft, the predicted earth pressures equaled the active pressure associated with the R-y curves. The predicted bending moments in Figure 104e resulted from the predicted earth pressures in Figure 105. Between the lower anchor and the bottom of the excavation, the predicted and measured moments are 70 percent of the design moments (Figure 58). The design moments were determined using a $25H$ trapezoidal earth pressure diagram assuming a hinge at the lower anchor and the bottom of the excavation. Similar to the one-tier wall, the measured bending moments in the two-tier soldier beams were less than the design moments developed from the apparent earth pressure diagram, and the earth pressures are 50 percent less than the apparent earth pressures. Therefore, the bending moment reductions recommended by Peck et al. (1974) also apply to the moments in the lower span of multi-tier walls.

The experimental R-y curves for the Texas A&M wall used back-calculated active and passive earth pressure coefficients (K_a = 0.15 and K_p = 6.6). Rankine earth pressure coefficient for the soils at the Texas A&M site are: K_a = 0.307 and K_p = 3.255. Rankine or Coulomb active earth pressure coefficients for the soils at the site are greater than the back-calculated active earth pressure coefficient. When using R-y curves with either Rankine or Coulomb active earth pressures, the one-tier or the two-tier Texas A&M walls failed. In these analyses the earth pressures over the lower part of the wall were too large and the lateral load-carrying capacity of the toe was exceeded. Predicted bending moments and earth pressures for an active earth pressure coefficient of 0.15 were similar to the measured moments and back-calculated earth pressures. Apparently, arching transfers load to the ground anchor locations and reduces pressures over the lower portion of the wall. No relationship was developed that could consider the reduction in earth pressure as a result of arching.

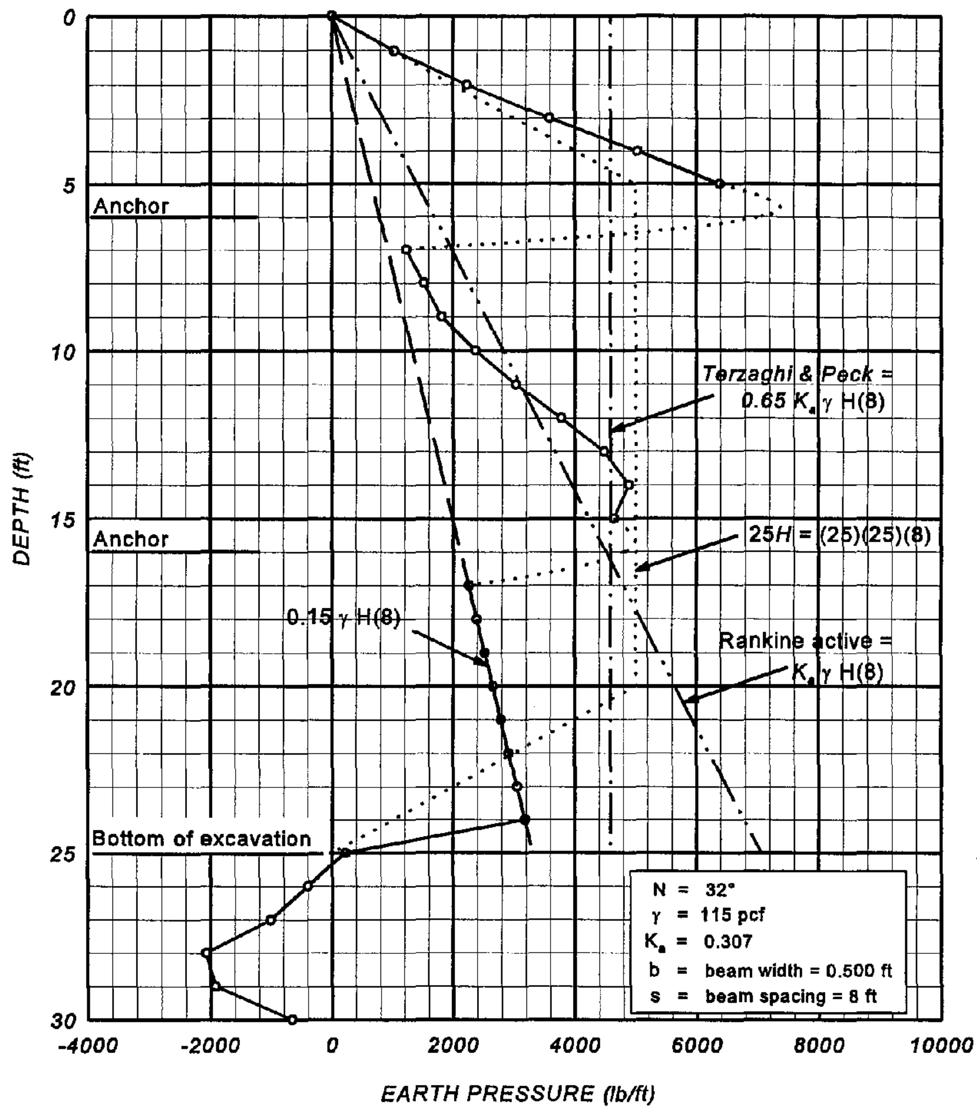

FIGURE 105
Comparison of BMCOL76 Predicted Earth Pressures with Apparent and Rankine Earth Pressures for the Two-tier Texas A&M Wall, Final Excavation (25 ft)

3.4.3 Bonneville Navigation Lock Diaphragm Wall (Sand)

Munger, et al. (1990) described an anchored reinforced concrete diaphragm wall built to support the Union Pacific Railroad line in the Columbia River Gorge at Bonneville Navigation Lock. Soils information at the site is summarized in Table 31. Soils at the site were assumed to be a homogeneous dense sand. Wall data required for the beam-column analysis are presented in Table 32. Tendon data for the four rows of ground anchor are summarized in Table 33. Anchor data were divided by the anchor spacing (11 ft).

TABLE 31
Soil Properties for Bonneville Wall

Unit weight	125 pcf
Angle of internal friction	30°
Angle of wall friction	30°
Standard penetration resistance (N)	15 blows/ft
Active earth pressure coefficient (K_a)	0.297
Passive earth pressure coefficient (K_p)	10.1
At-rest earth pressure coefficient (K_o)	0.5

TABLE 32
Data for Bonneville Wall

Wall height	42 ft
Toe embedment	8 ft
Wall thickness	3 ft
Lateral stiffness, EI	1.62×10^{11} lb.-in.^{2}
Ground anchor spacing	11 ft
Surcharge pressure	500 psf

TABLE 33
Ground Anchor Data for Bonneville Wall

ANCHOR NUMBER	UNBONDED LENGTH	TENDON BOND LENGTH	LOCK-OFF LOAD	TENDON STIFFNESS	ANCHOR ANGLE
1	74 ft	30 ft	28.1 kips/ft	5.48×10^3 lb/in/ft	20°
2	64 ft	30 ft	28.1 kips/ft	6.17×10^3 lb/in/ft	20°
3	53 ft	30 ft	28.1 kips/ft	7.17×10^3 lb/in/ft	20°
4	37 ft	30 ft	35.8 kips/ft	9.38×10^3 lb/in/ft	20°

Coulomb earth pressure coefficients were used to construct the R-y curves used in the analysis. Active, passive, and at-rest earth pressure coefficients were determined using Equations 3.17, 3.18, and 3.14, respectively. An angle of wall friction equal to 30° was selected since the slurry trench was constructed in a granular soil with large rock fragments. The reference deflections for the active and passive soil pressures were assumed to be 0.05 in and 0.5 in, respectively. These reference deflections were the same as the deflections back-calculated from the Texas A&M wall.

The construction sequence implemented in the beam-column analysis consisted of the following nine stages:

1. Excavate to 6 ft.
2. Stress the first anchor at 4 ft.
3. Excavate to 18 ft.
4. Stress the second anchor at 16 ft.
5. Excavate to 30 ft.
6. Stress the third anchor at 28 ft.
7. Excavate to 40 ft.
8. Stress the fourth anchor at 38 ft.
9. Excavate to 42 ft.

Predicted deflections and bending moments upon completion of the excavation are compared with the measured values in Figure 106. Measured and predicted deflection plots show that the wall was pulled back into the ground as the ground anchors were stressed. The R-y curves were shifted where the wall movements exceeded the reference deflections. This occurred only during the 6-ft excavation stage before stressing the upper anchor. Below 6 ft, wall movements were small and the R-y curves were not shifted to model the construction sequence. Since most R-y curves were not shifted, the predicted deflections and bending moments for the analysis where the construction sequence was not modeled were similar to those for the analysis where the construction sequence was modeled. The beam-column analysis predicted the wall deflections satisfactorily. Accurate deflection predictions may have resulted from the large anchor loads, which prevented plastic movements from developing. Ground anchor loads high enough to pull the wall into the ground are not economically feasible or justified on most projects. The magnitude of the anchor loads can be seen in Figure 106c, which shows that the predicted earth pressures are greater than the at-rest earth pressures. Comparing the predicted and measured bending moments was difficult since moments were only measured at nine locations. Most of the measured moments were close to the predicted moments. The analysis did not predict the bending moments measured at 22 and 30 ft.

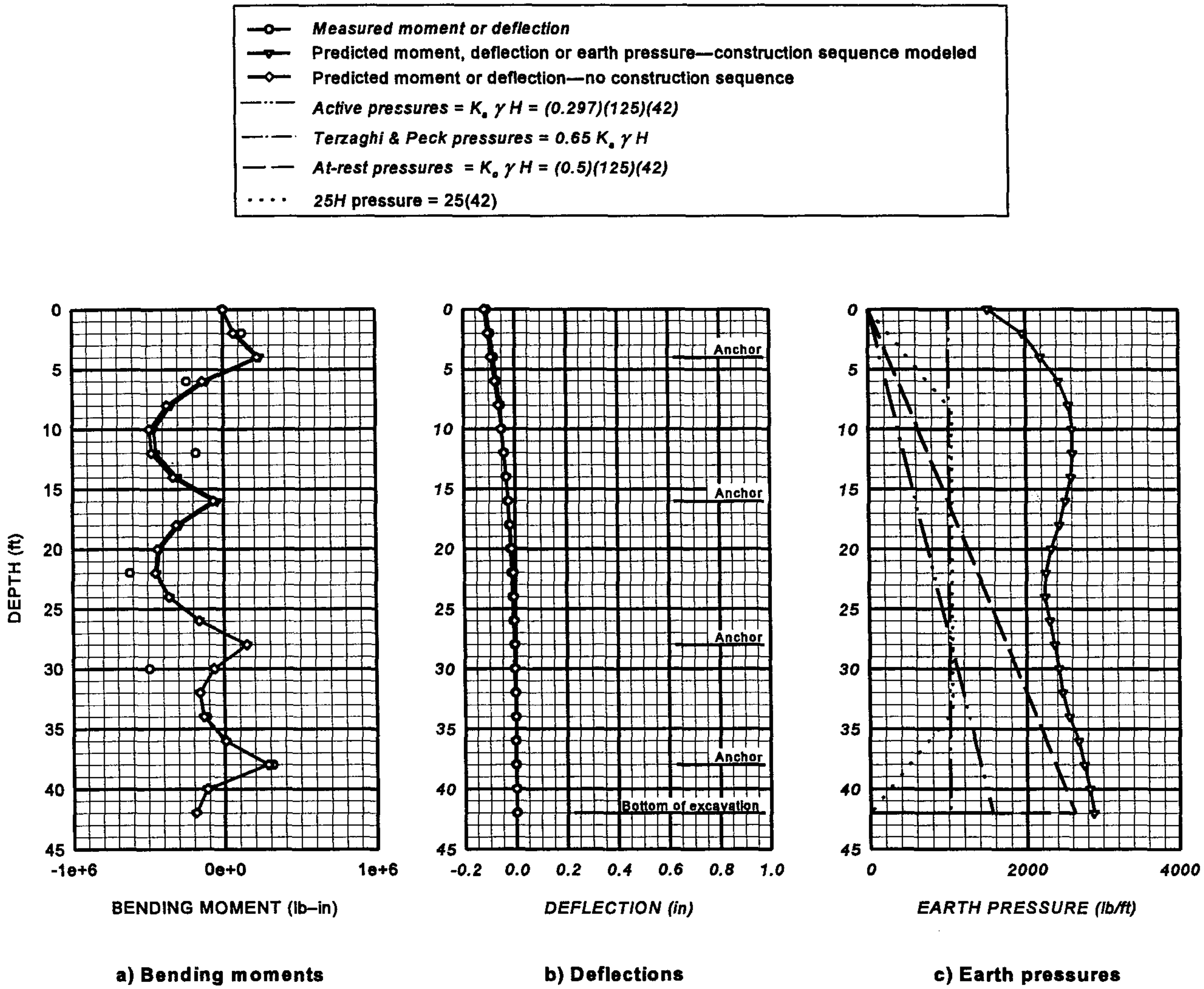

FIGURE 106
Measured and BMCOL76 Predicted Bending Moments and Deflections, and BMCOL76 Predicted Earth Pressures for the Bonneville Navigation Lock Wall, Final Excavation (42 ft)

3.4.4 Two-tier Wall at Lima, Ohio (Clay)

Lockwood (1988) and Cheney (1990) describe an anchored wall built for a grade separation within the city of Lima, Ohio. A partial description of the wall is contained in Section 2.5.3.3. In the beam-column analyses, the soils were assumed to be a uniform stiff lean clay. Soldier Beam 93 in the wall was instrumented and monitored as part of FHWA Demonstration Project 68. The soldier beams (double C15×33.9) were installed in 30-in-diameter drilled shafts on 6-ft centers. Two rows of hollow-stem-augered soil anchors were used to support the wall. Soil properties, wall data, and anchor tendon data used in the beam-column analyses are presented in Tables 34 to 36. Based on the results from the Texas A&M drilled-in beams, the soldier beam lateral bending stiffness was calculated ignoring composite action.

TABLE 34
Soil Properties for Lima Wall

Unit weight	134 pcf
Angle of internal friction	35°
Cohesion	340 psf
Over consolidation ratio	2.5
Undrained shear strength	1.65 tsf
Active earth pressure coefficient (K_a)	0.27
Passive earth pressure coefficient (K_p)	3.7
At-rest earth pressure coefficient (K_o)	0.68

TABLE 35
Data for Lima Wall

Wall height	27 ft
Toe embedment	15 ft
Lateral stiffness, EI	1.89×10^{10} lb-in^2
Ground anchor spacing	6 ft

TABLE 36
Ground Anchor Data for Lima Wall

ANCHOR NUMBER	UNBONDED LENGTH	TENDON BOND LENGTH	LOCK-OFF LOAD	TENDON STIFFNESS	ANCHOR ANGLE
1	30 ft	20 ft	70 kips	7.7×10^4 lb/in	20°
2	30 ft	20 ft	70 kips	7.7×10^4 lb/in	20°

Rankine earth pressure coefficients were used to construct the R-y curves used in the analysis. Active, passive, and at-rest pressure coefficients were determined using Equations 3.15, 3.16, and 3.14, respectively. Rankine coefficients were selected since axial load data suggested that the vertical component of the ground anchor load was transferred to the ground above the bottom of the excavation. Total stress and effective stress analyses were done. In the total stress analysis, the plane strain R-y curves above the bottom of the excavation were developed using resistances determined by Equations 3.25, 3.26, and 3.27. The plane strain R-y curves for the effective stress analysis were developed using resistances determined by Equations 3.28, 3.29, and 3.30. Resistances from the equations were multiplied by the soldier beam spacing to develop the active and passive resistances for the plane strain R-y curves. An active reference deflection of 0.1 in and a passive reference deflection of 1.0 in were used to develop both the effective and total stress R-y curves. Below the bottom of the excavation, the same single soldier beam R-y curves (Section 3.3.2.4) were used in both the total and effective stress analyses. The diameter of the drill shaft was used to develop lateral resistance for the single soldier beam R-y curves. A reference deflection of 0.7 in was used to develop the single soldier beam R-y curves.

Beam-column predictions were made for the following five construction stages using BMCOL 76 and effective and total stress R-y curves:

1. Excavate to 10 ft.
2. Stress the anchor at 8 ft.
3. Excavate to 18 ft.
4. Stress the anchor at 16 ft.
5. Excavate to 27 ft.

The anchor stressing load was simulated by applying a constant load. T-y curves (Section 3.3.3) were used to describe anchor behavior for subsequent construction stages.

Measured deflections after the excavation reached 18 ft and the final excavation depth are compared with those predicted using the beam-column method in Figure 107. An expanded horizontal scale was used in Figure 107 to enable the different curves to be distinguished from one another. Deflection predictions using total and effective stress R-y curves are shown. In Figure 107b deflection predictions assuming that the wall was wished into the ground are shown. When simulating the construction stages, the R-y curves are shifted when the wall deflections exceed either the active or passive reference deflections. Since the wall movements were small, only the upper R-y curves were shifted. Ground anchor loads were large enough to pull the wall into the ground and the predicted deflections were not sensitive to the type of R-y curves used or whether the construction sequence was modeled.

Figure 108 shows the predicted bending moments for the completed Lima wall using effective and total stress R-y curves. Results assuming that the wall was wished into the ground and results using shifted R-y curves to model the construction sequence are included. Figure 108 shows that each type of R-y curve predicted similar bending moments and the predictions were not sensitive to the selection of the R-y curves since the anchor loads were high. Figure 109 compares the predicted earth pressures with the apparent earth pressures and Rankine active and at-rest pressures. Above the lower anchor, predicted pressures were greater than the apparent earth pressures and the at-rest pressures. This confirms that the design pressures for the wall were greater than the at-rest pressures. Figure 109 shows that the mobilized earth pressures from the total stress or effective stress analyses were similar.

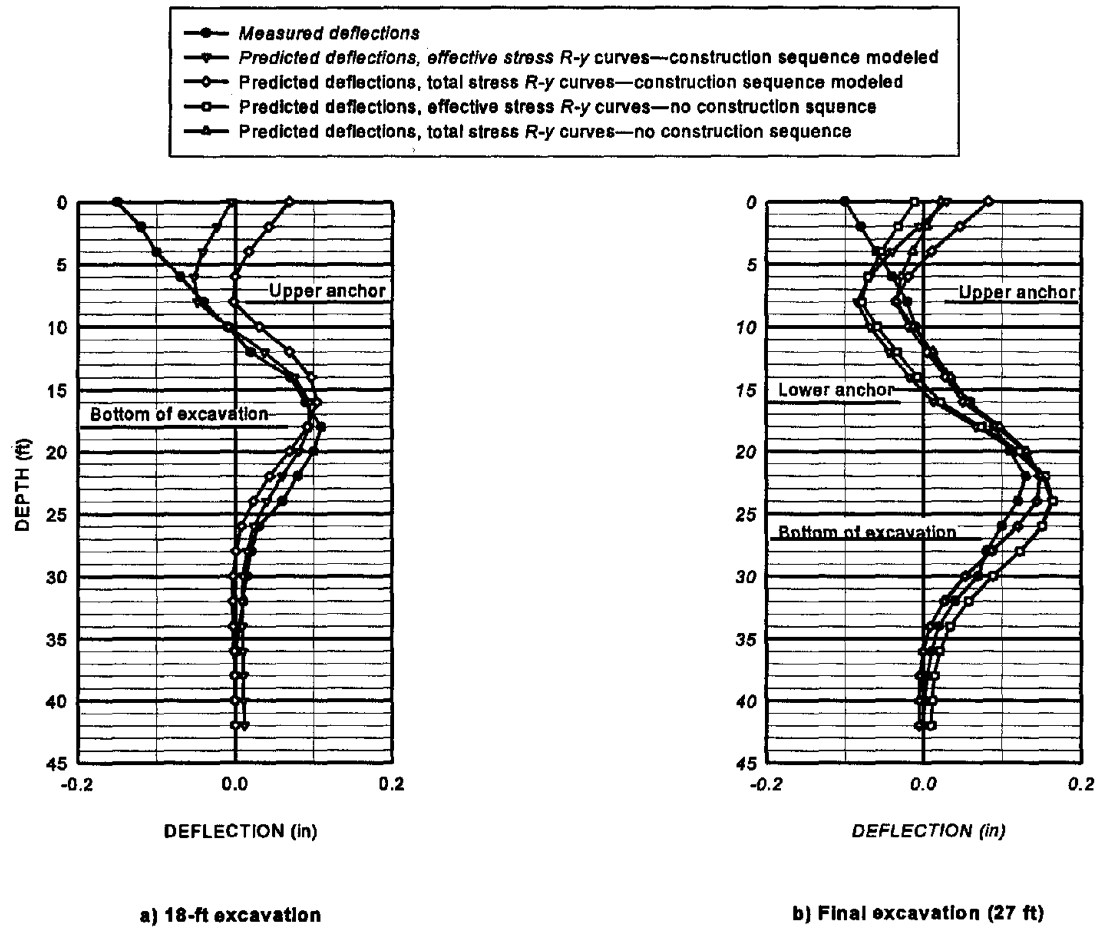

FIGURE 107
Measured and BMCOL76 Predicted Deflections for the Lima Wall

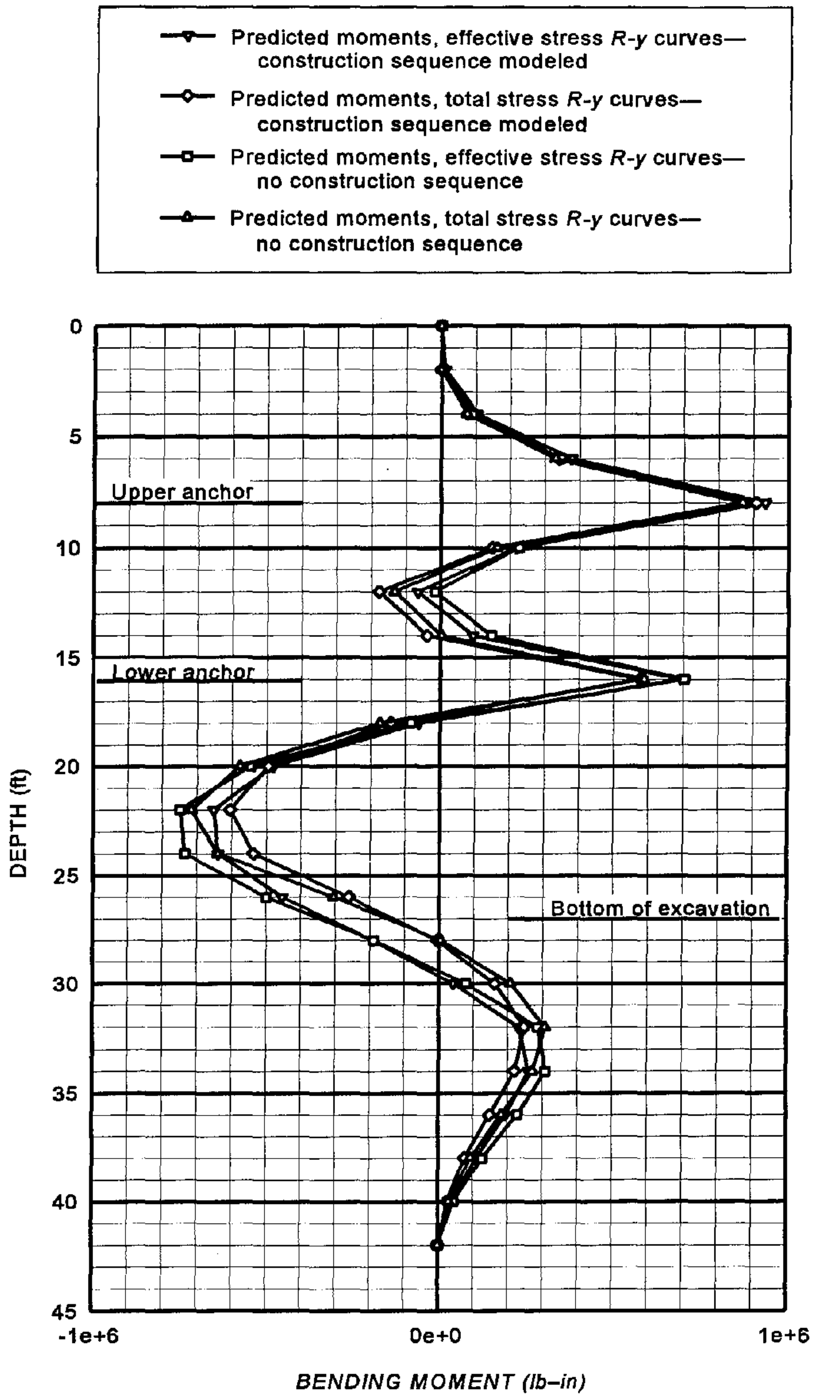

FIGURE 108
BMCOL76 Predicted Bending Moments for the Lima Wall, Final Excavation (27 ft)

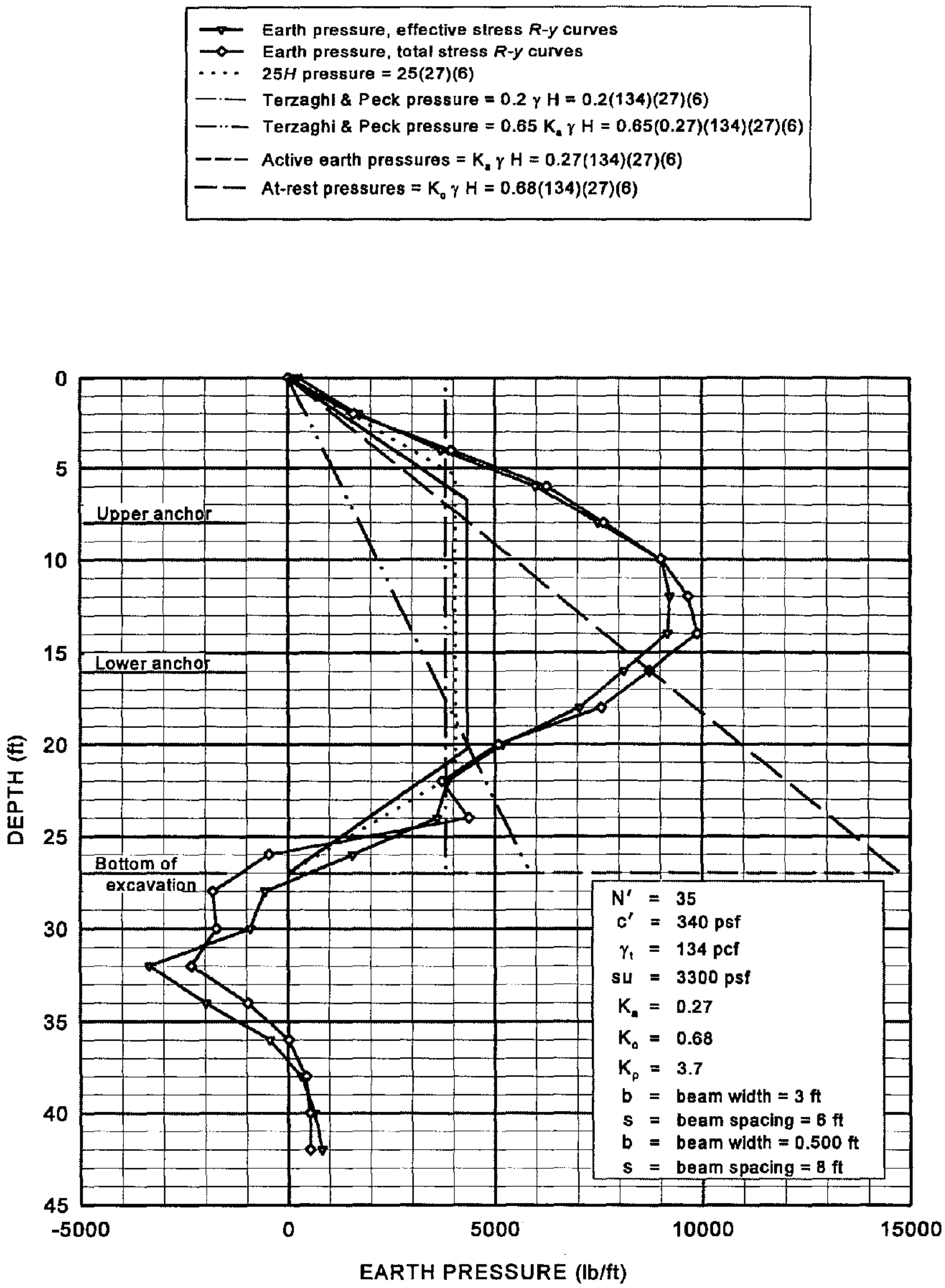

FIGURE 109
Comparison of BMCOL76 Predicted Earth Pressures with Apparent and Rankine Earth Pressures for the Lima Wall, Final Excavation (27 ft)

3.4.5 125 High Street Excavation Support System, Boston, Massachusetts (Clay)

Houghton and Dietz (1990) describe the behavior of two instrumented soldier beams installed in a temporary excavation support system built for an office building in downtown Boston. Section 3.5.3.2 of this report describes the installation. Soldier Beam 67 was instrumented and monitored by Schnabel Foundation Company. The soldier beams (double W12×30) were installed in 3-ft-diameter drilled shafts on 10-ft centers. Six rows of soil anchors supported the wall. Soil properties, wall data, and anchor tendon data used in the beam-column analyses are presented in Tables 37 to 39. Section properties for the steel beam were used in the analyses.

TABLE 37
Soil Properties for High Street Excavation Support Support Wall

Unit weight	135 pcf
Angle of internal friction	45°
Undrained shear strength	4.68 tsf
Active earth pressure coefficient (K_a)	0.17
Passive earth pressure coefficient (K_p)	5.83
At-rest earth pressure coefficient (K_o)	0.3

TABLE 38
Data for High Street Excavation Support System Wall

Wall height	54 ft
Toe embedment	8 ft
Lateral stiffness, EI	1.43×10^{10} lb-in^2
Ground anchor spacing	10 ft

TABLE 39
Ground Anchor Data for High Street Excavation Support System Wall

ANCHOR NUMBER	UNBONDED LENGTH	TENDON BOND LENGTH	LOCK-OFF LOAD	TENDON STIFFNESS	ANCHOR ANGLE
1	24 ft	25 ft	125 kips	5.9×10^4 lb/in	25°
2	33 ft	20 ft	150 kips	5.0×10^4 lb/in	25°
3	36 ft	19 ft	152 kips	4.8×10^4 lb/in	25°
4	20 ft	15 ft	105 kips	7.9×10^4 lb/in	25°
5	20 ft	15 ft	121 kips	7.9×10^4 lb/in	25°
6	20 ft	15 ft	121 kips	7.9×10^4 lb/in	25°

Rankine earth pressure coefficients were used to construct the R-y curves. Active, passive, and at-rest pressure coefficients were determined using Equations 3.15, 3.16, and 3.14, respectively. Rankine coefficients were selected since axial load data showed that part of the vertical component of the ground anchor load was transferred to the ground above the bottom of the excavation. Total stress and effective stress analyses were done. In the total stress analysis, the plane strain R-y curves above the bottom of the excavation were developed using resistances determined by Equations 3.25, 3.26, and 3.27. Plane strain R-y curves for the effective stress analysis were developed using resistances determined by Equations 3.28, 3.29, and 3.30. Resistances from the equations were multiplied by the soldier beam spacing to develop active and passive resistances for the R-y curves. An active reference deflection of 0.12 in and a passive reference deflection of 0.4 in were used to develop both the effective and total stress R-y curves. Below the bottom of the excavation, single soldier beam R-y curves (Section 3.3.2.4) were used in the total and effective stress analyses. The diameter of the drill shaft was used to develop lateral resistance for the single soldier beam R-y curves. A reference deflection of 0.1 in was used in developing the single soldier beam R-y curves.

The construction sequence used in the beam-column analyses consisted of the following 13 stages:

1. Excavate to 6 ft.
2. Stress the anchor at 4 ft.
3. Excavate to 12 ft.
4. Stress the anchor at 10 ft.
5. Excavate to 20 ft.
6. Stress the anchor at 18 ft.
7. Excavate to 30 ft.
8. Stress the anchor at 28 ft.
9. Excavate to 38 ft.
10. Stress the anchor at 36 ft.
11. Excavate to 48 ft.
12. Stress the anchor at 46 ft.
13. Excavate to 54 ft.

Each ground anchor was modeled as described in the earlier case histories.

Predicted bending moments and deflections using total and effective stress R-y curves are compared with the measured bending moments and deflections in Figures 110 and 111. Bending moments predicted using total stress R-y curves were closer to the measured moments than those predicted using effective stress curves. Moments predicted using the effective stress R-y curves are larger than the moments predicted using the total stress R-y curves. The maximum effective stress moment was about 20 percent greater than the total stress moment. Except at the 40-ft depth, moments calculated using shifted R-y curves and those calculated using unshifted curves were similar. Deflection predictions using total or effective stress R-y curves were similar and much smaller than the measured deflections. Deflection predictions did not change significantly when modeling the construction sequence using shifted R-y curves. Figure 111 suggests that R-y curves are not able to model lateral deflections of an anchored wall accurately.

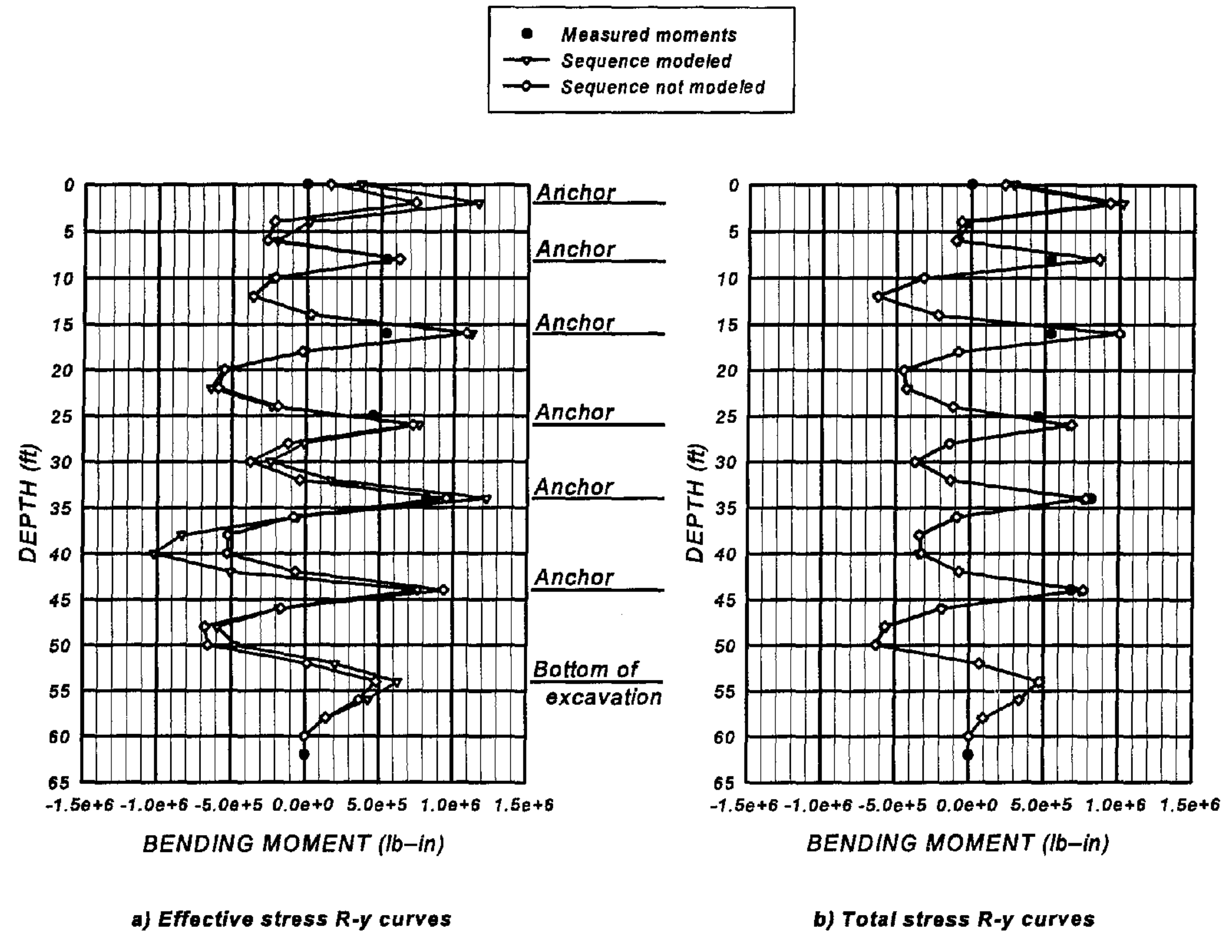

FIGURE 110
Measured and BMCOL76 Predicted Bending Moments
for the Boston Wall, Final Excavation (54 ft)

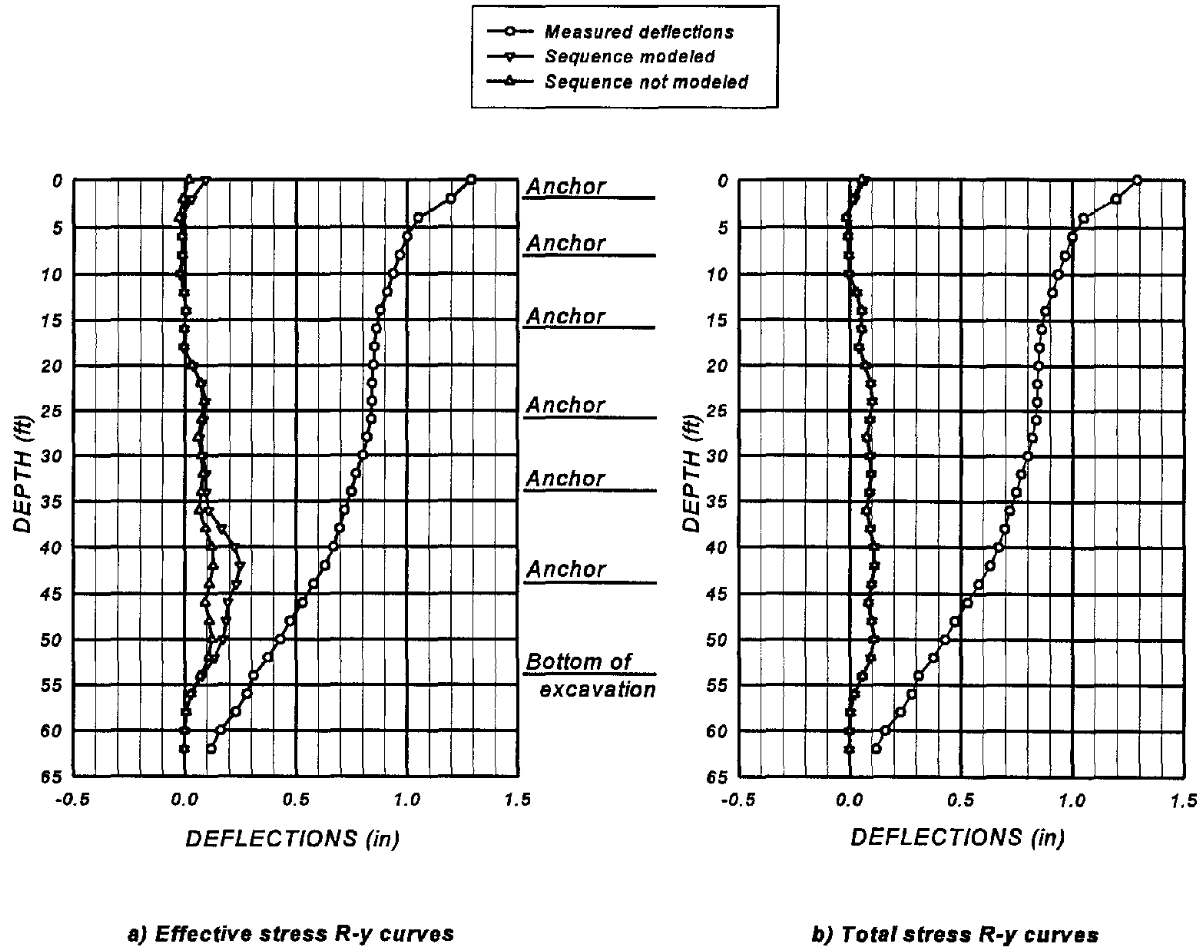

FIGURE 111
Measured and BMCOL76 Predicted Deflections
for the Boston Wall, Final Excavation (54 ft)

Figure 112 compares the earth pressures predicted from the analyses with several apparent earth pressure diagrams and the design pressure diagram. Pressures predicted using total stress and effective stress R-y curves were similar. Design pressures were between the total stress apparent earth pressures and the effective stress apparent earth pressures. Predicted earth pressures from a beam-column analysis should reflect the response of the wall to the applied ground anchor loads. Since the predicted earth pressures were similar to the design earth pressures, both the total stress and effective stress R-y curves were suitable for predicting the bending moments in the wall.

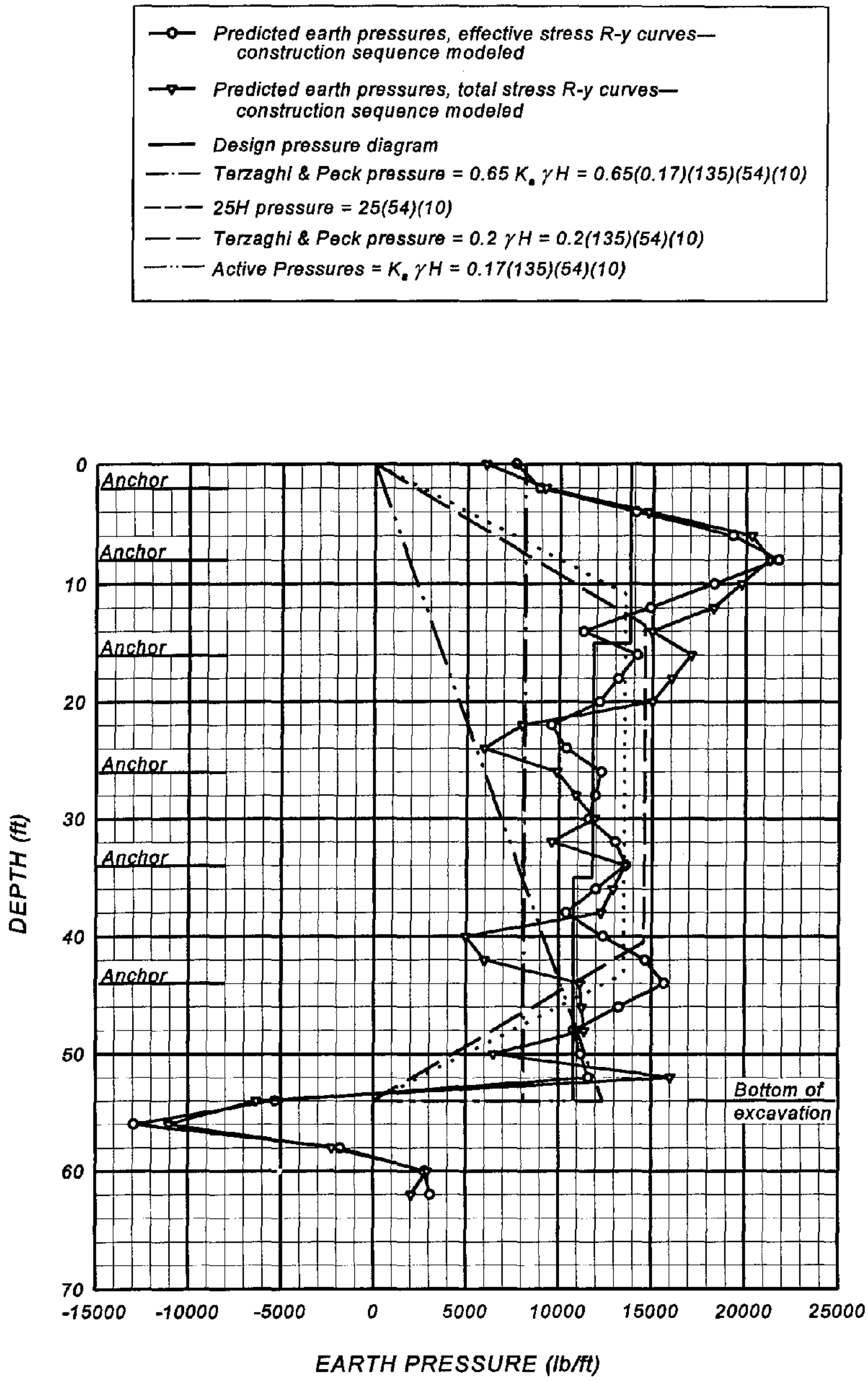

FIGURE 112
Comparison of BMCOL76 Predicted Earth Pressures with Apparent, Design, and Rankine Earth Pressures for the Boston Wall, Final Excavation (54 ft)

3.4.6 Discussion of Beam-column Predictions

Beam-column methods using R-y curves predicted the bending moments satisfactorily if the total lateral earth load was at or above the load resulting from at-rest pressures, or the active earth pressure coefficient was reduced. Deflection predictions using the beam-column analyses often were significantly less than the measured deflections. R-y curves only model bending deflections, and they are unable to model translation of the wall resulting from mass movements or settlement of the wall.

Bending moment and deflection predictions for the Texas A&M wall were made using the back-calculated plane strain R-y curves above the bottom of the excavation. An active earth pressure coefficient of 0.15 was used to develop the R-y curves for the Texas A&M wall. This active earth pressure coefficient is smaller than reasonable Rankine or Coulomb coefficients for the soils at the site. For example, the Coulomb active earth pressure coefficient for the soils at the site is 0.278 for an angle of wall friction equal to 16° (ϕ/2). The Coulomb coefficient is 1.85 times larger than the back-calculated coefficient. Attempts were made to model the Texas A&M wall using an earth pressure coefficient of 0.278 and the as-built 5-ft toe embedment. These attempts were unsuccessful. Apparently, the lateral loads were less than the applied loads resulting from an active earth pressure coefficient of 0.278.

Deflection predictions for the one-tier Texas A&M wall were reasonable, but the deflection predictions for the two-tier wall were significantly smaller than the measured deflections. R-y curves are unable to predict the lateral wall movements that resulted from soldier beam settlement. Since the two-tier wall settled more than the one-tier wall, the lateral movement predictions for the two-tier wall cannot be as accurate as the predictions for the one-tier wall.

Earth pressure predictions for the one-tier wall (Figure 102) and similar predictions for the two-tier wall (Figure 105) show that the analyses predicted reasonable earth pressure distributions. Predicted earth pressures at the ground anchor locations were large. Where the predicted earth pressures exceeded the active pressures, the ground anchor load controlled the bending moments. Near the anchor the analysis indicates that the wall acts to distribute the anchor load to the ground, and the bending moments depend on anchor load, beam stiffness, and soil resistance. Between the anchor and the bottom of the excavation the earth pressures for the one-tier and the two-tier wall decrease to the active earth pressure used to develop the R-y curves. Where the predicted pressures are equal to the active pressures used to develop the R-y curves, the moments predicted by the analysis depend upon the load applied by the soil.

Beam-column analysis predictions for the Bonneville Navigation Lock and Lima walls were similar. Earth pressure predictions for the walls (Figure 106 and 109) show that the anchor loads caused the pressures behind the wall to be greater than the at-rest pressures. Measured deflections (Figures 106 and 107) show that the upper portions of the walls were pulled back into the ground by the ground anchors. For these two cases, the R-y curves predicted the deflections satisfactorily. Predicted deflections were close to measured deflections because the ground was competent, the anchor loads were high, and mass movements were small. Predicted deflections did not exceed the R-y curve reference deflections at many locations. Therefore, the results of the analysis depended upon elastic soil behavior, and the R-y curves were not shifted to model the different construction stages.

Simulating the construction sequence improved the movement predictions, but the bending moment predictions were not affected significantly by using R-y curves that simulated the construction sequence. Since the beam-column deflection predictions do not include mass movement components, empirical charts, which take into account mass movements, should be used to estimate movements of anchored walls. If mass movements are controlled, and stiff walls and high ground anchor loads are used, lateral movement prediction using beam-column analyses and R-y curves may be reasonable. However, for most applications, it is not necessary or economical to design the wall and anchors to resist more than the apparent earth pressures.

In the beam-column analyses, lateral resistance of the soldier beam toes was predicted using R-y curves developed from laterally loaded pile theory. Lateral resistances calculated using laterally loaded pile theory were greater than results developed from classical methods. Lateral load-carrying capacity predictions based on laterally loaded pile theory modeled the behavior of the toes satisfactorily.

R-y curves developed using total and effective stress strength parameters were used in the analyses of the Lima and the 125 High Street walls. The results show that predictions made using the total stress R-y curves were better than the predictions made using effective stress R-y curves. Deflection predictions made using effective stress or total stress R-y curves did not describe the lateral movement of the 125 High Street wall satisfactorily. Ground anchor loads for the 125 High Street wall were close to the loads predicted by the apparent earth pressure diagrams. Ground anchor loads in the Lima wall were high (greater than at-rest pressures) and the movement predictions for the Lima wall were reasonable. Bending moment predictions using total stress or effective stress R-y curves were reasonably similar. R-y curves are not used to determine ground anchor loads. Anchor loads are determined using apparent earth pressure diagrams or other appropriate methods, and R-y curves are used to predict the wall's response to the applied loads. Beam-column analyses for the walls gave reasonable predictions for soldier beam bending moments and earth pressures. The design pressure diagram for the 125 High Street wall is known, and Figure 112 shows that the predicted pressures were similar to the design pressures. Similarity between the design and predicted earth pressures indicates that bending moments determined using the beam-column method have to be similar to the design moments.

R-y curves used in the analyses of the soldier beam walls assumed that the active load and passive resistance above the bottom of the excavation are determined by multiplying the unit loads by the soldier beam spacing. Results of the beam-column predictions for the Texas A&M wall, Lima wall, and 125 High Street wall indicate that use of these plane strain R-y curves is suitable for determining the response of the wall to the applied ground anchor loads.

3.5 SENSITIVITY ANALYSIS

The beam-column method in Section 3.3 models the wall as a beam with a lateral bending stiffness, EI, and the soil as a series of non-linear springs. The soil springs are defined by five parameters [y_a, y_p, K_a, K_o, and K_p (Figure 72)]. Analyses were done for the one-tier Texas A&M wall and the Lima wall to evaluate how sensitive the results were to variations in each soil spring parameter and bending stiffness of the wall.

Soil properties for each wall are contained in Section 3.4.1 and 3.4.4. The construction sequence was not considered for the sensitivity analyses, and the embedment depth of the Texas A&M wall was increased to 20 ft to ensure a stable wall for each case examined.

Analyses were done by varying the following parameters one at time:

- Vary the active earth pressure coefficient, K_a.
- Vary the at-rest earth pressure coefficient, K_o.
- Vary the passive earth pressure coefficient, K_p.
- Vary the reference deflection, y_a.
- Vary the reference deflection, y_p.
- Vary the lateral bending stiffness, EI, of soldier beam.

In Section 3.5, figures are used to present the results of the sensitivity analyses. In each figure, the solid curve presents the results of the beam-column analysis for the case where the R-y curve parameters and the beam stiffness represent the actual installation.

3.5.1 One-Tier Wall at Texas A&M (Sand)

Parameters used for the sensitivity analyses of the Texas A&M wall (sand) are shown in Table 40. In Table 40, the parameters for Analysis 1 represent the actual wall and the back-calculated R-y parameters. Bold parameters in the table indicate parameters varied for the sensitivity analyses. The T-y curve described in Section 3.4.1 was used to model the ground anchor. The actual anchor lock-off load was used in each analysis. Except Analyses 17, 18, and 19, the actual soldier beam stiffness was used.

Figures 113 and 114 show that predicted bending moments, deflections, and earth pressures are sensitive to variations in K_a and EI. Variations in K_o, K_p, y_a, and y_p affected the earth pressure distributions (Figure 115), but they did not affect the deflections and bending moments.

Increasing K_a by a factor of two caused the predicted bending moments to increase between 1.5 and 2.7 times depending upon location (Figure 113). Predicted bending moments at the ground anchor location did not increase as much as those below the ground anchor because bending moments near the anchor depended primarily upon anchor load. Predicted moments at 20 ft increased in proportion to increases in K_a. In the beam-column model, bending moments between the ground anchor and the bottom of the excavation depended primarily upon the earth pressure applied to the lower portion of the wall.

TABLE 40
Parameters Used in the Sensitivity Analysis of the Texas A&M Wall

ANALYSIS	K_a	K_o	K_p	y_a (in)	y_p (in)	EI (lb-in^2)
1	0.15	0.47	5.8	0.05	0.5	1.25×10^{10}
2	**0.20**	0.47	5.8	0.05	0.5	1.25×10^{10}
3	**0.25**	0.47	5.8	0.05	0.5	1.25×10^{10}
4	**0.30**	0.47	5.8	0.05	0.5	1.25×10^{10}
5	0.15	**0.3**	5.8	0.05	0.5	1.25×10^{10}
6	0.15	**0.6**	5.8	0.05	0.5	1.25×10^{10}
7	0.15	**1.0**	5.8	0.05	0.5	1.25×10^{10}
8	0.15	0.47	**3.3**	0.05	0.5	1.25×10^{10}
9	0.15	0.47	**7.5**	0.05	0.5	1.25×10^{10}
10	0.15	0.47	**9.3**	0.05	0.5	1.25×10^{10}
11	0.15	0.47	5.8	**0.1**	0.5	1.25×10^{10}
12	0.15	0.47	5.8	**0.2**	0.5	1.25×10^{10}
13	0.15	0.47	5.8	**0.3**	0.5	1.25×10^{10}
14	0.15	0.47	5.8	0.05	**1.0**	1.25×10^{10}
15	0.15	0.47	5.8	0.05	**1.5**	1.25×10^{10}
16	0.15	0.47	5.8	0.05	**2.0**	1.25×10^{10}
17	0.15	0.47	5.8	0.05	0.5	$\mathbf{6.25 \times 10^{9}}$
18	0.15	0.47	5.8	0.05	0.5	$\mathbf{6.25 \times 10^{10}}$
19	0.15	0.47	5.8	0.05	0.5	$\mathbf{1.25 \times 10^{11}}$

Variations in the bending stiffness of the wall affected the moments below the ground anchor (Figure 114). At the ground anchor, the bending moments only varied by 10 percent while the beam stiffness varied by a factor of 20. In the analysis, beam stiffness affects the distribution of the earth pressures at the anchor location, but it does not significantly affect the bending moments (Figure 114). Below the ground anchor, predicted bending moments were dependent upon the magnitude of the active earth pressures. Variations in the bending stiffness, EI, affected the bending moments below the anchor location to some extent, too (Figure 114). The stiffer the beam the larger the predicted bending moments were above the bottom of the excavation.

Increasing K_a by a factor of two had the effect of almost tripling the deflections (Figure 113). Decreasing the bending stiffness of the soldier beam by 50 percent resulted in increasing the deflections above the bottom of the excavation by 65 to 100 percent depending upon location (Figure 114). Increasing the bending stiffness by a factor of five reduced the deflections by a factor of approximately 2.5 to 3.0 times. A factor of 10 increase in the bending stiffness reduced the deflections approximately 3.5 to 4.0 times. These results indicate that, in the analysis, wall deflections are primarily dependent upon the magnitude of the applied earth pressures, and secondarily dependent upon the bending stiffness of the wall. The sensitivity analyses also indicate that there is a practical limit to controlling deflections by stiffening the wall. Deflections of a beam depend on the effective span length to the third or fourth power. Therefore, bending deflections can be controlled more effectively by reducing the span between supports than by increasing the stiffness of the wall.

Figure 115 shows that, for practical purposes, the magnitude and distribution of the earth pressures depended primarily upon K_a, and to some degree on the bending stiffness, EI. Changes in EI affected the predicted earth pressures at the ground anchor and below the bottom of the excavation. Earth pressures at the anchor were larger for the flexible beams. For stiffer beams, the earth pressures were distributed further from the ground anchor location. Variations in K_o, K_p, y_a, and y_p influenced the earth pressures close to the ground anchor, but they did not affect the predicted bending moments. Figure 115 shows that the maximum earth pressures at the ground anchor location occurred when y_a and y_p equaled the active and passive reference deflections used to develop the R-y curves (y_a = 0.05 in and y_p = 0.5 in).

Ground anchor loads for the Texas A&M wall were determined from the 25H apparent earth pressure diagram. Therefore, the anchor loads were between the Rankine active and at-rest loads. For this case, the sensitivity analyses indicated that the predicted bending moments, earth pressures, and deflections depended primarily on the active earth pressures (value of K_a used to develop the R-y curves). The analyses showed that bending stiffness also affected the predictions, but to a lesser extent. The analyses demonstrates that, when the anchor load is determined using appropriate apparent earth pressure diagrams, the selection of the active earth pressure coefficient for the R-y curves affects the bending moment predictions.

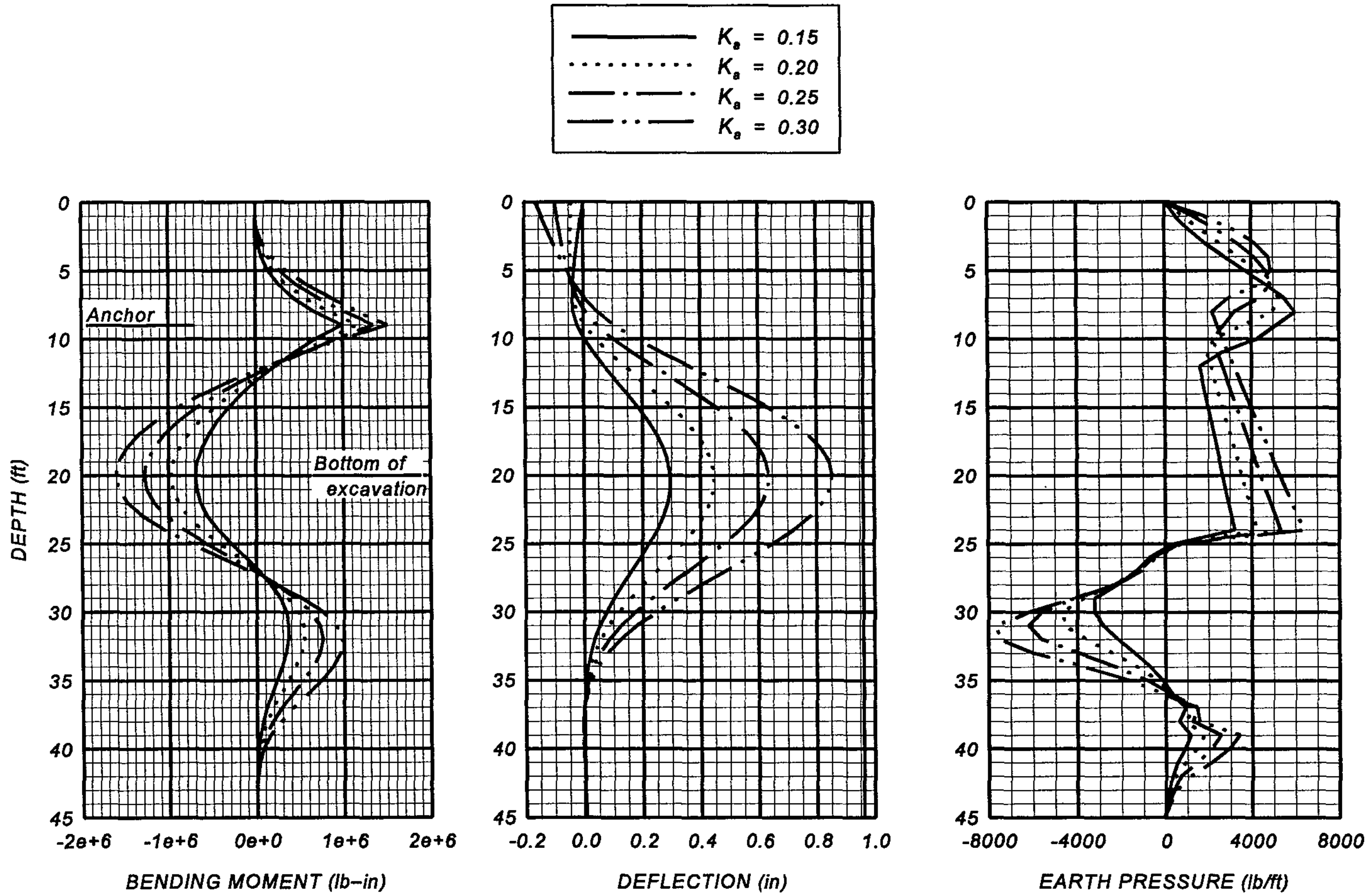

FIGURE 113
Sensitivity Analysis for BMCOL76 Predictions for the One-tier Texas A&M Wall, K_a Varies

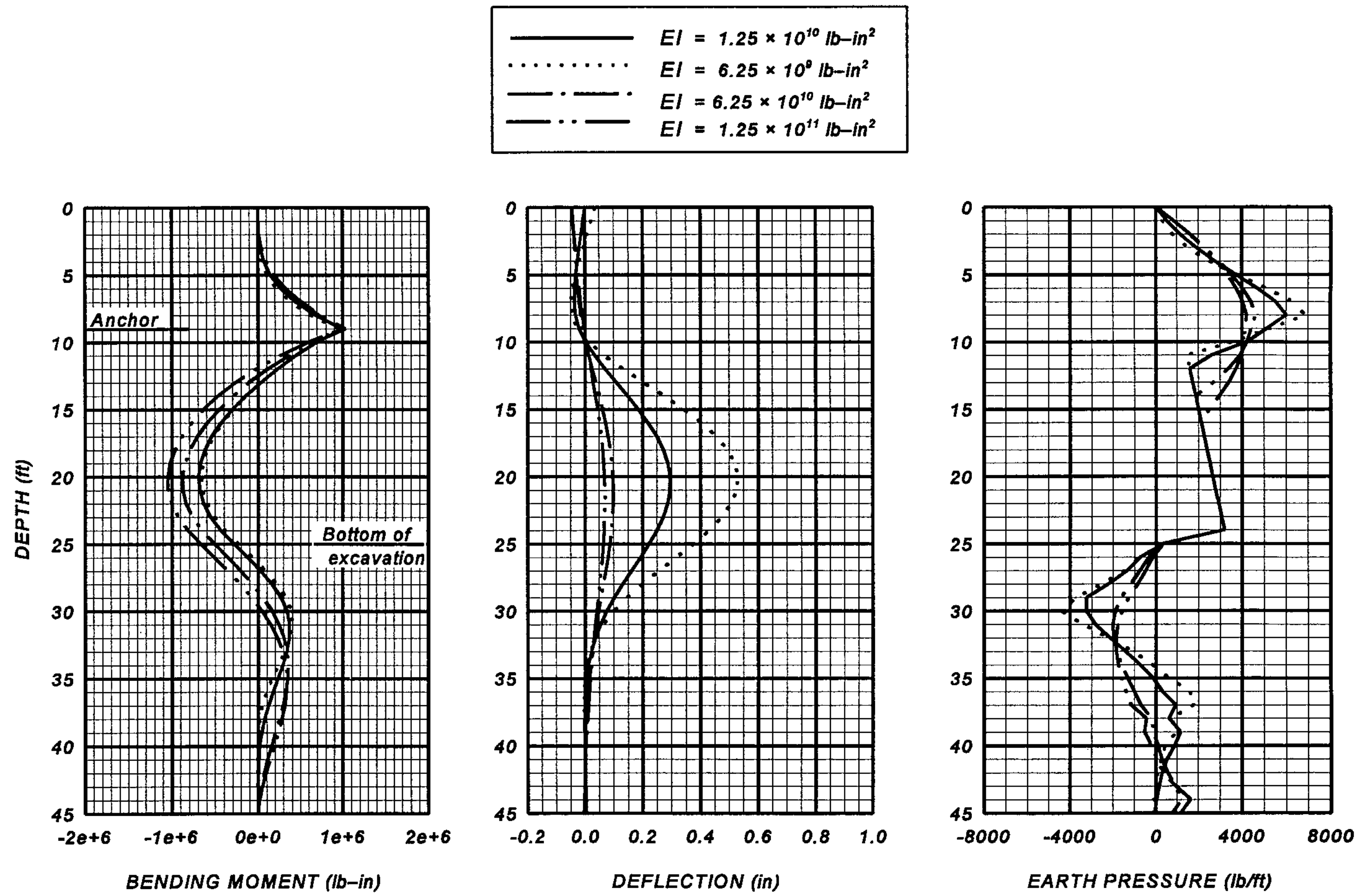

FIGURE 114
Sensitivity Analysis for BMCOL76 Predictions for the One-tier Texas A&M Wall, *EI* Varies

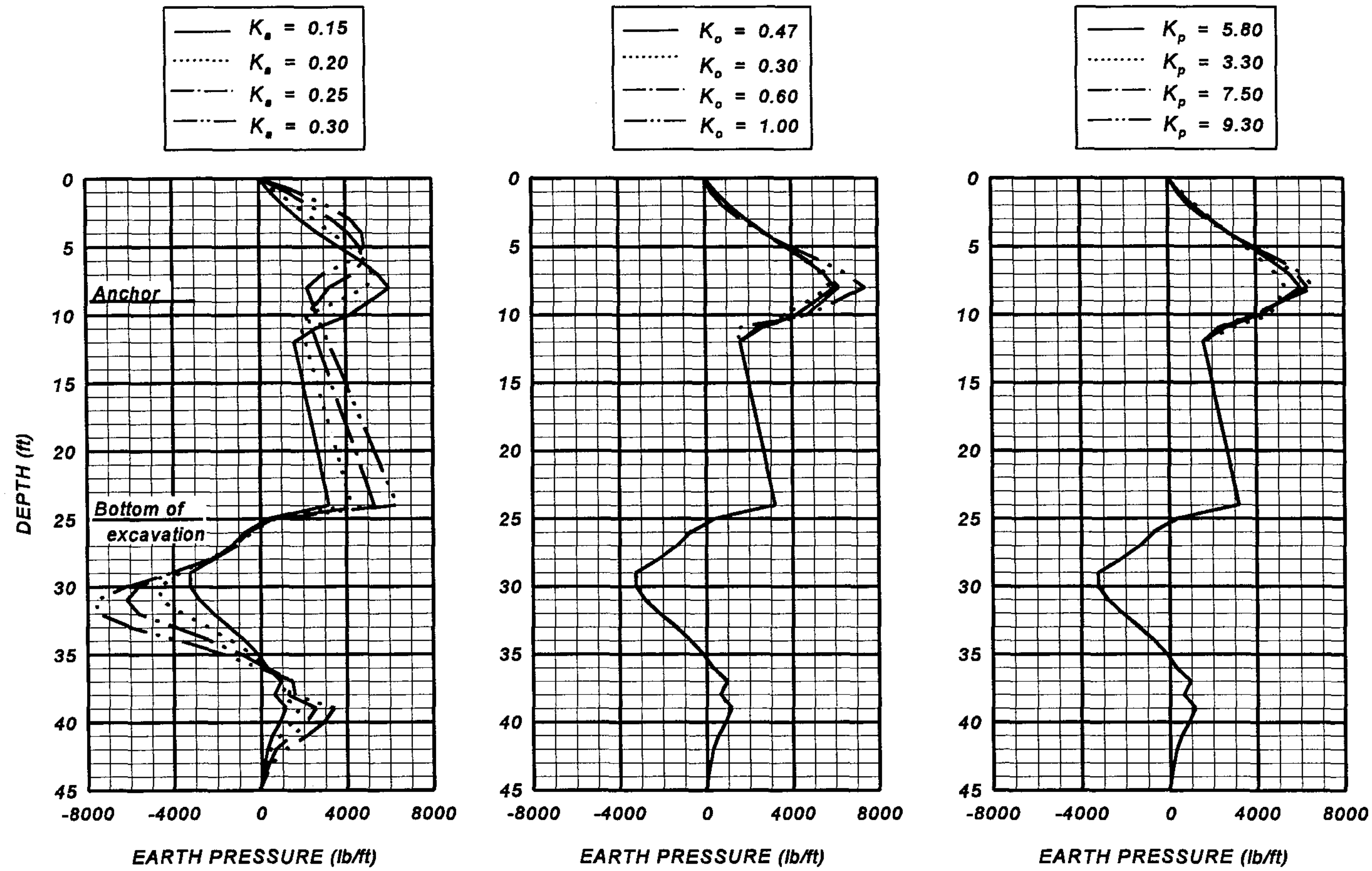

a) K_a Varies   b) K_o Varies   c) K_p Varies

FIGURE 115
Sensitivity Analysis for BMCOL76 Earth Pressure Predictions for the One-tier Texas A&M Wall

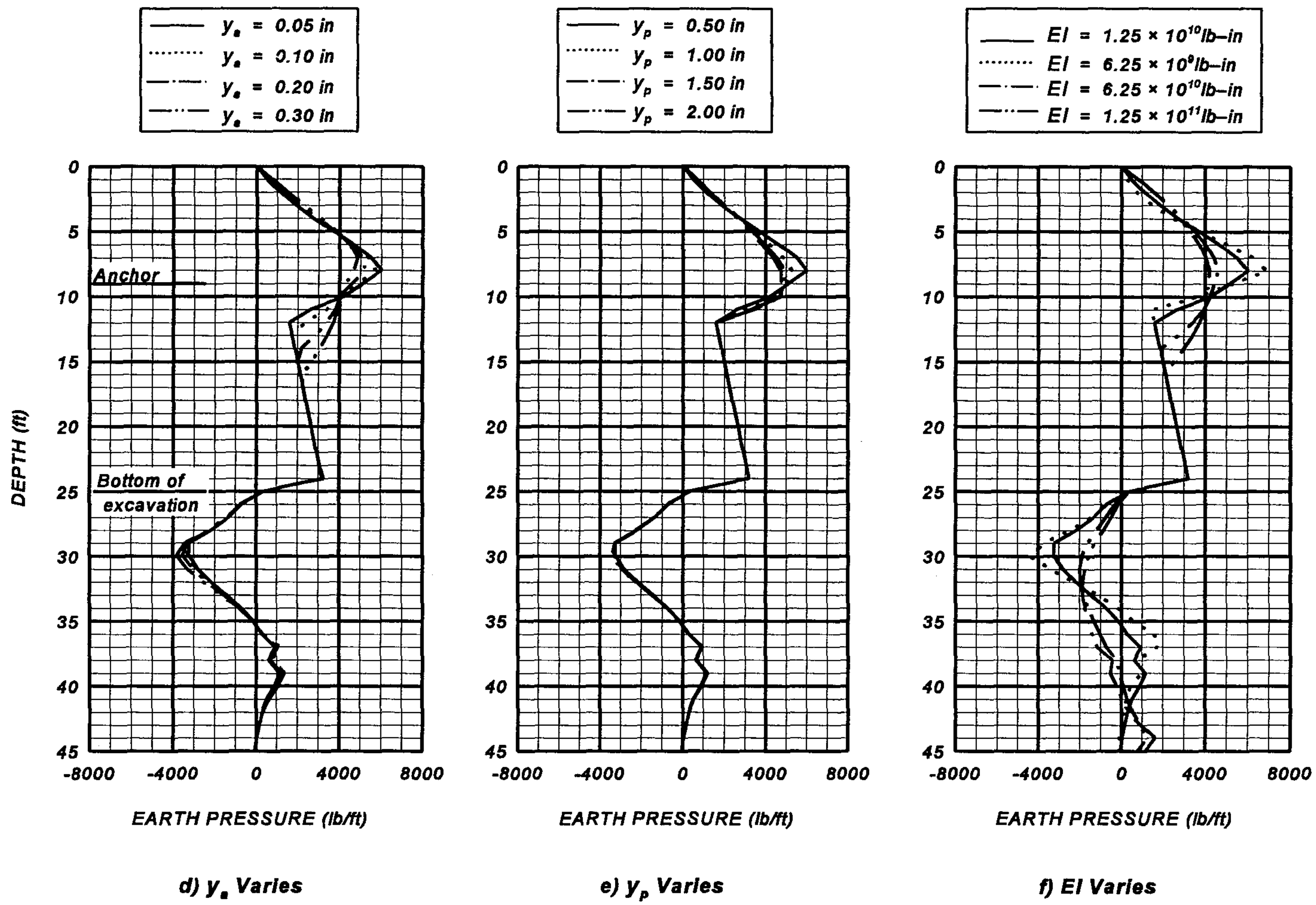

FIGURE 115
(continued)

3.5.2 Sensitivity Study Using Effective Stress R-y Curves in the Analyses of the Two-tier Lima, Ohio, Wall (Clay)

Parameters used in the effective stress sensitivity analyses of the Lima wall are contained in Table 41. The bending stiffness and the effective stress R-y curve parameters in Analysis 1 closely represented the actual conditions. Active, passive, and at-rest earth pressures used to develop the plane strain R-y curves above the bottom of the excavation are given by Equations 3.34 to 3.36.

$$R_{active} = (P_{active})\, s = (K_a \sigma'_v - 2c\sqrt{K_a})\, s \qquad \text{. . . [3.34]}$$

$$R_{passive} = (P_{passive})\, s = (K_p \sigma'_v + 2c\sqrt{K_p})\, s \qquad \text{. . . [3.35]}$$

$$R_{at\text{-}rest} = (P_{at\text{-}rest})\, s = (K_o \sigma'_v)\, s \qquad \text{. . . [3.36]}$$

where:

K_a = active earth pressure coefficient

K_p = passive earth pressure coefficient

K_o = at-rest earth pressure coefficient

σ'_v = effective vertical stress at depth z

c = drained cohesion of the soil

s = soldier beam spacing

Bold values in the table indicate the parameter that was varied for each analysis. The ground anchors were simulated using T-y curves described in Section 3.4.4. The actual soldier beam stiffness was used in each analysis except Analyses 17, 18, and 19.

TABLE 41
Parameters for the Effective Stress, Sensitivity Analyses of the Lima Wall

ANALYSIS	K_a	K_o	K_p	y_a (in)	y_p (in)	EI (lb-in^2)
1	0.25	0.7	5.8	0.3	0.8	1.89×10^{10}
2	**0.20**	0.7	5.8	0.3	0.8	1.89×10^{10}
3	**0.30**	0.7	5.8	0.3	0.8	1.89×10^{10}
4	**0.40**	0.7	5.8	0.3	0.8	1.89×10^{10}
5	0.25	**0.3**	5.8	0.3	0.8	1.89×10^{10}
6	0.25	**0.5**	5.8	0.3	0.8	1.89×10^{10}
7	0.25	**1.0**	5.8	0.3	0.8	1.89×10^{10}
8	0.25	0.7	**3.3**	0.3	0.8	1.89×10^{10}
9	0.25	0.7	**7.5**	0.3	0.8	1.89×10^{10}
10	0.25	0.7	**9.3**	0.3	0.8	1.89×10^{10}
11	0.25	0.7	5.8	**0.2**	0.8	1.89×10^{10}
12	0.25	0.7	5.8	**0.4**	0.8	1.89×10^{10}
13	0.25	0.7	5.8	**0.5**	0.8	1.89×10^{10}
14	0.25	0.7	5.8	0.3	**0.5**	1.89×10^{10}
15	0.25	0.7	5.8	0.3	**1.2**	1.89×10^{10}
16	0.25	0.7	5.8	0.3	**1.5**	1.89×10^{10}
17	0.25	0.7	5.8	0.3	0.8	$\mathbf{6.25 \times 10^{9}}$
18	0.25	0.7	5.8	0.3	0.8	$\mathbf{6.25 \times 10^{10}}$
19	0.25	0.7	5.8	0.3	0.8	$\mathbf{1.25 \times 10^{11}}$

The results of the sensitivity analyses are shown in Figures 116 to 121. Figure 116 shows that changes in K_a affected the bending moments between the supports and below the lower anchor. Moments at the ground anchor locations did not vary significantly in response to changes in K_a. Bending moments at the upper ground anchor varied 6 percent and moments at the lower anchor varied 16 percent as K_a changed from 0.2 to 0.4. Bending moments at the ground anchor locations were not sensitive to changes in K_a since the anchors pulled the wall back into the soil, which mobilized passive earth pressures. Bending moments between the anchors were small, but they responded to changes K_a. Moments in the span below the second row of anchors and above the bottom of the excavation were the most sensitive to changes in K_a. There, the moments changed 55 percent in response to changes K_a. The R-y curves below the bottom of the excavation (25 ft) were not affected by the value of K_a. However, the bending moment in the toe changed as the earth pressure above the bottom of the excavation changed. These changes reflected the mobilization of additional load-carrying capacity in the toe to support the increased load resulting from increases in K_a.

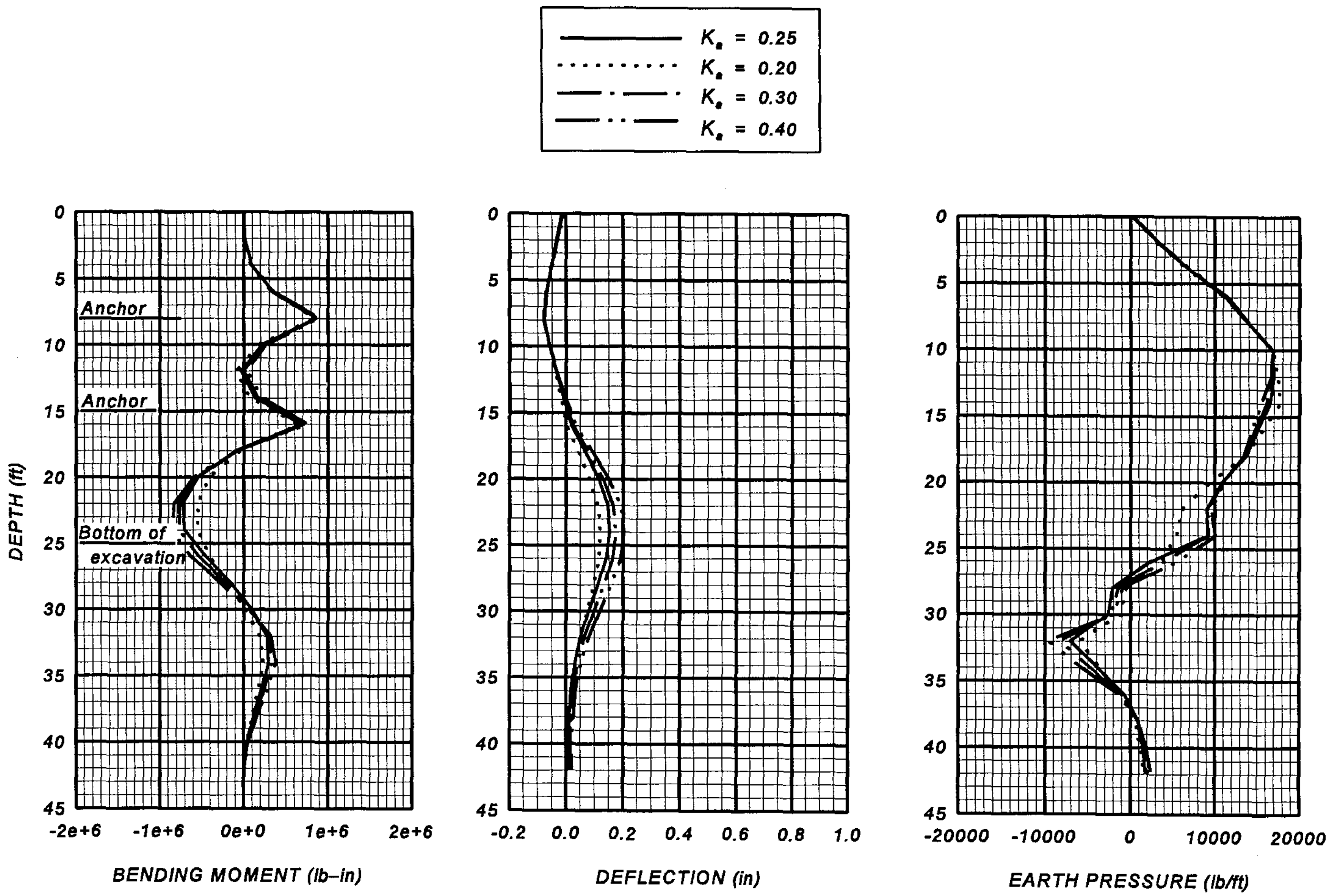

FIGURE 116
Sensitivity Analysis for BMCOL76 Predictions for the Lima Wall, Effective Stress *R-y* Curves, K_a Varies

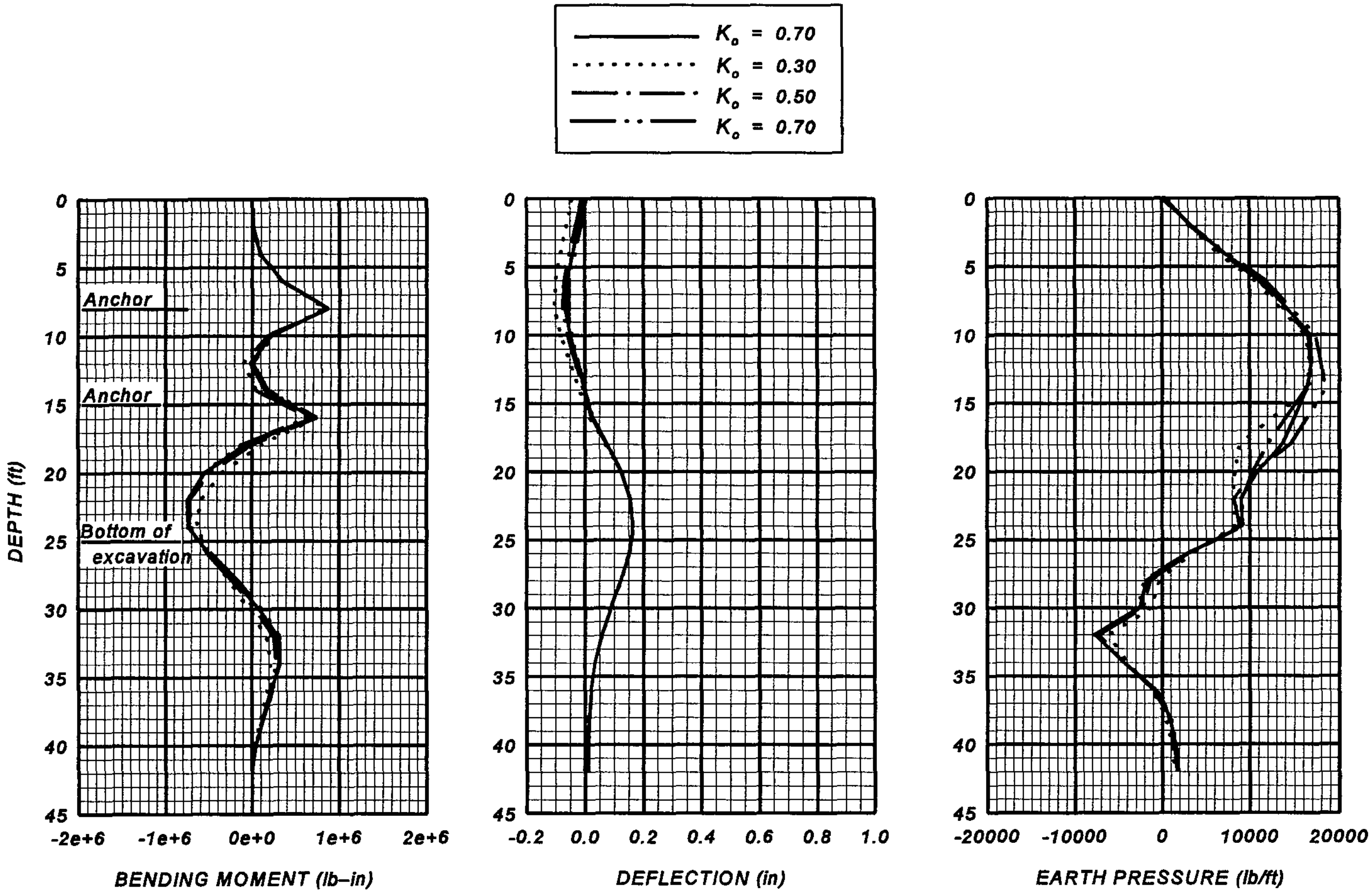

FIGURE 117
Sensitivity Analysis for BMCOL76 Predictions for the Lima Wall, Effective Stress *R-y* Curves, K_o Varies

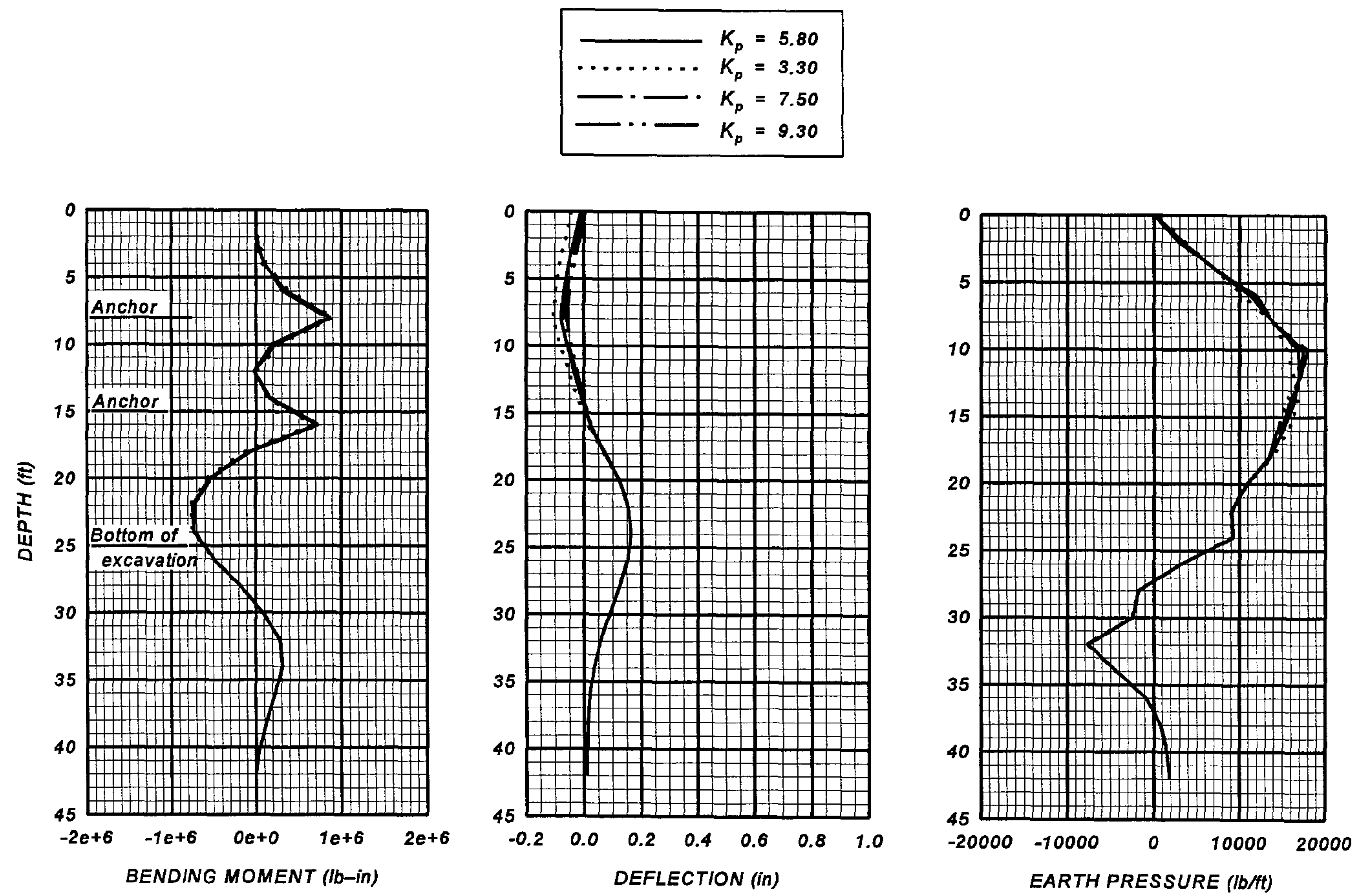

FIGURE 118
Sensitivity Analysis for BMCOL76 Predictions for the Lima Wall, Effective Stress *R-y* Curves, K_p Varies

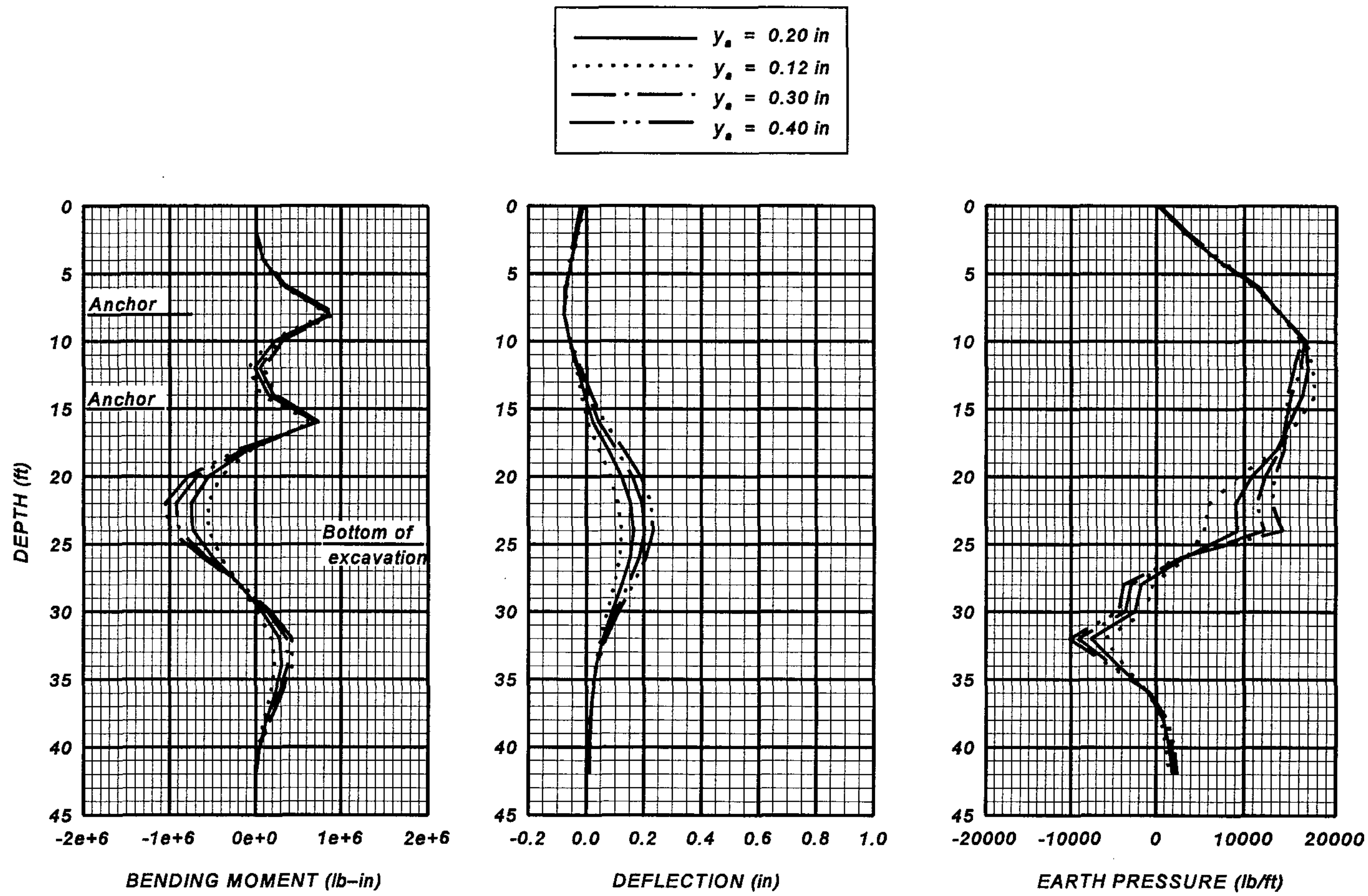

FIGURE 119
Sensitivity Analysis for BMCOL76 Predictions for the Lima Wall, Effective Stress *R-y* Curves, y_a Varies

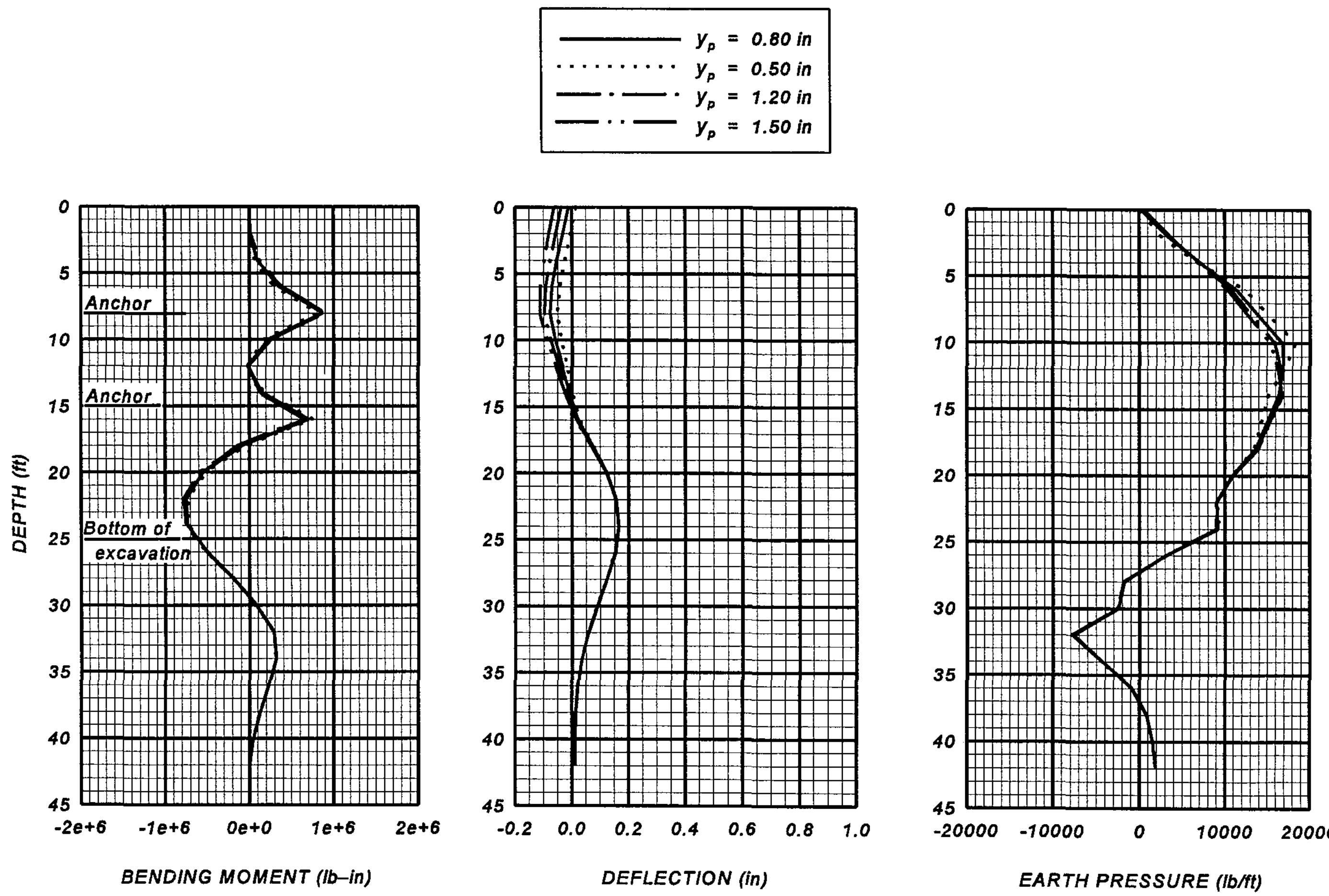

FIGURE 120
Sensitivity Analysis for BMCOL76 Predictions for the Lima Wall, Effective Stress *R-y* Curves, y_p Varies

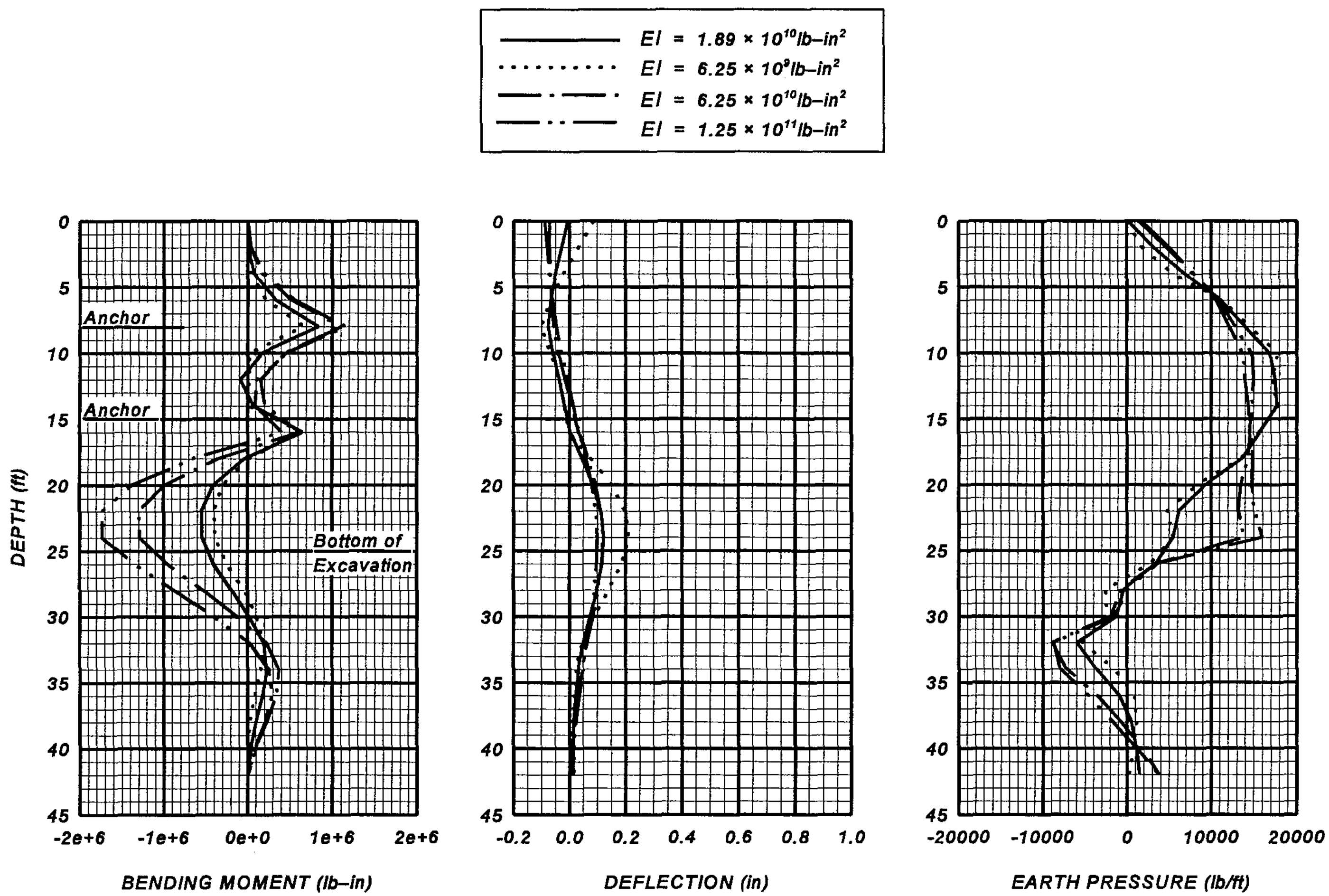

FIGURE 121
Sensitivity Analysis for BMCOL76 Predictions for the Lima Wall, Effective Stress *R-y* Curves, *EI* Varies

Figure 116 shows how predicted wall deflections and earth pressures were affected by changes in K_a. In the upper portion of the wall, deflections and earth pressures did not change as the active earth pressure coefficient, K_a, changed from 0.2 to 0.4. Wall deflections and earth pressures at the top of the wall were not affected by changes in K_a because the ground anchors pulled the wall back into the ground. Below 15 ft, deflections and earth pressures were sensitive to changes in the active earth pressure coefficient. There, the wall moved out in an attempt to reduce the earth pressures. Twenty-four ft below the top of the wall the deflections increased by 68 percent and the earth pressures increased by 82 percent as K_a changed from 0.2 to 0.4. Changes in earth pressures and deflections below the bottom of the excavation reflect the mobilization of passive resistance required to balance the increased earth pressures that developed as K_a increased.

Figure 117 shows the results of the sensitivity analyses when K_o was varied from 0.3 to 1.0. When K_o changes, the slope of the R-y curve between the active and passive soil pressures changes. A large K_o causes a steep slope between the active and at-rest pressures and a flat slope between the at-rest and the passive pressures. Since the predicted movements of the Lima wall were small ($0.0006H$) and within the elastic range of the R-y curves, changes in K_o affected the results of the sensitivity analyses. However, variations in the bending moment curves were not large. The bending moments at the upper ground anchor varied 4 percent and the moments at the lower anchor varied 7 percent for values of K_o between 0.3 and 1.0. Bending moments between the anchors were small, but they responded to changes K_o. Below the ground anchors and above the bottom of the excavation, the bending moments changed by 18 percent in response to changes K_o. The R-y curves below the bottom of the excavation (27 ft) were not affected by the value of K_o. Bending moment changes in the toe reflected the mobilization of additional load-carrying capacity required to support increased earth pressures above the bottom of the excavation. Wall deflections for the upper portion of the wall were affected by changes in K_o. Below 15 ft, the deflection of the wall was not affected by changes in K_o. Figure 117 shows that changes in K_o caused small changes in the earth pressures.

Figure 118 shows that the predicted bending moments did not change as K_p varied from 3.3 to 9.3. Since the ground anchors pulled the upper portion of the wall back into the ground, the passive earth pressure coefficient had some influence on wall deflections and the earth pressures. However, these changes were small since the passive capacity of the ground was not exceeded.

Results of the sensitivity analyses where the active reference deflection, y_a, was varied are shown in Figure 119. Predicted bending moments and deflections along the upper portion of the wall were not affected by changes in y_a. Along the upper portion of the wall the analyses predicted that the wall would be pulled back into the ground. Where the wall is pulled into the ground, bending moments, deflections, or earth pressures are not sensitive to changes in the active reference deflection. Below the ground anchors the wall deflects outward. There, the value of y_a affects the results because the slope of the R-y curve between the at-rest and the active pressures is determined by the value of y_a. When y_a was small, active earth pressures developed with small wall movement. For larger values of y_a, the wall had to deflect more to reduce the earth pressures to active. In the span below the lower ground anchor the bending moments and wall deflections increased by 90 percent as the value of y_a increased from 0.2 to 0.5. Earth pressures in the same span increased 160 percent as y_a increased.

Variation in the passive reference deflection, y_p, affected the bending moments, wall deflections, and earth pressures, as shown in Figure 120. When y_p changes, the slope of the R-y curve between the at-rest and the passive pressure changes. Bending moments in the soldier beam varied by less than 10 percent as y_p varied from 0.5 to 1.5. Deflections over the upper portion of the wall were more sensitive to changes in y_p. There, the ground anchors pulled the wall back into the ground and the slope of the R-y curves between the at-rest and the passive pressures affected the wall movement. Earth pressures near the ground anchors also depended upon the value of y_p. The maximum earth pressure between the ground anchors varied by 9 percent as y_p changed from 0.5 to 1.5.

Variations in wall stiffness, EI, affected bending moments, wall deflections, and earth pressures. Figure 121 shows how sensitive the results of the analyses were to changes in beam stiffness. Bending moments varied by 74 percent at the upper anchor, 60 percent at the lower anchor, 343 percent below the lower anchor, and 89 percent in the toe as EI changed from 6.25×10^9 to 1.25×10^{11} (a factor or 20). Except for the most flexible wall, the deflected shape of the wall did not change significantly in response to changes in bending stiffness. Predicted earth pressures did change in response to changes in wall stiffness. Stiffer walls had more uniform pressures and required more passive toe capacity. More flexible walls had concentrated pressures at the ground anchors and reduced pressures below the ground anchors and in the toe.

Figures 116 to 121 show that the predicted bending moments were primarily sensitive to variations in EI. Since the analyses predicted that the ground anchors would pull the wall back into the ground and the pressures would not exceed the passive resistance of the ground, the bending stiffness of the wall determined how the wall behaved.

3.5.3 Sensitivity Study Using Total Stress R-y Curves in the Analyses of the Two-tier Lima, Ohio, Wall (Clay)

Parameters used in the total stress sensitivity analyses of the Lima wall are contained in Table 42. Values for Analysis 1 closely represented the actual wall and the total stress R-y curve parameters in Section 3.4.4. Active, passive and at-rest earth pressures used to develop the total stress R-y curves above the bottom of the excavation were determined using Equations 3.37 to 3.39. Equation 3.37 gives a negative active pressure over the full height of the wall (Section 3.3.2.3 describes how the R-y curves are developed when the active pressures are negative), and Equation 3.38 gives a lower passive pressure than the effective stress passive pressure. Since the total stress R-y curves are different from the effective stress R-y curves, the predictions for the total stress analyses were different from those developed using effective stress R-y curves.

$$R_{active} = (P_{active})\, s = (\sigma_v - 2s_u)\, s \qquad \text{. . . [3.37]}$$

$$R_{passive} = (P_{passive})\, s = (\sigma_v + 2s_u)\, s \qquad \text{. . . [3.38]}$$

$$R_{at\text{-}rest} = (P_{at\text{-}rest})\, s = (\sigma_v)\, s \qquad \text{. . . [3.39]}$$

where:

σ_v = total vertical stress

s_u = undrained shear strength

s = soldier beam spacing

TABLE 42
Parameters for the Total Stress, Sensitivity Analyses of the Lima Wall

ANALYSIS	y_a (in)	y_p (in)	EI (lb-in²)
1	0.2	0.8	1.89×10^{10}
2	**0.3**	0.8	1.89×10^{10}
3	**0.4**	0.8	1.89×10^{10}
4	**0.5**	0.8	1.89×10^{10}
5	0.2	**0.5**	1.89×10^{10}
6	0.2	**1.2**	1.89×10^{10}
7	0.2	**1.5**	1.89×10^{10}
8	0.2	0.8	$\mathbf{6.25 \times 10^{9}}$
9	0.2	0.8	$\mathbf{6.25 \times 10^{10}}$
10	0.2	0.8	$\mathbf{1.25 \times 10^{11}}$

Bold values in the table indicate parameters that were varied for each analysis. The ground anchors were simulated using the T-y curves described in Section 3.4.4. Actual soldier beam stiffness was used in each analysis except Analyses 8, 9, and 10.

Figure 122 shows the results of the sensitivity analyses where the active reference deflection, y_a, was varied between 0.2 and 0.5 in. In the upper portion of the wall, the bending moments, deflections, and earth pressures changes were small in response to changes in y_a. Below the ground anchors, bending moments, deflections, and earth pressures were more sensitive to changes in the active reference deflection. Bending moments in the soldier beam varied by 14 percent at the upper anchor, less than 1 percent at the lower anchor, 71 percent below the lower anchor, and 87 percent in the toe as y_a changed from 0.2 to 0.5 in. Analyses using total stress R-y curves predicted slightly larger bending moments than the analyses using effective stress R-y curves (Figure 119). Below the lower anchor, wall deflections increased 90 percent as y_a increased. A similar increase was observed when effective stress R-y curves were used, but the deflections for the total stress cases were about 20 percent larger than the deflections calculated using effective stress R-y curves. As y_a increased, earth pressures in the span below the lower anchor and in the toe increased 68 and 79 percent, respectively. Earth pressures developed using total stress R-y curves were between 7 and 27 percent greater than the pressures developed using effective stress R-y curves above the bottom of the excavation.

Bending moments, wall deflections and earth pressures determined in the sensitivity analyses using total stress R-y curves were not sensitive to changes in y_p between 0.5 and 1.5 (Figure 123). Bending moments, deflections and earth pressures determined in the y_p sensitivity analyses using total stress R-y curves were similar to those determined using the effective stress R-y curves.

Variations in wall stiffness, EI, affected bending moments, wall deflections, and earth pressures. Figure 124 shows how sensitive the total stress analyses were to changes in beam stiffness. Bending moments varied by 64 percent at the upper anchor, 167 percent at the lower anchor, 385 percent below the lower anchor, and 183 percent in the toe as EI changed from 6.25×10^9 to 1.25×10^{11} lb-in^2 (a factor or 20). Comparing Figure 121 with Figure 124 shows that the bending moment and deflection curves developed using the total stress R-y curves were similar to those developed using effective stress R-y curves in the EI sensitivity analyses. Above the bottom of the excavation, the earth pressures developed using the total stress R-y curves were between 5 and 10 percent greater than the earth pressures developed with effective stress R-y curves.

Total stress and effective stress R-y curves were used to predict the response of the Lima wall system to the applied ground anchor loads. Ground anchor loads were large enough to pull the wall back into the ground. High ground anchor loads caused the predictions from the total stress and the effective stress analyses to be similar. When anchor loads are high, wall behavior depends upon the passive resistance. Passive resistance for the total stress of effective stress R-y curves was high relative to the applied ground anchor loads.

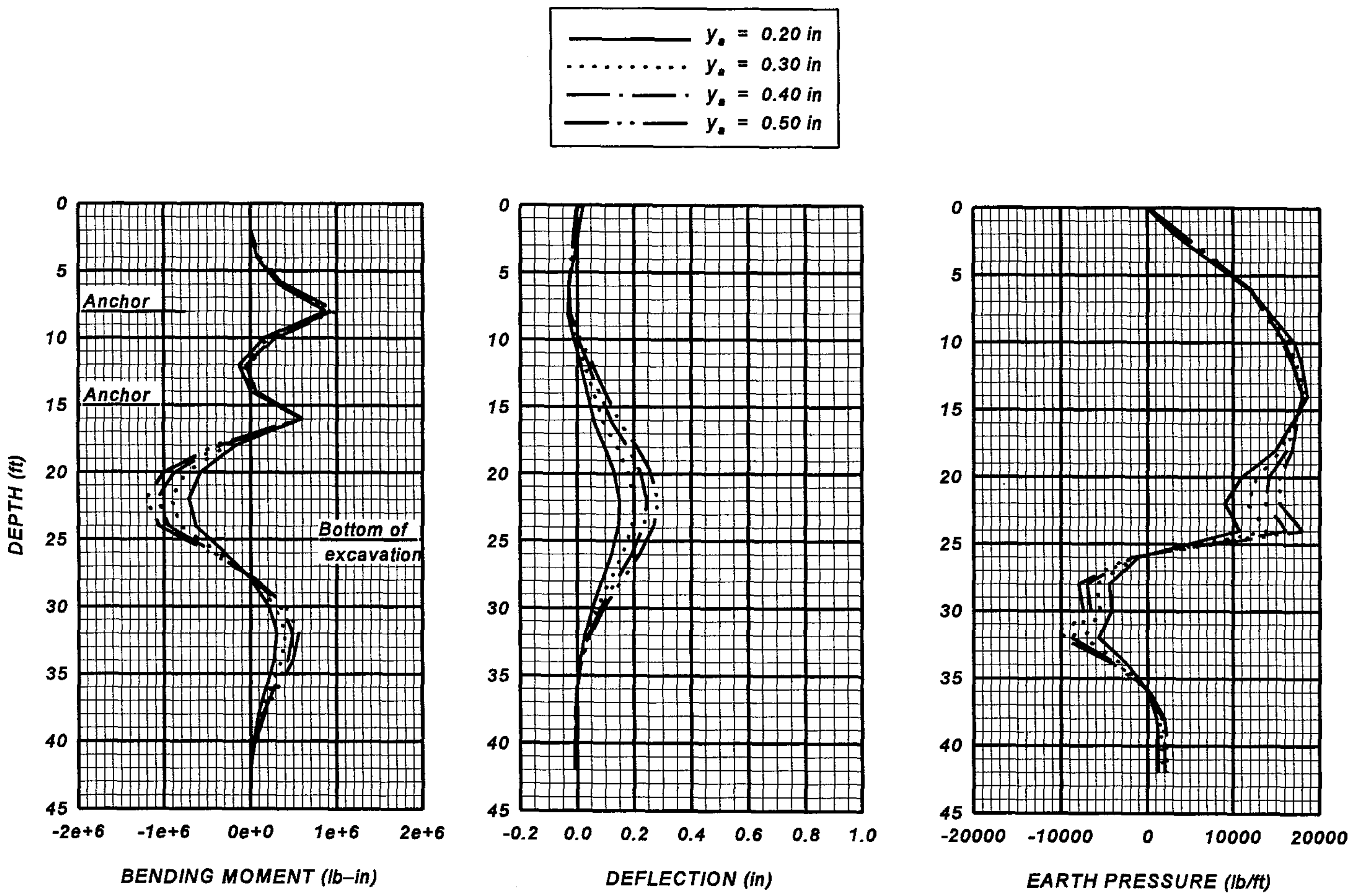

FIGURE 122
Sensitivity Analysis for BMCOL76 Predictions for the Lima Wall, Total Stress *R-y* Curves, y_a Varies

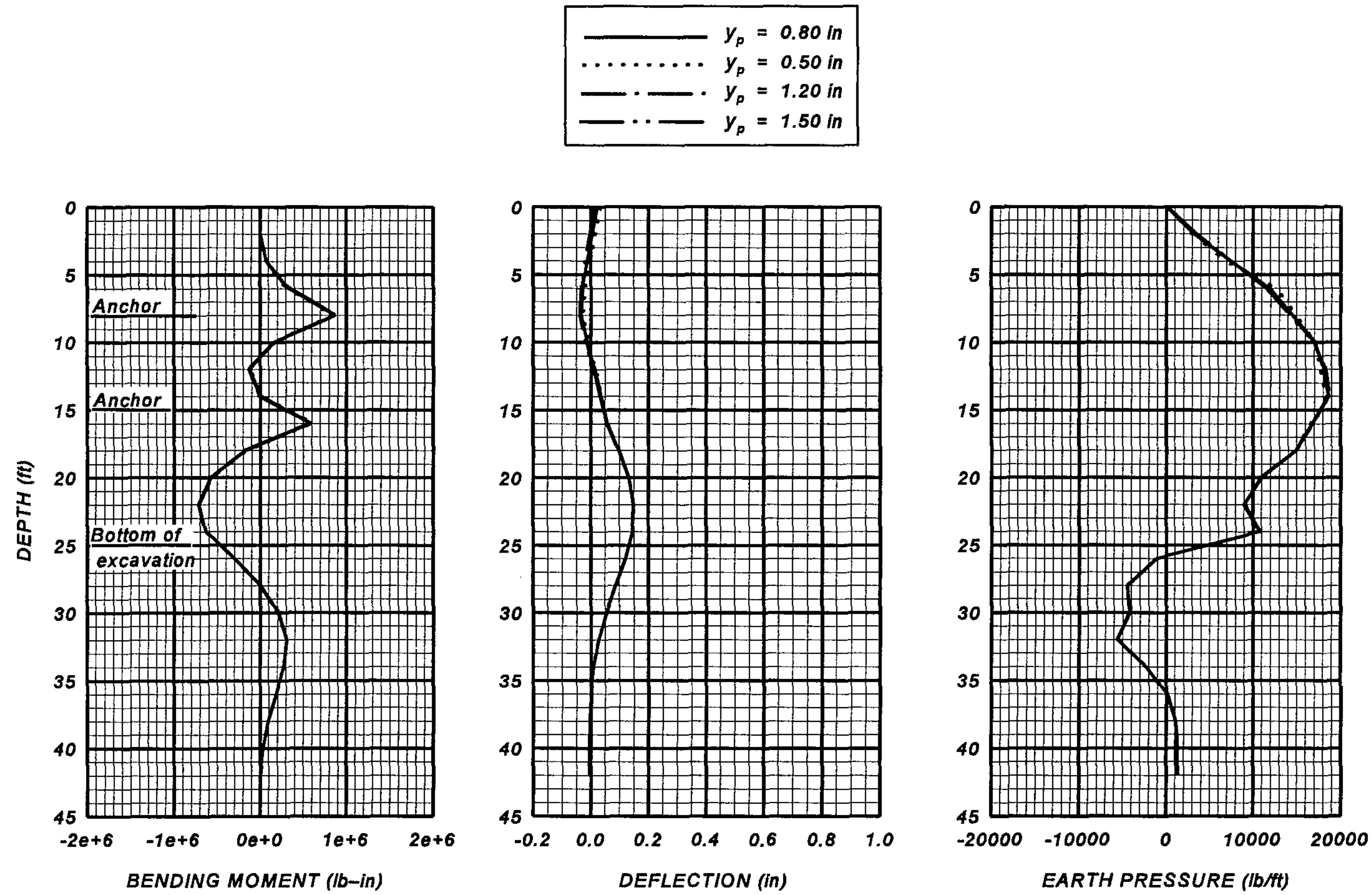

FIGURE 123
Sensitivity Analysis for BMCOL76 Predictions for the Lima Wall, Total Stress *R-y* Curves, y_p Varies

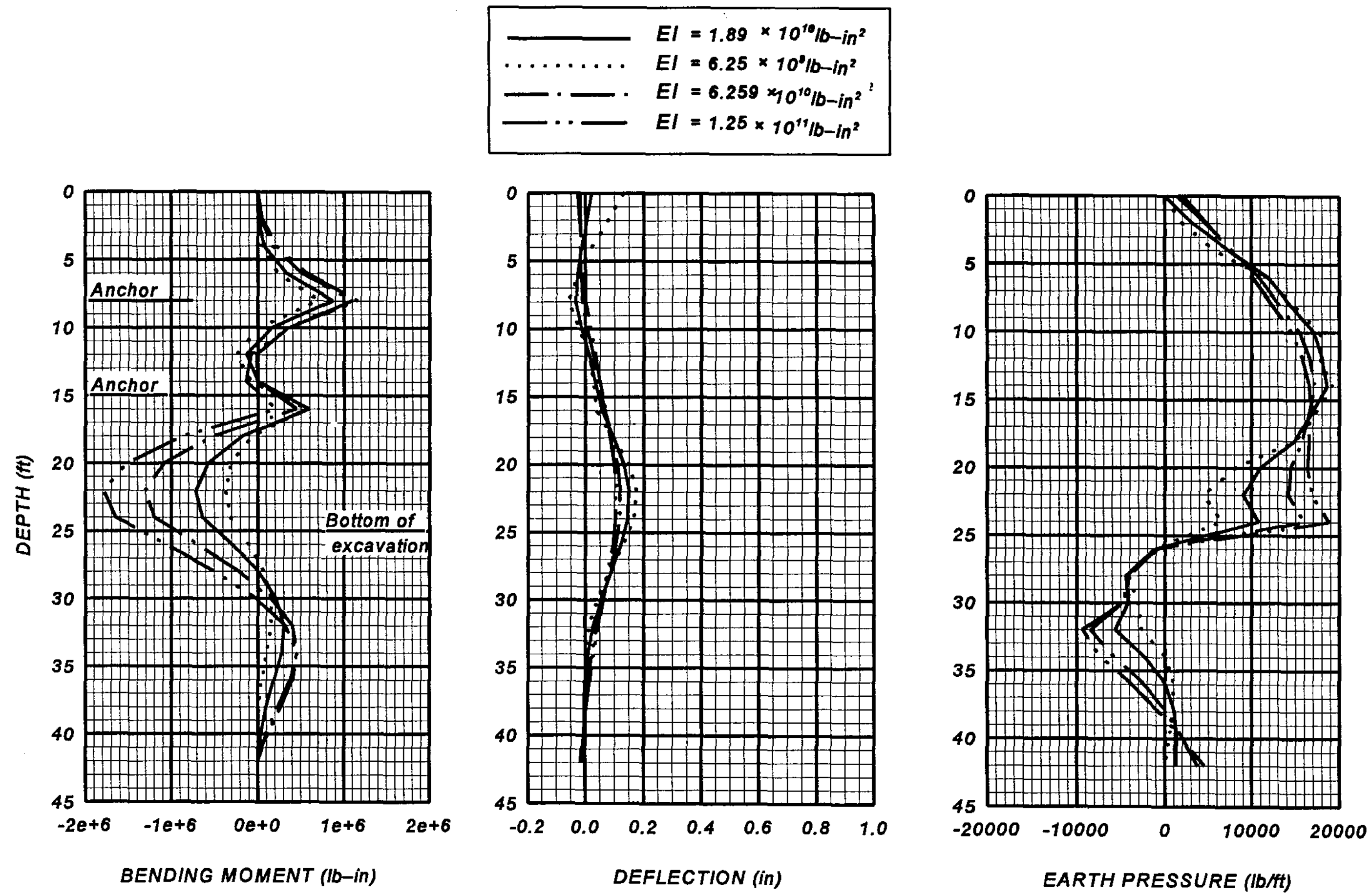

FIGURE 124
Sensitivity Analysis for BMCOL76 Predictions for the Lima Wall, Total Stress *R-y* Curves, *EI* Varies

3.6 SOIL-STRUCTURE INTERACTION ANALYSIS USING APPARENT EARTH PRESSURE DIAGRAMS AND R-y CURVES TO MODEL THE LATERAL TOE RESISTANCE

Section 3.4 showed that non-linear soil springs did not accurately model the earth pressures behind flexible walls when the ground anchors were locked-off at loads determined from apparent earth pressure diagrams. To match predicted behavior with the measured behavior, the active earth pressure used to define the minimum load associated with the springs behind the wall had to be reduced by 50 percent. The active pressures had to be reduced, since they were defined in terms of Rankine or Coulomb coefficients, and they could not model the redistribution of pressures that occurs behind flexible walls. Arching, stressing the ground anchors, the construction sequence, and facial stiffness cause the earth pressures on flexible walls to redistribute to the supports. On the other hand, apparent earth pressure diagrams were developed from measured loads and include the effects of arching, soldier beam flexibility, preloading of supports, facial stiffness, and the construction sequence. Apparent earth pressure diagrams give lower lateral earth pressures than triangular active earth pressures near the bottom of the excavation. The apparent earth pressure diagram introduced in Section 2.5.9 also considers the locations of the supports. A soil-structure interaction analysis that combined the apparent earth pressure diagrams with R-y curves to model the lateral resistance of the soldier beam toe was evaluated to determine if could predict the measured bending moments for the one-tier and two-tier walls built at Texas A&M.

CBEAMC (Dawkins, 1994), a soil-structure interaction computer code based on a simple finite element method , was used for the analyses. Figure 125 illustrates how the apparent earth pressure, toe resistance, and ground anchors were modeled in the analyses. The apparent earth pressures were modeled as a distributed load. Analyses were made using the design pressure diagrams (Figures 130 and 131) and the apparent earth pressure diagrams in Figure 60. The total lateral load from each diagram was 100 kips. Below the bottom of the wall, the passive resistance was modeled by a series R-y curves. Active R_a-y curves were on the back of the wall and passive R_p-y curves were on the front of the wall. The soldier beam was modeled as a continuous member. The maximum resistance is related to the passive capacity of the beam and the minimum resistance is related to the active pressure. The resistances for the R-y curves were developed using relationships described in Section 3.6.1. API single pile resistance (discussed in Section 3.3.2.2) was not used since it did not include the interaction of adjacent soldier beams. Ground anchors were modeled as concentrated T-y curves (Section 3.3.3), where T is the anchor load and y is the deflection of the wall at the anchor location.

3.6.1 Modeling the Lateral Resistance of the Toe

Figure 125 shows the general nature of the R-y curves used to describe the load-deflection behavior of the toe of the wall. Relationships developed by Wang and Reese (1986) were used to determine the lateral resistances for the R-y curves. These relationships were developed to compute the ultimate passive resistances for a drilled shaft wall. Wang and Reese considered three modes of failure. To incorporate their equations in the analysis, the ultimate resistances for each failure mode are determined, and the smallest resistance is used to describe the passive resistance of the toe at any depth. Figures showing the different failure mechanisms are presented below. One mode of failure assumes that the passive resistance results from a wedge failure in front of an individual drilled shaft (Figure 126). This failure mechanism is similar to the mechanism modeled by the API single pile curves. When the drilled shafts become too close or too deep, the individual wedges will overlap and the lateral resistance for an individual drilled shaft will be reduced (Figure 127). At some depth, the soil in front of the shaft will be confined and the lateral resistance will not depend upon a wedge failure, but it will be limited by flow of the soil around the shafts. Flow resistance will control when the soil plastically flows (Figure 128) between the soldier beams rather than a wedge failure up to the surface. Lateral resistance can be limited by a fourth failure mode not considered by Wang and Reese. At no point can the passive resistance be greater than that computed for a two-dimensional failure surface (Figure 129).

Equations for each failure mode are presented here. Those interested in studying their derivation are directed to the work by Wang and Reese (1986) and the *COM624 Manual* (Wang and Reese, 1992).

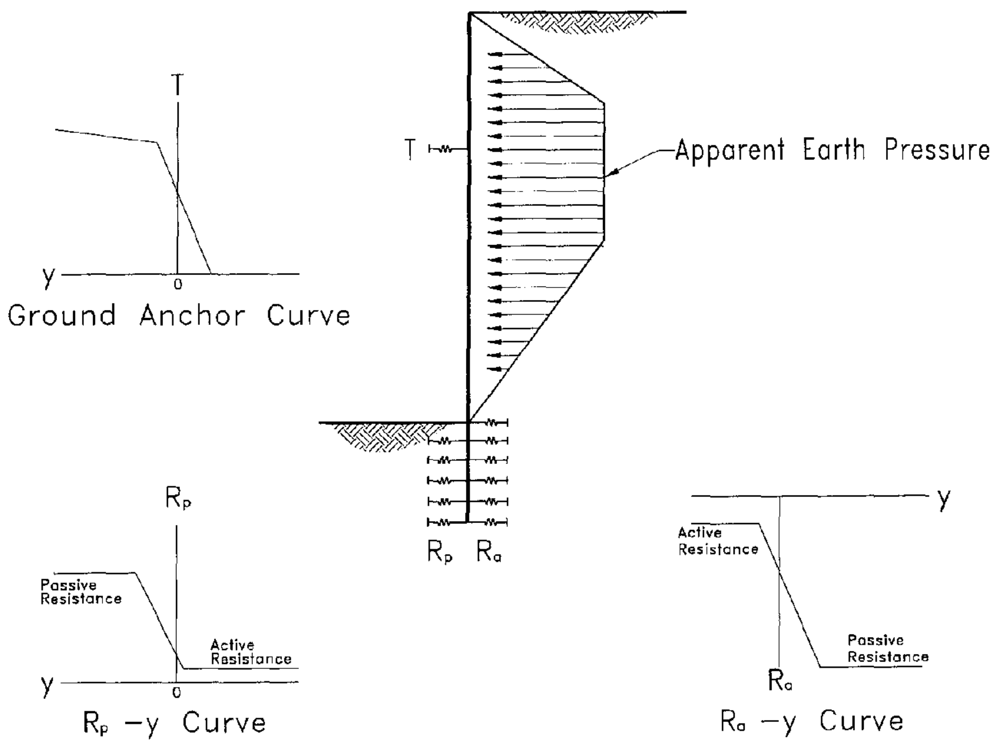

FIGURE 125
Diagram Illustrating the Modeling of Earth Pressures, Toe Resistance, and Ground Anchors in a Soil-structure Interaction Analyses

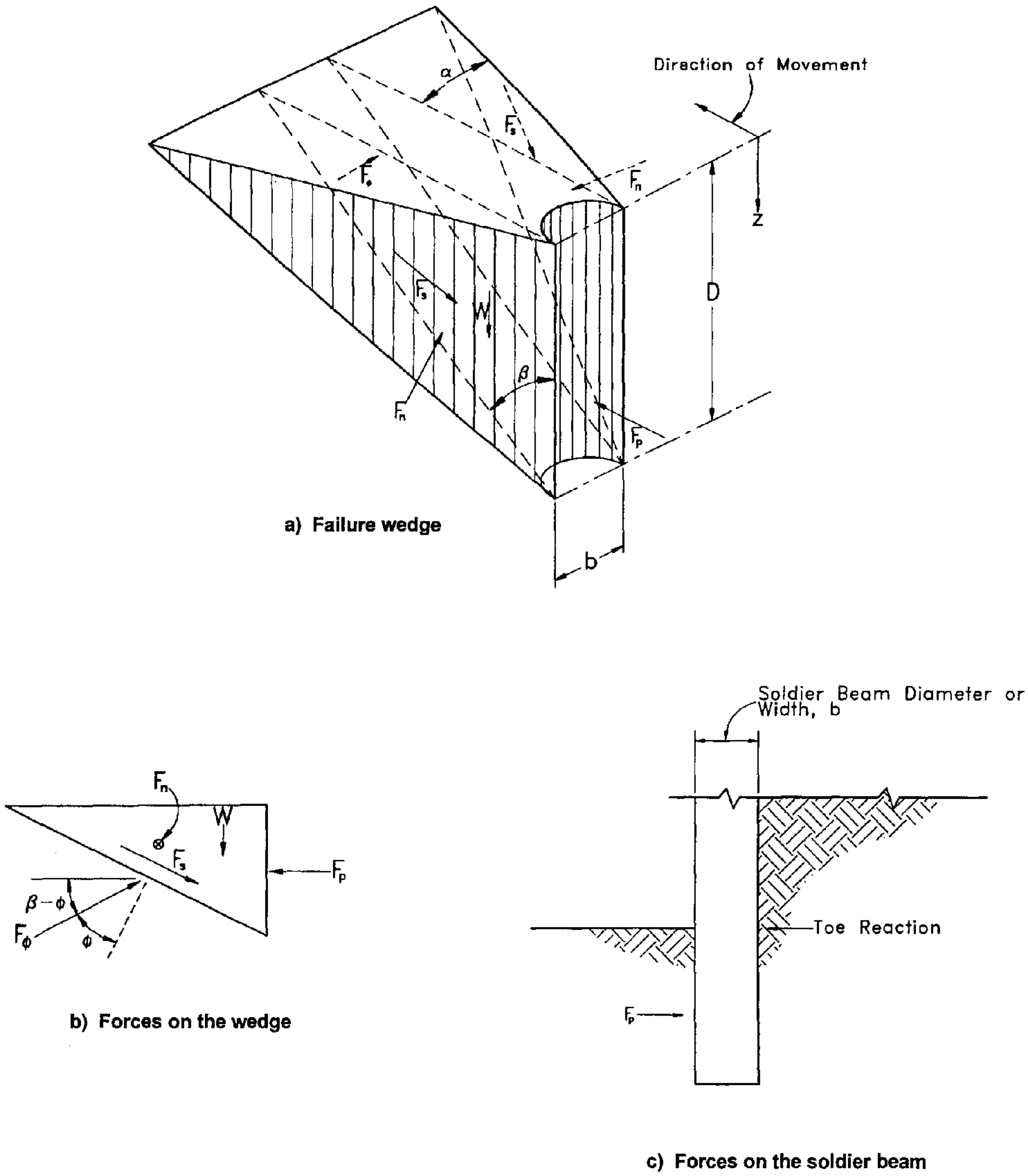

FIGURE 126
Passive Wedge Failure for a Soldier Beam Toe in Sand
(after Reese, et al., 1974)

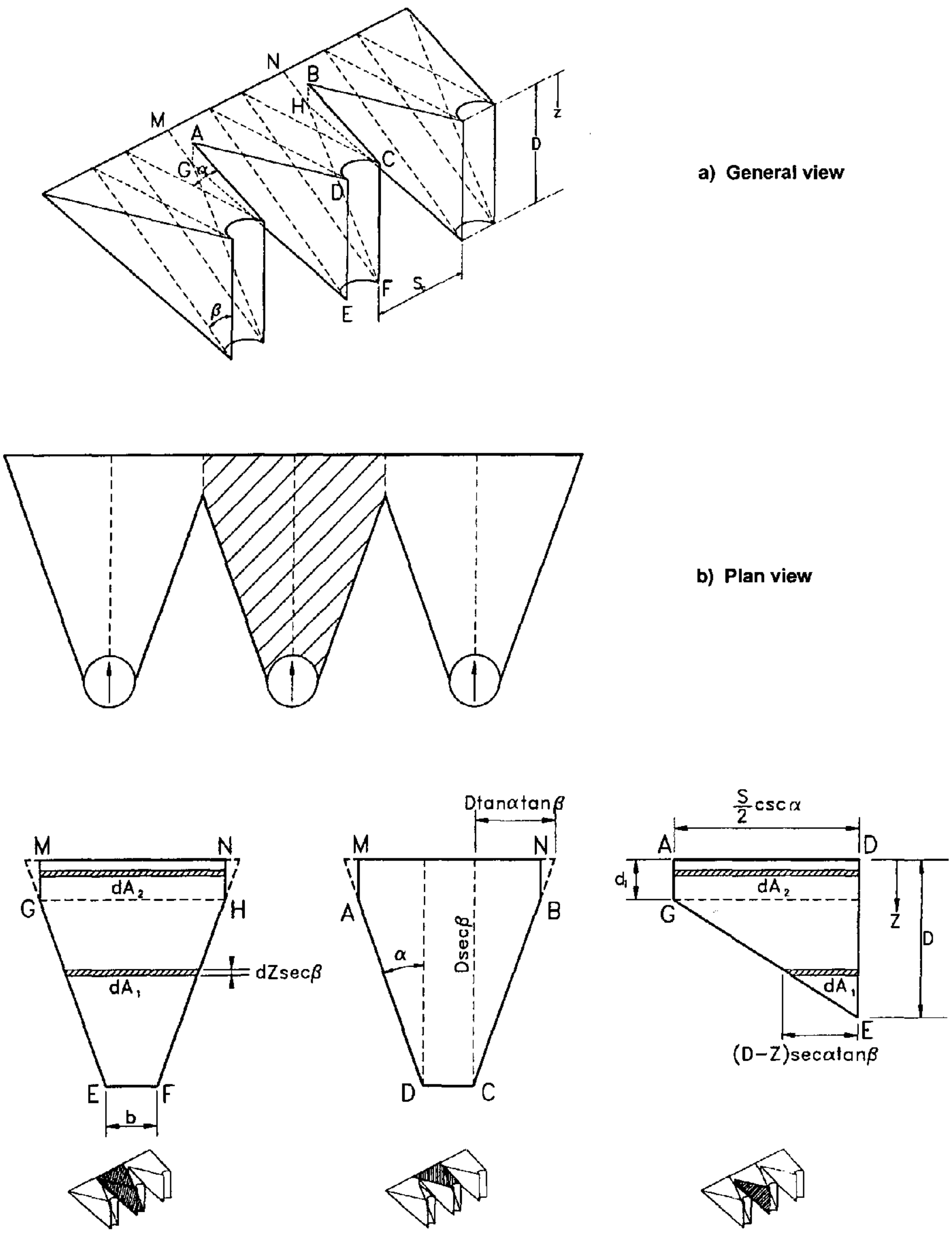

FIGURE 127
Intersecting Failure Wedges for Soldier Beam Toes in Sand
(after Wang and Reese, 1986)

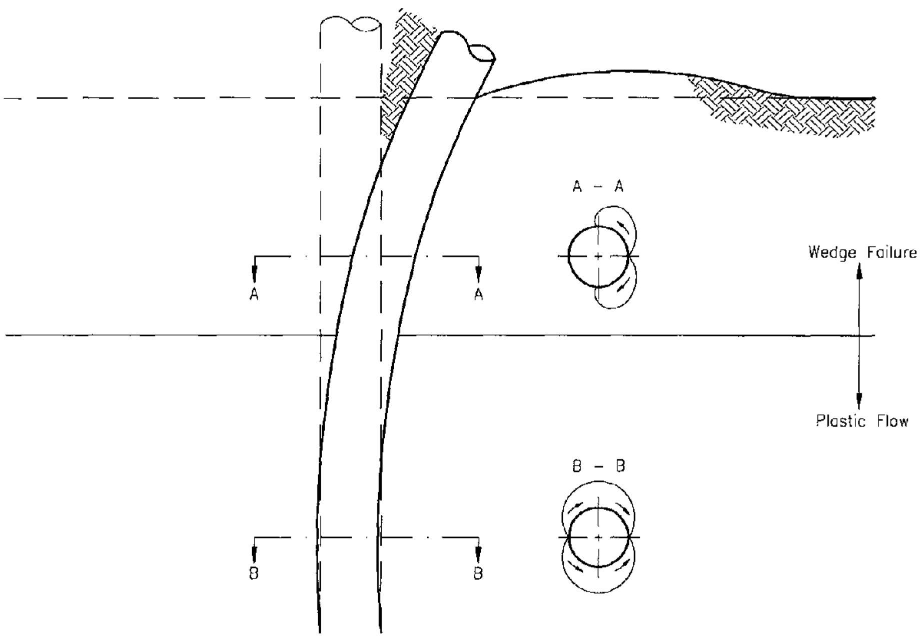

FIGURE 128
Plastic Soil Flow Around a Soldier Beam Toe
(after Wang and Reese, 1986)

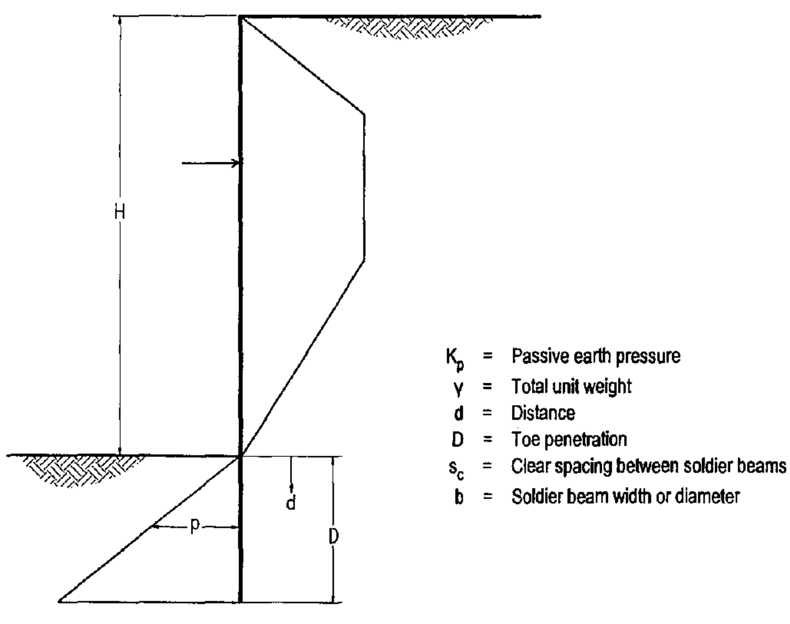

$p=(K_p \gamma d)(s_c+b)$

FIGURE 129
Passive Resistance for the Toe of a Continuous Wall in Sand

Figure 126 shows the wedge failure for a single soldier beam in sand. The passive force, F_p, is given by Equation 3.40.

$$F_p = \gamma D^2 \left[\frac{K_o D \tan\phi \sin\beta}{3\tan(\beta-\phi)\cos\alpha} + \frac{\tan\beta}{\tan(\beta-\phi)} \left(\frac{b}{2} + \frac{D}{3}\tan\beta\tan\alpha \right) + \frac{K_o D \tan\beta}{3}(\tan\phi - \sin\beta - \tan\alpha) \right] \quad \ldots [3.40]$$

where:

γ = total unit weight
K_o = at-rest earth pressure coefficient
K_a = active earth pressure coefficient
β = 45 + ϕ/2
α = ϕ for dense sands, ϕ/3 – ϕ/2 for loose sands

Equation 3.40 is differentiated to give the ultimate soil resistance at depth, d (Equation 3.41).

$$p = \gamma d \left[\frac{K_o d \tan\phi \sin\beta}{\tan(\beta-\phi)\cos\alpha} + \frac{\tan\beta}{\tan(\beta-\phi)}(b + d\tan\beta\tan\alpha) + K_o d \tan\beta(\tan\phi\sin\beta - \tan\alpha) \right] \quad \ldots [3.41]$$

Figure 127 shows the individual failure wedges intersecting as the soldier beam spacing decreases or the toe depth increases. Equation 3.42 gives the depth of the intersection of adjacent wedges.

$$d_i = D - \frac{s_c}{2\tan\alpha\tan\beta} \quad \ldots [3.42]$$

where:

D = toe depth
s_c = clear spacing between soldier beams

When d_i is positive, the failure wedges intersect. If d_i is negative, the failure wedges do not intersect. At depths greater than, d_i, the passive resistances are not affected by adjacent soldier beams, and they are computed using Equation 3.41. Above the point of intersection, the passive resistances are reduced to account for the intersection of the failure wedges. To account for the intersection of the wedges, the passive resistances determined from Equation 3.41 are reduced by the resistances determined for a wedge with a height, d_i, and a soldier beam with a width of zero. Resistances down to the depth, d_i, are given by Equation 3.43.

$$p = \gamma d \left[\frac{K_o d \tan\phi \sin\beta}{\tan(\beta-\phi)} \left(\frac{1}{\cos\alpha} - 1 \right) + \frac{d\tan\beta\tan\alpha}{\tan(\beta-\phi)} - K_o d \frac{\sin^2\beta}{\cos\beta}\tan\phi(\tan\alpha + 1) \right] \quad \ldots [3.43]$$

where:

$d \le d_i$

At depth, the ultimate lateral resistance will be limited to the resistance that can develop before the soil flows between the soldier beams (Figure 128). Equation 3.44 gives the ultimate lateral flow resistance.

$$p = K_a b \gamma d \tan^8 \beta + K_o \gamma d \tan\phi \tan^4 \beta \qquad \ldots [3.44]$$

Figure 129 shows the two-dimensional failure wedge. Lateral resistances cannot exceed the value given by Equation 3.45.

$$p = K_p \gamma d (s_c + b) \qquad \ldots [3.45]$$

where:

s_c = clear spacing between soldier beams

b = soldier beam width or shaft diameter

Wang and Reese's sand equations included an active earth pressure term subtracted from the passive resistance to give a net resistance at a given depth. The active earth pressure term was dropped from each equation since the ground surface for a wall is not level. Equations 3.41 to 3.45 give the passive resistance at a location, and the Rankine active pressures must be applied to the other side of the wall when computing the capacity of the toe (Figure 130).

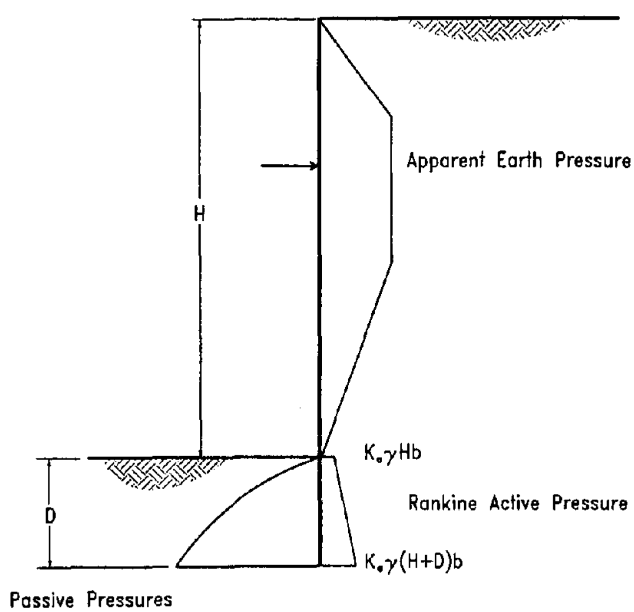

FIGURE 130
Diagram Illustrating the Active and Passive Pressures on a Soldier Beam Toe

3.6.2 Predicted and Measured Bending Moments for the One-tier Wall

Soil-structure interaction analyses were performed on one-tier wall sections with the earth loading behind the wall given by the 25*H* trapezoid apparent earth pressure diagram (design diagram) and the modified trapezoidal diagram shown in Figure 60. The lateral resistance of the embedded portion of the soldier beams was modeled using R-y curves. Wang and Reese relationships were used to determine the ultimate lateral resistance for the R_a-y and the R_p-y curves. The active reference deflection, y_a, equaled 0.05 in, and the passive reference deflection, y_p, equaled 0.5 in. The same R-y curves were used for both analyses.

Figure 131 compares the bending moment diagrams from the soil-structure interaction analyses with the average bending moments in Soldier Beams 15 and 16, 84 days after completion of the wall. Bending moment diagrams for the two trapezoidal diagrams assuming a hinge at the bottom of the excavation also are shown. The total lateral load for each apparent earth pressure diagram was 100 kips. The soldier beam in the analysis using the 25*H* diagram had to be lengthened 1 ft to obtain a solution. The 25*H* diagram requires the soldier beam toe to carry more load than the modified trapezoidal diagram. The soil-structure interaction analysis for the modified trapezoidal diagram predicted bending moments similar to those given by the design diagram with a hinge at subgrade. Soldier beams are modeled as continuous members in the soil-structure interaction analyses. Modeling the soldier beam as a continuous member causes the effective span between the ground anchor and the result of the lateral toe reaction to be longer, and the lower bending moments to increase.

Using the modified trapezoidal apparent earth pressure diagram in a soil-structure interaction analysis predicted reasonable bending moments and allowed the soldier beam to be modeled as a continuous member. The analysis using the modified trapezoidal apparent earth pressure diagram and R-y curves to describe the lateral resistance along the soldier beam toe modeled the behavior of the wall with a 5-ft embedment depth. Section 3.4.1 noted that a solution could not be obtained using Rankine or Coulomb active pressures behind the wall above the bottom of the excavation and a 5-ft toe embedment.

3.6.3 Predicted and Measured Bending Moments for the Two-tier Wall

Soil-structure interaction analyses were performed on two-tier wall sections with the earth loading behind the wall given by the 25*H* trapezoid apparent earth pressure diagram (design diagram) and the modified trapezoidal diagram shown in Figure 60. The lateral resistance of the embedded portion of the soldier beams was modeled using R-y curves. Wang and Reese relationships were used to determine the ultimate lateral resistance for the R_a-y and the R_p-y curves. The active reference deflection, y_a, equaled 0.05 in, and the passive reference deflection, y_p, equaled 0.5 in. The same R-y curves were used for both analyses.

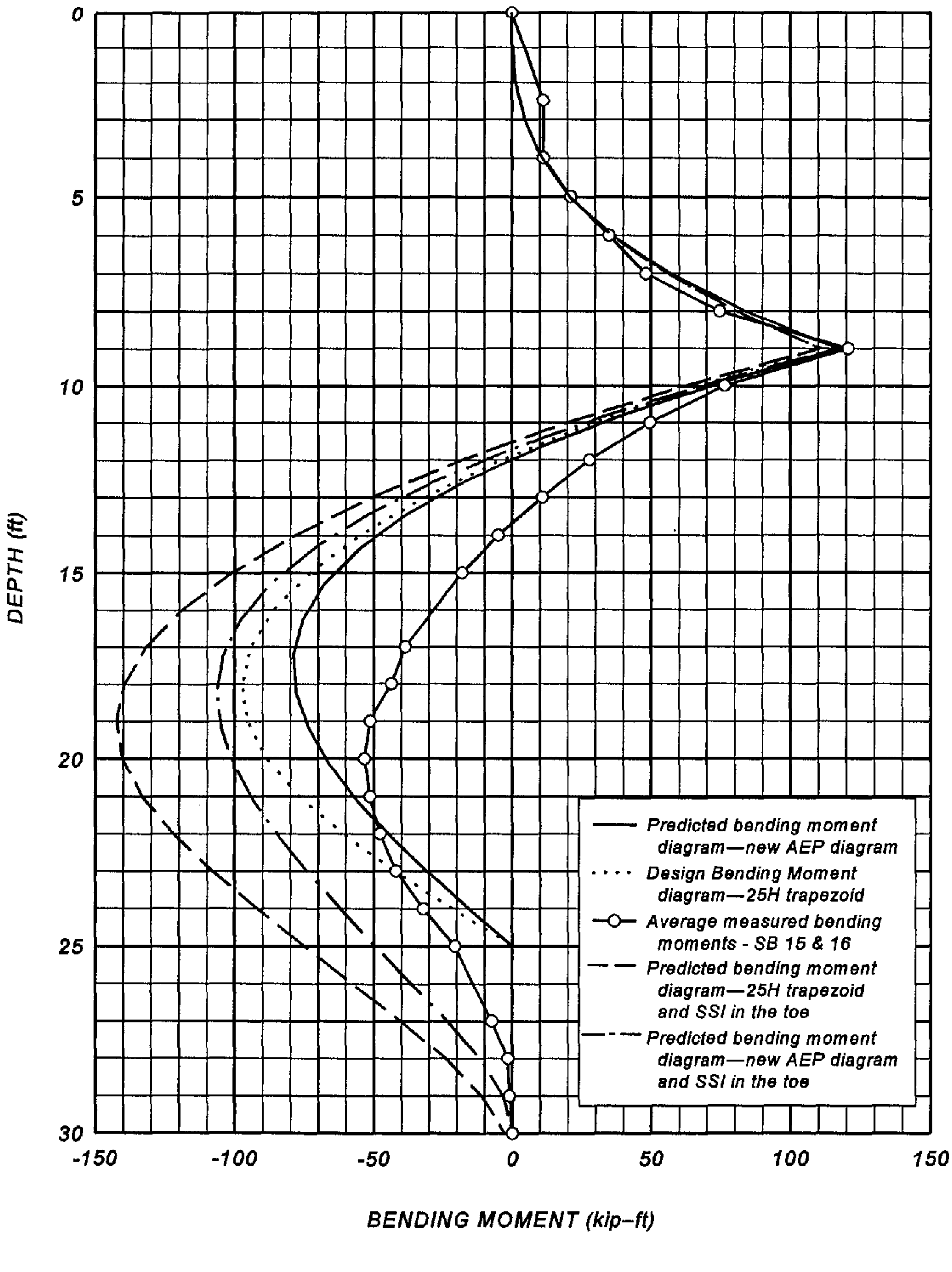

FIGURE 131
Comparison of Predicted Bending Moments Using Trapezoidal Apparent Earth Pressure (AEP) Diagrams and *R-y* Curves with Predicted Bending Moments Using Trapezoidal Apparent Earth Pressure (AEP) Diagrams Assuming a Hinge at the Bottom of the Excavation and the Average Measured Bending Moments in Soldier Beams 15 and 16

Figure 132 compares the bending moment diagrams from the soil-structure interaction analyses with the average bending moments in Soldier Beams 7 and 8, 84 days after completion of the wall. Bending moments for the trapezoidal diagrams assuming a hinge at the lower ground anchor and the bottom of the excavation also are shown. The total lateral load for each apparent earth pressure diagram was 100 kips. Figure 132 shows that the soil-structure interaction analyses modeled the soldier beam as a continuous structural member. Maximum predicted bending moments occurred at the ground anchor locations. The soil-structure interaction analysis using the modified trapezoid predicted the bending moments satisfactorily at the upper ground anchor location and below the lower ground anchor. Predicted moments between the ground anchors and at the lower anchor were higher than the measured bending moments. The maximum bending moments predicted by the design diagram and the maximum moment predicted by the soil-structure interaction analysis using the modified apparent earth pressure diagram were the same.

3.6.4 Observations

Soil-structure interaction analyses using apparent earth pressure diagrams above the bottom of the excavation, and R-y curves based on Wang and Reese (1986) relationships to model the lateral resistance of the soldier beam toe, predicted the bending moments satisfactorily. Apparent earth pressure diagrams include the effects of arching, soldier beam flexibility, preloading of the supports, facial stiffness, and the construction sequence. Attempts to use R-y curves based on Rankine or Coulomb earth pressure coefficients above the bottom of the excavation and modeling the construction sequence were not able to predict the behavior of the soldier beams in the full-scale test wall. Reasonable predictions for the full-scale wall could only be obtained when the active earth pressure coefficient was reduced by 50 percent to account for load redistribution.

Figures 131 and 132 show that trapezoidal apparent earth pressure diagrams with a hinge at subgrade predict bending moments in the soldier beams satisfactorily. Bending moment at the upper ground anchor must be the same for the hinge method and the soil-structure interaction analysis. Below the upper ground anchor, the maximum bending moments computed using the hinge method were similar to the maximum bending moments predicted by the soil-structure interaction analysis. For anchored walls with competent ground at subgrade it is not necessary to perform a soil-structure interaction analysis to determine the design moments. A soil-structure interaction analysis can be used to determine the bending moments in a wall where the toe resistance is poor and the wall cantilevers around the ground anchor.

Wang and Reese relationships for clays are presented in *Design Manual for Permanent Ground Anchor Walls* (Weatherby, 1997).

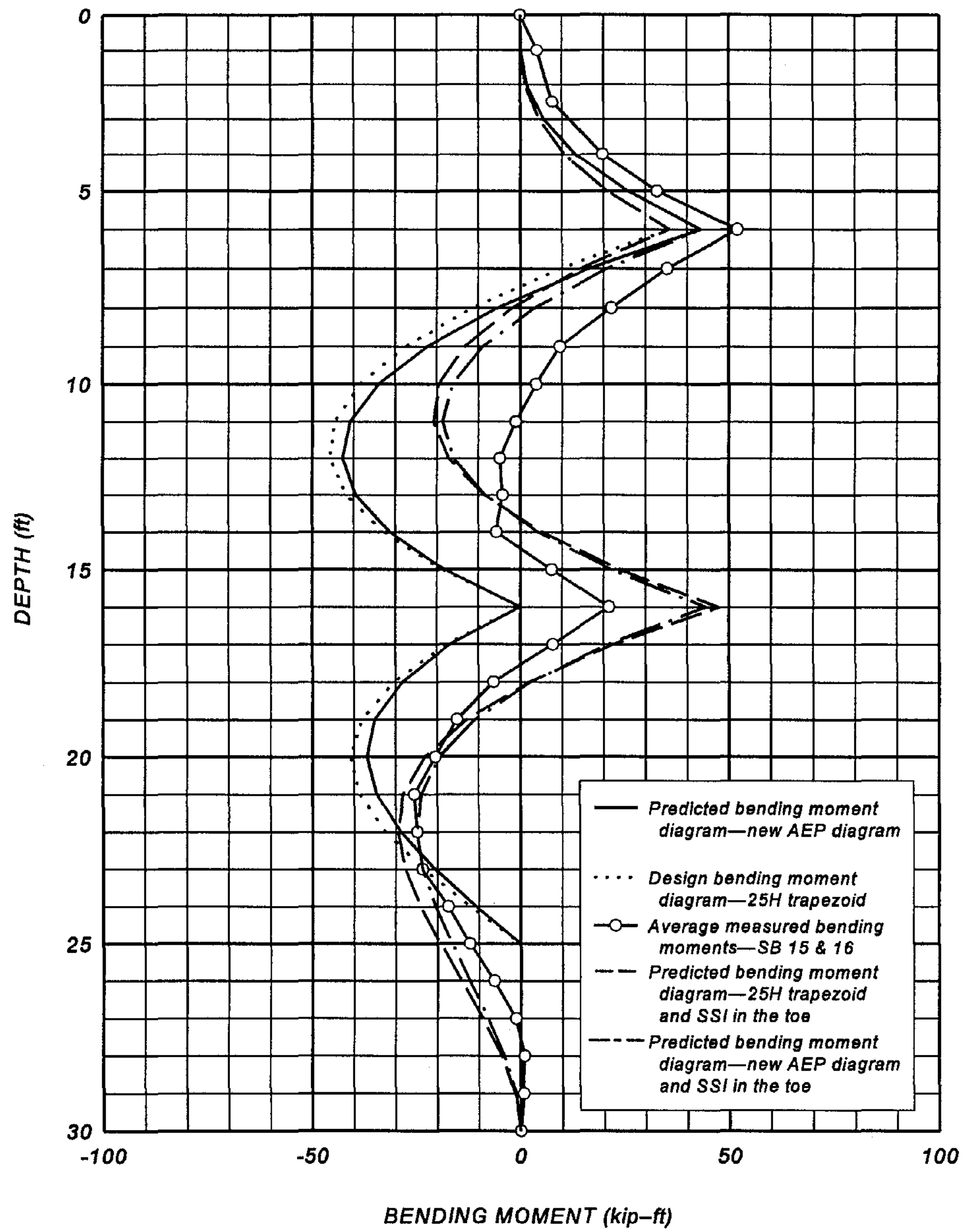

FIGURE 132
Comparison of Predicted Bending Moments Using Trapezoidal Apparent Earth Pressure (AEP) Diagrams and *R-y* Curves with Predicted Bending Moments Using Trapezoidal Apparent Earth Pressure (AEP) Diagrams Assuming a Hinge at the Bottom of the Excavation and the Average Measured Bending Moments in Soldier Beams 7 and 8

APPENDIX

Figures 133 through 142 show the bending moments, axial loads, inclinometer profiles, and settlement profiles for drilled-in Soldier Beams 13 and 14 at different construction stages. Soldier Beam 13 has Class A concrete in the toe and Soldier Beam 14 has lean-mix backfill in the toe. Soldier Beams 13 and 14 are in the one-tier wall section.

Figures 143 through 154 show the bending moments, axial loads, inclinometer profiles, and settlement profiles for driven Soldier Beams 15 and 16 at different construction stages. Soldier Beams 15 and 16 are in the one-tier wall section.

Figures 155 through 170 show the bending moments, axial loads, inclinometer profiles, and settlement profiles for driven Soldier Beams 7 and 8 at different construction stages. Soldier Beams 7 and 8 are in the two-tier wall section.

Figures 171 through 184 show the bending moments, axial loads, inclinometer profiles, and settlement profiles for drilled-in Soldier Beams 9 and 10 at different construction stages. Soldier Beam 9 has Class A concrete in the toe and Soldier Beam 10 has lean-mix backfill in the toe. Soldier Beams 9 and 10 are in the two-tier wall section.

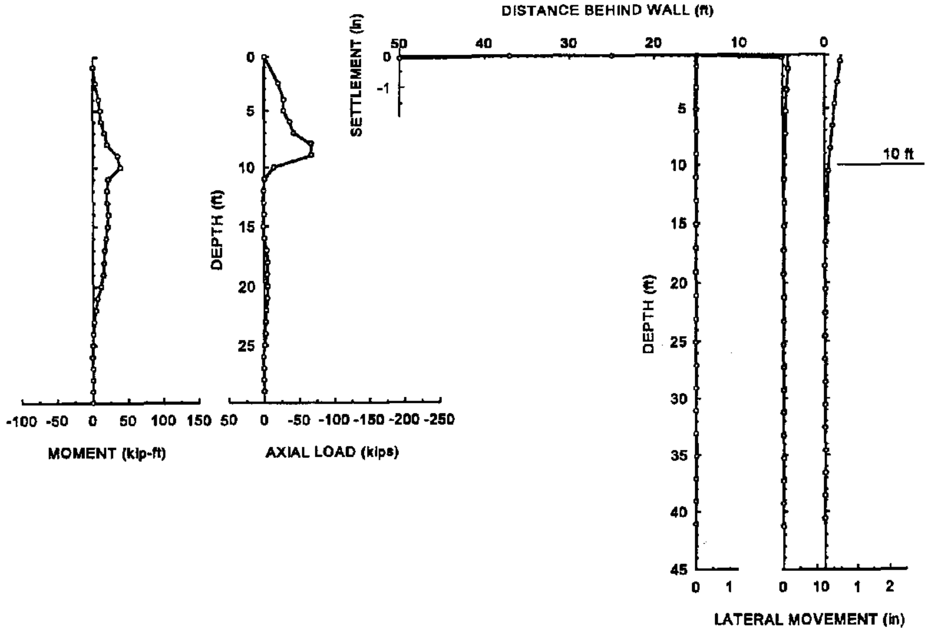

FIGURE 133
Bending Moments, Axial Loads, Lateral Movements, and Settlements: Drilled-in Soldier Beam No. 13; 10-ft Excavation – Day 96

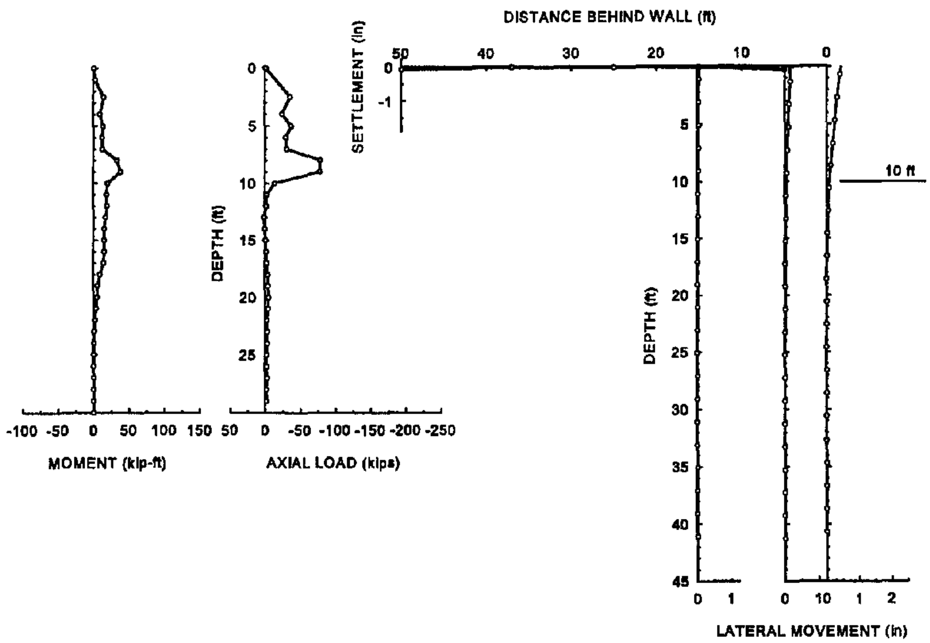

FIGURE 134
Bending Moments, Axial Loads, Lateral Movements, and Settlements: Drilled-in Soldier Beam No. 14; 10-ft Excavation – Day 96

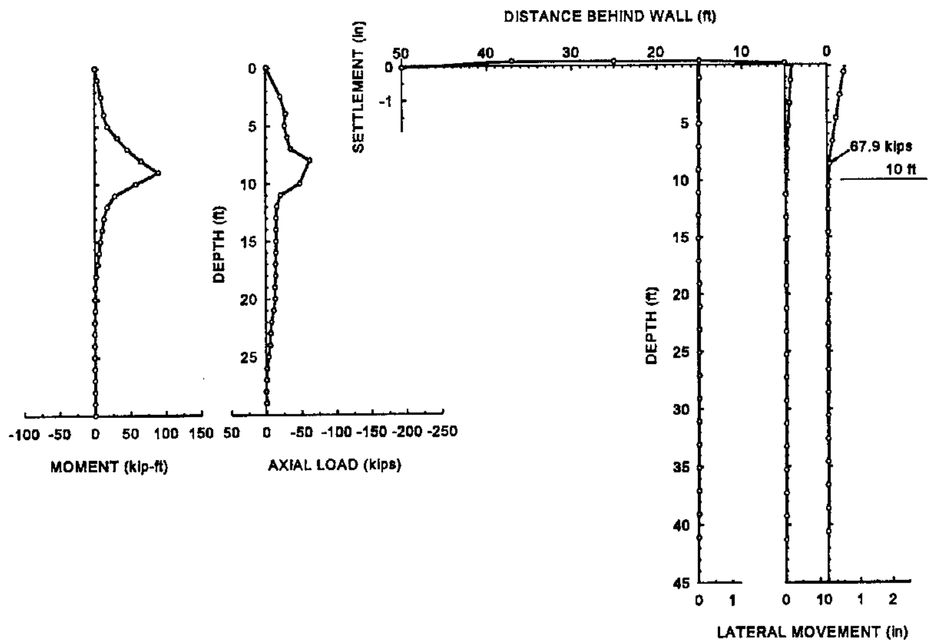

FIGURE 135
Bending Moments, Axial Loads, Lateral Movements, and Settlements: Drilled-in Soldier Beam No. 13; Stress Ground Anchor – Day 101

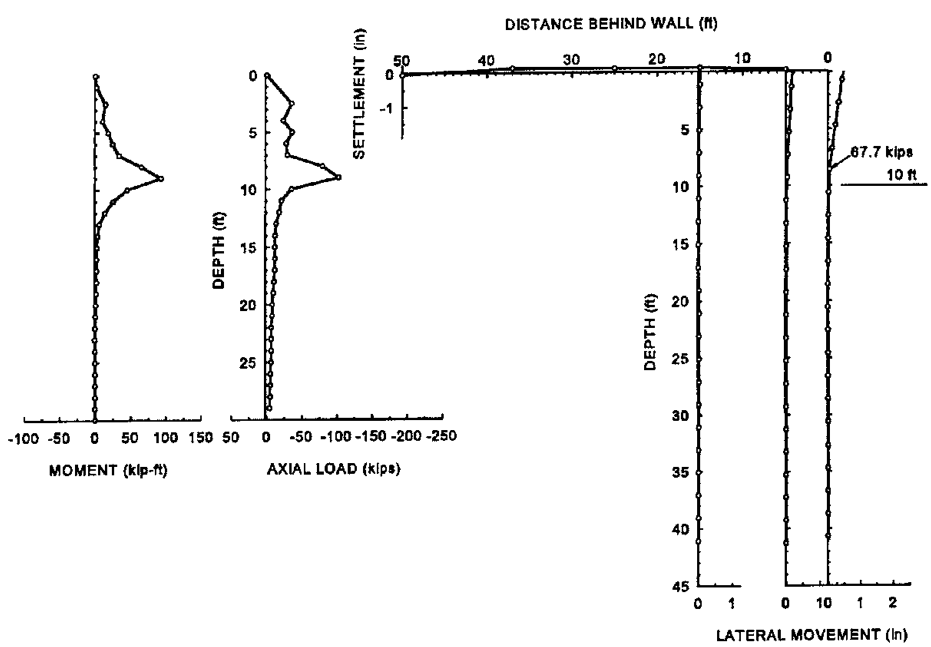

FIGURE 136
Bending Moments, Axial Loads, Lateral Movements, and Settlements: Drilled-in Soldier Beam No. 14; Stress Ground Anchor – Day 101

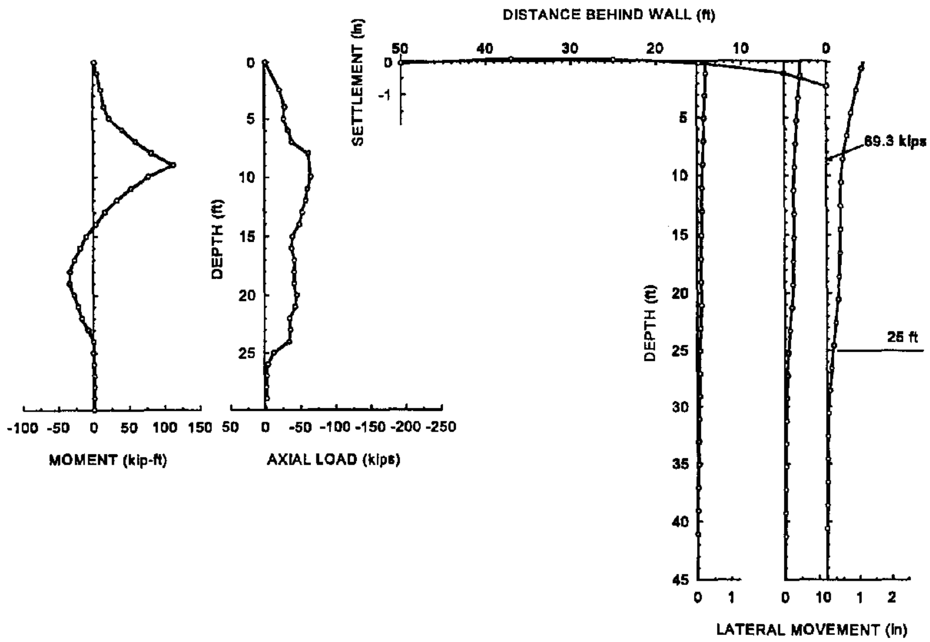

FIGURE 137
Bending Moments, Axial Loads, Lateral Movements, and Settlements: Drilled-in Soldier Beam No. 13; 25-ft Excavation – Day 122

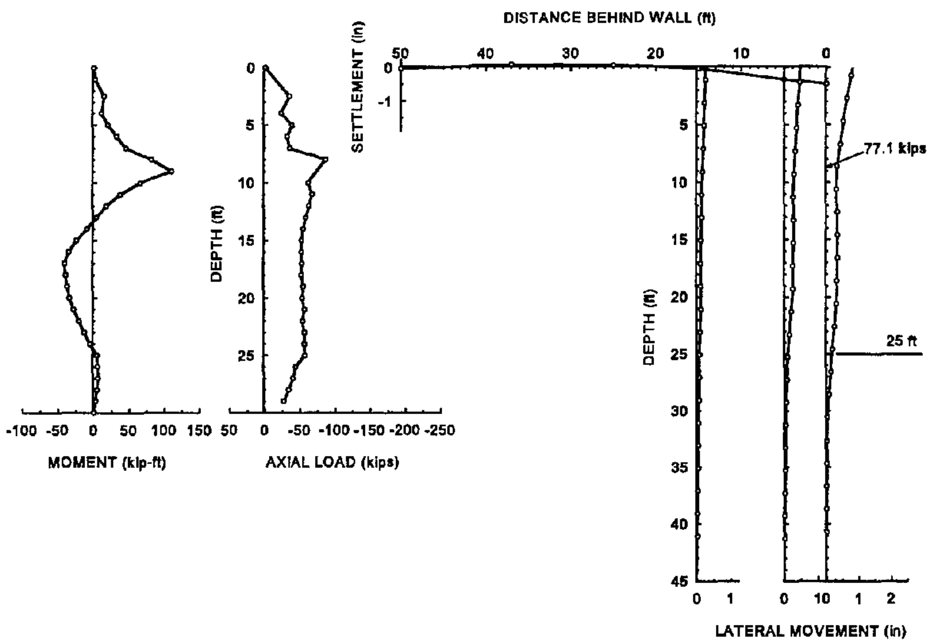

FIGURE 138
Bending Moments, Axial Loads, Lateral Movements, and Settlements: Drilled-in Soldier Beam No. 14; 25-ft Excavation – Day 122

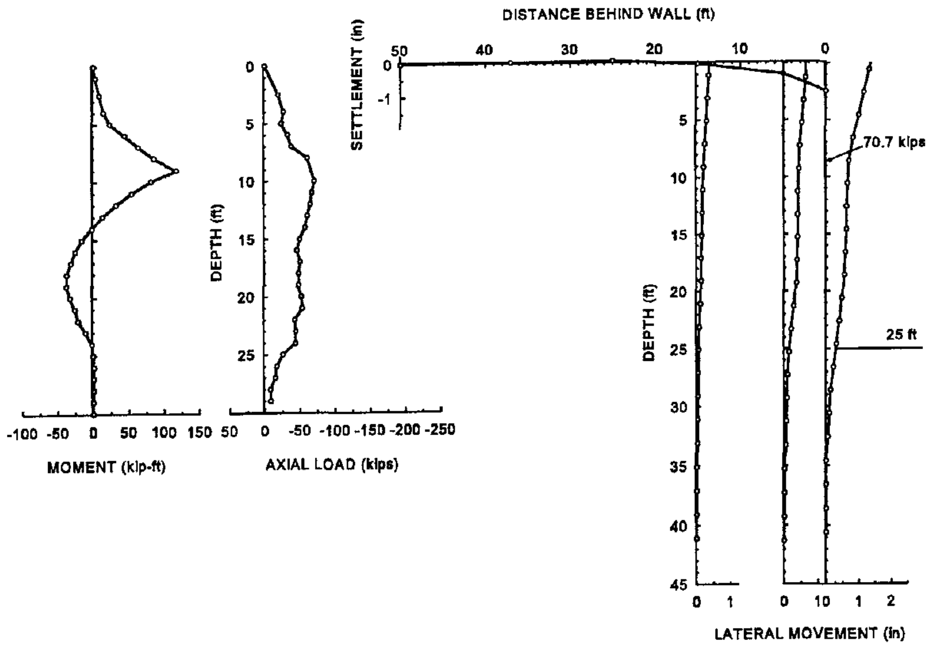

FIGURE 139
Bending Moments, Axial Loads, Lateral Movements, and Settlements: Drilled-in Soldier Beam No. 13; Long-term Reading – Day 206

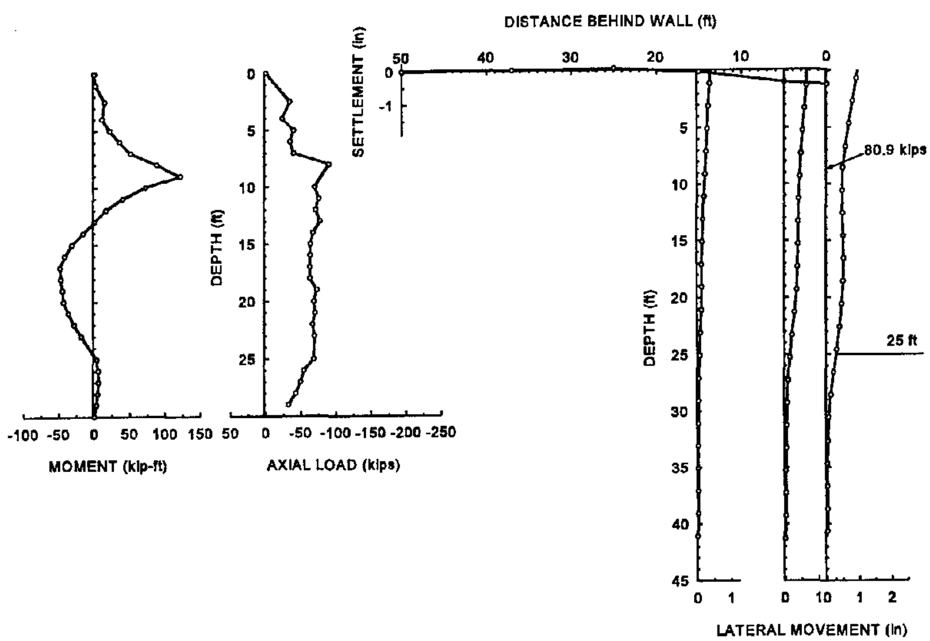

FIGURE 140
Bending Moments, Axial Loads, Lateral Movements, and Settlements: Drilled-in Soldier Beam No. 14; Long-term Reading – Day 206

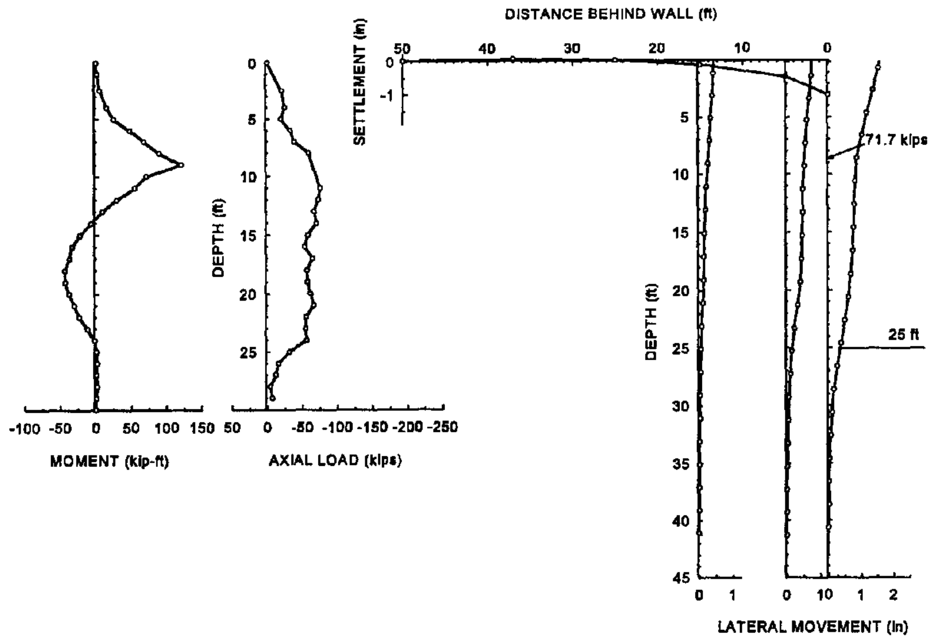

FIGURE 141
Bending Moments, Axial Loads, Lateral Movements, and Settlements: Drilled-in Soldier Beam No. 13; Final Reading – Day 573

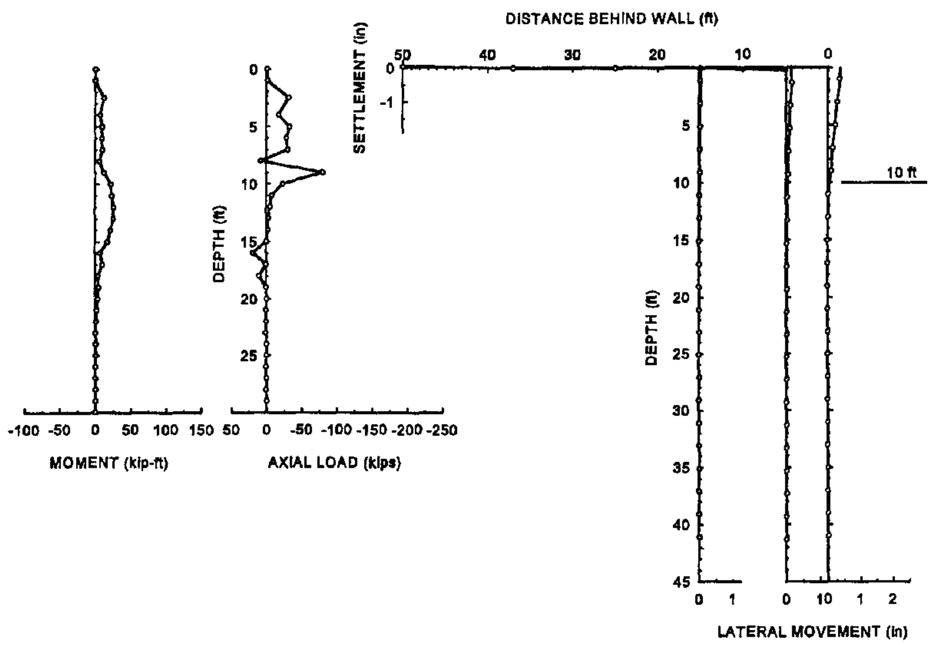

FIGURE 142
Bending Moments, Axial Loads, Lateral Movements, and Settlements: Drilled-in Soldier Beam No. 14; Final Reading – Day 573

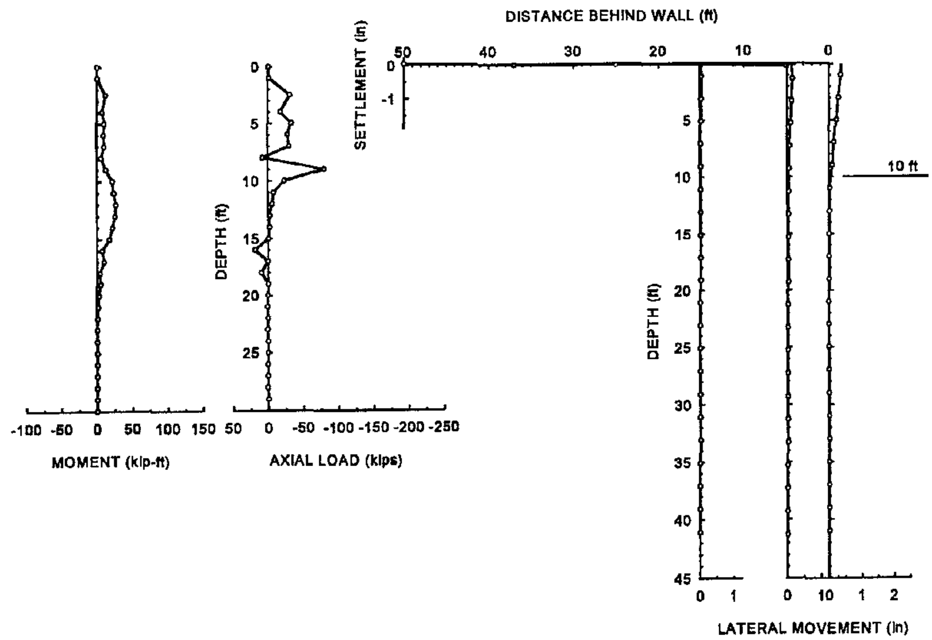

FIGURE 143
Bending Moments, Axial Loads, Lateral Movements, and Settlements: Driven Soldier Beam No. 15; 10-ft Excavation – Day 96

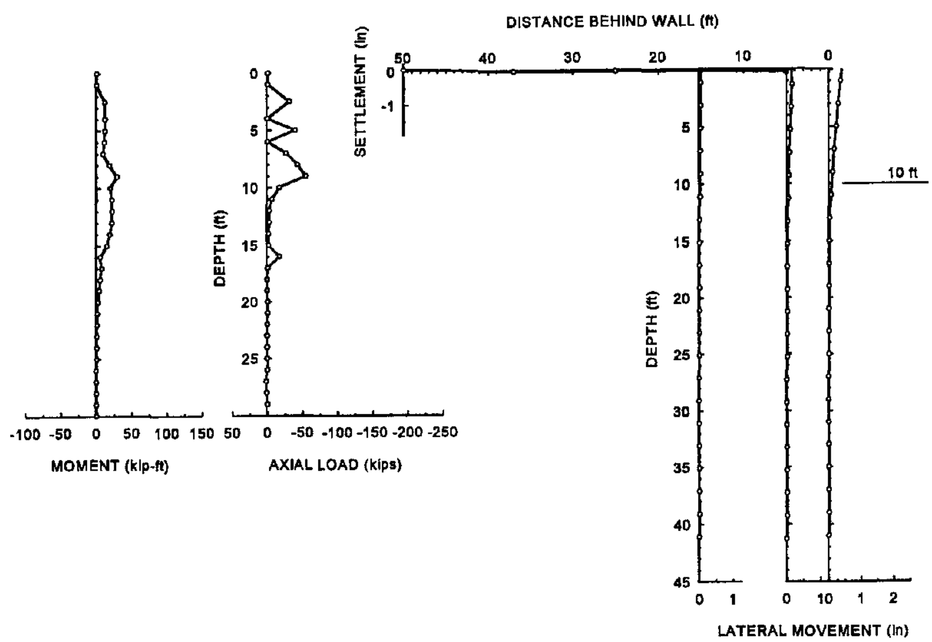

FIGURE 144
Bending Moments, Axial Loads, Lateral Movements, and Settlements: Driven Soldier Beam No. 16; 10-ft Excavation – Day 96

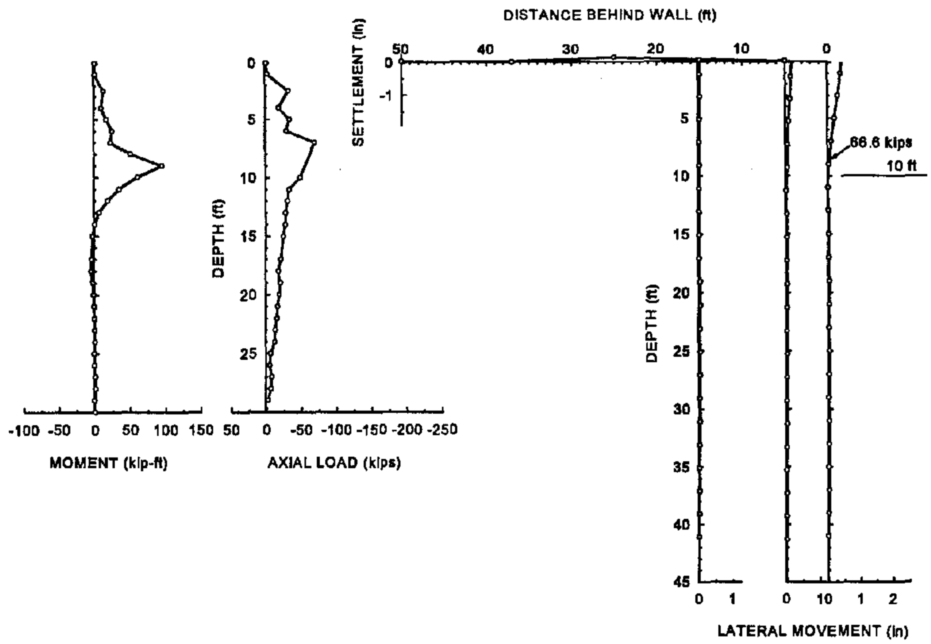

FIGURE 145
Bending Moments, Axial Loads, Lateral Movements, and Settlements: Driven Soldier Beam No. 15; Stress Ground Anchor – Day 101

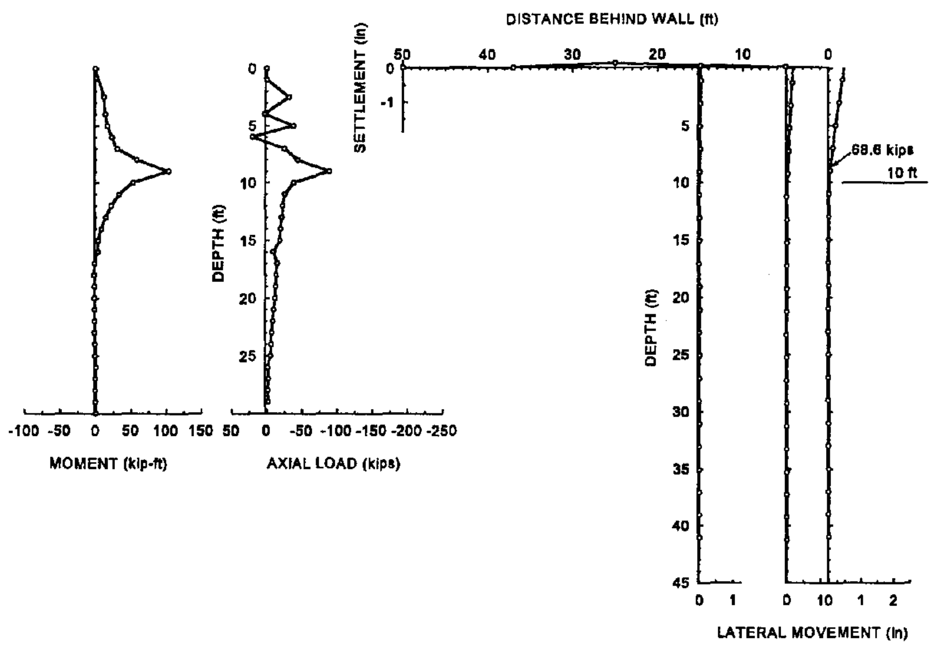

FIGURE 146
Bending Moments, Axial Loads, Lateral Movements, and Settlements: Driven Soldier Beam No. 16; Stress Ground Anchor – Day 101

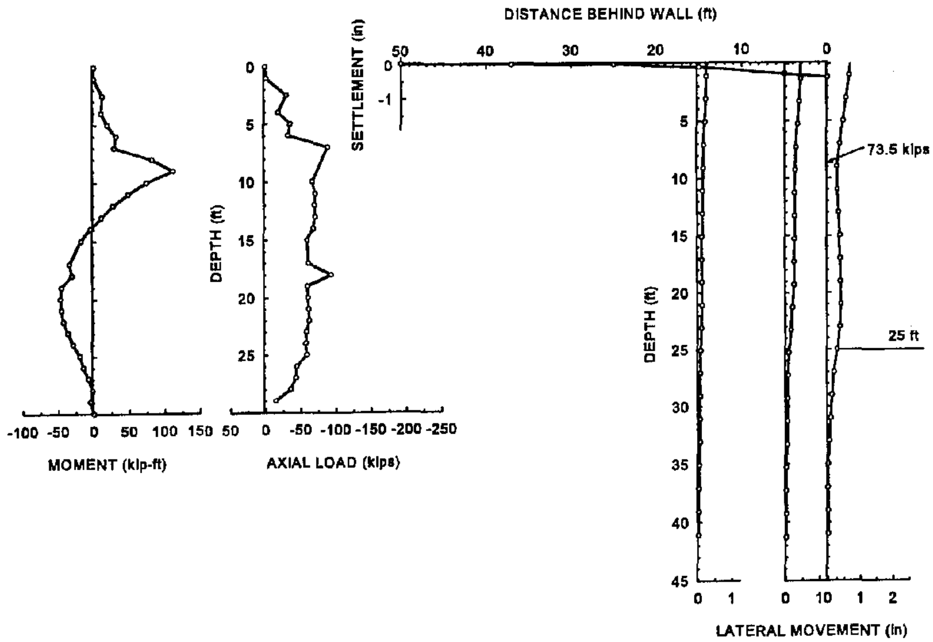

FIGURE 147
Bending Moments, Axial Loads, Lateral Movements, and Settlements: Driven Soldier Beam No. 15; 25-ft Excavation – Day 122

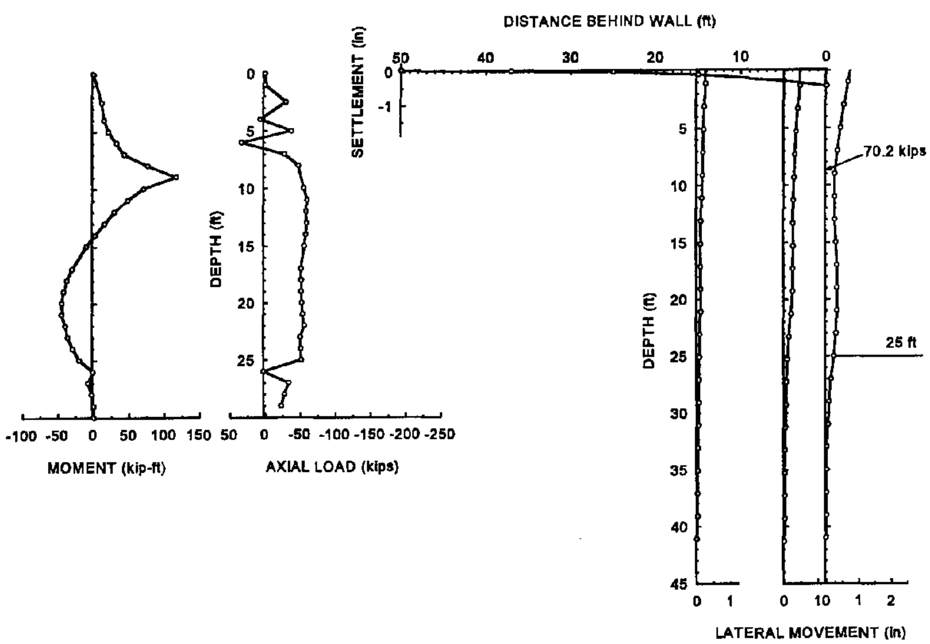

FIGURE 148
Bending Moments, Axial Loads, Lateral Movements, and Settlements: Driven Soldier Beam No. 16; 25-ft Excavation – Day 122

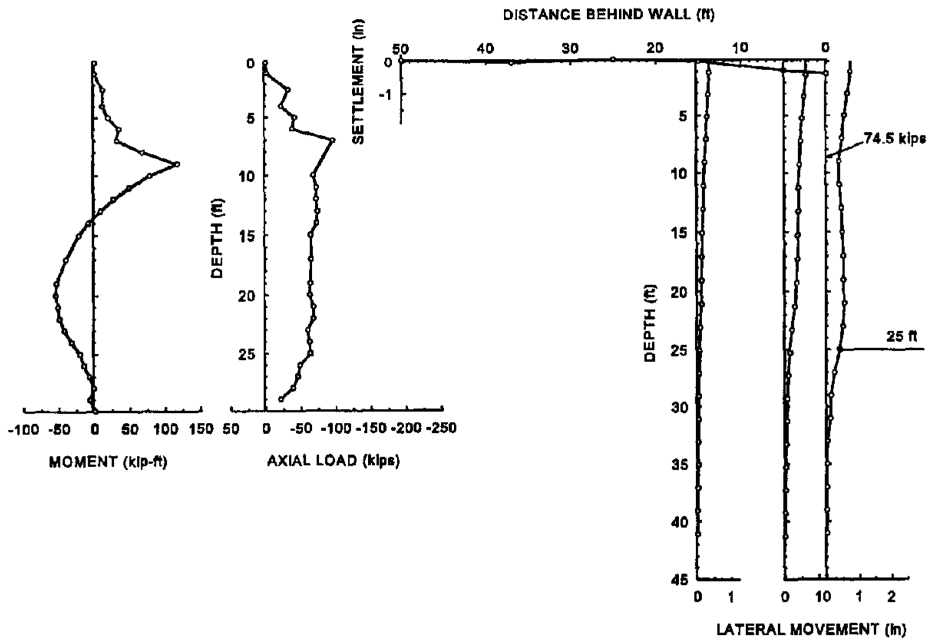

FIGURE 149
Bending Moments, Axial Loads, Lateral Movements, and Settlements: Driven Soldier Beam No. 15; Long-term Reading – Day 206

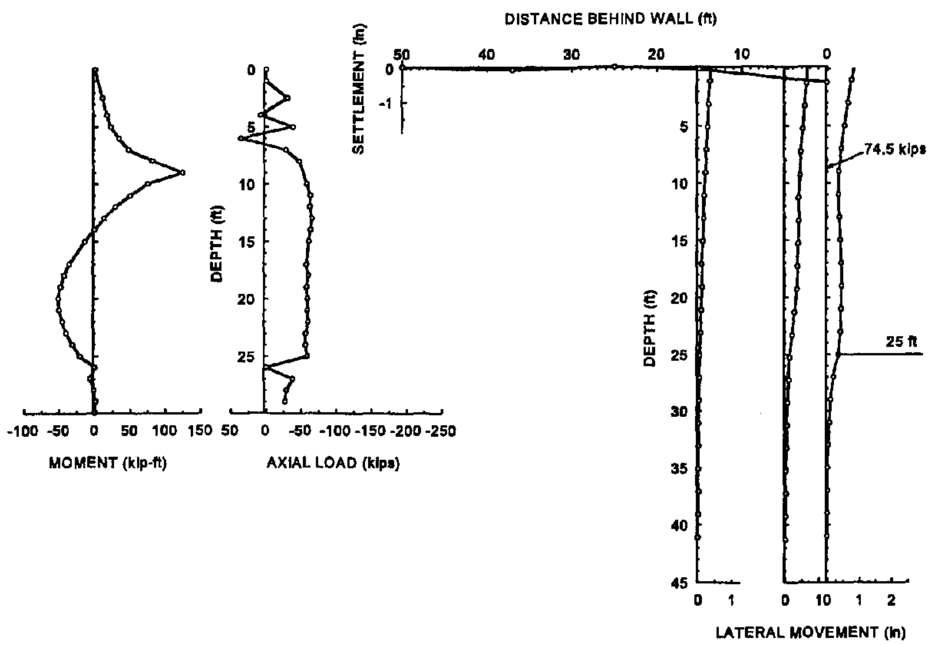

FIGURE 150
Bending Moments, Axial Loads, Lateral Movements, and Settlements: Driven Soldier Beam No. 16; Long-term Reading – Day 206

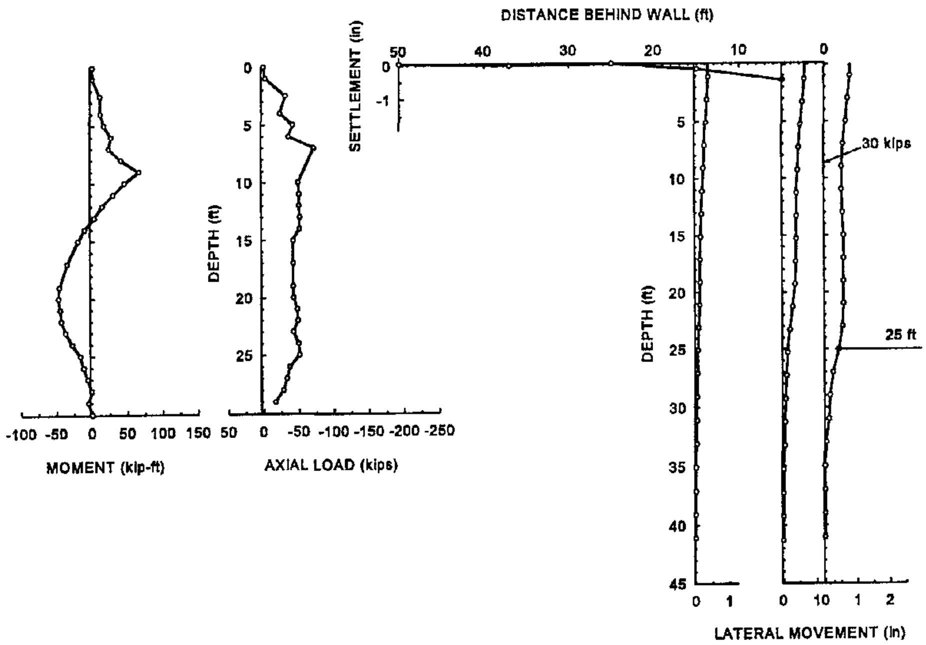

FIGURE 151
Bending Moments, Axial Loads, Lateral Movements, and Settlements: Driven Soldier Beam No. 15; Ground Anchor Load Reduced – Day 226

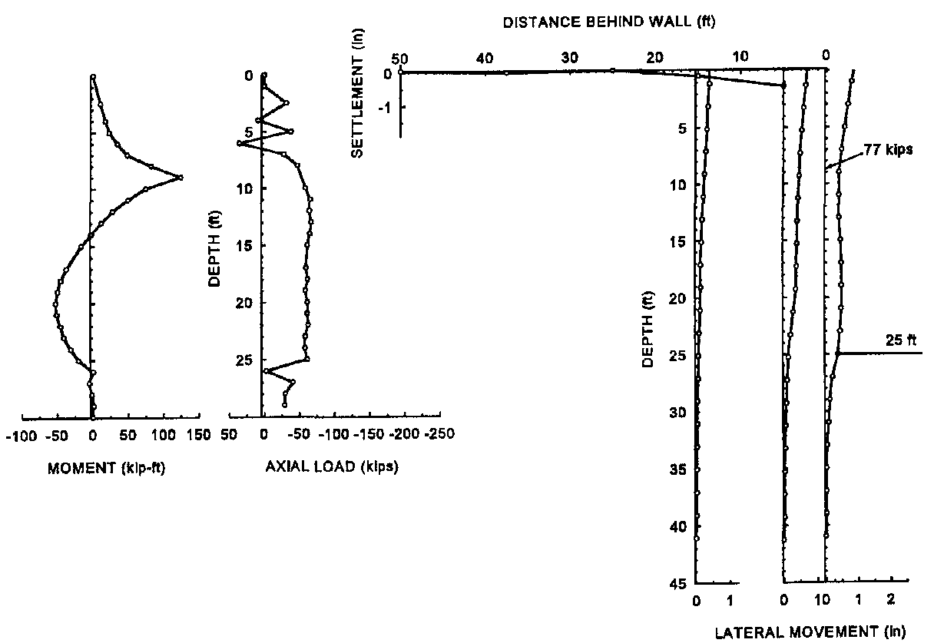

FIGURE 152
Bending Moments, Axial Loads, Lateral Movements, and Settlements: Driven Soldier Beam No. 16; Load Reduced on Ground Anchor Supporting Soldier Beam No. 15 – Day 226

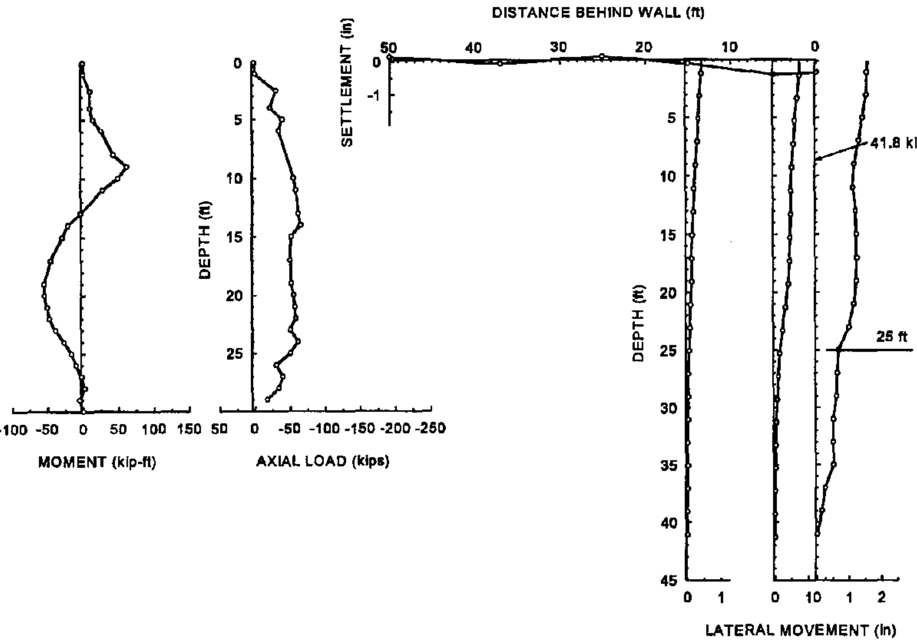

FIGURE 153
Bending Moments, Axial Loads, Lateral Movements, and Settlements: Driven Soldier Beam No. 15; Final Reading After Ground Anchor Load Reduced – Day 573

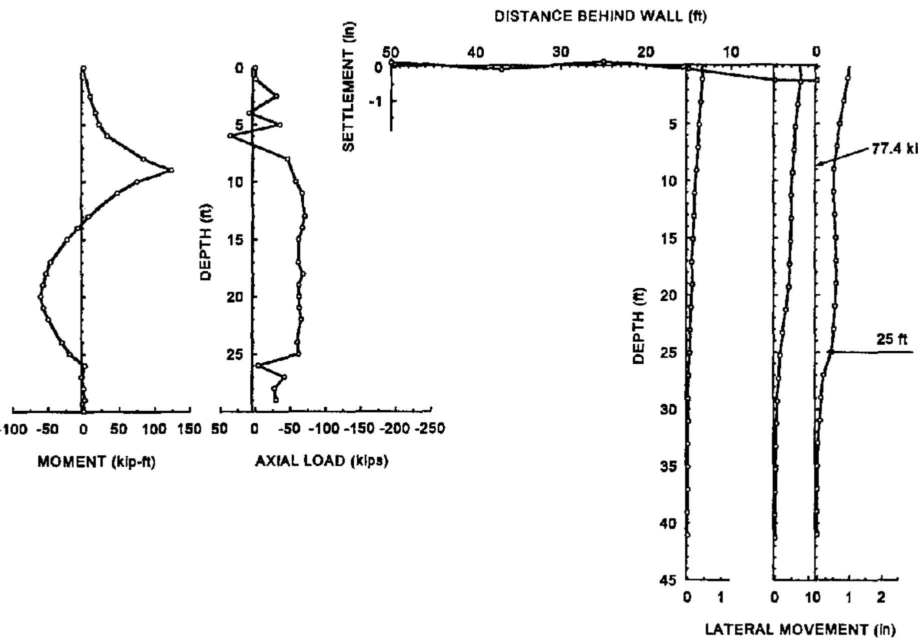

FIGURE 154
Bending Moments, Axial Loads, Lateral Movements, and Settlements: Driven Soldier Beam No. 16; Final Reading After Ground Anchor Load Reduced – Day 573

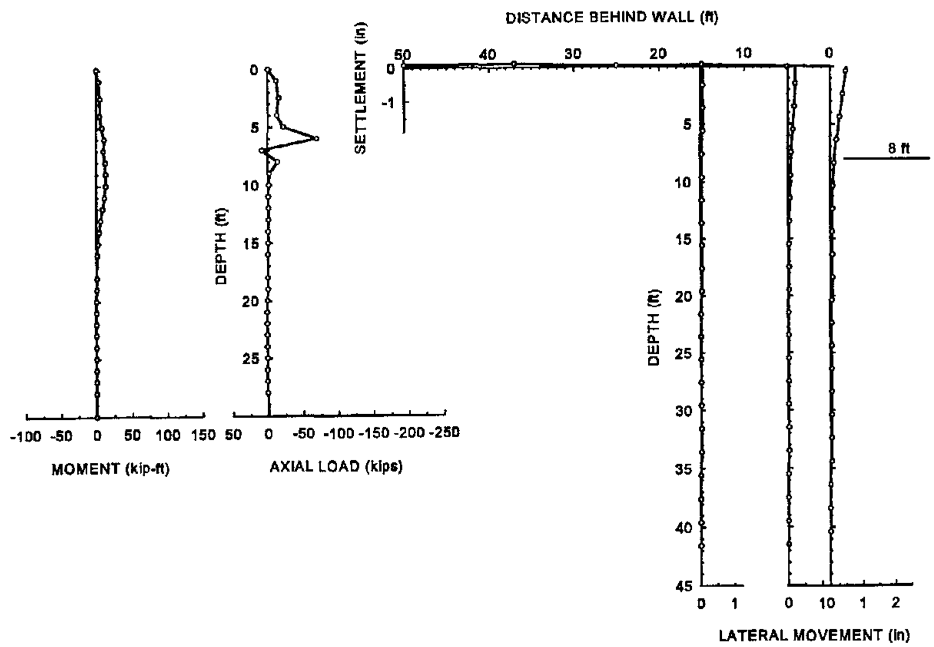

FIGURE 155
Bending Moments, Axial Loads, Lateral Movements, and Settlements: Driven Soldier Beam No. 7; 8-ft Excavation – Day 86

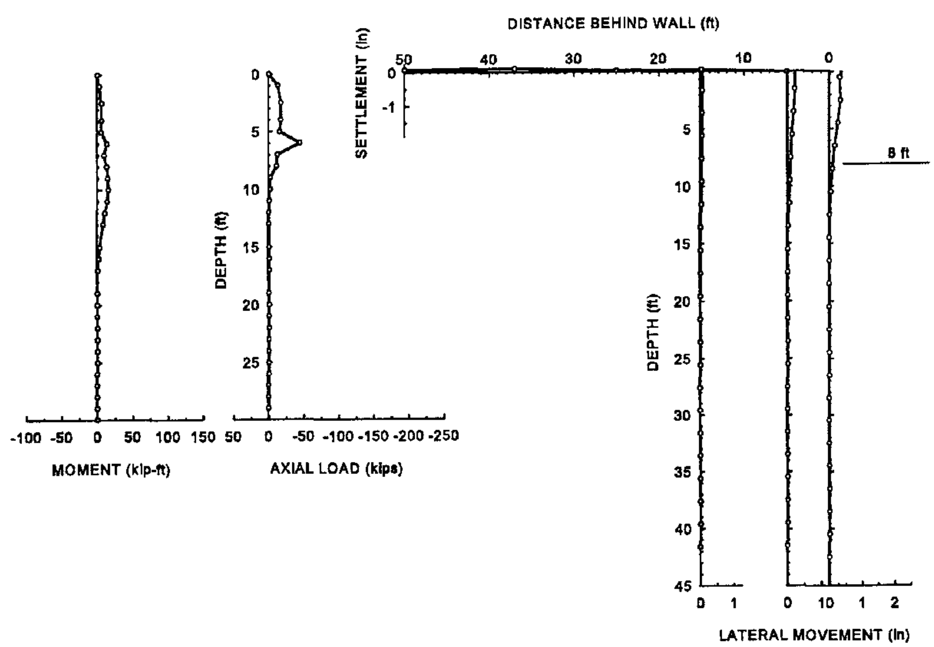

FIGURE 156
Bending Moments, Axial Loads, Lateral Movements, and Settlements: Driven Soldier Beam No. 8; 8-ft Excavation – Day 86

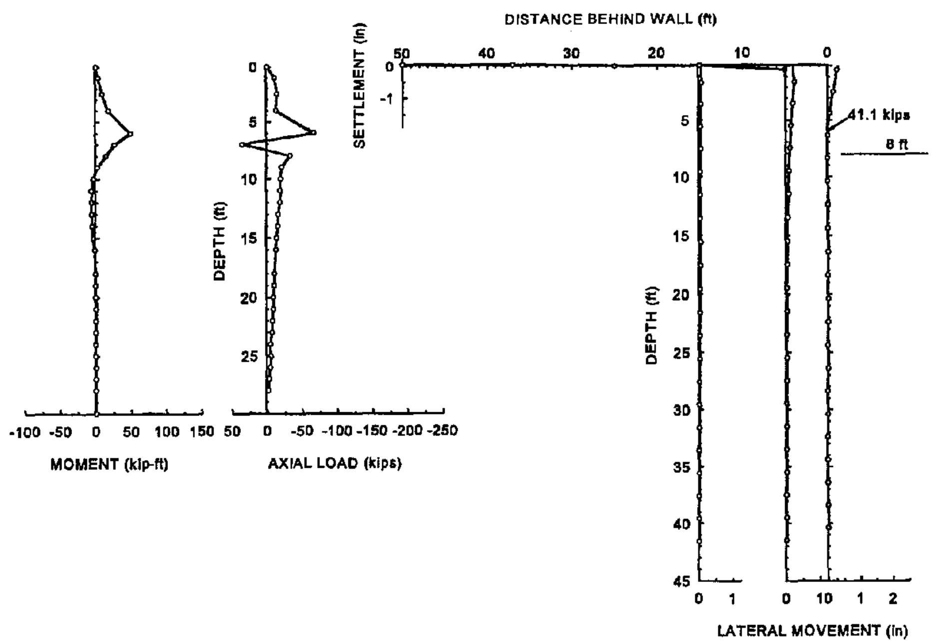

FIGURE 157
Bending Moments, Axial Loads, Lateral Movements, and Settlements: Driven Soldier Beam No. 7; Stress Upper Ground Anchor – Day 95

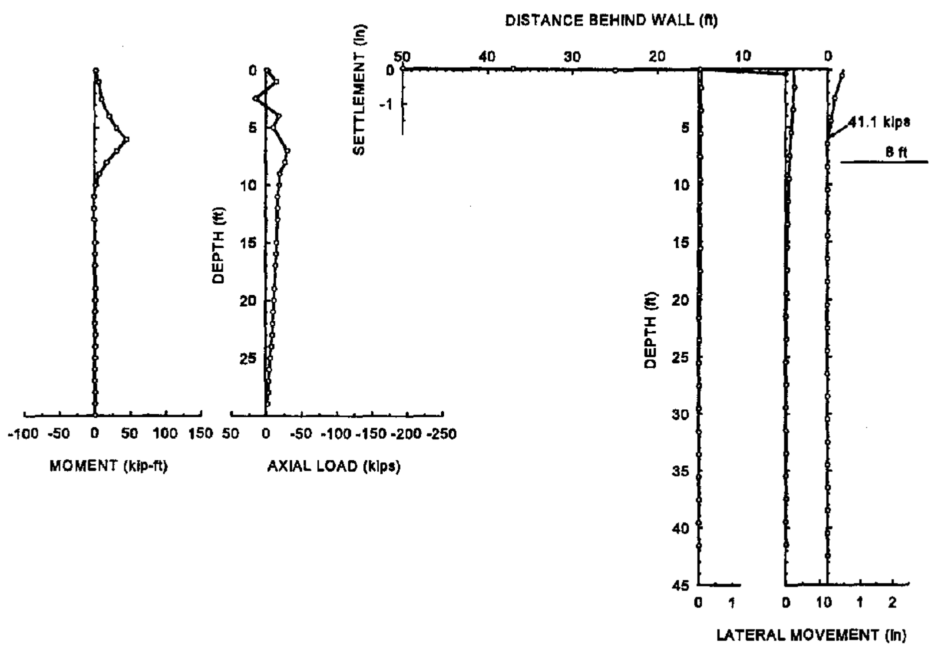

FIGURE 158
Bending Moments, Axial Loads, Lateral Movements, and Settlements: Driven Soldier Beam No. 8; Stress Upper Ground Anchor – Day 95

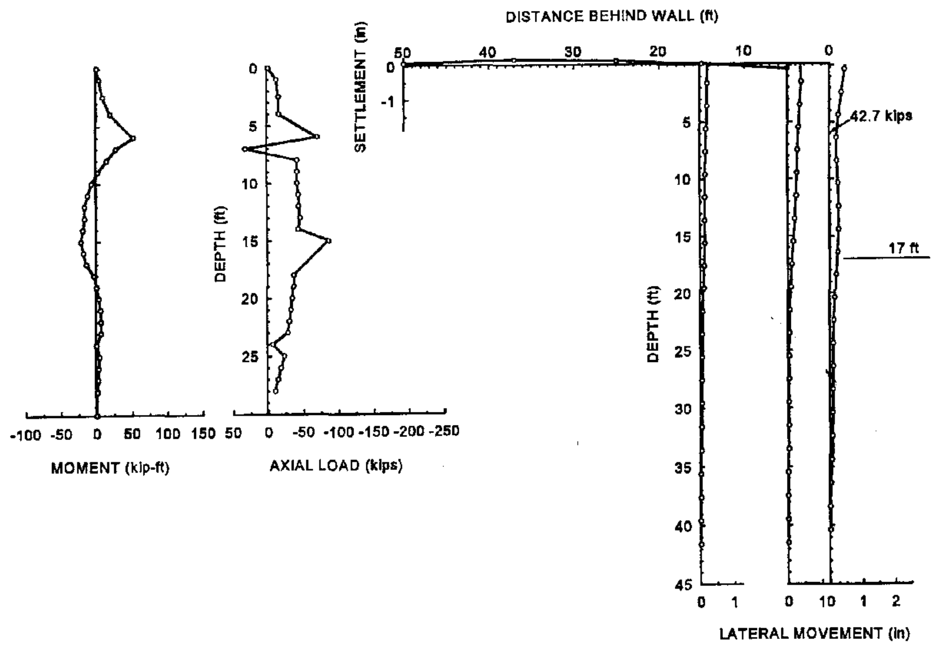

FIGURE 159
Bending Moments, Axial Loads, Lateral Movements, and Settlements: Driven Soldier Beam No. 7; 17-ft Excavation – Day 108

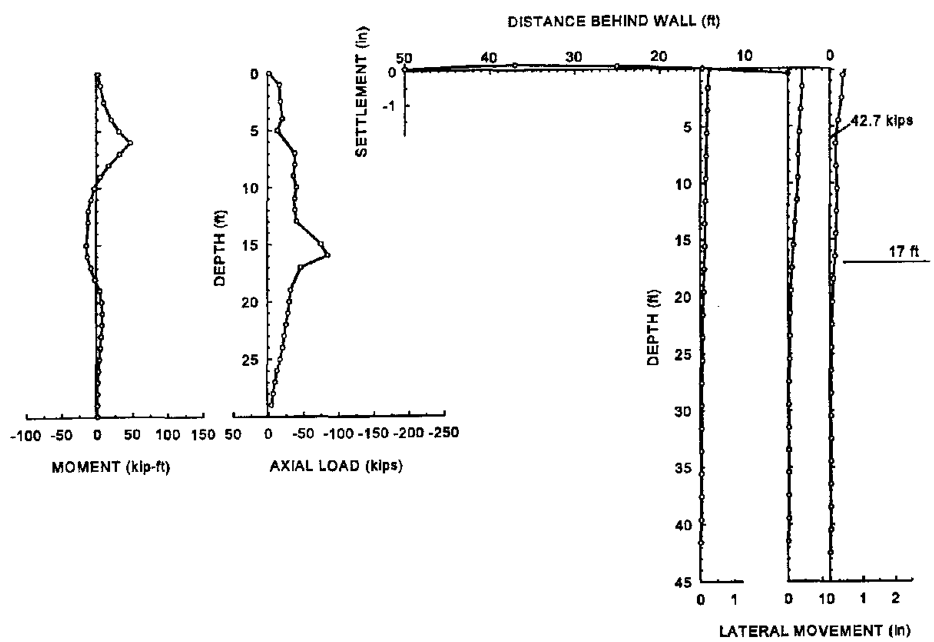

FIGURE 160
Bending Moments, Axial Loads, Lateral Movements, and Settlements: Driven Soldier Beam No. 8; 17-ft Excavation – Day 108

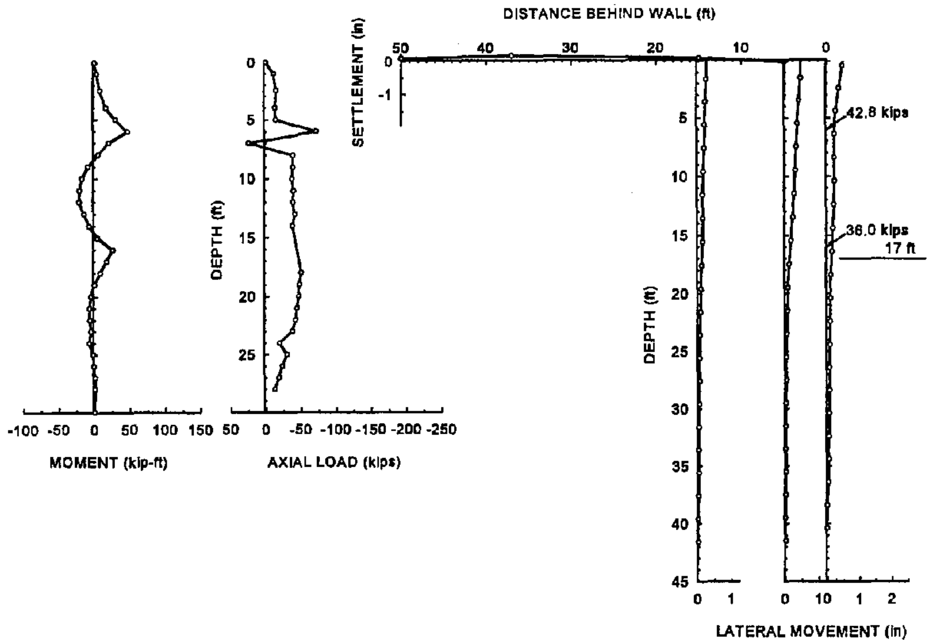

FIGURE 161
Bending Moments, Axial Loads, Lateral Movements, and Settlements: Driven Soldier Beam No. 7; Stress Lower Ground Anchor – Day 114

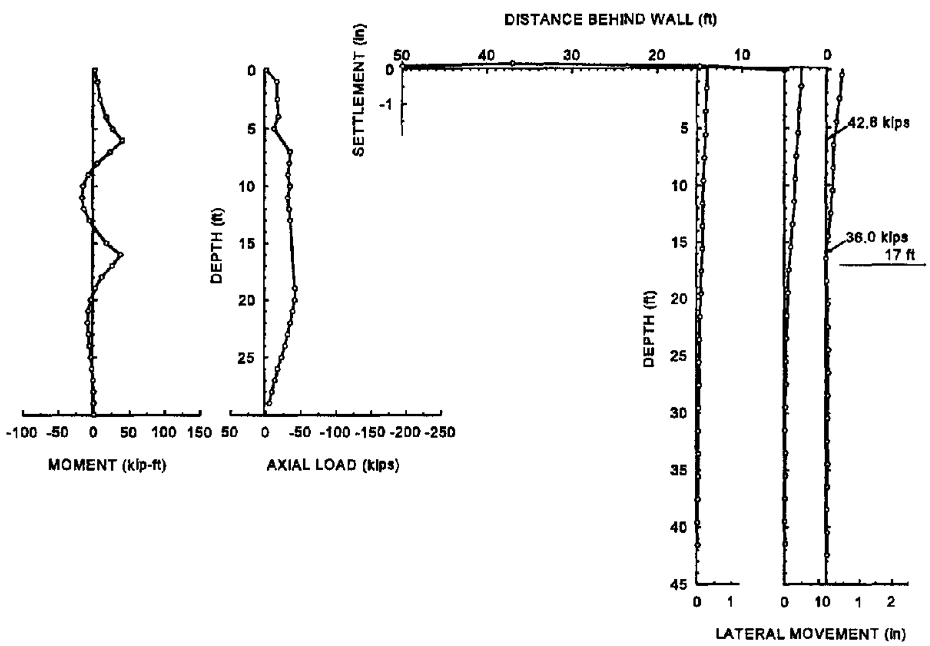

FIGURE 162
Bending Moments, Axial Loads, Lateral Movements, and Settlements: Driven Soldier Beam No. 8; Stress Lower Ground Anchor – Day 114

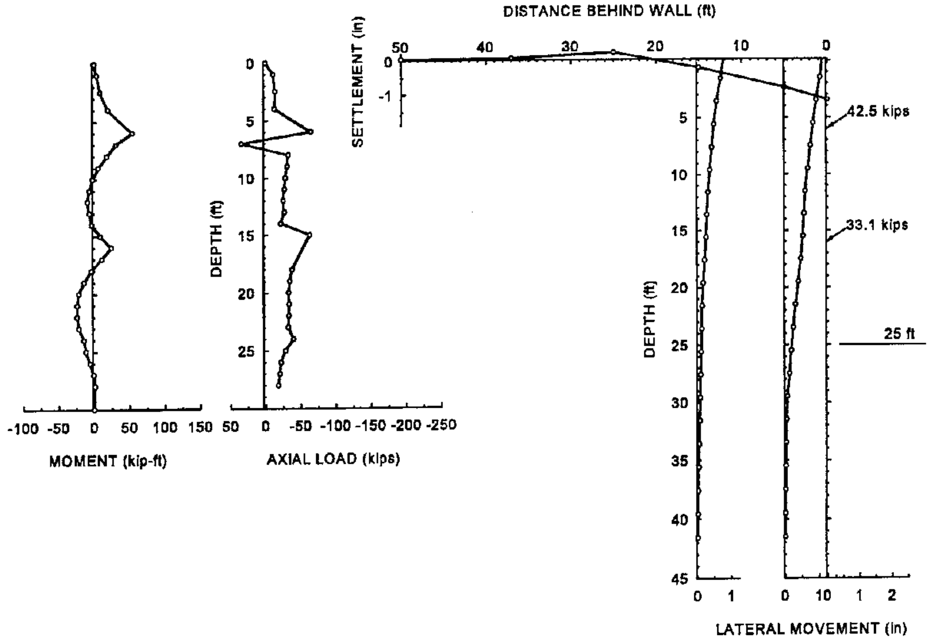

FIGURE 163
Bending Moments, Axial Loads, Lateral Movements, and Settlements: Driven Soldier Beam No. 7; 25-ft Excavation – Day 122

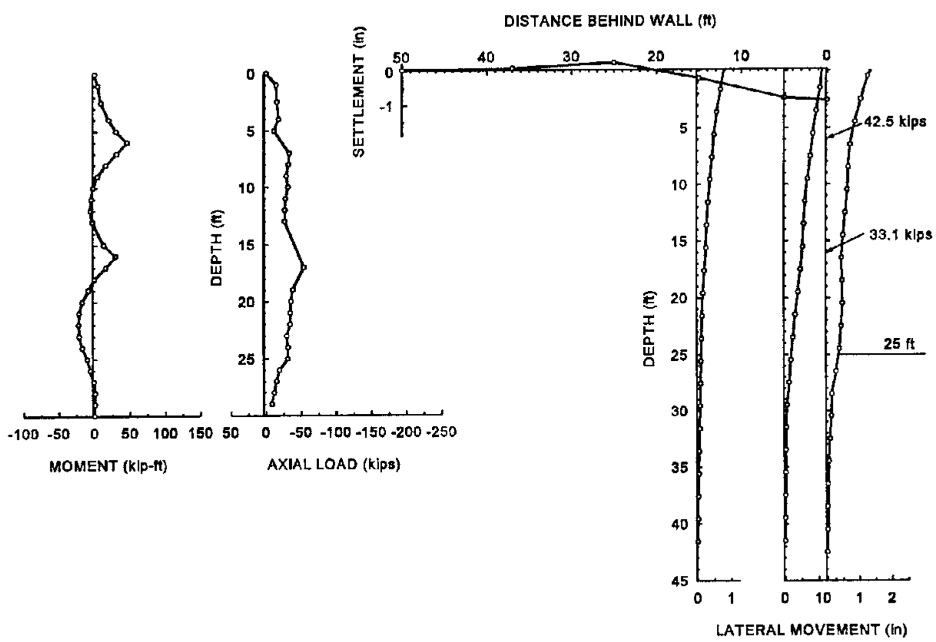

FIGURE 164
Bending Moments, Axial Loads, Lateral Movements, and Settlements: Driven Soldier Beam No. 8; 25-ft Excavation – Day 122

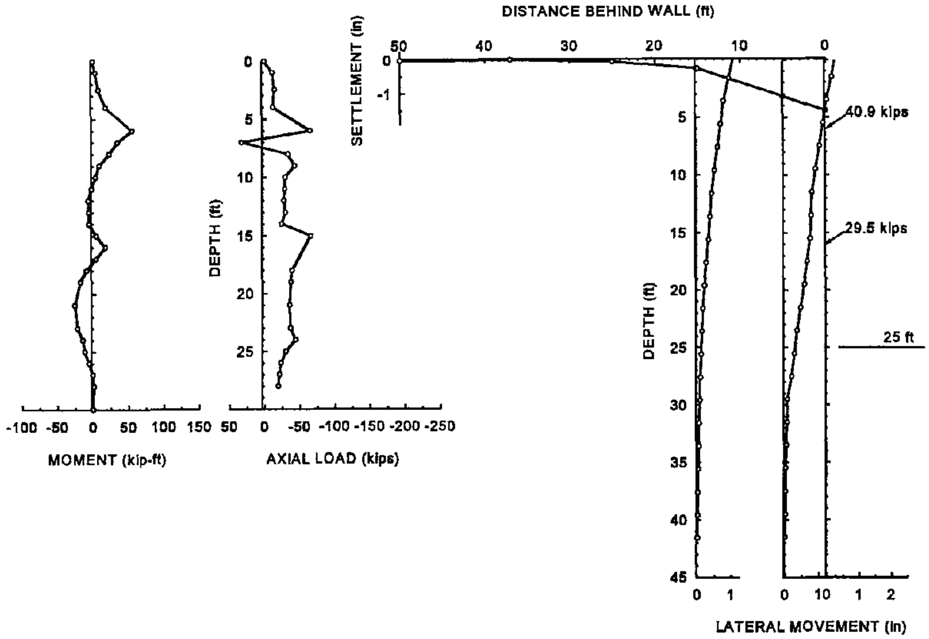

FIGURE 165
Bending Moments, Axial Loads, Lateral Movements, and Settlements: Driven Soldier Beam No. 7; Long-term Reading – Day 206

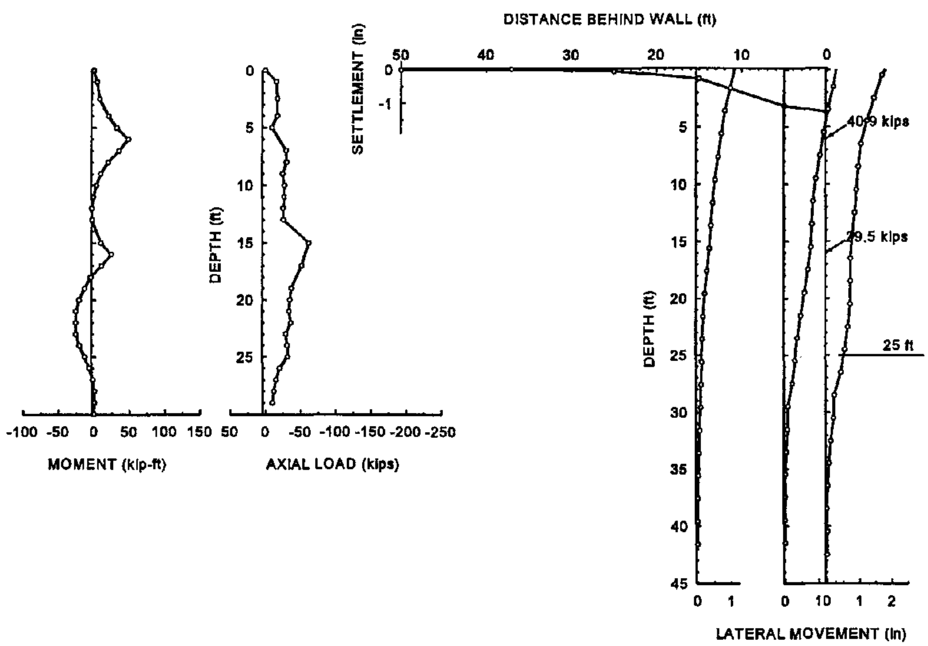

FIGURE 166
Bending Moments, Axial Loads, Lateral Movements, and Settlements: Driven Soldier Beam No. 8; Long-term Reading – Day 206

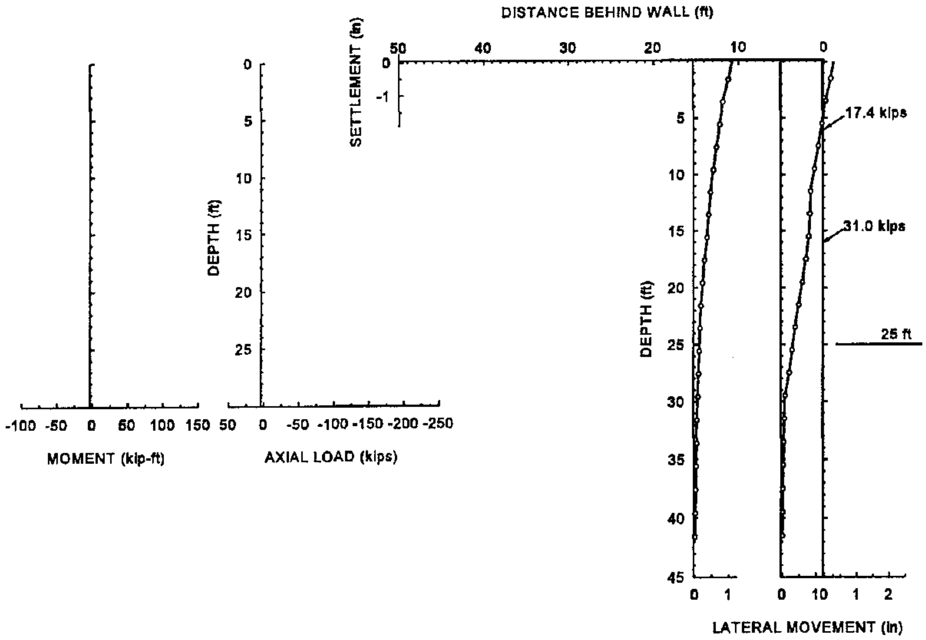

FIGURE 167
Bending Moments, Axial Loads, Lateral Movements, and Settlements: Driven Soldier Beam No. 7; Upper Ground Anchor Load Reduced – Day 226

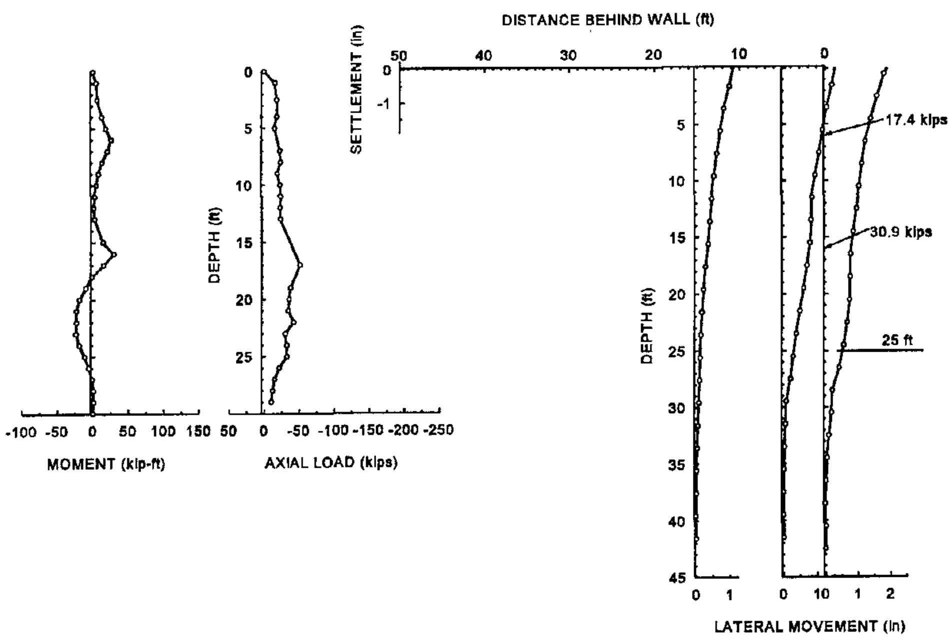

FIGURE 168
Bending Moments, Axial Loads, Lateral Movements, and Settlements: Driven Soldier Beam No. 8; Upper Ground Anchor Load Reduced – Day 226

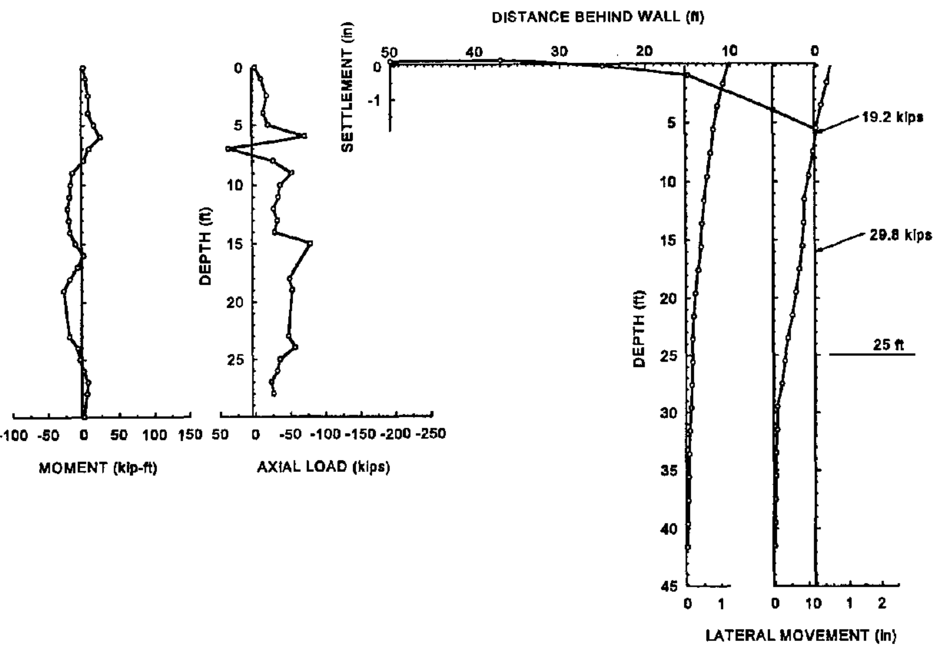

FIGURE 169
Bending Moments, Axial Loads, Lateral Movements, and Settlements: Driven Soldier Beam No. 7; Final Reading After Upper Ground Anchor Load Reduced; Day 573

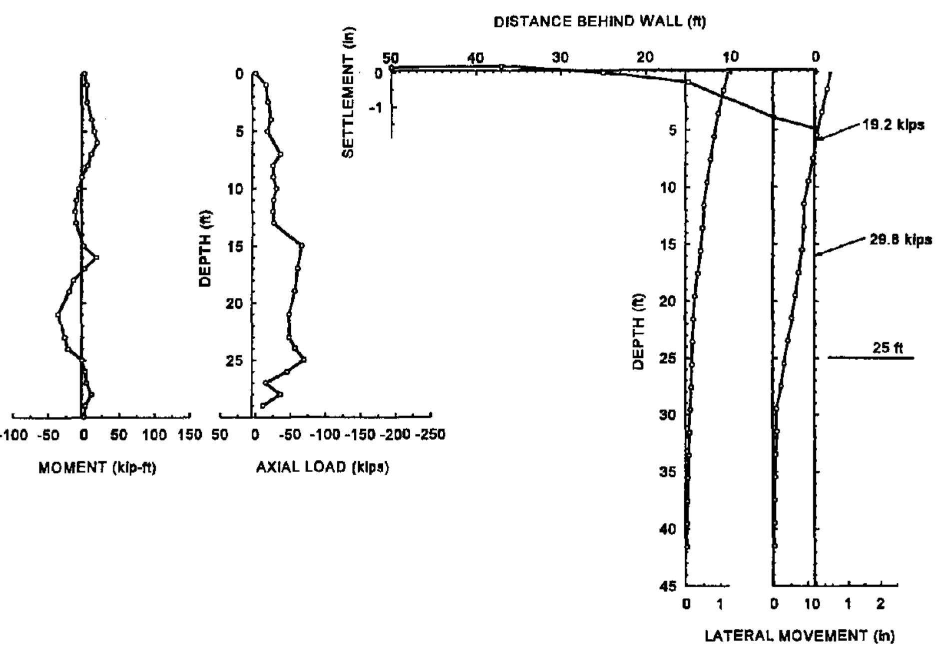

FIGURE 170
Bending Moments, Axial Loads, Lateral Movements, and Settlements: Driven Soldier Beam No. 8; Final Reading After Upper Ground Anchor Load Reduced; Day 573

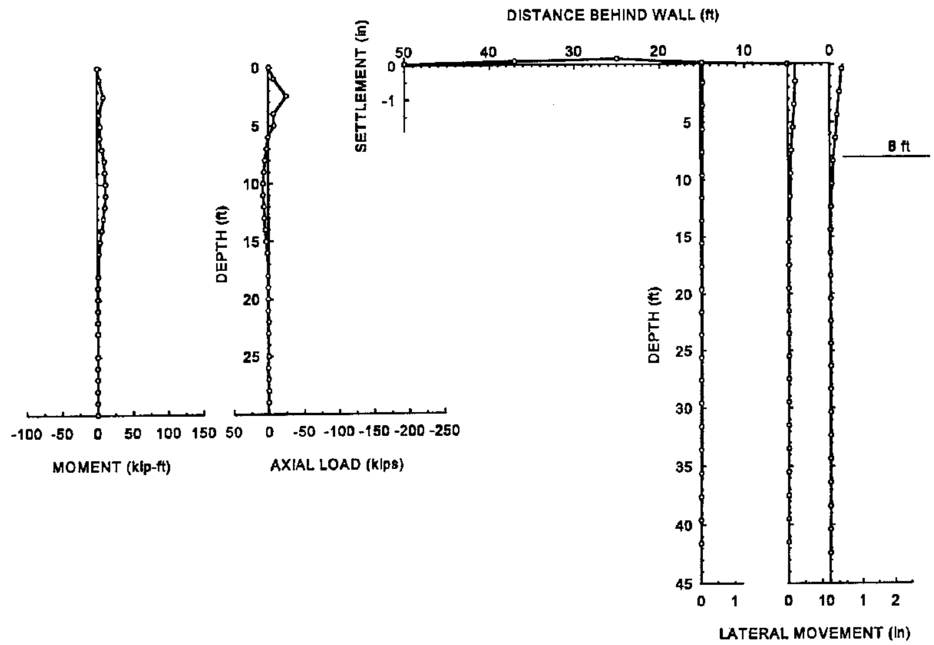

FIGURE 171
Bending Moments, Axial Loads, Lateral Movements, and Settlements: Drilled-in Soldier Beam No. 9; 8-ft Excavation – Day 86

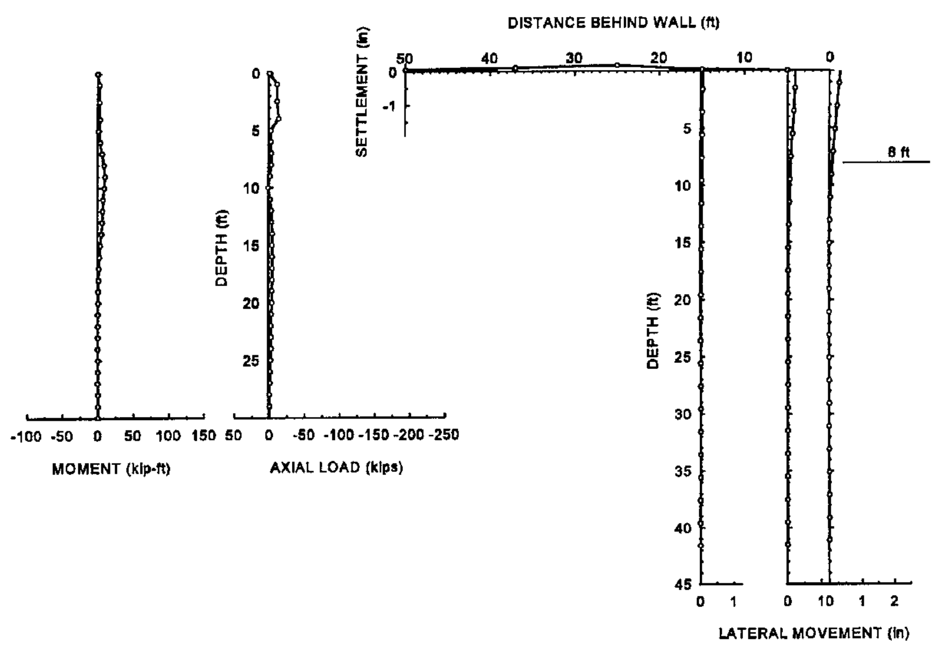

FIGURE 172
Bending Moments, Axial Loads, Lateral Movements, and Settlements: Drilled-in Soldier Beam No. 10; 8-ft Excavation – Day 86

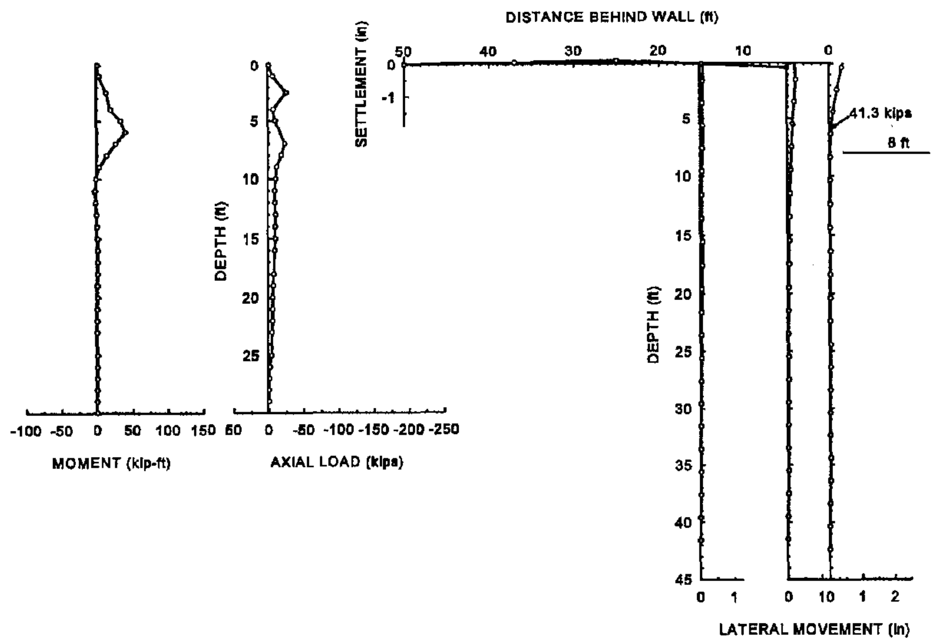

FIGURE 173
Bending Moments, Axial Loads, Lateral Movements, and Settlements: Drilled-in Soldier Beam No. 9; Stress Upper Ground Anchor – Day 95

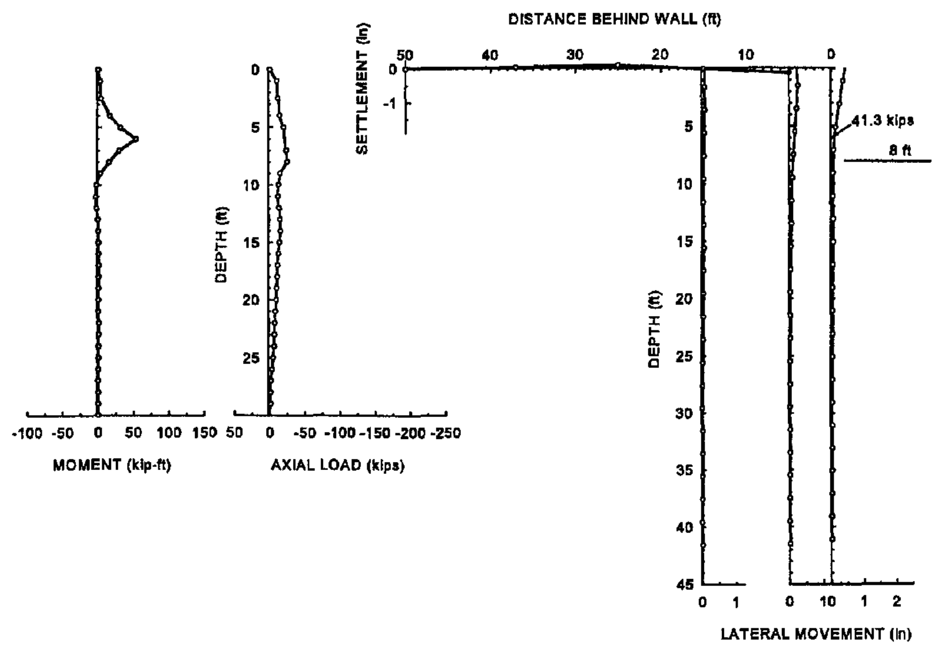

FIGURE 174
Bending Moments, Axial Loads, Lateral Movements, and Settlements: Drilled-in Soldier Beam No. 10; Stress Upper Ground Anchor – Day 95

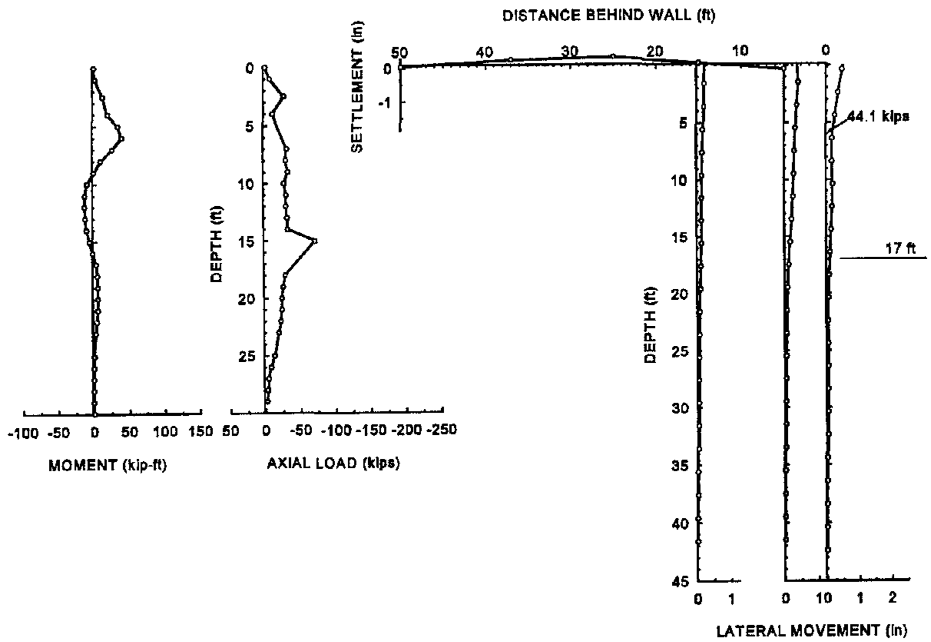

FIGURE 175
Bending Moments, Axial Loads, Lateral Movements, and Settlements: Drilled-in Soldier Beam No. 9; 17-ft Excavation – Day 108

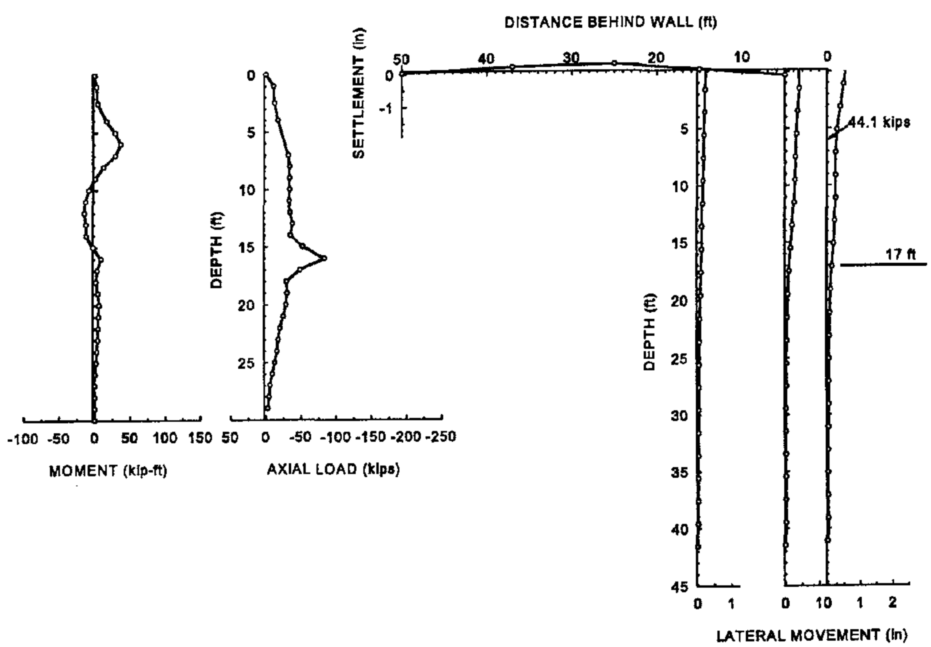

FIGURE 176
Bending Moments, Axial Loads, Lateral Movements, and Settlements: Drilled-in Soldier Beam No. 10; 17-ft Excavation – Day 108

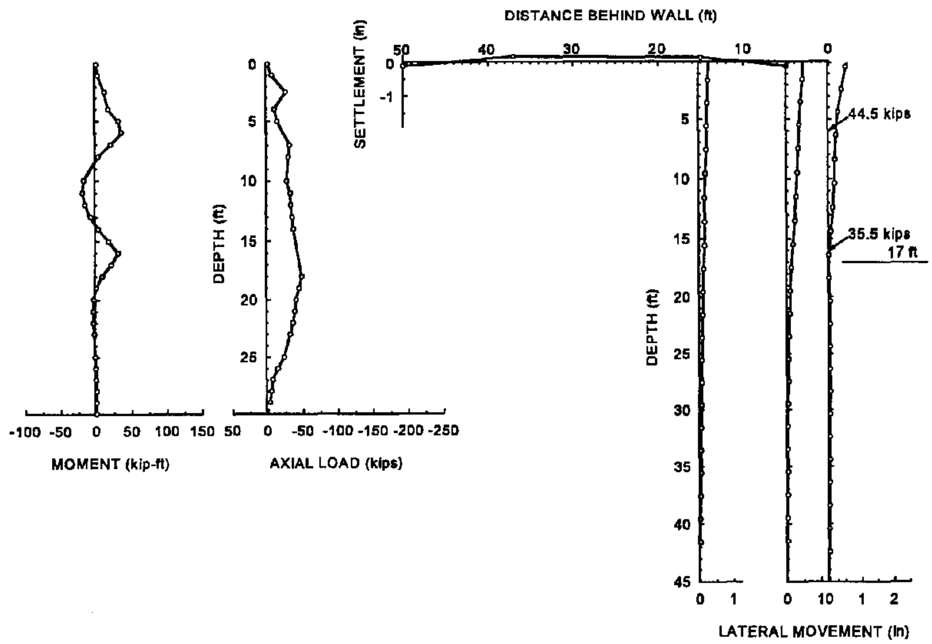

FIGURE 177
Bending Moments, Axial Loads, Lateral Movements, and Settlements: Drilled-in Soldier Beam No. 9; Stress Lower Ground Anchor – Day 114

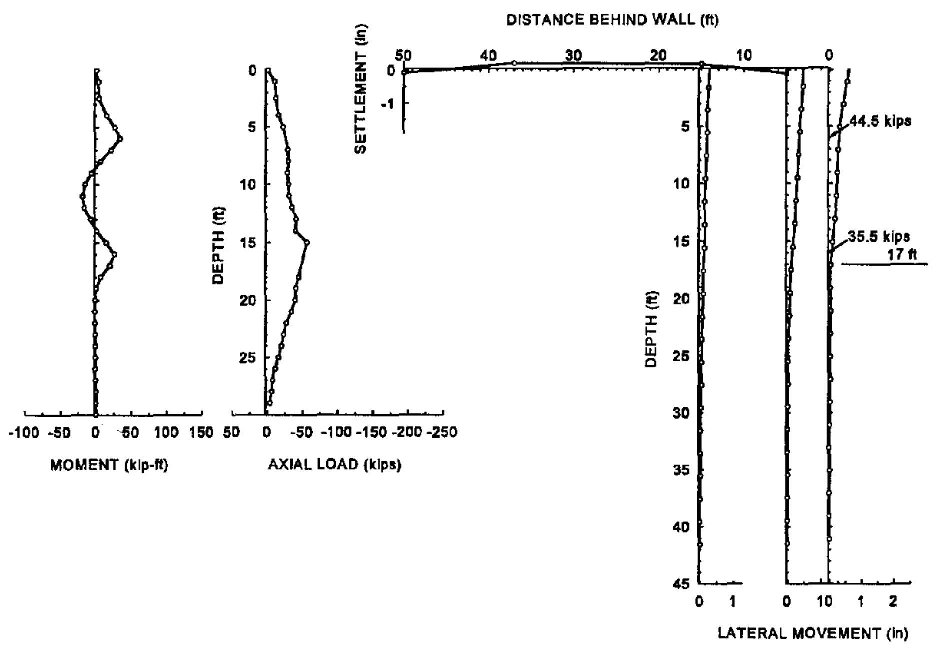

FIGURE 178
Bending Moments, Axial Loads, Lateral Movements, and Settlements: Drilled-in Soldier Beam No. 10; Stress Lower Ground Anchor – Day 114

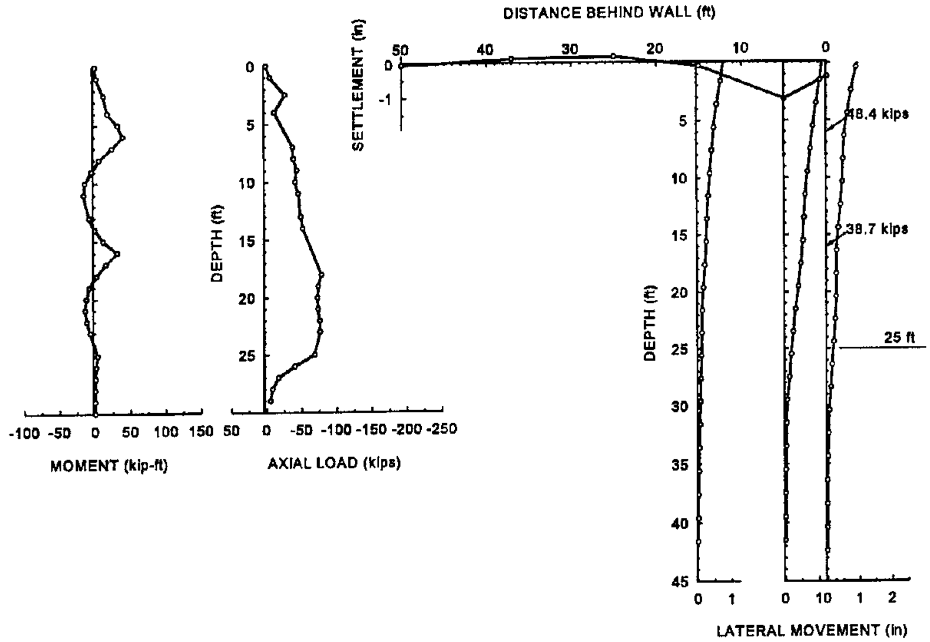

FIGURE 180
Bending Moments, Axial Loads, Lateral Movements, and Settlements: Drilled-in Soldier Beam No. 9; 25-ft Excavation – Day 122

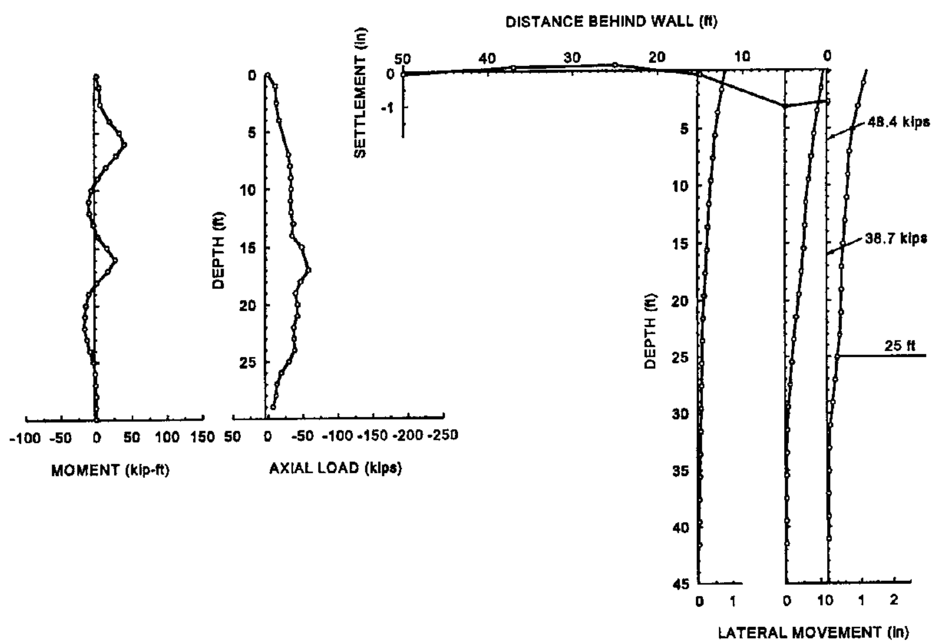

FIGURE 180
Bending Moments, Axial Loads, Lateral Movements, and Settlements: Drilled-in Soldier Beam No. 10; 25-ft Excavation – Day 122

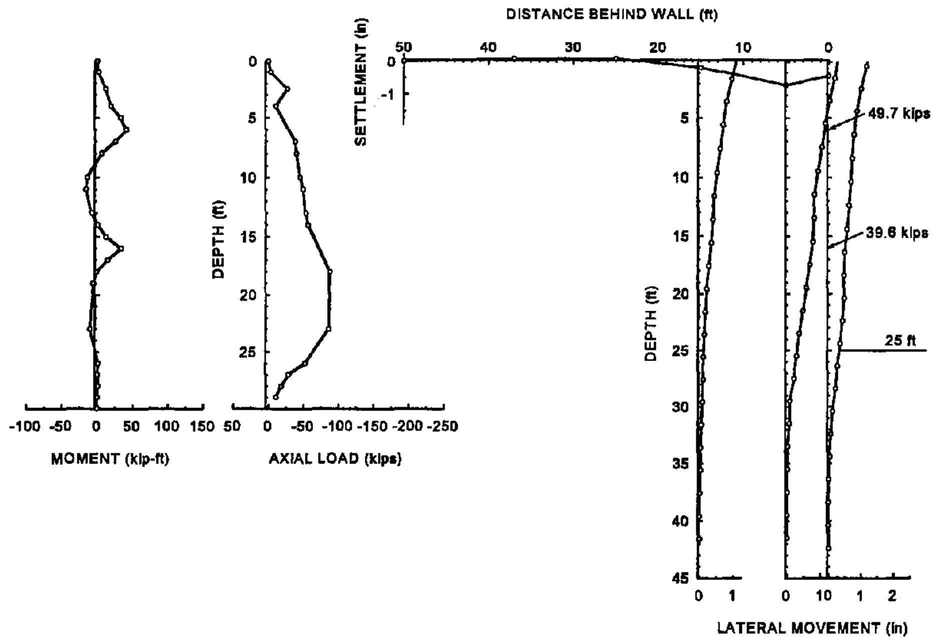

FIGURE 181
Bending Moments, Axial Loads, Lateral Movements, and Settlements: Drilled-in Soldier Beam No. 9; Long-term Reading – Day 206

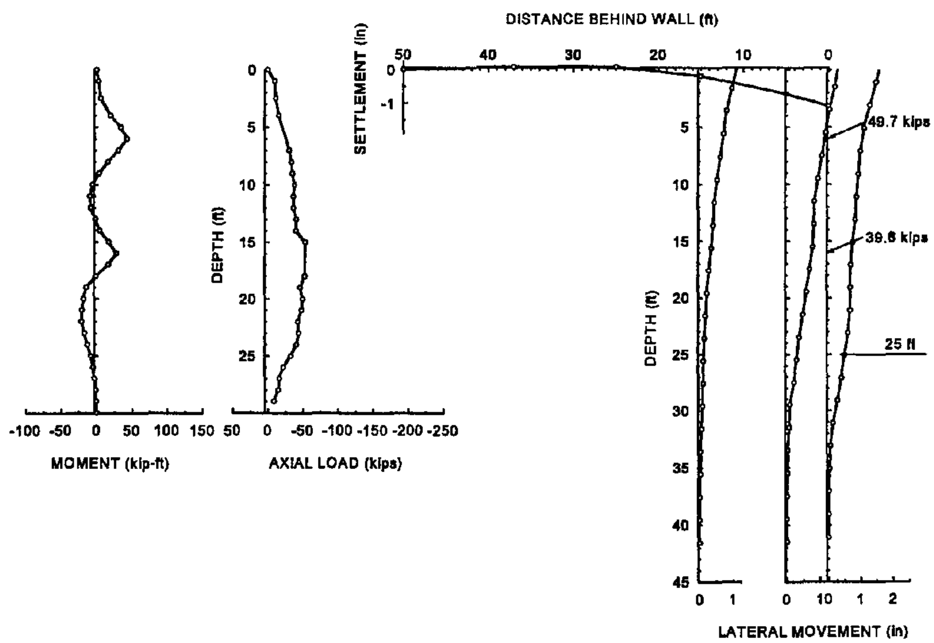

FIGURE 182
Bending Moments, Axial Loads, Lateral Movements, and Settlements: Drilled-in Soldier Beam No. 10; Long-term Reading – Day 206

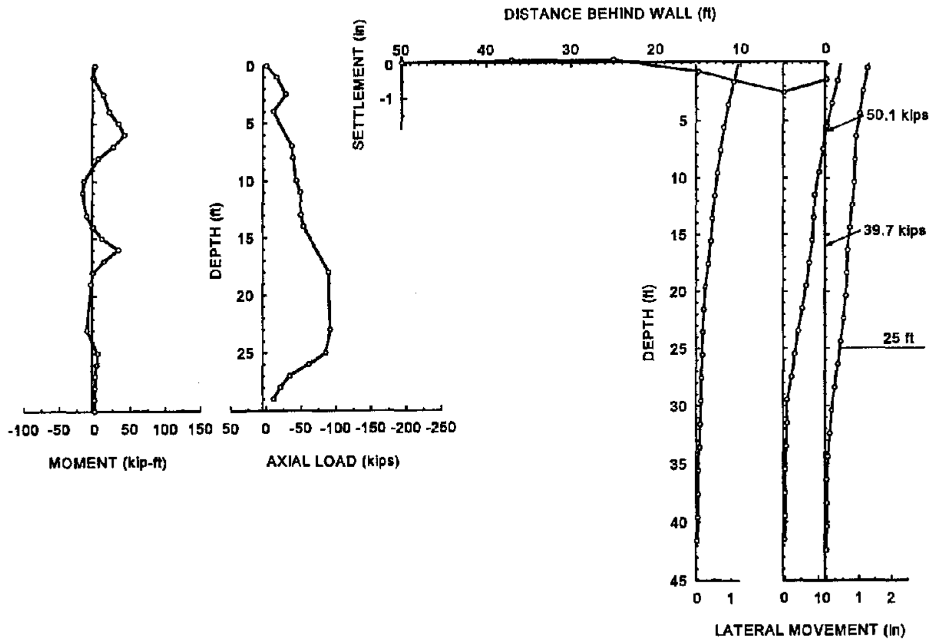

FIGURE 183
Bending Moments, Axial Loads, Lateral Movements, and Settlements: Drilled-in Soldier Beam No. 9; Final Reading After Load Reduced on Ground Anchor Supporting Soldier Beams 7 & 8 – Day 573

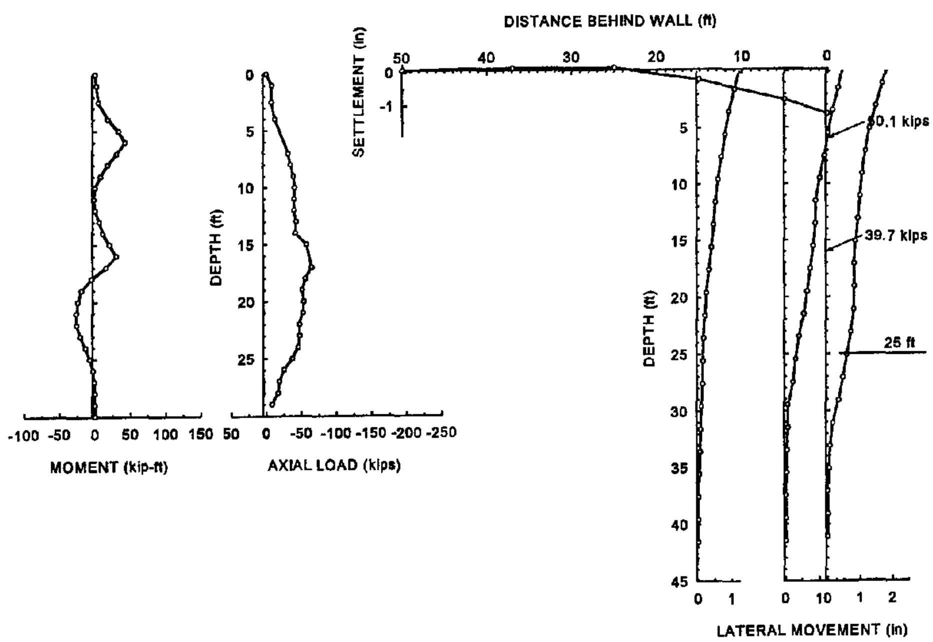

FIGURE 184
Bending Moments, Axial Loads, Lateral Movements, and Settlements: Drilled-in Soldier Beam No. 10; Final Reading After Load Reduced on Ground Anchor Supporting Soldier Beams 7 & 8 – Day 573

REFERENCES

AASHTO (1996). *The Standard Specification for Highway Bridges,* 16th Edition, Washington, DC.

Army Corps of Engineers (1993). "Design of Pile Foundations," *Technical Engineering and Design Guides*, ASCE, New York.

Bowles, J.E. (1974). *Analytical and Computer Methods in Foundation Engineering*, McGraw-Hill, Inc., 1974.

Cheney, R.S. (1988). *Permanent Ground Anchors*, Federal Highway Administration Report, FHWA-DP-68-1R.

Cheney, R (1990). *Permanent Ground Anchors, Volume 2, Field Demonstration Project Summaries,* FHWA Report No. DP-90-068-003.

Clough, G.W. and O'Rourke, T.D. (1990). "Construction Induced Movements of In-situ Walls," *Proceedings: Design and Performance of Earth Retaining Structures*, ASCE and Cornell University, Geotechnical Special Publication No. 25, pp. 439-470.

Coulomb, C.A. (1776). "An Attempt to Apply the Rules of Maxima and Minima to Several Problems of Stability Related to Architecture," *Mem. Acad. Roy. des Sciences* 3, Paris, p 38.

Dawkins, W.P. (1994). *User's Guide: Computer Program for Analysis of Beam-column Structures with Nonlinear Supports (CBEAMC)*, U.S. Army Corps of Engineers.

Goldberg, D.T., Jaworski, W.E. and Gordon, M.D. (1976). *Lateral Support Systems and Underpinning*, Vol. I, II, and III, Federal Highway Administration, FHWA-RD-75-103, April.

Haliburton, T.A. (1968). "Numerical Analysis of Flexible Retaining Structures," *Proceedings ASCE,* 94(SM3), pp.1233-1251.

Houghton, R.C. and Dietz, D.L. (1990). "Design and Performance of a Deep Excavation and Support System in Boston, Massachusetts," *Proceedings: Design and Performance of Earth Retaining Structures*, ASCE and Cornell University, Geotechnical Special Publication No. 25, pp. 795-816.

Jaky, J (1944). "A nyugalmi nyomas tenyezoje" (The coefficient of earth pressure at rest), *Magyar Mernok es Epitesz-Egylet Kozlonye*, pp. 355-358.

REFERENCES
(continued)

Lockwood, M.E. (1988). *Retention System Monitoring Demonstration Project No.68,* Progress Report for Ohio Dept. of Transportation, Cincinnati, OH.

Long, J.H., Weatherby, D.E., and Cording, E.J. (1998). *Summary Report of Research on Permanent Ground Anchor Walls*, "Volume I: Current Practice and Limiting Equilibrium Analyses," Report No. FHWA-RD-98-065, Federal Highway Administration, McLean, VA.

Long R. P. (1987). *Report on the Forces in soldier Pile No. 77 at the Danbury, CT Tieback Wall.*

Matlock, H., Bogard, D., and Lam, I. (1981). *BMCOL 76: A Computer Program for the Analysis of Beam-columns Under Static Axial and Lateral Loading*, Program Developed at the University of Texas at Austin, Program Documented at The Earth Technology Corporation, Long Beach, CA.

Mayne, P.W. and Kulhawy, F.H. (1982). "Ko-OCR Relationships in Soil," *Proceedings ASCE Journal* 108, GT.6, pp 851-872.

Mitre Software Corporation (1989). *G-TILT Inclinometer Data Reduction Computer Program*, Mitre Software Corporation, Edmonton, Alberta, Canada.

Mueller, C.G., Long, J.H., Weatherby, D.E., Cording, E.J., Power III, W.F., and Briaud, J.-L. (1998). *Summary Report of Research on Permanent Ground Anchor Walls*, "Volume III: Model-scale Wall Tests and Ground Anchor Tests," Report No. FHWA-RD-98-067, Federal Highway Administration, McLean, VA.

Munger, D.F., Jones, P.T., and Johnson, J. (1990). "Temporary Tieback Wall, Bonneville Navigation Lock," *Proceedings: Design and Performance of Earth Retaining Structures*, ASCE and Cornell University, Geotechnical Special Publication No. 25, pp. 778-793.

Murchison, J.M. and O'Neill, M.W. (1984). "Evaluation of P-y Relationships in Cohesionless Soils," *Analysis and Design of Pile Foundation, Proceedings ASCE,* San Francisco, CA.

NAVFAC (1982). *Foundations and Earth Structures*, DM-7.2, Department of Navy, Alexandria, VA, p. 63.

REFERENCES
(continued)

Nutting Company, H.C. (1988). *Progress Report: Tied-back Retaining Wall Performance Study, Demonstration Project No. 68, North Street Grade Separation, Lima, Ohio*, Prepared for the Ohio Department of Transportation, May 12.

O'Neill, M.W. and Murchison, J.M. (1983). *An Evaluation of P-y Relationships in Sands*, Research Report GT-DF02-83, Univ. of Houston, Houston, TX.

Peck, R.B. (1969). "Deep Excavations and Tunneling in Soft Ground," State-of-the-Art Report, *7th International Conference on Soil Mechanics and Foundation Engineering*, Mexico City, State-of-the-Art Volume, pp. 225-290.

Peck, R.B., Hanson, W.E., and Thornburn, T.H. (1974). *Foundation Engineering*, Second Edition, John Wiley & Sons, New York.

Pfister, P., Evers, G., Guillaud, M., and Davidson, R. (1982). *Permanent Ground Anchors, Soletanche Design Criteria*, FHWA/RD-81/150, U.S. Dept. of Transportation, FHWA, Washington, DC.

Reese, L.C., Cox, W.R., and Koop, F.D. (1974), "Field Testing and Analysis of Laterally Loaded Piles in Sand," *Proceedings of the 5th Offshore Technology Conference*, Houston, TX, Paper No. OTC 2080, Vol. II.

Reese, L.C., Cox, W.R., and Koop, F.D. (1975). "Field Testing and Analysis of Laterally Loaded Piles in Stiff Clay," *Proceedings 7th Offshore Technology Conference*, Vol. II, Dallas, Texas, pp. 671-690.

Rowe, P.W. (1952). "Anchored Sheet Pile Walls," *Proceedings of the Institution of Civil Engineers*, Part 1, pp. 27-70.

Schmertmann, J.H. (1970). "Static Cone to Compute Static Settlement Over Sand," *Proceedings ASCE, J. Soil Mechs. and Found. Engrg. Div.*, Vol. 96, No. SM3, May, pp. 1011-1043.

Schmertmann, J.H. (1977). *Guidelines for CPT Performance and Design*, Pub. No. FHWA-TS-78-209, Federal Highway Administration, Washington, DC.

Schnabel, H.S. (1982). *Tiebacks in Foundation Engineering and Construction*, McGraw-Hill, Inc., 170 pp.

REFERENCES
(continued)

Terzaghi, K., Peck, R.B., and Mesri, G. (1996) *Soil Mechanics in Engineering Practice*, 3rd Edition, John Wiley & Sons, New York.

Trofimenkov, J.G. (1974). "Penetration Testing in USSR," *State-of-the-Art Report, European Symp. Penetration Testing,* Stockholm, Vol. I.

Tschebotarioff, G. (1979). *Soil Mechanics, Foundations and Earth Structures*, McGraw-Hill Book Company, New York.

Urzua, A. and Weatherby, D. E. (1998). *TB Wall - Anchored Wall Design and Analysis Program for Personal Computers*, Report No. FHWA-RD-98-098, Federal Highway Administration, McLean, VA.

Wang, S.-T. and Reese, L.C. (1986). *Study of Design Methods for Vertical Drilled Shaft Retaining Walls*, Texas State Department of Highways and Public Transportation, Austin, TX.

Wang, S.-T. and Reese, L.C. (1992). *COM624P: Laterally Loaded Pile Analysis Program for the Microcomputer, Version 2.0*, FHWA Report No. SA-91-048, Washington, DC.

Weatherby, D.E. (1997). *Design Manual for Permanent Ground Anchor Walls*, Report No. FHWA-RD-97-130, Federal Highway Administration, McLean, VA.

Weatherby, D. E. (1998). *Summary Report of Research on Permanent Ground Anchor Walls*, "Volume IV: Conclusions and Recommendations," Report No. FHWA-RD-98-068, Federal Highway Administration, McLean, VA.